Surface Modification of Polymer Membranes by Self-Organization

by

Jonathan F. Hester

B.S. Materials Science and Engineering
Purdue University, 1993

Submitted to the Department of Materials Science and Engineering
in Partial Fulfillment of the Requirements for the Degree of
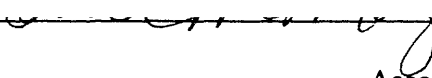
DOCTOR OF PHILOSOPHY IN POLYMERS

at the

MASSACHUSETTS INSTITUTE OF TECHNOLOGY

February, 2001

Signature of Author: _____
Department of Materials Science and Engineering
September 11, 2000

Certified by: _____
Anne M. Mayes
Associate Professor of Polymer Physics
Thesis Supervisor

Accepted by: _____
Carl V. Thompson
Stavros Salapatas Professor of Materials Science and Engineering
Chair, Departmental Committee on Graduate Students

Surface Modification of Polymer Membranes by Self-Organization

by
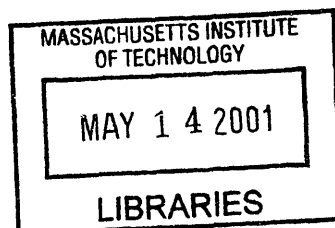
Jonathan F. Hester

Submitted to the Department of Materials Science and Engineering
on September 11, 2000 in partial fulfillment of the
requirements for the Degree of Doctor of Philosophy in Polymers

ABSTRACT

Water filtration processes employing polymer membranes have become increasingly important over the past forty years. Due to their high efficiency and modularity relative to conventional processes, membrane separations are among a suite of emerging water treatment technologies which will make possible future water use sustainability, by enabling the decentralization of wastewater treatment and the recycling of currently unused wastewater streams. The application of these highly efficient processes is presently limited, however, by their high operating costs relative to conventional processes, the most important cause of which is low fluxes and membrane failure due to fouling of the *hydrophobic* membrane materials by organics pervasive in feed waters. Current approaches to abate membrane fouling include substitution of more hydrophilic materials, as well as hydrophilic surface modification of hydrophobic membranes using coating and surface graft polymerization techniques. In many applications, the first approach results in unacceptable compromises in mechanical, thermal, and chemical stability. Coating and grafting techniques have been successful in reducing membrane fouling, but suffer from the disadvantages that (1) they require additional processing steps during membrane fabrication, increasing capital costs, (2) the coated or grafted layers obstruct membrane pores, reducing permeability, and (3) the hydrophilic surface layers have limited long-term stability.

This thesis explores the preparation of membranes having tailored surface chemistries from polymer blends composed of poly(vinylidene fluoride) (PVDF, an important commercial hydrophobic membrane material) and a small proportion (5-10%) of an amphiphilic, comb-shaped additive polymer designed for compatibility with PVDF. These blends *self-organize* during the aqueous coagulation and heat treatment steps of the standard immersion precipitation process for membrane fabrication, such that the amphiphilic polymer component is localized preferentially at the surface. The near-surface compositions of self-organizing membranes are quantified at the molecular level by X-ray photoelectron spectroscopy (XPS), and the surface chemistries so determined are related to membrane performance in a variety of adsorption, filtration, and wetting tests. The effect of the amphiphilic additive on membrane morphology is studied using electron microscopy.

Much of the work presented herein centers on blends containing an inexpensive, free-radically synthesized comb additive designed for fouling resistance, P(MMA-*r*-POEM), which has a poly(methyl methacrylate) (PMMA) backbone and poly(ethylene oxide) (PEO) side chains. Using this additive, processing conditions and molecular architecture are optimized to take full

advantage of surface segregation during the conventional steps of the commercial membrane fabrication process. Significant surface segregation is observed to occur during both the coagulation and aqueous heat treatment steps of the process. Using a coagulation bath heated to 90°C, a near-surface compositon of ~50 vol % comb (approaching 100% surface monolayer coverage) is obtained on a membrane with a bulk comb concentration of 15 vol % (10 wt %), requiring no post-coagulation processing. In an ultrafiltration experiment, membranes prepared using this single-step process exhibit fouling resistances comparable to membranes hydrophilized using coating and grafting methods. Significantly, addition of the comb results in an *increase* in the membrane porosity of up to an order of magnitude, compared to unmodified membranes having similar pore size distributions. Thus, due to the combined benefits of fouling resistance and increased porosity, a membrane containing 10 wt % of a comb having 45-unit PEO side chains has a flux over 20 times that of an unmodified PVDF membrane with equivalent separation characteristics after 3 h of filtration of a concentrated protein foulant solution. It is predicted and observed that the kinetics of membrane coagulation favor the surface segregation of *higher* molecular weight additives. Thus, the near-surface concentraion of P(MMA-*r*-POEM) after coagulation increases monotonically with its molecular weight up to at least $\overline{M}_w = 516\,000$ g/mol, based on polystyrene standards. This enables the preparation of membranes having robust, highly entangled surface layers composed of a water-insoluble comb. Surface layers prepared by self-organization are shown to be completely stable over at least 32 mo. of aqueous storage.

Self-organization is shown to have significant advantages over the current surface modification methods. First, self-organization results in surface modification of all internal pore channels, in addition to the external surfaces modified by coating and line-of-site grafting techniques. This has important consequences with respect to fouling by through-pore foulants, as well as the use of immersion precipitation for the facile preparation of advanced devices having tailored surfaces, including filters for toxic metal recovery and scaffolds and barrier materials for biomedical applications. Second, self-organizing membranes containing P(MMA-*r*-POEM) are potentially *self-healing*, in that surface layers damaged by acid exposure can be largely regenerated by subsequent heat treatment in water, which results in further surface segregation of residual comb from the bulk.

Using a novel, industrially-relevant atom transfer radical polymerization technique, comb polymers having PVDF backbones and POEM or poly(methacrylic acid) (PMAA) side chains are prepared. PVDF membranes prepared in a single step from blends containing ≥5 wt % PVDF-*g*-POEM are spontaneously wettable by water. Similarly prepared membranes containing 10 wt % PVDF-*g*-PMAA are *environmentally-responsive*, in that the pores can be reversibly opened and closed by adjustment of the feed solution pH, which controls the conformation of the weak polyacid PMAA side chains expressed at the membrane surface. A reversible flux variation of over an order of magnitude is observed as the feed pH is changed from 2 to 8. Conformational changes of surface-expressed PMAA are confirmed by atomic force microscopy force-distance measurements. These results make "intelligent," environmentally responsive filtration membranes available with no extra processing steps, and demonstrate the versatility of self-organization as a technique for imparting highly tailored surfaces to polymer membranes.

Thesis Supervisor: Anne M. Mayes
Title: Associate Professor of Polymer Physics

Table of Contents

6

List of Illustrations and Figures

10

List of Tables

Acknowledgments

result of simultaneous experimentation by myself, Dr. Banerjee, Ariya Akthakul, and Darrell Irvine.

1. Scope and Structure of this Thesis

1.1 Scope

This thesis is directed toward a new strategy for the surface modification of polymer membranes used for water filtration. Membrane-based separation technologies have been used for about forty years in water treatment applications, where they offer important benefits over conventional processes in terms of separation effectiveness and efficiency. Due to technological improvements resulting in lower costs, membrane water treatment processes have grown steadily both in terms of scale and market share, such that they now compete economically with conventional water treatment technologies in some applications. Indeed, membrane separation processes will play an important role in achieving future water use sustainability, as continuing population growth and industrialization require substantial and global improvements in water use efficiency.

The widespread application of membrane separations on scales sufficient to realize *global* sustainability will require substantial reductions in operating cost. Polymer membranes continue to suffer from fundamental materials deficiencies, which contribute strongly to current high process costs. The most severe of these is their susceptibility to *fouling*, the obstruction of membrane pores by organic material pervasive in wastewater streams. Fouling contributes substantially to the operating costs of membrane separations by dramatically reducing permeate throughputs, necessitating frequent membrane cleaning, and limiting membrane lifetimes. In addition, advanced applications of polymer membranes (*e.g.*, protein separations, heavy metal removal, drug delivery

applications) will require better *selectivities* on the part of membranes toward particular target species in their environments. A number of criteria will determine the future success of polymer membranes in these advanced applications and in contributing to water use sustainability. Table 1.1 summarizes these criteria, as well as the design attributes to be considered in meeting them. Reference to the criteria and attributes set forth in Table 1.1 will be made repeatedly throughout this thesis.

Table 1.1 Applicability Criteria for Water Treatment Membranes

Applicability Criteria	*Design Attributes*

Low Operating Cost
– Long membrane lifetimes
– High permeate throughput
	• Durability
	  – Mechanical stability
	  – Thermal stability
	  – Chemical resistance
	• High membrane porosity
	• Fouling Resistance
	  – Hydrophilic surface chemistries
	  – Robust and/or *self-healing* surface
	    chemistries

High Selectivity – Highly engineered surface chemistries – Control of pore size	• Flexibility in surface chemistry selection • *Functional* surface chemistries • *Environmentally-responsive* pore sizes
Low Capital Cost	• Inexpensive membrane materials • Minimal processing

Current methods for improving the fouling resistance and selectivity of polymer membranes have generally focused on either the bulk modification of the polymers used in their fabrication to render them hydrophilic, or the surface modification of existing membranes by coating or surface graft polymerization (see Figure 1.1). While these approaches have often been successful in achieving enhanced fouling resistance or

16

selectivity, these benefits generally come at the expense of higher fabrication costs (due to additional processing), reduced membrane permeability, and/or reduced durability.

The subject of this thesis is the surface modification of polymer membranes through *self-organization*, wherein a small proportion of an inexpensive additive polymer blended with a conventional membrane polymer becomes preferentially localized at the membrane surface during the *standard* fabrication process (Fig. 1.2), thereby delivering a desirable surface chemistry without significantly impacting the bulk membrane properties. The work presented herein will demonstrate that this strategy is capable of *simultaneously* satisfying all of the applicability criteria outlined in Table 1.1.

polymer membrane

COATING

GRAFTING

membrane with modified surface
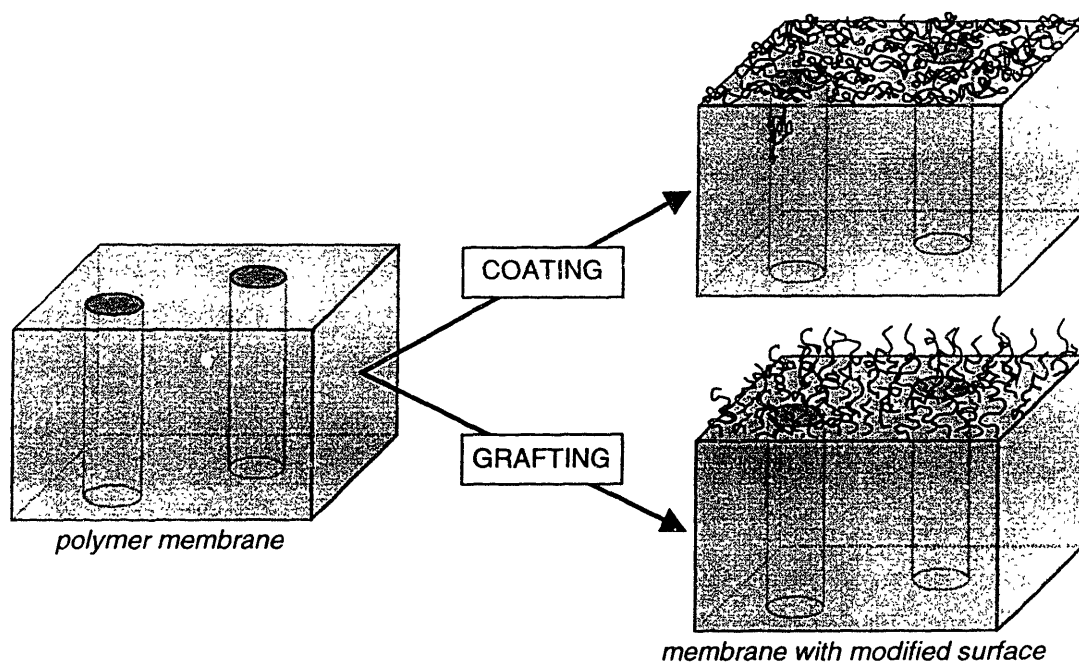
Figure 1.1 Coating and grafting strategies for surface modification
After membrane fabrication, additional processing is done to impart a desired surface chemistry. This may involve the coating of polymers or the surface graft polymerization of monomers onto the membrane surface.

1.2 Structure

Chapter 2, *Motivation and Background*, outlines the current applications of polymer membranes, describes their potential role in achieving future water use sustainability, and details their present limitations. Necessary background information related to membrane fabrication is also provided, as well as a review of past work related to the surface modification of polymer membranes. At the end of this chapter, the intelligent design of self-organizing blends for membrane applications is considered.

Chapter 3, *Experimental Techniques*, details the materials and methods used in the work presented herein, including the synthesis and characterization of polymer additives and the fabrication and characterization of polymer membranes. The results of the experiments are discussed in Chapters 4 and 5.

Chapter 4, *Implementation of Self-Organization During Membrane Fabrication*, explores the degree of additive surface localization obtainable. The effects on membrane

polymer blend
(matrix polymer + additive polymer)

membrane with tailored surface
chemistry
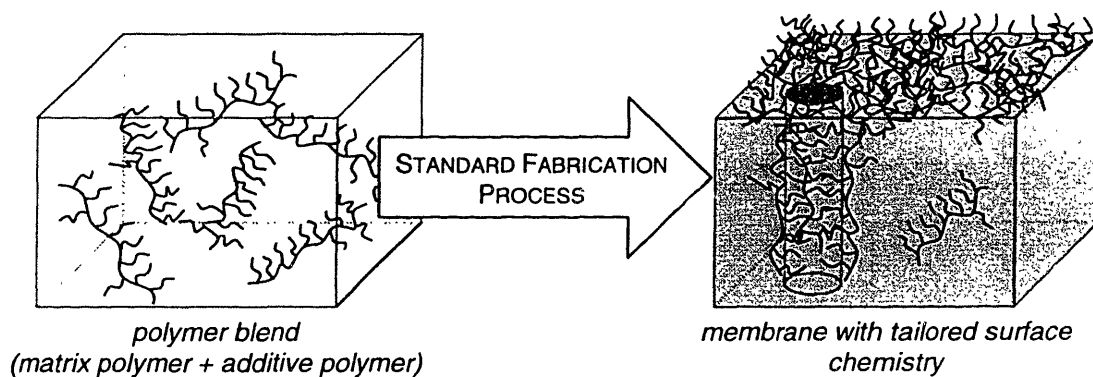
Figure 1.2 Self-organization strategy for surface modification
A small proportion of a comb-shaped additive polymer is blended with the conventional membrane-forming polymer. The additive surface-segregates during the standard membrane fabrication process, providing the desired surface chemistry with no extra processing steps.

18

surface composition of additive molecular architecture and processing conditions are explored, as well as the effect of the second polymer component on membrane morphology. It is shown that, with proper selection of molecular and process variables, a high degree of additive surface localization is obtainable using the conventional membrane fabrication steps, with no deleterious effects on membrane morphology.

In Chapter 5, *Performance of Self-Organizing Membranes*, the benefits realized through self-organization are discussed. Specifically, self-organizing membranes containing three principal additive materials are considered. The three additives are designed to impart fouling resistance, water wettability, and pH-responsive separation characteristics, respectively, to membranes. Moreover, it is shown that the modified surface chemistries produced by self-organization are potentially *self-healing*, in that surface layers damaged by exposure to aggressive chemicals can be largely regenerated through a simple heat treatment in water.

Chapter 6 is a summary of the main conclusions made from this work. This chapter closes with some suggestions for future study and extension of the self-organization strategy put forth in this thesis.

2. Motivation and Background

2.1 Polymer Membranes and Their Applications

Polymer membranes are polymeric devices which enable the separation of materials based roughly on their molecular or aggregate size,[1] although other attributes of the materials,[2] such as solubility, diffusivity, and electrical charge, may be important. Polymer membranes are used for gas/gas, liquid/gas, liquid/liquid, and solid/liquid separations. This thesis is directed toward the liquid/liquid and solid/liquid separations encountered in water treatment applications. In most of these applications, the driving force for the separation is a pressure gradient applied across the membrane.[2] One or more species in the feed water is retained and concentrated, while the remainder of the feed solution permeates the membrane. Figure 2.1 is a simple schematic diagram of such an operation.

The simplest polymer membranes are flat sheets anywhere from 10 μm to 200 μm in thickness.[1-3] Membranes are also fabricated as hollow fibers 1 mm or less in diameter. Most membranes of commercial importance are characterized by an *asymmetric* structure
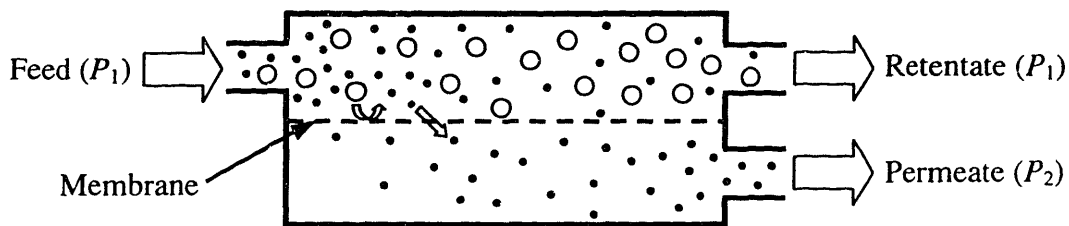
Figure 2.1 Schematic illustrating the principle of membrane separation
The feed side of the membrane is held at a pressure P_1 greater than the pressure P_2 on the permeate side.
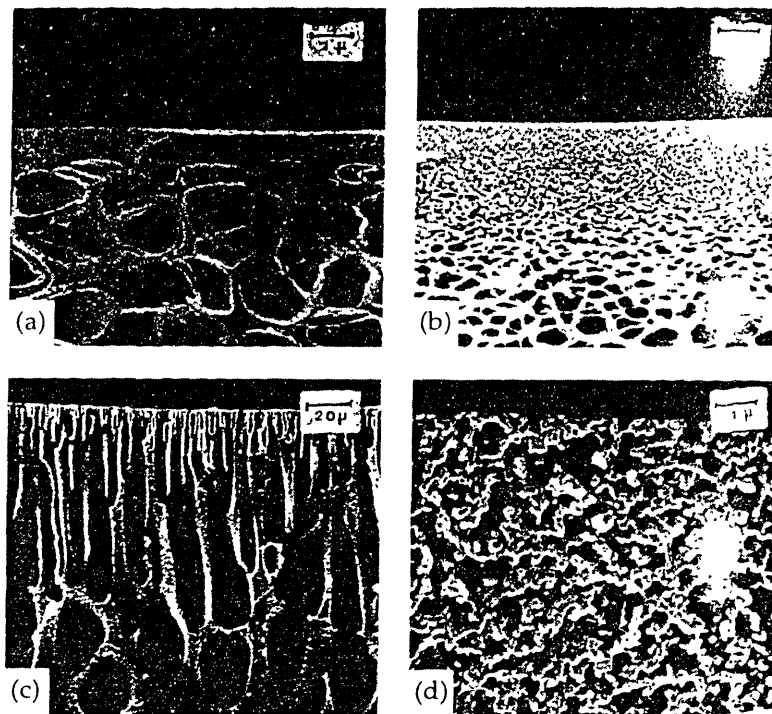
Figure 2.2 Typical membrane cross-sections

(a) Asymmetric "sponge" membrane with uniform pore structure; (b) asymmetric "sponge" membrane with graded pore structure; (c) asymmetric "finger" type membrane; (d) symmetric membrane without a dense surface layer. *(Figure reprinted from reference 47)*

(see Figure 2.2), consisting of a relatively dense, 0.1 to 1 μm surface layer overlaying a highly porous sublayer.[4] The separation characteristics of the membrane are determined by the pore size distribution in the surface layer, while the porous substructure provides mechanical support. This asymmetric structure is advantageous, since separation is achieved at the membrane surface, while relatively high fluxes are allowed through the large pore channels which comprise the bulk of the membrane volume. With respect to the asymmetric structure, hollow fiber membranes are entirely analogous to flat membranes, with the dense separation layer usually on the interior surface of the fiber.[14,5]

Polymer membranes are assembled into modules used for water treatment. A common

module geometry used for flat membranes is shown in Figure 2.3. An important and general characteristic of module design is that fluid flow is *tangential* to the membrane surface and of sufficient velocity to inhibit deposition of materials onto the membrane. Thus, species in the feed water unable to pass through the membrane are concentrated as they are swept across the membrane surface, finally exiting the module at the downstream side.

Table 2.1 Characteristics of the Various Types of Water Treatment Membranes

Membrane Type	Separation Surface Structure	Mechanism of Separation	Species Retained
Microfiltration (MF)	Micropores (0.01 to 10 μm)	Aggregate size	Particulates, microorganisms, bacteria
Ultrafiltration (UF)	Mesopores (1 to 50 nm)	Molecular/aggregate size	Colloidal particles, oil droplets, macromolecules, viruses
Nanofiltration (NF)	Nanopores (<2 nm)	Molecular size + solution/diffusion	Sugars, divalent ionic species
Reverse Osmosis (RO)	Dense	Solution/diffusion	Monovalent ionic species

Polymer membranes are often classified according to their separation surface pore sizes.[1,2,6,7] The major types of membranes used in water treatment applications, their separation surface structures, and the types of species retained are listed in Table 2.1. These various membrane types, alone or in combination, are capable of physically removing from water species ranging in size from monovalent salts to macroscopic particulate matter. Current applications of polymer membranes include the desalination of sea and brackish water, water softening, municipal wastewater treatment, the

purification of wastewater produced by such industries as electroplating, metal finishing,

petroleum and petrochemical, and pulp and paper, and the production of ultrapure water

for the electronics and pharmaceutical industries.[8]

The *physical* nature of membrane separation operations, as well as their high

degree of modularity, gives them notable advantages over conventional water treatment

processes with respect to water use efficiency. These advantages are discussed in the

next section in the context of their significant implications for future water use
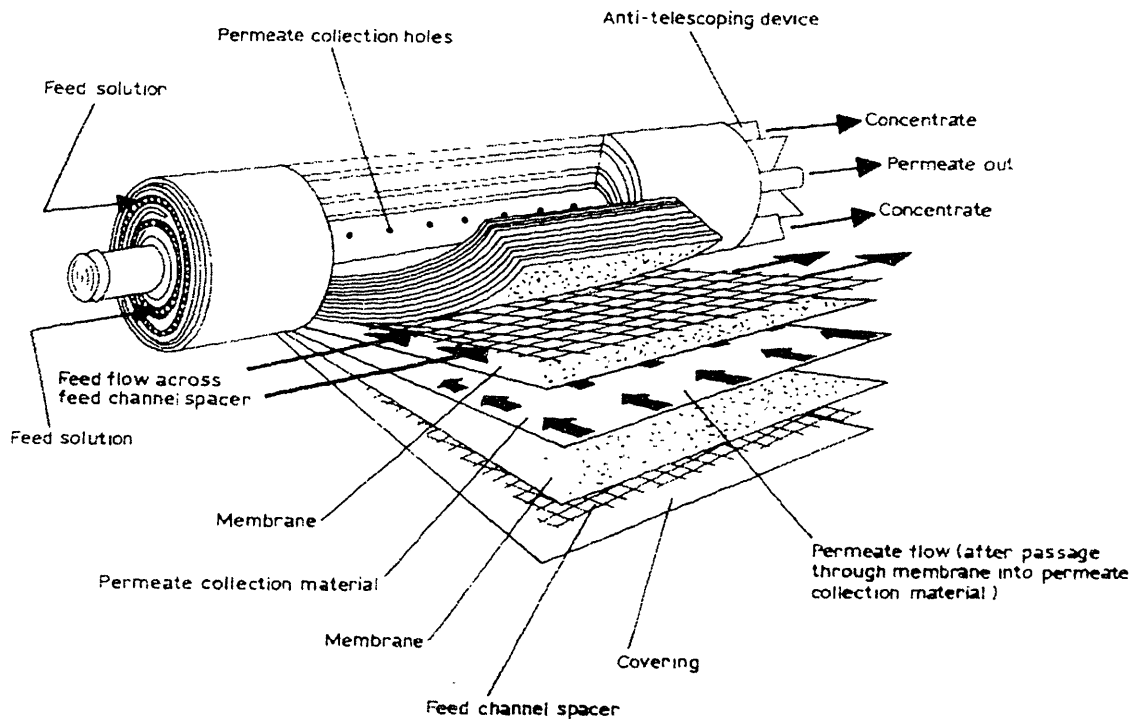
Figure 2.3 Schematic of a "spiral wound" membrane filtration module
Two flat membrane sheets are separated by a permeate collection material and bonded around three sides. The open end of the resulting envelope is connected to the central tube as the only outlet by means of the permeate collection holes. A spacer material is then placed on top of the envelope, and the resulting assembly is wound many times about the central tube. The feed solution is concentrated in the spacer material, and permeate is collected from the central tube. This geometry packs a large, flat sheet (with a large surface area) into a small volume. Note that feed solution flow is tangential to the membrane surface. *(Figure reprinted from reference 1)*

sustainability. Despite their advantages, however, the use of membrane-based processes is strongly limited by fundamental materials deficiencies with the membranes themselves. The challenges posed by these materials deficiencies will also be considered in the next section.

2.2 The Need for Better (and Cheaper) Polymer Membranes

2.2.1 The Promise: Polymer Membranes for Water Use Sustainability

Annually, the world's land masses receive approximately 40,700 cu. km of runoff, the source of freshwater for all human use.[9] Of this amount, only about 12,500 cu. km is geographically accessible on demand. Currently, people use approximately 35% of this *accessible water supply* (AWS) for agriculture, industry, and household needs. An additional 19% is used for "instream" purposes – to dilute pollutants, sustain fisheries, and transport goods. Thus, over half of the world's AWS is currently in use.

Figure 2.4 projects global human appropriation of freshwater into the future. The projections are based on estimated historical per capita water withdrawals compiled by the Global Water Policy Project[9-11] and expected world populations published by the United Nations.[12] Two projections are shown. The more conservative projection assumes that the future per capita rate of water use remains constant at the 1995 value. The more liberal projection assumes that per capita water use increases at the same rate as it did between 1950 and 1990, when per capita withdrawals increased by roughly 50% as the world population grew by 2.7 billion.[10,11] The solid, horizontal line denotes the AWS as of 1995. In the past, the AWS has been expanded to meet increasing freshwater

demands mainly through the construction of new dams and reservoirs. Due to environmental constraints, such constructions are expected to offer fewer sustainable solutions in the near future. In fact, new dam systems are not expected to increase the AWS by more than 10% over the next thirty years.[9] The expected AWS in 2025 is plotted as a dotted line in Figure 2.4.

Clearly, present patterns of freshwater use are not sustainable. Even by the most conservative estimate,[9] current practices may be expected to completely outstrip the AWS around 2050, resulting in extensive environmental degradation and wildlife habitat destruction. Evidence of severe environmental degradation due to human water use
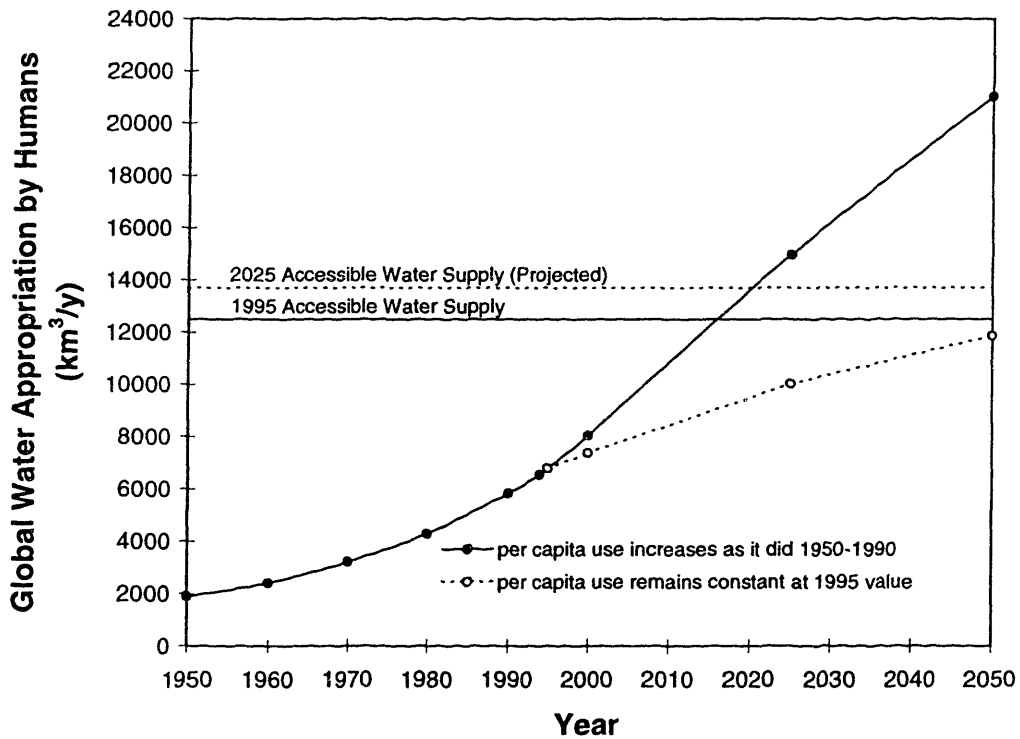
Figure 2.4 Projected global water use by humans through 2050
Projections are based on historical per capita water withdrawals compiled by the Global Water Policy Project[9-11] and expected world populations published by the United Nations.[12]

intensification exists today, for example, in the American Southwest, where the Colorado River Delta has been dessicated due to man-made dams and river diversions, resulting in extensive loss of biodiversity and destruction of fisheries, and threatening the Cocopa Indians with cultural extinction.[10,13] Moreover, the current and historical withdrawals plotted in Figure 2.4 do not include water obtained by unsustainable overpumping of groundwater. Groundwater overpumping currently provides water in many important food-producing regions, including China, India, and the western United States, and some Middle Eastern nations rely on this practice for significant portions of their water needs.[11]

The global account presented above does not reveal the severe cases of regional water scarcity which exist even now, due to the non-uniform distribution of global runoff. In fact, greater than 20% of the world population, mostly in the arid regions of Africa and the Middle East, currently live without access to acceptable drinking water.[11] In the Nile, Euphrates, Ganges, and Jordan river basins, water scarcity has directly resulted in international conflict.[14] We can only expect these problems to worsen if unsustainable water use continues.

Clearly, future sustainability will require that we do much more with much less water. This will be made possible in large part by emerging water treatment technologies which will

a) enable the decentralization of water treatment processes, and

b) produce useable, and even potable, water from wastewater streams which are currently unused.

Among these technologies are filtration technologies based on polymer membranes. Unlike conventional wastewater treatment technologies (flocculation, settling, and sand

filtration), membrane-based processes are highly modular, and thus easily and economically scaled down to sizes amenable to *on-site* industrial wastewater treatment. Such processes have recently found wide-spread use, for example, in the automotive paint industry,[15] where large-scale paint mixers are routinely flushed with water to remove residual paint. The resulting waste stream was traditionally diluted with additional water and discharged to the environment. Membrane processes now enable the on-site reclamation of valuable paint from these waste streams, along with the recycling of flushing water in a closed loop. Thus, the modularity of membrane processes enables the decentralization of wastewater treatment operations, allowing the reclamation of water "impurities" while they are unmixed and therefore valuable. Water savings result not only from the ability to recycle water on-site, but also from reduced sludge generation and the reduced quantity of water required to dilute pollutants.

In concert with other advanced treatment processes, membrane processes are capable of removing from wastewater species which cannot be removed by traditional wastewater treatment methods. This capability has the potential to dramatically increase the efficiency of municipal water use. Municipal water systems are traditionally characterized by a complete separation of potable water and wastewater treatment systems. Water is collected in a reservoir and undergoes potable treatment before being distributed to the municipal water supply. Wastewater is then collected, undergoes a level of treatment dictated by environmental impact upon the receiving body, and is discharged as downstream waste. Using this "open loop," each water molecule may be utilized by the municipality as potable water, at most, once per annual cycle. An

advanced water treatment plant based on membrane filtration processes is scheduled to close San Diego, California's water loop in 2000.[16,17] Water discharged into the city's sewer system will be repurified to *potable standards* by the advanced treatment plant, then blended with water in one of the city's potable source reservoirs. If implemented worldwide, such closed-loop schemes would result in dramatically reduced per capita water withdrawal rates by enabling municipalities to utilize each source water molecule multiple times before surrendering it to the natural water cycle.

The above examples illustrate how polymer membranes are creating two important paradigm shifts in the treatment of wastewater streams: from centralized to decentralized, and from open-loop to closed-loop. Both paradigm shifts convert traditional "*waste*water" streams to available water *resources*. Membrane separation processes have a number of additional advantages over conventional wastewater treatment processes.[18,19] Conventional processes require the addition of chemical coagulants and flocculants to the feed waste stream. If not properly handled, such processes can leave residual waste material in treated water. Furthermore, they generate sludges containing concentrated quantities of man-made waste products, in addition to the natural particulates removed from the feed water. These sludges must be diluted in a receiving water body or landfilled, practices which often threaten the quality of existing potable water sources.[20] Moreover, these concentrated wastes contain a large amount of water which might otherwise be useful – as much as 10% of the water treated by a conventional wastewater treatment plant may be lost in the disposed sludge.[8] Polymer membranes provide an absolute filter capable of physically separating from wastewater

streams species ranging in size from viruses to particulate matter, and thus enable the treatment of water without the addition of chemicals. For this reason, membrane processes are capable of decreasing by 20 to 50 times the sludge volume which must be recovered or disposed of by other processes.[21]

Similarly, polymer membranes offer a desirable alternative to the conventional use of chlorine and ozone for water disinfection.[8] Chlorine and ozone can react with organic impurities in water to produce chlorinated organic products, the presence of which have been correlated with occurrences of cancer.[4] Various membrane separation processes have been shown to completely disinfect water (physically removing viruses as well as larger organisms) without the addition of chlorine or ozone.

Finally, the capability of RO membranes to physically remove salts from sea and brackish water offers the possibility of significantly expanding the AWS. Because RO processes require no phase change, they are inherently less energy-intensive than conventional distillation methods for desalination. Until recently, however, the high material costs of RO processes have prevented them from competing with multi-stage flash (MSF) distillation in most cases.[22] Thanks to steady improvements in membrane materials and a simultaneous ten-fold reduction in membrane costs over the last twenty years,[23,24] RO is now more economical than MSF in situations where fuel costs are high.[22] Due to their energy-intensive nature, desalination technologies currently offer real alternatives only to energy-rich nations. Moreover, they are practical only in coastal regions. Still, for many arid nations, the prospect of an affordable physical separation process for desalination remains a tantalizing, if in many cases distant, possibility.

2.2.2 The Challenges: Flux, Fouling, and Selectivity

Membrane processes for water treatment and ultrapure water production are a proven technology, having been used on large scales since the early 1970s. In 1994, MF, UF, NF, and RO processes together produced municipal drinking water at a rate of roughly 3.6 million m^3/day worldwide.[25] Membrane processes for on-site industrial wastewater treatment are routinely employed in the paint, motor manufacture, metal plating, and wire drawing industries, where they enable the recovery of valuable constituents (*i.e.*, paints and oils) from waste streams.[8] As a business, membrane technology expands by roughly 15% per year worldwide.[26]

However, the operating costs of membrane processes remain high compared to conventional processes. For example, a 1993 pilot-scale comparison[27] between conventional and MF processes for the treatment of domestic effluent concluded that, while MF was significantly more effective at removing the species of interest, it was not economically viable because its operating cost was *14 times* that of the conventional process. Thus, membrane processes are often not applied in situations where their use would have clear benefits. Car washing facilities, which elute gallons of a water/detergent mixture to the municipal sewer each time a car is washed, are one example.[15] Small-scale membrane filtration units are capable of enabling the recycling of this mixture by removing oils and dirt particles suspended in the eluted water. However, the high operating cost of the membrane separation process is not economically justified by the low value of the water/detergent mixture recovered. A second example is the general failure of membrane processes to replace chlorination and ozonification for water

31

disinfection, although these conventional methods have been linked to cancer deaths.[4,8] Because of their high costs, membrane technologies are largely beyond the means of developing nations.[22] In fact, 75% of the market for polymer membranes is confined to the United States, Europe, and Japan.[25] Thus, the benefits of these technologies are currently unavailable to many of the most water-starved regions of the world.

The capital and operating costs of membrane separation processes are typically direct functions of the trans-membrane flux,[28] since this parameter establishes the trade-off between the trans-membrane pressure (*i.e.*, fuel usage) and the overall membrane surface area needed to obtain the required permeate throughput.[22,29] Indeed, although cellulosic membranes existed as early as the 1930s,[4] their commercial use was impractical until the development in the late 1950s of asymmetric membrane structures[30] capable of high fluxes. Currently, the limiting attribute with respect to flux is not membrane morphology or process design, but rather the nature of the membrane materials themselves.

MF and UF membranes are most commonly fabricated from hydrophobic polymers such as polysulfones, polypropylene, polycarbonate, and poly(vinylidene fluoride) (PVDF). These materials have excellent chemical resistance, thermal stability, and mechanical properties under the application conditions.[31] However, their hydrophobic character makes them highly susceptible to fouling, the occlusion of membrane pores due to the adsorption of proteins, oils, and other organic material commonly present in feed waters.[29,32,33] Fouling can occur very rapidly – it has been estimated that roughly half of the porous volume in a typical MF or UF membrane is

fouled within less than one day in a typical operation[32] – and it can have a dramatic effect

on the trans-membrane flux. In fact, in the worst cases, the flux is completely controlled

by a "secondary membrane," a film of organic material deposited on the membrane

surface.[4] Moreover, fouling can result in irreversible changes in membrane selectivity

with time.[32,34]

Figure 2.5 is a schematic illustration of the reality faced by the operators of

membrane processes as a result of fouling, which necessitates frequent cleaning

operations to maintain acceptable fluxes. Membrane cleaning is generally accomplished

by periodic "backwashes," during which flow through the membrane is reversed, and by

occasional chemical cleanings, typically with caustic and/or detergent solutions. In
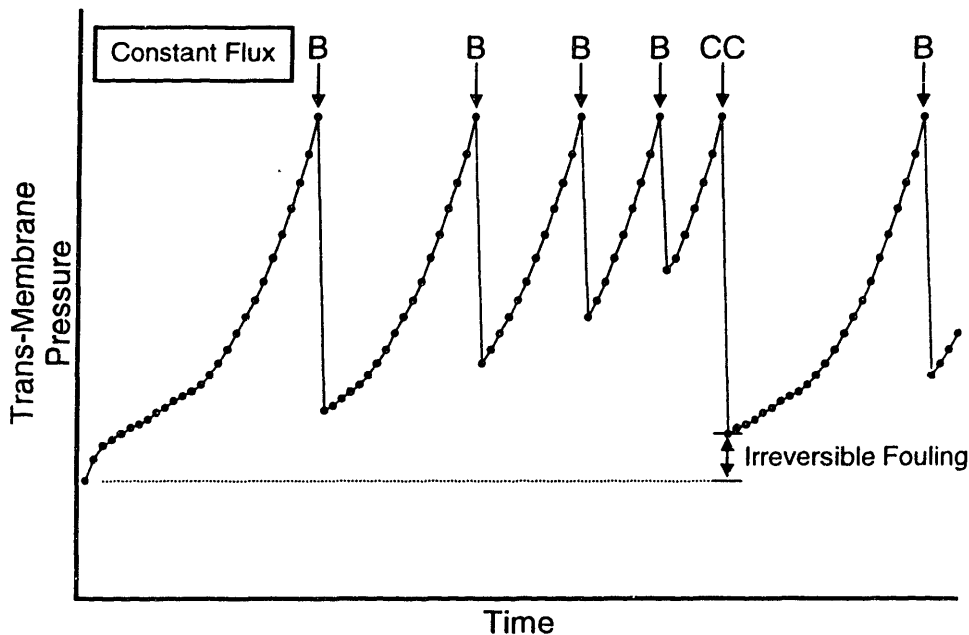
Figure 2.5 Schematic pressure vs. time plot for an UF operation
In this example, as in many UF operations, the trans-membrane pressure is controlled in order
to maintain a constant permeate flux.   B = backwash operation;   CC = chemical cleaning
operation.   In UF, the time between backwash operations is often on the order of 30 minutes.
As shown, both cleaning strategies become gradually less effective with time.

addition, pre-treatment of feed waters with chemical coagulants is often employed to precipitate foulant species before they contact the membrane, significantly increasing the inclusive operating cost and negating some of the potential advantages of membrane separations.[35,36] Ultimately, fouling limits membrane lifetimes. In all, membrane cleaning and replacement costs associated with fouling in UF processes are estimated to account for 47% of the total process costs,[37] quite apart from the role fouling plays in determining the operation size and pressure required to obtain a given permeate throughput. Thus, the problem of fouling is a ripe target for process cost reduction.

Cellulosic and polyamide-based membranes, used commonly in RO and NF and frequently in UF applications, are hydrophilic, and thus significantly less susceptible to fouling.[2,19] However, water acts as a plasticizer for these hydrophilic materials, resulting in comparatively poor thermal and mechanical properties.[4] Moreover, these materials are subject to chemical and biological attack. Hydrolysis and biodegradation of cellulosic membranes generate physical holes over time, compromising their separation characteristics and reducing their lifetimes.[2,7,38] Polyamide-based membranes, for their part, are highly sensitive to oxidants, such as chlorine, which are commonly found in feed water.[2,22,39] Clearly, a need exists for membranes which combine the superior bulk properties of the hydrophobic materials with the surface chemistries of the hydrophilic materials.

A second problem limiting the application of current polymer membranes is their poor selectivity. For example, one potentially significant application of polymer membranes is the high-speed fractionation of macromolecules (e.g., proteins).[1,40] This

market is currently satisfied almost entirely by chromatography processes, which are inherently slow since they rely on the achievement of chemical equilibrium. Physical separation processes based on UF membranes would operate at much higher speeds and thus lower costs. However, UF is not currently useful in this application due to *time-dependent* separation characteristics caused both by fouling and by gradual compaction of the membrane pores under pressure,[4] which result in poor selectivity between macromolecules of different sizes.[1] Additionally, one might imagine the application of polymer membranes capable of specifically removing target species from feed water streams based on their chemical nature, rather than simply their size. For example, a MF or UF membrane capable of retaining a specific heavy metal ion based on a chemical binding event would do so at a much higher throughput than a dense RO membrane relying on a slow diffusion mechanism for separation.

An obvious approach to solving the problems of fouling and selectivity, without sacrificing the optimized bulk properties of the current membrane materials, is the surface modification of hydrophobic membranes to impart engineered surface chemistries. For the prevention of fouling, the dominant cause of which is the chemical attraction between organics in the feed solution and the membrane surface,[4,41] the modification of hydrophobic membrane surfaces with hydrophilic chemical groups is often successful. Similarly, higher selectivities may be achieved by surface modification using moieties capable of responding chemically to the environment and to species of interest in the feed stream. A number of surface modification techniques are currently used, with varying degrees of success. These are reviewed in Section 2.4. First, it is

necessary to understand the method used for membrane fabrication, which is the subject of the next section.

2.3 Fabrication of Polymer Membranes

2.3.1 The Immersion Precipitation Process: An Overview

Polymer membranes for water treatment applications are fabricated almost exclusively by *immersion precipitation.* A schematic of the continuous process for production of flat membranes is shown in Figure 2.6. Following are the elementary steps in the process.[2,3,42-46]

1. The polymer is dissolved in a solvent to form a solution containing 10 to 30 wt % polymer. A small quantity of a nonsolvent "pore former" is usually added to this solution.

2. The solution is cast under a doctor blade onto a moving, nonwoven polyester or mylar belt. Often, this belt will serve as a permanent support for the finished membrane. The thickness of the cast film is typically between 10 and 500 μm.

3. Partial evaporation of the solvent may or may not be allowed to occur.

4. The film is immersed in a nonsolvent, usually water or a water-rich mixture, resulting in precipitation (or "coagulation") of the polymer to form the asymmetric, porous structure. The nonsolvent temperature is typically between −10 and +20°C.

5. The membrane may be heat treated in a second water bath for morphology refinement, such as pore shrinkage. The heat treatment temperature is usually between 50 and 90°C.

6. The membrane is rinsed and taken up on a roll.

Hollow fiber type membranes are made by an entirely analogous process;[2] the casting solution is extruded into a hollow fiber geometry by means of a spinneret, after which the extruded mixture is immersed in a precipitant bath to induce polymer coagulation.

The final membrane structure depends upon each of the following critical process variables: (1) composition of the casting solution, (2) optional solvent evaporation rate and time, (3) composition and temperature of the precipitation medium, and (4) optional heat treatment duration and temperature.
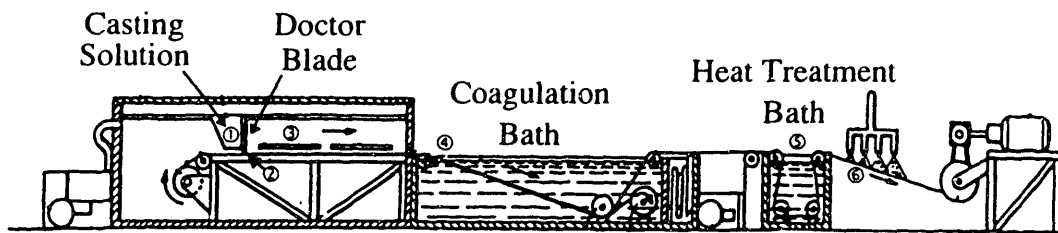
Figure 2.6 Schematic of the continuous immersion precipitation process
(1) Polymer is dissolved in a solvent. (2) The resulting casting solution is cast under a doctor blade onto a moving belt. (3) Evaporation of solvent may be allowed to occur. (4) The casting solution is immersed in a nonsolvent, resulting in precipitation of polymer. (5) The membrane may be heat treated in a second nonsolvent bath. (6) The membrane is rinsed and taken up on a roll. *(Figure adapted from reference 44)*

2.3.2 Mechanism of Membrane Formation

Depending on the processing conditions outlined in the previous section, polymer membranes fabricated by immersion precipitation may exhibit any of the four major morphology types shown in Figure 2.2.[43,47] The morphology of a membrane has a profound effect upon its performance. For example, "sponge" type membranes generally retain small solutes and exhibit low fluxes, while "finger" type membranes exhibit high fluxes but relatively poor retention of small solutes.[48] In addition to the substructure

37

morphology, the pore size distribution in the separation surface, which directly affects the selectivity and permeability of the membrane, varies substantially with the above processing conditions. Indeed, by manipulation of the processing conditions, it is often possible to prepare RO, UF, and MF membranes from the same material.[49]

Extensive empirical work has been conducted to connect the various process parameters to the resulting membrane structures. Morphological elements of interest include the occurrence, thickness, and porosity of the dense surface "skin,"[43,47,50] the pore volume and interconnectivity[51] in the substructure, and the presence or absence of the *macrovoids*[52-55] characteristic of "finger" type membranes (Fig. 2.2c). Based on the large body of experimental work, a number of mechanistic frameworks, both qualitative[47,48,56-59] and computational,[43,49,60-68] have been developed to explain and predict membrane structures. The most sophisticated computational models[60-64] are semi-quantitatively predictive for a limited number of systems and preparation conditions. This section outlines the basic processes operating during membrane fabrication, an understanding of which is essential to the design of self-organizing membranes.

Equilibrium Thermodynamic Considerations

The formation of the membrane structure during the coagulation step of the fabrication procedure is fundamentally a phase separation process, and it is therefore instructive to consider the equilibrium properties of the three-component solvent-nonsolvent-polymer system. Figure 2.7 is a schematic ternary phase diagram describing a system containing a *semi-crystalline* polymer (component 3), a solvent (component 1), and a precipitant (component 2).[2,47,69-71] Energetic interactions between any tw

38

POLYMER
3

E′

Binodal

E

Crystallization
Boundary

D

C

A

B

solid
+
liquid

liquid
+
liquid

E″

1 phase

1

2

E″

SOLVENT
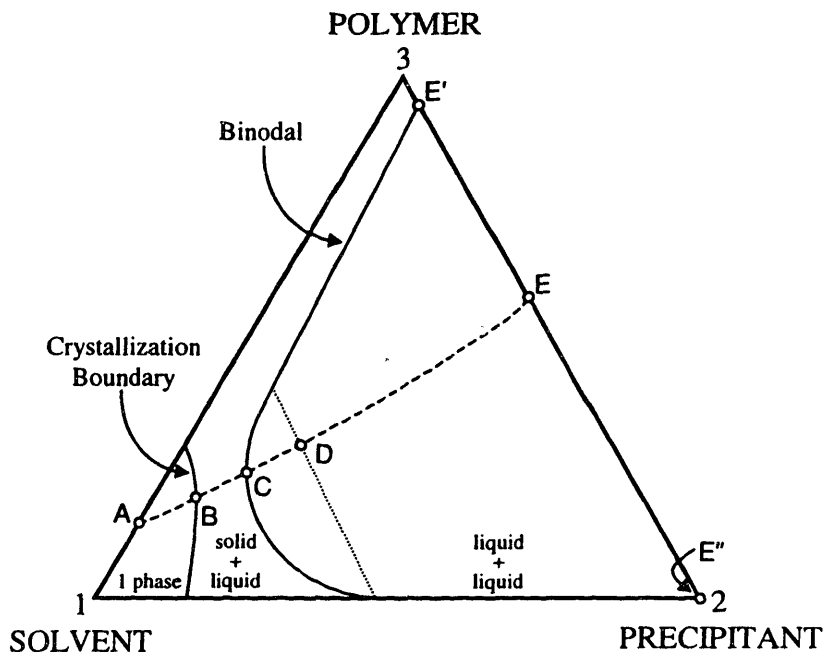
PRECIPITANT

Figure 2.7 Ternary phase diagram describing immersion precipitation

components i and j may be described by the Flory-Huggins interaction parameter, χ_{ij}.

For the case shown in Figure 2.7, the polymer is soluble in liquid component 1 ($\chi_{13}<\frac{1}{2}$)

and insoluble in liquid component 2 ($\chi_{23}>\frac{1}{2}$), and the two liquid components are miscible

in all proportions ($\chi_{12}<2$).[72] The phase diagram contains three regions:

   a) a one-phase region at low concentrations of the polymer and precipitant,

   b) a two-phase region defined by the equilibrium crystallization boundary
      (absent in systems containing noncrystalline polymers), within which the
      liquid phase is in equilibrium with crystallized polymer, and

   c) a second two-phase region, defined by the binodal, within which a liquid
      polymer-rich phase is in equilibrium with a liquid polymer-poor phase.

The relative positions of the crystallization boundary and binodal vary widely for systems

containing crystallizable polymers.[60,69,73]

The dashed line *ABCDE* represents a typical "composition path" for a casting solution during membrane formation. A homogeneous casting solution of initial composition *A* imbibes precipitant from the coagulation bath (and loses solvent to it) until the occurrence of instability at composition *B*. At *B*, solid-liquid demixing may occur by nucleation and growth of polymer crystals. The extent to which solid-liquid demixing actually occurs depends on the duration of the compositional change from *B* to *C*, where the considerably faster liquid-liquid phase separation process begins. Nucleation and growth of a liquid polymer-lean phase within the continuous liquid polymer-rich phase then proceeds while, at the same time, continuing solvent/precipitant exchange causes the viscosity of the polymer-rich phase to increase rapidly. At an overall composition *D*, macroscopic polymer transport in the polymer-rich phase is significantly hindered, and this phase may be regarded as a solid. Exchange of solvent for precipitant continues until a final composition *E* is reached. At *E*, an immobile polymer-rich phase of composition *E'* is in equilibrium with a polymer-poor phase (*E''*), which constitutes the precipitant-filled pores. Shrinkage of the polymer-rich phase always takes place throughout the precipitation process since the casting solution is composed of 10-30% polymer, while the ultimate composition of the polymer-rich phase is typically nearly 100% polymer.

Kinetic Considerations

The equilibrium thermodynamic considerations presented above provide a useful framework for analysis of the events occurring during membrane formation. However, it is the kinetics of mass transfer during the coagulation process which determine the composition pathway *ABCDE* and the *dispersion* of the phases (*i.e.*, the pore size).[57]

Moreover, an important feature of this system is the high polymer concentration in the casting solution, which leads to slow mass transfer and a consequent tendency of the system to assume metastable states throughout the phase separation process.[42,47,66] Thus, diffusion kinetics play a role in the determination of membrane morphology as important as that of equilibrium thermodynamics.[60]

The mass transfer processes occurring throughout membrane formation take place during four major time frames:

1. During evaporation of solvent from the casting solution prior to its contact with the coagulation bath;

2. After immersion in the coagulation bath, but prior to any demixing processes;

3. During solid-liquid and/or liquid-liquid demixing, but prior to gelation of the polymer;

4. After gelation of the polymer.

The evaporation step was long thought critical to the formation of the surface skin characteristic of asymmetric membranes.[50,74,75] However, several workers have demonstrated that the nature of the membrane surface can be entirely controlled in the complete absence of solvent evaporation.[43,49,76] Thus, the evaporation step will not be considered in this thesis.

Mass Transfer Processes Near the Nascent Membrane Surface. This thesis is concerned with the modification of the membrane surface composition during the coagulation step. Thus, mass transfer processes occurring in the nascent surface layer will be a central consideration. A mechanistic framework which will be particularly useful was proposed by Strathman, *et al.*[47,48] to explain several features of the observed

membrane morphologies, most notably the occurrence of the dense surface skin in the absence of an evaporation step. The model is based on the evolution of precipitant concentration gradients in the cast film at various times after its immersion in the coagulation bath.

Figure 2.8 schematically illustrates precipitant concentration profiles near the interface between the cast film and the precipitant bath at four different times during membrane coagulation. The significant feature of Figure 2.8 is the steep precipitant concentration gradients in the near-surface region of the cast film at early times during membrane formation. The function of the precipitant is to raise the chemical potential of the polymer in solution such that it ultimately precipitates. Thus, the local gradient in the chemical potential of the polymer scales approximately with the local concentration gradient of water,

$$\nabla \mu_3 \sim \nabla c_2 \qquad (2.1)$$

This gradient in the polymer chemical potential, in turn, results in a macroscopic flux of polymer directed into the casting solution. The local magnitude of this flux scales with the magnitude of the local gradient in chemical potential,

$$\vec{J}_3 \sim -\nabla \mu_3 \qquad (2.2)$$

according to the diffusion equation.

Figure 2.9 illustrates the variation of polymer chemical potential with position in the cast film at an early time, when the precipitant exhibits a steep concentration gradient near the interface. The arrows represent the drift velocities experienced by polymer molecules at various depths in the cast film as a result of the chemical potential gradient.

42
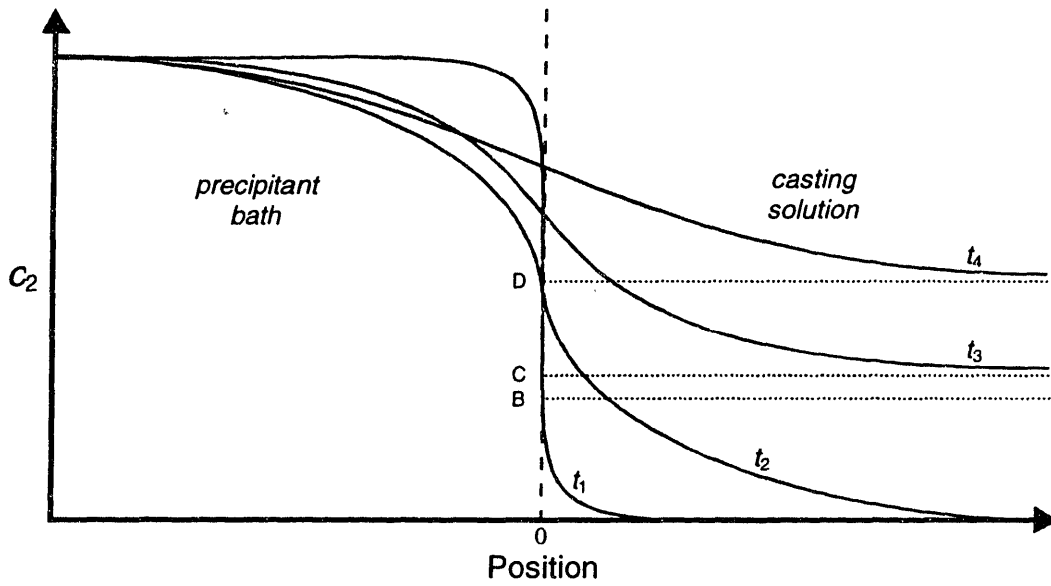
Figure 2.8 Precipitant concentration as a function of position and time in cast film

Solid-liquid demixing, liquid-liquid demixing, and gelation begin at precipitant concentrations B, C, and D, respectively. At time t_1, compositional changes have taken place, but no demixing has occurred. At time t_2, demixing has occurred in a portion of the film near the interface, but gelation has not occurred. At time t_3, demixing has occurred throughout the film, and a portion of the membrane structure has been fixed by gelation. At time t_4, the gross structure of the membrane has been fixed, although solvent-precipitant exchange will continue.
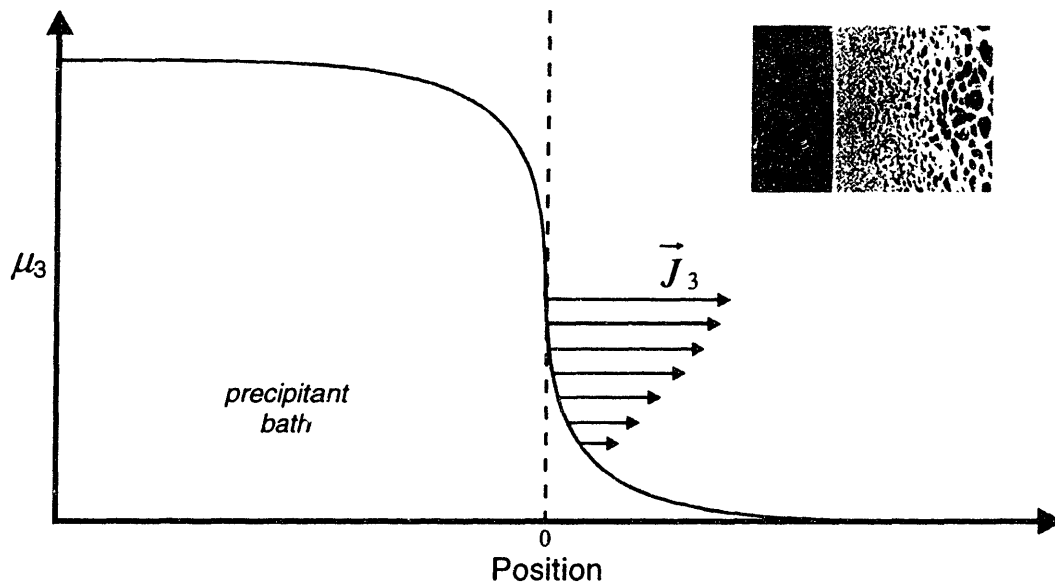
Figure 2.9 Polymer chemical potential vs. position in cast film at early time

The arrows represent the magnitudes of the drift velocities experienced by polymer molecules at various depths as a result of the chemical potential gradient. Steep chemical potential gradients lead to densification of the polymer in the near-surface region of the film, resulting in an asymmetric membrane structure (inset).

43

The polymer flux profile illustrated in Figure 2.9 results in an increase in polymer concentration in the near-surface region of the cast film prior to gelation of the polymer. According to Strathmann, *et al.*, this mechanism is responsible for the formation of the dense surface skin on asymmetric membranes. Arguments based on the evolution of precipitant concentration gradients in the cast film have also been used to explain qualitatively the conditions under which symmetric membranes (Fig. 2.2d) are formed, as well as the conditions resulting in gradient-pore (Fig. 2.2b) and uniform-pore (Fig. 2.2a) substructures.[47]

More recently, several workers[43,49,60-66] have demonstrated the utility of mathematical models combining modified Flory-Huggins polymer solution theory and ternary diffusion theory, which are remarkably effective in predicting the effects of various processing conditions on the resulting membrane morphologies. These models verify the existence at early times of a boundary layer at the interface between the cast film and precipitant bath in which exists a steep gradient in water concentration, as proposed by Strathmann, *et al.*[49,65] However, they also indicate that kinetic processes other than polymer diffusion contribute to the formation of the dense surface layer. All of the present computational models are predicated on the assumption that macroscopic polymer diffusion is negligible compared to the much faster diffusion of the solvent and nonsolvent components.[43] Nevertheless, they correctly predict the formation of a dense surface layer under the appropriate processing conditions. According to these models, a dense surface skin may be formed when, at early times, the flux of solvent out of the cast film exceeds the flux of precipitant into it.[43,64] Regardless of the role of polymer diffusion

in the determination of membrane morphologies, we will find in Chapter 4 that significant polymer diffusion *does* occur during membrane coagulation. Indeed, for a *quaternary* system containing two polymer components, it will be shown that differences in the diffusion kinetics of the two polymers can result in *surface segregation* of one of them.

Macrovoid Formation. "Finger" type and "sponge" type membranes are differentiated from one another by the presence in finger type membranes of large macrovoids near the separation surface, which sometimes extend through nearly the entire membrane cross-section (Fig. 2.2c). These macrovoids provide for high fluxes and are therefore desirable for many moderate-pressure UF applications, but they result in mechanical properties unsuitable for high-pressure RO operations.[48,52,55,68] Over the years, macrovoid formation has been attributed to a number of mechanisms, and these have been reviewed by Smolders, *et al.*[52] and by Lin, *et al.*[55]

Light transmission experiments have related macrovoid formation to *instantaneous demixing.*[48,52,55] In these experiments, the onset of demixing in the casting solution is monitored as a change in turbidity after its immersion in the coagulation bath. Instantaneous demixing occurs when the composition of the cast film near the interface enters the miscibility gap immeasurably quickly upon contact with the precipitant, resulting in formation of the polymer-poor phase. By contrast, membranes exhibiting *delayed demixing* after immersion in the coagulation bath are typically free of macrovoids. During the period prior to liquid-liquid demixing in such membranes, the near-surface membrane composition is in a stable region of the phase diagram and

diffusion processes occur without disruption by spinodal decomposition or nucleation and

growth processes. Monte Carlo simulations of polymer coagulation have similarly

revealed a dramatic decrease in the velocity of the liquid-liquid demixing front upon

transition from "finger" to "sponge" morphologies.[67,68,77] Conditions which tend to

suppress instantaneous demixing and macrovoid formation include choice of a solvent-

nonsolvent pair with a low free energy of mixing,[47,78,79] high polymer concentrations in the

casting solution, concentration of the near-surface region of the cast film by

evaporation,[48,79] and addition of solvent to the coagulation bath.[48]

Recent ternary diffusion models[49,52,65] shed some light on the experimentally

observed link between instantaneous demixing and macrovoid formation. These models

suggest that a casting solution exhibiting instantaneous demixing near the interface may

undergo a transition to delayed demixing, illustrated in Figure 2.10. In (a), the precipitant

enters the cast film and the casting solution in the region of the interface undergoes

instantaneous demixing, resulting in the formation of nuclei of a polymer-poor phase. In

(b), polymer gels at the casting solution interface (behind the advancing precipitant

diffusion front). This results in a higher resistance to precipitant diffusion from the
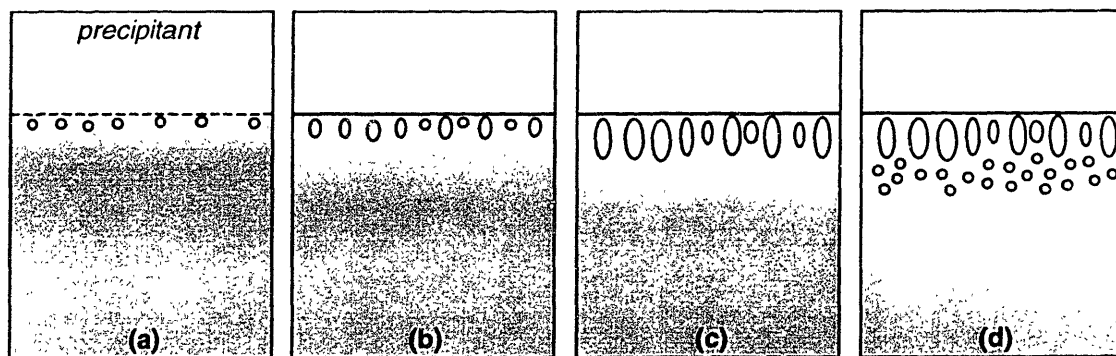
Figure 2.10 Illustration of transition from instantaneous to delayed demixing

coagulation bath and a consequent transition to delayed demixing at the diffusion front. In (c), stable compositions exist for some delay time in front of the previously nucleated droplets of the polymer-poor phase. During this time, those droplets coarsen, becoming macrovoids. Coarsening of the incipient macrovoids is arrested when, after the delay, new nuclei begin to form in front of them (d). This diffusional model appears to be the only current model for macrovoid formation capable of explaining all of the available empirical data.[52]

Crystallization. As alluded to above in the discussion of thermodynamics, the structures of membranes prepared from crystallizable polymers are commonly controlled completely by the liquid-liquid demixing process, even when solid-liquid demixing is thermodynamically favored and the composition path enters the solid-liquid two-phase region at an earlier time, as in Figure 2.7. The reason for this is the slow nucleation and growth of solid polymer crystallites compared with the equivalent processes for liquid-liquid demixing.[56,69,73,80-82] Thus, in most cases, crystallization takes place in the polymer-rich phase after the gross membrane morphology has been determined, resulting in fibrillar structures in the polymer-rich phase and no evidence of spherulites.[52] Membranes having porous spherulitic structures have been obtained from semicrystalline polymers such as PVDF.[69,83] Processing conditions that favor solid-liquid demixing are those that shift the liquid-liquid binodal toward the polymer-precipitant axis of the ternary phase diagram, such as use of a relatively poor precipitant,[69] and those that allow slow exchange of the solvent and precipitant, such as introduction of the precipitant from the vapor phase.[83]

47

2.4 Current Methods for Membrane Surface Modification

Numerous strategies for the surface modification of polymer membranes have been investigated. These modifications have been performed to improve the two "problem" attributes of polymer membranes outlined in Chapter 1 and discussed in Chapter 2: fouling susceptibility and low selectivity. Most methods have focused on the coating or grafting of species onto the surfaces of membranes following their preparation by immersion precipitation (Figure 1.1). As discussed in more detail below, all coating and grafting techniques suffer from one or more of the following disadvantages:

1. Surface modifying agents are subject to removal by long-term exposure to aggressive species in the feed solution or during aggressive chemical cleaning procedures.

2. Grafting and coating typically result in changes in the membrane pore size distribution, often reducing permeability.

3. Hydrophilicity is typically imparted to the membrane separation surface only,[31,45,84-89] while foulant accumulation can occur both at the separation surface and within the internal pore channels.[90-92]

4. These methods require post-coagulation processing steps, increasing membrane fabrication costs.

This section provides a brief review of the relevant literature related to surface modification techniques.

2.4.1 Surface Modification for Fouling Resistance

Introduction

Several strategies to impart surface hydrophilicity to conventional hydrophobic membrane materials have been investigated. In many cases, researchers have conducted filtration tests to determine the benefits of the modification methods used in terms of fouling resistance. Such tests typically involve measurement of the trans-membrane flux of pure water (J_o), followed by measurement of the trans-membrane flux of a foulant solution after a fixed period of foulant solution filtration (J_f). A quantitative review of such studies available in the literature is presented in Appendix A.

The success of a given surface modification method can be characterized by four key performance metrics. The ratio J_f/J_o is a measure of the inherent fouling resistance of a membrane. In Appendix A, this ratio is reported for both modified membranes (J_f^M/J_o^M) and the corresponding unmodified controls (J_f^C/J_o^C). The effect of surface modification on the initial pure water flux, characterized by the ratio J_o^M/J_o^C, must also be considered when assessing the benefit of a particular method. From a practical point of view, perhaps the most important measure of success is the ratio of the absolute trans-membrane fluxes of the modified and unmodified membranes after foulant filtration (J_f^M/J_f^C). Following are brief discussions of coating, grafting, and other methods presently used for membrane surface modification.

49

Coating Methods

Coating is often accomplished by the adsorption of water-soluble polymers[91,93] or surfactants[93-95] onto membranes in aqueous solution. One might envision the routine performance of such pretreatments during a filtration operation, simply by addition of polymer or surfactant to the feed stream. This approach is economical, and has been marginally successful in increasing the fouling resistance of polysulfone (PSf), polyamide, and polyacrylonitrile (PAN) based membranes relative to untreated membranes (Appendix A).

This strategy has two significant shortcomings. First, the polymers and surfactants that comprise the coating occlude the membrane pores substantially, such that the initial pure water flux for a treated membrane might be as little as 10% of that for an untreated membrane.[93] Thus, even when significant resistance to foulant adsorption has been achieved, the absolute throughput of foulant solution after several hours has been at most 40% better than that for the corresponding untreated membrane. The second shortcoming of this approach is the fragile nature of the surfaces produced. Surfactants and polymers used for membrane pretreatment desorb from membrane surfaces, both during exposure to water and during chemical cleanings.[93] The use of this strategy thus precludes any fine control over membrane selectivity, since adsorption and subsequent desorption of the modifying species result in unpredictable changes in the membrane pore size distribution over time.

Coating has also been accomplished by dipping or spraying steps immediately following membrane fabrication.[45,88,89] These coating methods have an effect on the initial pure water flux similar to that of adsorption pretreatment. However, substantially better

50

fouling resistance has been achieved. In fact, the coating of PVDF membranes with a poly(ethylene oxide)-*b*-polyamide copolymer provided an absolute flux improvement of greater than 7 times compared to untreated membranes at the end of an 8-h filtration of an oil-water emulsion, despite the fact that the coating process resulted in an initial pure water flux reduction of 89%.[45] The effect of the coated layers on membrane selectivity is significant, however, and surface stability remains an issue, especially at extreme pH's.[45]

Under the appropriate conditions, aqueous adsorption of polymers and surfactants can modify pore channels throughout the membrane cross-section, as well as the separation surface. Through-pore modification requires the use of a macromolecule or surfactant having a dimension in solution sufficiently small compared to the separation surface pore size.[91,93,95] Kinetic studies[95] of the adsorption of various macromolecules and surfactants onto commercial UF membranes show that complete coverage of the internal pore channels requires diffusion times on the order of 12 h, however. Coatings applied by dipping and spraying steps affect the properties of the separation surface only.[45,88,89]

Grafting Methods

More robust surface layers have been prepared by the surface graft polymerization of vinyl monomers or macromonomers onto membranes from solution. For this purpose, free radicals may be produced on membrane surfaces by exposure to redox initiators,[96,97] low-temperature plasmas,[84,86,98-102] or ultraviolet,[31,87,103-105] γ-ray,[106] or electron beam[107,108] radiation. Like coating, grafting occludes the surface pores, often resulting in reduced permeability (see Ref. 104, Appendix A). However, reductions in the initial pure water flux due to grafting are usually far less severe than those from

coating processes. In fact, the pure water fluxes for grafted membranes are frequently better than those for the corresponding unmodified membranes due to the hydrophilicity of the surface layers produced.[86,87,100,105] Graft-modified PSf and poly(ethersulfone) (PES) membranes have been prepared which exhibit fluxes after several hours of protein solution filtration over 2 times those of unmodified membranes.[86,100]

Grafting methods, which result in covalent bonding of the modifying species to the membrane, are expected to create surfaces with much greater long-term stability than coated surfaces. However, the grafted surface layers are subject to chemical degradation, especially during aggressive chemical cleaning procedures. The long-term stability of grafted layers exposed to aggressive environments has not been well studied.[105] In addition, the grafting density and grafted chain length are kinetically limited and difficult to control. Much trial and error is involved in the optimization of each combination of membrane and graft polymerized monomer. Often, the achievable degree of surface coverage is limited by the occurrence of unacceptable pore blockage at high grafting densities.[87]

Only a few researchers have directly assessed the depth of modification achieved by grafting methods. Yamagishi, et al.[31] surface graft polymerized methacrylic acid (MAA) onto PES membranes by UV irradiation, incubated the membranes in cupric sulfate solution, and used x-ray photoelectron spectroscopy (XPS) to determine the concentration of copper ions bound to the anionic MAA as a function of depth. They found that the depth of modification increased roughly linearly with irradiation time, reaching a depth of 15 μm (20% of the membrane thickness) at a long irradiation time of

10 min. Chain degradation can be a problem at such long irradiation times, however. UV irradiation of a PES/chloroform solution for 10 min under identical conditions resulted in a reduction of the PES molecular weight to 33% of its original value due to primary bond cleavage. Grafting of PES membranes using UV irradiation times longer than 10 min resulted in significantly changed separation characteristics due to pore enlargement as a result of PES degradation. Thus, in this study, there appeared to be a limit to the depth of modification achievable. Iwata and Matsuda[84] surface graft polymerized acrylic acid (AA) onto plasma-treated PVDF membranes and stained the anionic AA with a cationic fluorescent dye. Fluorescence microscopy of sections of the stained membranes clearly indicated the presence of AA in a sharply-defined region limited to the top 12 μm (~10% of the membrane thickness). Chen and Belfort[86] surface graft polymerized N-vinyl-pyrrolidone (NVP) onto plasma-treated PES membranes. Comparison of the XPS spectra for the two external surfaces of the grafted membranes showed no NVP on the side opposite the plasma-exposed separation surface. Kanamori, et al.[85] grafted poly(ethylene glycol) (PEG) to cellulosic membranes. The results of water swelling experiments performed on these membranes were consistent with modification of the external surfaces only.

A few workers using grafting techniques have reported some evidence of pore channel modification at depths >15 μm. Peng and Cheng[109] studied polyethylene membranes grafted with MAA from water/methanol mixtures by UV irradiation. While grafting appeared to take place predominantly on the exposed surface, SEM and water swelling studies indicated that a high proportion of methanol in the reaction mixture

promoted significant grafting within the membrane substructure. The amount and distribution of material within the substructure was not clear. Using SEM, Ulbricht and Belfort[100] observed "agglomerates" of grafted material on the internal pore channel surfaces of plasma-treated PAN membranes grafted with AA. The authors did not provide micrographs, however, and the distribution of AA within the membrane substructure was again unclear. In addition, XPS of the external membrane surface opposite the plasma-treated separation surface showed no AA. Based on the available data, it appears that, though grafting techniques have occasionally achieved some level of modification of internal pore channels, they have not been shown to be reliable for this purpose.

Other Methods

Other strategies have been used to hydrophilize membranes. Perhaps the most straightforward approach is the chemical modification of the bulk membrane material. For example, membranes cast from sulfonated PVDF exhibit better fouling resistance than PVDF membranes.[110] Membranes cast from chemically modified "hydrophilic polysulfones" exhibit similar advantages over PSf membranes.[111] These approaches are not really "surface modification" approaches, however, since they may be expected to significantly impact the bulk properties of the membrane as well.[4] Thus, the ultimate properties of the membrane will reflect some compromise between desirable bulk and surface characteristics.

Exposure of PSf, PAN, and PES membranes to low-temperature plasma has been used to generate peroxide groups on the surface, which result in increased hydrophilicity

and fouling resistance.[86,100,112] This strategy still involves post-coagulation processing, albeit less complex processing than grafting methods. In addition, plasma exposure is known to ablate material from the membrane surface, frequently resulting in increases in pore size and consequent changes in selectivity.[86,100] Perhaps most importantly from a fundamental design point of view, both bulk chemical modification methods and surface plasma treatment methods offer extremely limited flexibility in the choice of membrane surface chemistry. When considering the surface modification of membranes for *selectivity*, it will be desirable to have a large "toolbox" of chemical groups from which to choose.

2.4.2 Surface Modification for Selectivity

Control over pore sizes at the level of Ångstroms is difficult during membrane fabrication by immersion precipitation. Even worse, the separation characteristics of membranes always change with time during operation due to fouling and pore compaction. Thus, polymer membranes are currently not very effective in applications such as the fractionation of macromolecules (*e.g.*, proteins). To address this issue, recent work has opened an intriguing new avenue of research directed toward the development of *environmentally responsive* (ER) membranes. These so-called "intelligent" membranes can adjust their own pore sizes in response to environmental stimuli. Thus, for protein separation, one might envision the employment of an ER membrane in concert with a feedback loop capable of continuously measuring the size of the permeating solute and adjusting some feed solution attribute to maintain the desired separation characteristics (Figure 2.11).
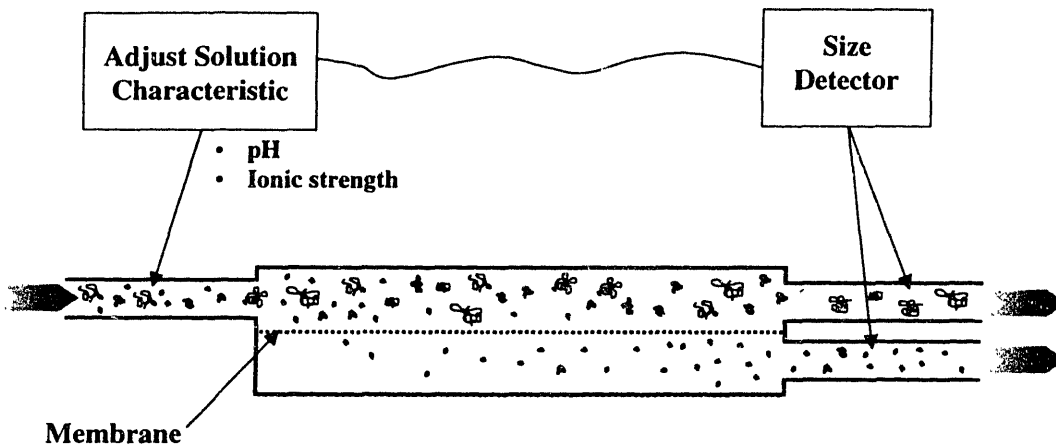
Figure 2.11 High-speed protein separation using an "intelligent" membrane
The membrane is capable of changing its pore size in response to a characteristic of the feed solution, enabling *in situ* size selection of the permeating species.
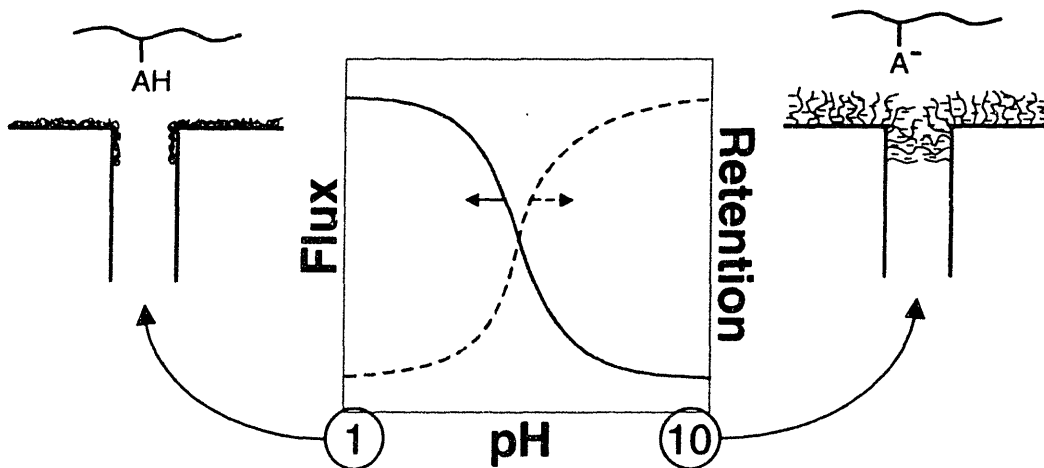
Figure 2.12 Grafted weak polyacid environmentally responsive membrane

The most widely studied ER membranes are prepared by the surface graft polymerization of weak polyacid chains onto a support membrane.[84,99,107,113-117] Monomers commonly used in this approach include acrylic acid and methacrylic acid. The weak acid groups on the grafted chains become negatively charged through the dissociation of a proton (Figure 2.12),

$$HA \rightleftharpoons A^- + H^+ \qquad (2.3)$$

and the degree of dissociation depends sensitively on the local pH and ionic strength.[118] At high pH, the degree of dissociation is high, and mutual repulsion between neighboring like charges causes the chains to assume an extended conformation, closing the membrane pores. At low pH, the chains become essentially neutral and assume a relatively more collapsed configuration, opening the pores. Thus, the chains provide a mechanochemical "pore valve" by which separation characteristics and trans-membrane flux can be controlled simply through adjustment of the feed solution pH or ionic strength. This effect is completely reversible and quite dramatic – the difference in trans-membrane flux between the "open" and "closed" pore conditions can be greater than an order of magnitude.[84,114] ER membranes sensitive to pH[115,117] and to glucose concentration[119] have been evaluated for use as drug delivery capsules, which would release a drug at appropriate times in response to an environmental stimulus (Figure 2.13). Membranes having grafted chains capable of photonically[120] and thermally[121] induced conformational changes have also been fabricated.
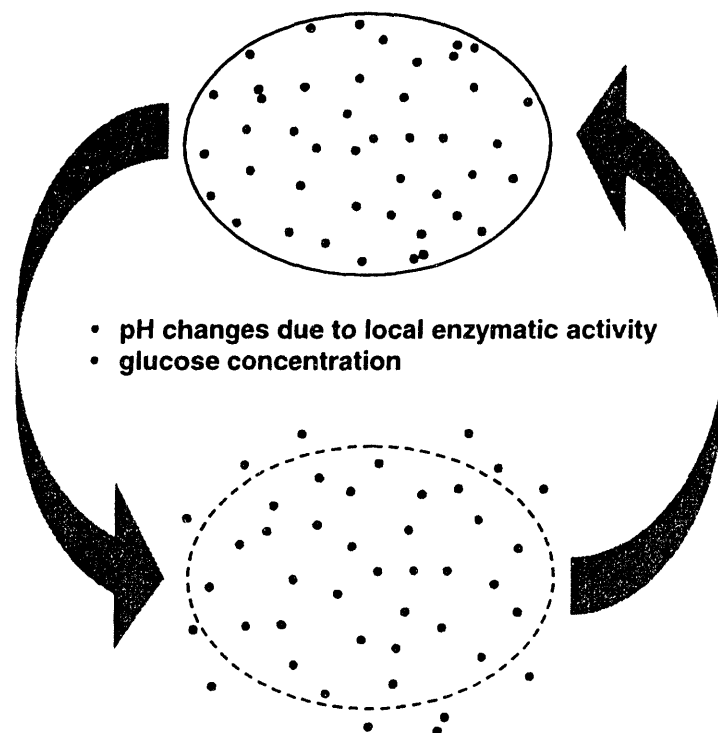
Figure 2.13 Schematic of an environmentally responsive drug delivery capsule

2.5 Membranes from Polymer Blends

Past work on membranes cast from polymer blends has generally been for the purpose of modifying the membrane morphology. For example, Uragami, *et al.*[122] cast membranes from blends of PVDF and *water soluble* poly(ethylene oxide) (PEO). The PEO was then extracted by a heat treatment in water, resulting in membranes with higher porosities than those cast from PVDF alone.

Extensive work has been conducted on blends of PSf, PES, and poly(ether imide) (PEI) with a water soluble additive polymer, poly(vinyl pyrrolidone) (PVP).[5,51,53,80,123-130] Compared to membranes prepared without the addition of PVP, membranes prepared from these blends often exhibit higher porosities, higher pore connectivities, and

suppression of macrovoid formation. To explain these observations, Boom et al.[51,53,127-129] defined two diffusional time scales during membrane coagulation. On the short time scale, solvent and water can interchange, but the two polymers do not diffuse relative to one another. The system is quasi-ternary and, owing to the favorable interactions between the two polymers and the water-solubility of PVP, the system exhibits an "effective" binodal situated near the polymer-precipitant axis. Diffusion models show that, on the short time scale, the composition path may nearly reach this virtual binodal. On the long time scale, the polymers diffuse relative to one another. PVP remains soluble and is extracted from the casting solution, resulting in a rapid shift of the effective binodal toward the polymer-solvent axis. The previously stable composition thus becomes rapidly unstable with respect to phase separation, creating the conditions for instantaneous demixing (see Section 2.3.2). Thus, instantaneous demixing (and an associated high porosity) is achieved throughout the casting solution, without the transition to delayed demixing commonly responsible for macrovoid formation.

Nunes, et al.[131] prepared membranes from compatible blends of PVDF with 5-34% poly(methyl methacrylate) (PMMA) in N,N-dimethylacetamide (DMAc) solution. UF experiments with pure water and with aqueous solutions of PEG showed significant increases in permeability with increasing PMMA content, without loss of retention of PEG in many cases. The authors concluded that the increased permeabilities were a result partially of increased membrane hydrophilicity and partially of morphology changes brought about by addition of PMMA. Overall porosity and macrovoid size were observed to increase with increasing PMMA content.

Nunes, *et al.* hypothesized that these morphological changes resulted from a change in the balance of the water and solvent transport rates at the interface between the cast film and the water bath. That is, the presence of the relatively hydrophilic PMMA in the casting solution increased the rate of water transport into the cast film relative to the rate of solvent transport out of it. This would cause liquid-liquid phase separation and subsequent polymer gelation to occur at a lower overall polymer concentration (see Figure 2.14), resulting in increased porosity. We might also hypothesize that PMMA, a relatively amphiphilic polymer with respect to water and DMAc, increased the affinity of water and solvent, enhancing the conditions for instantaneous demixing and a corresponding tendency toward macrovoid formation and increased porosity. Support for
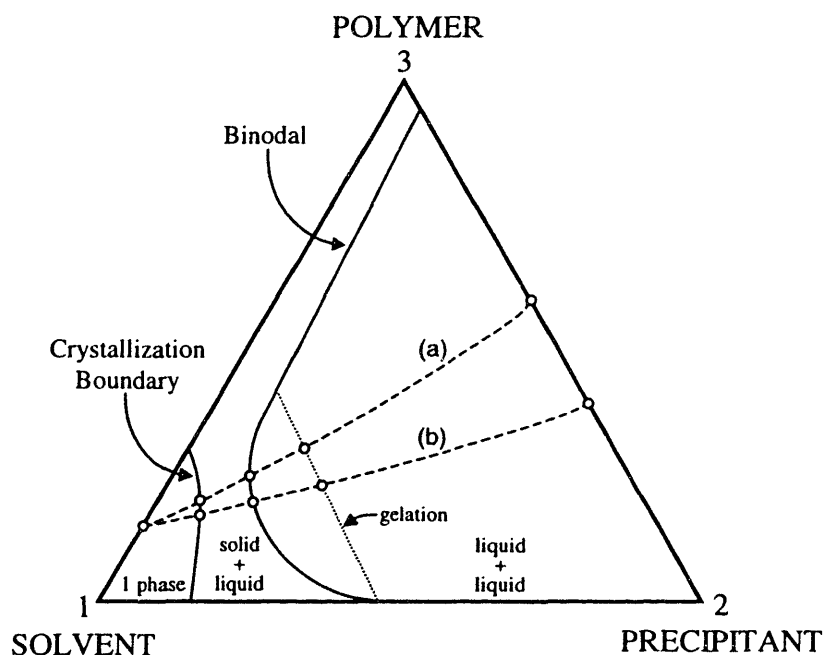
Figure 2.14 Effect of a relatively hydrophilic second polymer on composition path
(a) Schematic composition path for a casting solution containing a single, hydrophobic polymer, and (b) composition path for a casting containing a second, relatively hydrophilic polymer. For the blend, liquid-liquid phase separation and polymer gelation occur at lower overall polymer concentrations, resulting in increased porosity.

this second hypothesis comes from the work of Lin, *et al.*,[55] who observed a shift to instantaneous demixing and a corresponding tendency toward macrovoid formation and increased separation surface porosity with increasing concentration of a variety of small-molecule surfactants in PMMA membrane casting solutions.

From their work on membranes prepared from PVDF/PMMA blends, Nunes, *et al.* concluded an increase in membrane hydrophilicity with the addition of PMMA based on water contact angle measurements performed on the surfaces of dried membranes. While it is likely that increased hydrophilicity was achieved, these measurements are an unreliable evaluation of membrane surface chemistry, since surface roughness can easily control the sessile drop contact angle to an extent equal to or exceeding surface chemistry,[132] and SEM studies conducted by the authors indicated significant changes in surface morphology with PMMA content. Specifically, an increase in surface roughness with increasing PMMA content (which might be expected[55]) would have the same effect on the contact angle as an increase in hydrophilicity. While it is possible that some surface segregation of PMMA occurred in these blends during membrane fabrication, the authors did not directly assess the surface chemistry.

2.6 Surface Modification by Self-Organization

2.6.1 Objectives

An ideal strategy for modifying the surfaces of polymer membranes would have the following attributes (refer to Table 1.1):

1. It would provide a high degree of surface coverage and result in surfaces with good long-term stability.

2. It would provide surface coverage of the internal pore channels of the membrane, as well as the separation surface.

3. It would require inexpensive materials and minimal post-coagulation processing.

4. It would have a minimal impact on the bulk membrane properties (mechanical and thermal stability, chemical resistance).

5. It would not decrease membrane permeability due to pore size modification, and ideally would enhance it.

6. It would offer a high degree of flexibility in the selection of surface chemistry.

This thesis will show that these criteria can be simultaneously met by casting membranes from polymer blends composed of a conventional hydrophobic membrane-forming polymer and a small proportion of an inexpensive, highly branched, amphiphilic additive polymer.* PVDF, one of the most important commercial membrane materials (see Section 2.2.2), is used as the matrix polymer in all of the work presented in this thesis.

The work in this thesis differs from all published work related to membranes prepared from polymer blends in the following ways:

1. The additive polymer will be specifically engineered to *surface segregate* during the standard phase inversion process (Fig. 1.2), and at the same time express a surface chemistry optimized for a property of interest (*e.g.*, fouling resistance, wettability, pH-responsiveness).

2. Processing conditions will be optimized to take full advantage of surface segregation, such that a minimal proportion of the additive polymer can be used to achieve maximal delivery of the desired surface chemistry.

---

* A patent on this approach to membrane surface modification is pending.[133]

3. A number of experimental techniques, including x-ray photoelectron spectroscopy (XPS), atomic force microscopy (AFM), protein adsorption experiments, and UF experiments, will be used to determine, at the molecular level, the surface chemistries achieved and their relation to the properties of interest.

The intelligent selection of additive polymers with optimized properties for surface segregation and delivery of desirable surface chemistries is the subject of the next two sections.

2.6.2 Surface Segregation in Polymer Blends: Available Driving Forces

Thermodynamic Driving Forces

The migration of a surface-active additive from a polymer melt during processing is commonly used commercially for the chemical modification of polymer surfaces. However, this strategy has generally been limited to highly mobile, small-molecule additives.[134] These additives are easily removed from the surface over time, and their presence typically degrades the bulk mechanical properties of the matrix polymer. Over the past ten years, a large body of research has been directed toward the development of methods to modify the surfaces of polymeric articles through surface segregation of *macromolecular* additives, which have the potential to provide more robust surfaces with less impact on bulk mechanical properties.[134] Reviews of much of this work have been provided by Garbassi, *et al.*[135] and by Mayes and Kumar.[134]

We might expect that the interface between a polymer blend and its surroundings will be enriched in the component with the lower interfacial free energy. However, surface enrichment requires some degree of demixing of the components in the bulk.

That is, surface segregation of one component will occur only if the associated reduction of the interfacial free energy more than compensates for the loss of combinatorial entropy upon demixing and, in the case of exothermic mixing, the loss of mixing enthalpy. The balance between the driving forces favoring surface segregation and those favoring mixing determines both the amplitude and scale of any near-surface deviation from the bulk composition.[136] Recent research has identified a number of driving forces capable of producing substantial surface segregation in polymer blends. The intelligent design of a polymer additive for the surface modification of polymer membranes should begin with an accounting of these available driving forces. They are reviewed here in the context of our system of interest, a blend of PVDF and a relatively hydrophilic additive polymer, which forms an interface with an aqueous environment.

Interfacial Energy. Surface segregation of one component in a polymer blend is most commonly due to its lower interfacial energy,[136] which can result from favorable enthalpic interactions between the surface-active component and the surrounding medium, or from a lower cohesive energy density.[137] Blends of polystyrene (PS) with deuterated polystyrene (d-PS) have received much attention.[138-144] PS and d-PS are miscible, and d-PS has a surface tension ~0.1 dyne/cm lower than that of PS.[138] In blends of high molecular weight PS and d-PS, the lower-energy d-PS is preferentially localized at the air surface. Similar results have been found, for example, in compatible blends of hydrogenated and deuterated poly(ethylene propylene)[145,146] and in PS/poly(vinylmethylether),[147,148] where the surface is enriched in the lower surface energy component in both cases. Polar dipole-dipole interactions and hydrogen bonding are

examples of enthalpic interactions which commonly exist between hydrophilic polymers and water,[149] and which might be used to drive the segregation of such a polymer to a polymer/water interface.

Configurational Entropy. Though enthalpic driving forces dominate most observed surface segregation phenomena in polymer blends, entropic driving forces can be important as well. In bulk polymer melts, the spatial conformation of a polymer chain is typically well-represented by Gaussian statistics, with each polymer segment being approximately equivalent to a step in a three-dimensional random walk. A polymer chain near a surface experiences a reflecting boundary condition which reduces the total number of configurations available to the chain, and thus the total system entropy. To reduce the frequency of chain reflections at the material boundary, chain ends preferentially segregate to the surface of a monodisperse polymer melt, in the absence of strong enthalpic interactions.[150-153] Similarly, in a polymer blend, the component having the higher pure-component chain end density is preferred at the surface based on configurational entropy, since this increases the concentration of chain ends at the surface.[136] Thus, in bimodal polymer blends of structurally identical components, small surface excesses of the lower molecular weight component (typically a few percent greater than the bulk concentration) are predicted by simulation[154] and observed.[144,155,156] In fact, in bimodal PS/d-PS blends, surfaces slightly enriched in the *higher-energy* PS are produced if the PS is of sufficiently low molecular weight relative to the d-PS.[142-144]

Besides molecular weight, chain branching can be used to increase the chain end density of one polymer component relative to another, resulting in surface segregation of

the more highly-branched component.[136,157-159] Recent work on blends of branched and linear polymers has made the entropic driving force for surface segregation available as a bona fide engineering surface modification technique. Walton, et al.[159] studied blends of PMMA with a comb-shaped polymer, P(MMA-r-POEM), comprising a methyl methacrylate backbone with pendant PEO side chains approximately 9 EO units long. In vacuum-annealed blends containing only 2% P(MMA-r-POEM), complete surface coverage of the comb component was observed by neutron reflectivity, despite the fact that its surface tension exceeded that of the PMMA matrix by 2.4 dyne/cm. Thus, polymer architecture can be an important consideration in the design of additive polymers for surface segregation.

The Hydrophobic Effect. Water molecules near a surface incapable of hydrogen bond formation (*e.g.*, alkanes, hydrocarbons, fluorocarbons) assume a highly ordered arrangement which enables them to minimize the surface-induced loss of energetically favorable hydrogen bonds. This ordered restructuring of water molecules is entropically unfavorable, however. The consequent immiscibility of inert substances with water has been termed the *hydrophobic effect* and such substances are commonly referred to as *hydrophobic.*[149,160-162] Liberation of water layers from the constraint of existing adjacent to a hydrophobic surface provides an entropic driving force which might contribute to surface segregation of a polymer additive capable of hydrogen bond formation.

Incompatibility. Thermodynamic incompatibility between the components of a polymer blend has been shown to enhance enthalpically-driven surface segregation.[163] Self-consistent mean-field (SCF) calculations of surface segregation in miscible polymer

blends as a function of the surface energy difference and interaction parameter χ show that, while the surface energy difference determines which component will surface segregate, the degree of surface segregation increases significantly with increasing χ.[164] This result is expected, since an increased χ implies a less favorable free energy of mixing. In thermodynamically immiscible blends, where the driving forces for surface segregation add to a *positive* free energy of mixing, the more surface active component often completely dominates the surface composition. For example, marginally miscible blends containing low surface energy poly(dimethylsiloxane) (PDMS) typically display nearly 100% PDMS at their surfaces.[165,166]

In general, however, incompatibility is not a useful tool for engineering surface composition. As the incompatibility of a blend increases, so does its potential for macroscopic phase separation, which might result in degradation of bulk mechanical properties and exudation of the surface-active additive over time. In polymer membranes, phase separation might also result in unacceptable changes in pore morphology. Imparting a desired chemical functionality through the blending of an additive polymer with a matrix polymer usually requires the synthesis of a copolymer coupling the desired functionality with a block or graft segment which provides compatibility, or, at least, some favorable energetic interaction, with the matrix polymer.[135,167] Such a copolymerization strategy will be used in this thesis to combine desired surface chemistries with PVDF compatibility.

Crystallinity. A thermodynamically compatible blend composed of a crystallizing polymer A and a non-crystallizing polymer B can be represented as a two-phase system,

consisting of a crystalline phase and an amorphous, compatible A/B blend, as long as the concentration of B is not sufficient to suppress crystallization of A.[135,168] Thus, for example, in blends of poly(vinyl chloride) (PVC) with crystalline poly(ε-caprolactone) (PCL), crystallization enhances the surface segregation of PCL by causing rejection of PVC from the lower surface energy PCL crystals.[169] PVDF is highly crystalline, and we might expect that its crystallization would contribute to the surface segregation of an amorphous additive polymer having a lower interfacial energy with water.

A Kinetic Mechanism for Surface Segregation During Membrane Coagulation

In Section 2.3.2, a kinetic mechanism proposed by Strathman, *et al.*[47,48] to explain the asymmetric structure typical of polymer membranes prepared by immersion precipitation was presented. According to this mechanism, steep water concentration gradients are created at the interface between the casting solution and the aqueous precipitation bath at early times during membrane coagulation (Fig. 2.8), which in turn result in steep gradients in the chemical potential of the water-insoluble polymer (Eqn. 2.1). The polymer diffuses "down" this chemical potential gradient into the casting solution (Fig. 2.9, Eqn. 2.2), resulting in densification of the polymer at the interface prior to its gelation. The presence of such concentration gradients has been verified by more recent theoretical models.[49,65]

We now consider this kinetic framework in the context of a *quaternary* system containing two polymer components, a hydrophobic matrix polymer (component 3) and a relatively hydrophilic additive polymer (component 4). That is, polymer component 4, though water-insoluble, has some favorable interaction with water, through hydrogen
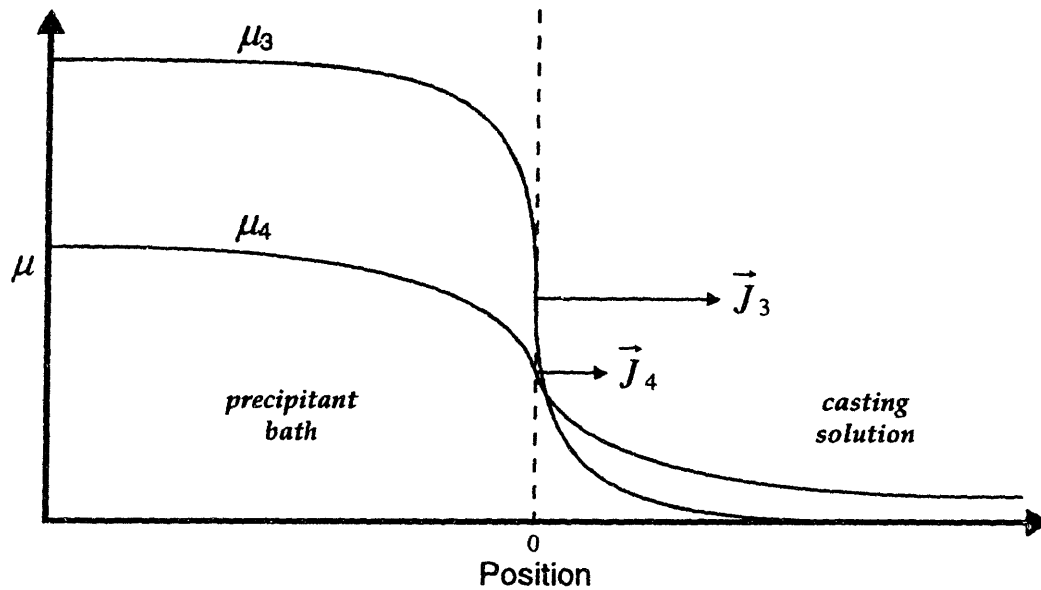
Figure 2.15 Schematic describing a kinetic mechanism for surface segregation
Schematic chemical potentials of hydrophobic polymer component 3 and relatively hydrophilic polymer component 4 as a function of position near the interface between the cast film and water bath at early times during coagulation. The hydrophilic polymer has a lower chemical potential in pure water, and consequently a smaller chemical potential gradient near the interface, resulting in slower transport into the casting solution. The hydrophilic polymer is effectively "left behind" at the interface.

bond formation or a polar dipole-dipole interaction. We expect the chemical potential of the hydrophilic component in pure water to be substantially less than that of the hydrophobic component (see Figure 2.15). Thus, we expect that, near the interface between the casting solution and the water bath,

$$|\nabla \mu_4| < |\nabla \mu_3| \tag{2.4}$$

and, consequently,

$$|\vec{J}_4| < |\vec{J}_3| \tag{2.5}$$

69

The hydrophilic component 4 is transported more slowly into the casting solution than the hydrophobic matrix component 3, resulting in surface enrichment of the hydrophilic additive.

Summary

In typical observations of surface segregation phenomena in polymer blends, prolonged heat treatments are required to allow the driving forces for surface segregation to overcome slow polymer-polymer interdiffusion. By comparison, the immersion precipitation process for membrane fabrication would appear well-suited to surface modification by surface segregation of a hydrophilic additive polymer. The thermodynamic driving forces for surface segregation afforded by the favorable interactions between the hydrophilic component and water are expected to work in concert with the above kinetic mechanism for surface segregation in the early stages of membrane coagulation, a period during which the polymers are solvated and therefore highly mobile. If surface segregation during membrane coagulation is not sufficient, we can, of course, expect to achieve further surface segregation by heat treatment of the membranes in water at a temperature above the glass transitions of PVDF (roughly -40°C[170]) and the additive polymer. In fact, we will explore in Section 5.2 the possibility of utilizing such a heat treatment to *regenerate* surface-segregated layers damaged by chemical exposure through migration of residual additive polymer from the bulk.

It is of interest to note that the kinetic mechanism for surface segregation described above would predict an increase in the degree of surface segregation of the

hydrophilic additive as its molecular weight *increases*, since polymer diffusivity scales as an inverse power of its molecular weight,[171]

$$D \sim \frac{1}{M^x} \tag{2.6}$$

That is, increasing the molecular weight of the surface-active polymer would further retard its transport into the casting solution prior to gelation, causing it to be "left behind" in greater proportion at the interface. This prediction is contrary to typical surface segregation phenomena, in which the surface-active polymer migrates from the bulk and the degree of surface segregation realized during a given time is inversely related to its molecular weight. In Chapter 4, this prediction will be used to test the validity of the above proposed kinetic surface segregation mechanism.

2.6.3 Molecular Design

As discussed above, the preparation of a robust surface by surface segregation requires a favorable energetic interaction, and preferably miscibility, between the additive and matrix polymers. At the same time, we would like to design the additive polymer to efficiently express a surface chemistry tailored for a surface property of interest (*e.g.*, protein adsorption resistance). We would like its architecture to take advantage of as many of the available driving forces for surface segregation as possible. Finally, we would like to prepare the additive polymer using a synthesis technique that is economical and amenable to common commercial production methods.

Much of the work in this thesis will focus on a comb-shaped additive polymer, P(MMA-*r*-POEM), having a PMMA backbone and PEO side chains (Figure 2.16a). This amphiphilic polymer is synthesized as a random copolymer of methyl methacrylate

71

(MMA) and poly(oxyethylene methacrylate) (POEM) using an economical solution free-radical technique (see Section 3.1.2), and is specifically designed to impart oil and protein resistance to PVDF membrane surfaces. PEO is chosen for its well-known, extraordinary ability to resist protein adsorption, which arises from its hydrophilicity, its strong propensity to participate in hydrogen bonds, its large excluded volume, and its unique coordination with surrounding water molecules in aqueous solution.[172-180] Surface-grafted PEO has rendered UF membranes resistant to oil[102] and protein[103,104,106] fouling.
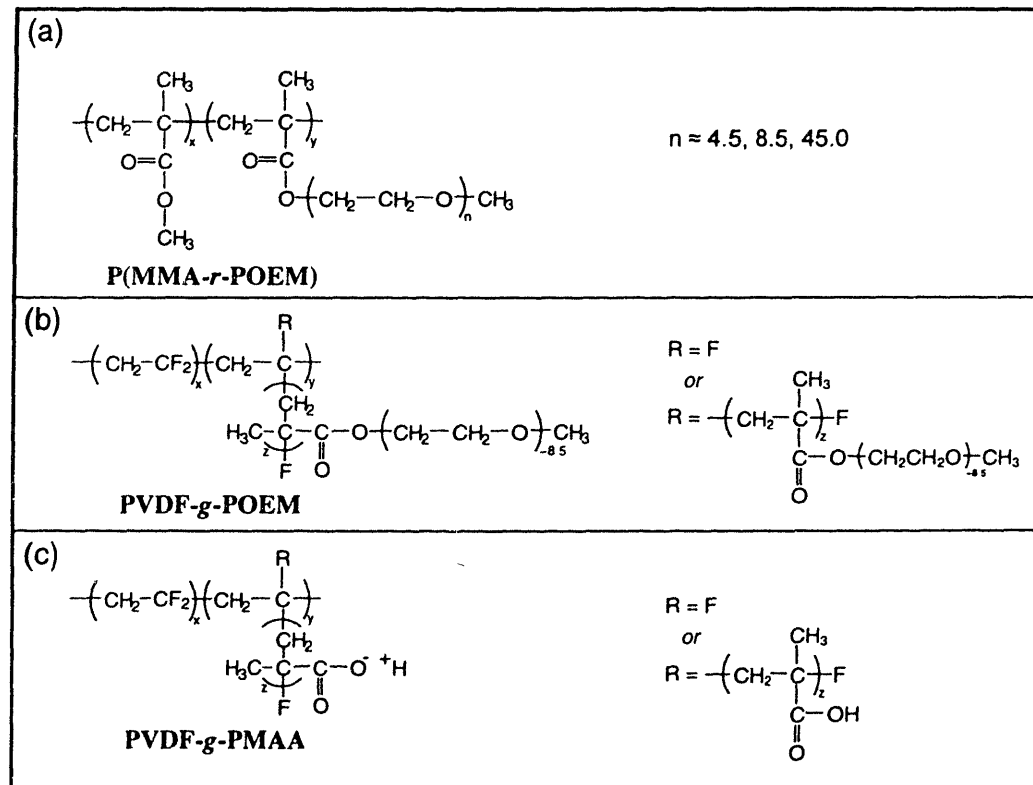
Figure 2.16 Chemical structures of comb additive polymers
(a) P(MMA-r-POEM), a random copolymer of methyl methacrylate and poly(oxyethylene methacrylate) (POEM), imparts fouling resistance to membranes. (b) PVDF-g-POEM, a graft copolymer of PVDF and POEM, imparts spontaneous wettability to membranes. (c) PVDF-g-PMAA, a graft copolymer of PVDF and poly(methacrylic acid), imparts wettability and a pH valving capability to membranes.

Selection of a comb architecture with PEO side chains creates a high yield of surface-localized PEO for each additive molecule near the surface and prevents bulk crystallization of PEO. Moreover, the comb architecture permits compatibilization of the additive and matrix polymers through the backbone, by exploiting the well-known miscibility of PVDF and PMMA.[131,181-184] Finally, the selection of a comb architecture affords a high chain end density to take advantage of the entropic driving force for surface segregation introduced in Section 2.6.2. In fact, as discussed in that section, entropically-driven surface segregation of a P(MMA-r-POEM) copolymer has been shown to *overcome* a mild enthalpic barrier in blends with lower-energy PMMA. P(MMA-r-POEM) copolymers have also been used in self-organizing blends with acrylic latex materials[185] and with poly(L-lactide) (PLLA).[186] In the latter work, surface segregation of the comb during heat treatment in water provided cell-resistant surfaces.

Two additional branched additive polymers will be utilized in this thesis to prepare membranes having desirable surface properties other than fouling resistance. A graft copolymer of PVDF and POEM, PVDF-g-POEM (Figure 2.16b), will provide membranes which are spontaneously wettable with water. Surface segregation of a graft copolymer of PVDF and methacrylic acid (MAA), PVDF-g-PMAA (Figure 2.16c), will be used for the facile preparation of ER membranes having tunable pore sizes. Both of these materials will be synthesized by a novel, controlled free-radical technique (see Section 3.1) which should be amenable to economical, large-scale production.

3. Experimental Techniques

3.1 Synthesis of Comb Additive Polymers

In this thesis, tailored surface properties were imparted to PVDF membranes through the surface segregation of comb additive polymers of three principal types, each designed for a different surface property. These three comb polymer chemistries are illustrated in Figure 2.16. Properties of all of the polymers synthesized are summarized in Table 3.1. A major objective of this thesis was to provide an *economical*, industrially-relevant approach for the surface modification of polymer membranes. Thus, a great deal of attention was paid to the selection of synthesis routes amenable to large-scale production methods and having minimal requirements with respect to reagent purity.

3.1.1 Materials

Methyl methacrylate (MMA), methyl acrylate (MA), poly(ethylene glycol) methyl ether methacrylate, referred to herein as polyoxyethylene methacrylate (POEM$_5$, $\overline{M}_n$ = 300 g/mol), POEM$_9$ ($\overline{M}_n$ = 475 g/mol), POEM$_{45}$ ($\overline{M}_n$ = 2080 g/mol, 50% solution in water), poly(ethylene glycol) methacrylate (HPOEM$_{10}$, $\overline{M}_n$ = 526 g/mol), tert-butyl methacrylate (tBMA), poly(vinylidene fluoride) (PVDF$_{250K}$, $\overline{M}_n$ *ca.* 107 000 g/mol, $\overline{M}_w$ *ca.* 250 000 g/mol), 2,2'-azobisisobutyronitrile (AIBN), copper(I) chloride (CuCl), 4,4'-dimethyl-2,2'-dipyridyl (bpy), p-toluenesulfonic acid monohydrate (TSA), tetrahydrofuran (THF, anhydrous), ethyl acetate (reagent grade), 1-methyl-2-pyrrolidinone (NMP, reagent grade), and toluene (anhydrous) were purchased from Aldrich Chemical Co. (Milwaukee, WI). Methanol, ethanol, petroleum ether, hexane,

and deuterated solvents were purchased from VWR. Diphenylmethylpotassium was prepared by Dr. Pallab Banerjee in the research group of Prof. A. M. Mayes at MIT. Unless otherwise specified, all reagents were used as received. Based on their molecular weights, $POEM_5$, $POEM_9$, and $POEM_{45}$ have pendant PEO chains with number-average degrees of polymerization of ~4.5, 8.5, and 45.0, respectively. $HPOEM_{10}$ has a pendant PEO chain with a number-average degree of polymerization of 10.0.

Table 3.1 Physical Characteristics of Additive Comb Polymers

polymer	$\overline{M}_w^{GPC}$ (g/mol)	$\overline{M}_n^{NMR}$ (g/mol)	$\overline{M}_w/\overline{M}_n$	composition[‡‡]	water solubility
P(MMA-r-POEM$_9$)[a]	14 400[†]	-	1.30[†]	49.8 wt % POEM$_9$	soluble
P(MMA-r-POEM$_9$)[b]	18 600[†]	-	1.81[†]	29.4 wt % POEM$_9$	insoluble
P(MMA-r-POEM$_9$)[c]	41 300[†]	-	2.09[†]	33.1 wt % POEM$_9$	insoluble
P(MMA-r-POEM$_9$)[d]	15 200[†]	-	1.78[†]	38.9 wt % POEM$_9$	insoluble
P(MMA-r-POEM$_9$)[e]	14 500[†]	-	1.68[†]	42.9 wt % POEM$_9$	soluble
P(MMA-r-POEM$_9$)[f]	14 800[†]	-	1.77[†]	48.6 wt % POEM$_9$	soluble
P(MMA-r-POEM$_9$)[g]	6 100[†]	-	1.14[†]	38.4 wt % POEM$_9$	insoluble
P(MMA-r-POEM$_9$)[h]	10 800[†]	-	1.12[†]	40.2 wt % POEM$_9$	insoluble
P(MMA-r-POEM$_9$)[i]	67 700[†]	-	1.37[†]	38.9 wt % POEM$_9$	insoluble
P(MMA-r-POEM$_9$)[j]	515 800[†]	-	1.19[†]	36.3 wt % POEM$_9$	insoluble
P(MMA-r-POEM$_5$)	155 000[†]	-	1.60[†]	50.9 wt % POEM$_5$	insoluble
P(MMA-r-POEM$_9$)[k]	63 300[†]	-	1.43[†]	50.7 wt % POEM$_9$	insoluble
P(MMA-r-POEM$_{45}$)	73 800[†]	-	1.42[†]	41.2 wt % POEM$_{45}$	insoluble
P(MA-r-POEM$_9$-r-HPOEM$_{10}$)	106 400[†]	-	2.59[†]	40.5 wt % (POEM$_9$ + HPOEM$_{10}$)	soluble
PVDF-g-POEM[a]	-	189 400[‡]	-	43.5 wt % POEM$_9$	insoluble
PVDF-g-POEM[b]	2 979 900[††]	323 200[‡]	1.38[††]	66.9 wt % POEM$_9$	insoluble
PVDF-g-PMAA	3 007 100[††]	211 300[‡]	1.11[††]	49.4 wt % MAA	insoluble

[†] GPC run in THF at 30°C, calibrated with PS standards.

[††] GPC run at 30°C in DMF containing 1 wt % $LiNO_3$, calibrated with PMMA standards. $\overline{M}_w^{GPC}$ and $\overline{M}_w/\overline{M}_n$ for the parent polymer $PVDF_{250K}$ (using the same method) are 1 218 300 g/mol and 2.10, respectively.

[‡] Calculated from ^1H NMR using Equation 3.10 (below).

[‡‡] Measured by ^1H NMR (see below).

3.1.2 Synthesis of P(MMA-r-POEM) Combs for Fouling Resistance

Anionic Polymerization

Synthesis Protocol. For initial studies of comb surface segregation during membrane fabrication, P(MMA-r-POEM9)[a] was prepared anionically by Dr. Pallab Banerjee in the research group of Prof. A. M. Mayes at MIT. THF was distilled over sodium benzophenone ketyl. MMA and POEM9 were separately stirred over calcium hydride overnight. Then, MMA and POEM9 were each vacuum distilled once over calcium hydride and a second time over trioctyl aluminum, and the middle fraction of each was collected for use. Five grams of each monomer were introduced to distilled THF at room temperature, after which the mixture was cooled to -45°C. The mixture was titrated against the initiator, 0.062 M diphenylmethylpotassium in THF, until a yellow color was stable for 3-4 min. A calculated quantity of the initiator solution (8.1 mL) was then injected into the reactor. After 12 h, the reaction was terminated by the injection of excess methanol. The reaction mixture was then warmed to room temperature, and the polymer was precipitated in excess petroleum ether. The polymer was purified by twice redissolving it in THF, concentrating the solution by evaporation under partial vacuum, and reprecipitating it in petroleum ether. Finally, the polymer was dried for 12 h in a vacuum oven at room temperature.

Characterization. The copolymer molecular weight was characterized by gel permeation chromatography (GPC) in THF at 30°C, based on PS standards. GPC was conducted at a flow rate of 1 mL/min using a Waters 510 HPLC pump, Waters Styragel™ columns, and a Waters 410 differential refractometer (Millipore Corp., Bedford, MA).

The copolymer composition was determined by ^{1}H nuclear magnetic resonance spectroscopy (^{1}H NMR) in deuterated chloroform using a Bruker DPX-400 spectrometer, as detailed in the next section. The molecular weight and composition of P(MMA-*r*-POEM$_9$)[a] appear in Table 3.1.

Free-Radical Polymerization

Living anionic polymerization is an attractive means to prepare model polymers for exploratory studies, since the resulting polymers are of nearly monodisperse molecular weight and have highly controlled architectures due to the virtual absence of termination reactions.[187] However, the low temperatures required, particularly for the anionic polymerization of methacrylates,[187] along with the rigorous requirements with respect to reagent purity, make it an unattractive method from a commercial point of view. Thus, the bulk of the P(MMA-*r*-POEM) additive polymers used in this thesis were synthesized by an inexpensive solution free-radical method. Bulk free-radical copolymerization of MMA and POEM to appreciable conversion results in gelation, most likely due to side reactions involving the ether bonds in POEM. However, it has been found by our research group and by others[188] that this can be avoided by diluting the
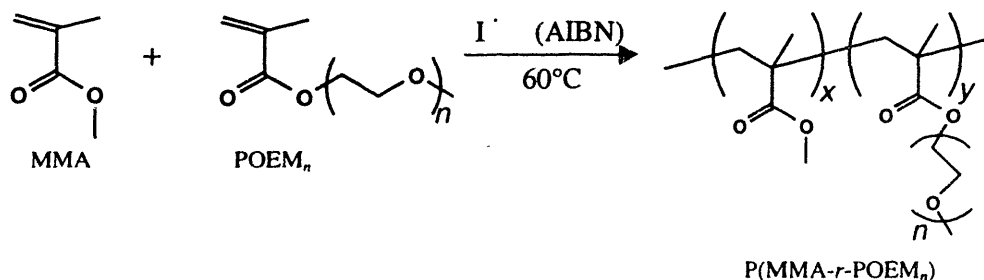
Figure 3.1 Synthesis scheme for P(MMA-*r*-POEM)

monomer with a solvent such as ethyl acetate, toluene, or THF to prepare a solution containing ≤10% monomer.

Synthesis Protocol. Figure 3.1 is a scheme for the free-radical synthesis of P(MMA-*r*-POEM). In a typical polymerization, MMA and POEM were dissolved in ethyl acetate at room temperature to make a solution containing 10% monomer. A calculated amount of AIBN was then dissolved in the mixture. The amount of AIBN added was based on empirical relationship of the ratio [M]/[AIBN], where [M] and [AIBN] are the monomer and AIBN concentrations, respectively, to the resulting comb molecular weights. The reaction vessel was sealed with a rubber septum, and argon gas was bubbled through the reaction mixture at a moderate rate for 10-15 min to remove oxygen. The reaction vessel was then placed in a silicone oil bath preheated to 60°C, and polymerization was allowed to proceed for 12 h. The polymer was precipitated in a mixture containing 9 parts petroleum ether and 1 part methanol (petroleum ether is a marginal solvent for POEM, while methanol is a good solvent for it). It was then purified by redissolving it in THF, concentrating the solution by evaporation, and reprecipitating it in similar petroleum ether/methanol mixtures at least two times. Finally, the polymer was dried overnight in a vacuum oven at room temperature. Details of each synthesis are tabulated in Appendix B. The synthesis protocols for comb polymers P(MMA-*r*-POEM$_9$)$^{b-f}$, P(MMA-*r*-POEM$_9$)^j, and P(MMA-*r*-POEM$_{45}$) differed somewhat from the above general procedure. These differences are detailed in Appendix B.

Characterization. All P(MMA-*r*-POEM) copolymers were characterized by GPC in THF at 30°C using PS standards, and by ^{1}H NMR in deuterated chloroform. The

NMR spectra for P(MMA-r-POEM) copolymers (see example, Figure 3.2) exhibit peaks in the range 0.7-2.3 ppm due to the C-CH$_x$ bonding environments and peaks in the range 3.2-4.3 ppm due to the O-CH$_x$ bonding environments present.[189,190] The number of protons in each type of bonding environment per repeat unit of MMA and POEM is given in Table 3.2.
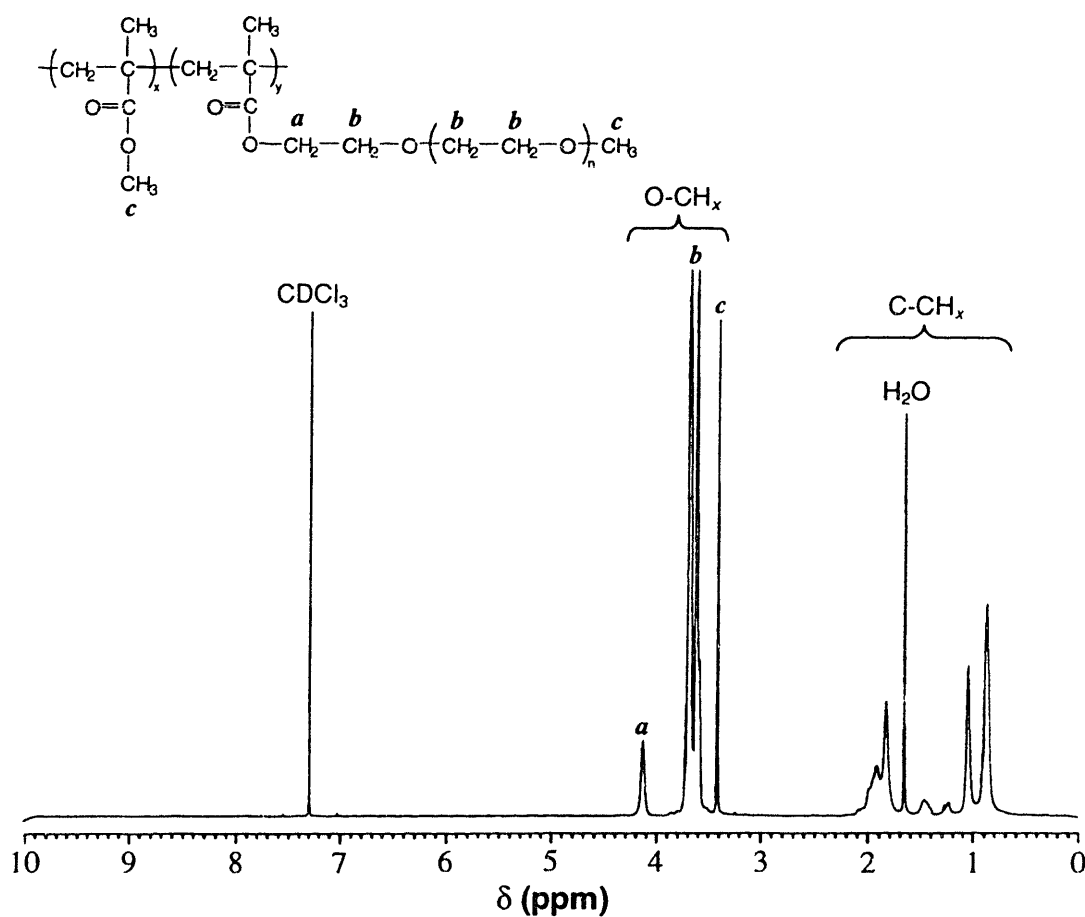
Figure 3.2 400 MHz ^{1}H NMR spectrum for P(MMA-r-POEM$_5$)

Assignments for the O-CH$_x$ resonances are indicated on the inset molecular structure. The water peak at ~1.6 ppm[191] was commonly present, and was not included in the calculation of copolymer compositions.

Table 3.2 Number of C-CH$_x$ and O-CH$_x$ Protons in MMA and POEM

	Number of Protons per Repeat Unit	
	MMA	*POEM*
C-CH$_x$	5	5
O-CH$_x$	3	$4n + 3$[†]

[†] n = 4.5, 8.5, 45.0 for POEM$_5$, POEM$_9$, and POEM$_{45}$, respectively

The mole fraction of POEM was thus calculated from the NMR data as,

$$X_{POEM} = \frac{B}{A + B} \tag{3.1}$$

where A and B are the solutions to the simultaneous system of equations,

$$5A + 5B = I_{C-CH_x} \tag{3.2}$$

and

$$3A + (4n + 3)B = I_{O-CH_x} \tag{3.3}$$

and where I_{C-CH_x} and I_{O-CH_x} are the total intensities of the resonances for each type of bonding environment. The weight fraction of POEM was then given by,

$$W_{POEM} = \frac{X_{POEM} M_o^{POEM}}{X_{POEM} M_o^{POEM} + (1 - X_{POEM}) M_o^{MMA}} \tag{3.4}$$

where M_o^{POEM} and M_o^{MMA} are the molecular weights of POEM and MMA, respectively. The molecular weights and compositions of all P(MMA-r-POEM) copolymers appear in Table 3.1.

3.1.3 Synthesis of P(MA-r-POEM-r-HPOEM) for Wettability

It will be shown in Chapter 5 that the addition of P(MMA-r-POEM) copolymer additives to membranes results in substantially enhanced fouling resistance. However, this additive does not successfully impart to PVDF membranes a second property of

interest, namely, wettability. To impart enhanced wettabity to membranes, a comb similar to P(MMA-r-POEM) in terms of preparation method and architecture, but with two chemistry changes, was synthesized. Firstly, the methyl methacrylate (MMA) backbone was changed to methyl acrylate (MA). Like PMAA, PMA has been shown to be miscible with PVDF.[181] Secondly, two comonomers were used: $POEM_9$, having a methoxy ($-OCH_3$) terminated PEO chain, and $HPOEM_{10}$, having a hydroxy (-OH) terminated PEO chain. Thus, the polymer was a terpolymer, P(MA-r-$POEM_9$-r-$HPOEM_{10}$), having a methyl acrylate backbone and PEO side chains, roughly half of which were methoxy-terminated, the other half being hydroxy-terminated. The significance of these two chemistry changes will be discussed in Section 5.3.2.

Synthesis Protocol. MA (30 g), $POEM_9$ (15 g), $HPOEM_{10}$ (15 g), and AIBN (0.084 g) were dissolved in ethyl acetate (~600 mL) at room temperature. The reaction vessel was sealed with a rubber septum, and argon gas was bubbled through the reaction mixture for 10 min to displace oxygen. The reaction vessel was then placed in a silicone oil bath preheated to 60°C, and polymerization was allowed to proceed for 16 h. The polymer was precipitated in a mixture containing 9 parts hexane and 1 part ethanol. It was then purified twice by redissolving it in THF, concentrating the solution by evaporation, and reprecipitating it in similar hexane/ethanol mixtures. Finally, the polymer was dried overnight under vacuum at room temperature.

Characterization. P(MA-r-$POEM_9$-r-$HPOEM_{10}$) was characterized by GPC in THF at 30°C using PS standards, and by ^{1}H NMR in deuterated chloroform. The NMR spectrum for the terpolymer is very similar to that for P(MMA-r-POEM) (see Section

3.1.2), having two separate groupings of resonances due to the C-CH_x and O-CH_x bonding environments. An additional peak appears at ~2.3 ppm (convolved with the C-CH_x resonances) due to the terminal $-OH$ proton of HPOEM. The number of protons in each type of bonding environment per repeat unit of MA, $POEM_9$, and $HPOEM_{10}$ is given in Table 3.3.

Table 3.3 Number of C-CH_x, $-OH$, and O-CH_x Protons in MA, POEM, and HPOEM

	Number of Protons per Repeat Unit		
	MA	*POEM$_9$*	*HPOEM$_{10}$*
C-CH_x + $-OH$	3	5	6
O-CH_x	3	37	40

With the assumption that the weight fractions of $POEM_9$ and $HPOEM_{10}$ in the terpolymer were equal (reflecting the equal weight fractions of the monomers used in the synthesis), the combined mole fraction of $POEM_9$ and $HPOEM_{10}$ was calculated from the NMR data as,

$$X_{(POEM_9 + HPOEM_{10})} = \frac{B + C}{A + B + C} \tag{3.5}$$

where A, B, and C are the solutions to the simultaneous system of equations,

$$475B = 526C \quad \text{\{assumption of equal wt. fractions\}}, \tag{3.6}$$

$$3A + 5B + 6C = I_{C-CH_x} + I_{-OH} \tag{3.7}$$

and

$$3A + 37B + 40C = I_{O-CH_x} \tag{3.8}$$

and where I_{C-CH_x}, I_{-OH}, and I_{O-CH_x} are the total intensities of the resonances for each type of bonding environment. Mole fractions were converted to weight fractions using an

equation analogous to Equation 3.4. The molecular weight and composition of P(MA-*r*-

POEM$_9$-*r*-HPOEM$_{10}$) appear in Table 3.1.

3.1.4 Synthesis of PVDF-g-POEM for Spontaneous Wettability

Introduction to Atom Transfer Radical Polymerization

Atom transfer radical polymerization (ATRP) is a relatively new synthesis technique, having been described only 5 years ago by Matyjaszewski, *et al.*[192] and Sawamoto and Kamigaito.[193] ATRP is a controlled/"living" free-radical technique which has classically been used to prepare polymers having polydispersities as low as 1.1[194] from vinyl monomers. ATRP is performed using an initiator which is an organic halide (R-X, where X = Br,Cl,F). A catalytic complex composed of a transition metal halide (M^{+z}X$_n$) and a suitable organic ligand (Ln) facilitates the repeated insertion of a vinyl monomer between the organic portion of the initiator and its terminal halogen atom. Repeated insertion of the monomer occurs via the *activation-propagation-deactivation cycle* illustrated in Figure 3.3.
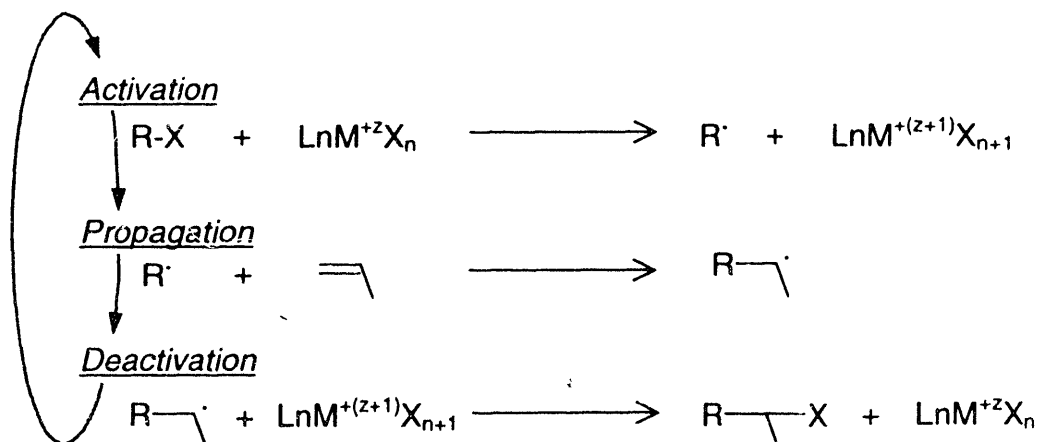
Figure 3.3 Schemata of the general steps in ATRP

During the *activation* step, the R-X bond is activated to yield a carbon-centered radical (R·) and an oxidized metal complex $[M^{+(z+1)}X_{n+1}]$. During the *propagation* step, the radical may react with a vinyl monomer. During the *deactivation* step, the metal complex is reduced to restore the dormant, halogen-endcapped chain end (R-X). The advantages of ATRP synthesis with respect to standard free-radical techniques arise from the fact that the equilibrium between the dormant and activated chain end species strongly favors the dormant one. Thus, the overall concentration of free-radicals remains very low throughout the polymerization,[195,196] and the termination and chain transfer reactions which contribute to chain branching and increased polydispersity in standard free-radical polymerizations[197] are much less probable. On the other hand, because polymerization proceeds by a free-radical mechanism, ATRP can be carried out without the stringent requirements of living ionic polymerizations with regard to reagent purity.

While these attributes of ATRP are attractive, the characteristic of the technique of greatest interest for the purposes of this thesis is the *nature of the initiator*. Indeed, PVDF is an organic halide that can act as an ATRP *macroinitiator*, enabling the facile grafting of vinyl side chains directly onto PVDF. ATRP macroinitiators, polymer chains with pendant chemical groups containing radically transferable halogen atoms, have been used previously for the preparation of ft copolymers. Matyjaszewski, *et al.*[198] polymerized 2-(2-bromopropionyloxy) acrylate free-radically to obtain a macroinitiator with a pendant Br atom on every repeat unit. The pendant Br atoms were then used as initiation points for ATRP of PS and poly(butyl acrylate) side chains. Similarly, PS and various poly(meth)acrylate side chains have been grafted onto a

poly[(vinyl chloride)-*co*-(vinyl chloroacetate)] macroinitiator, using the chloroacetate groups as the initiation sites for ATRP polymerization of the monomers.[199]

It has been reported[199] that *secondary* halogen atoms of the type found in PVDF are too strongly bonded to serve as initiation sites for ATRP. However, work in our laboratory has demonstrated that the secondary halogen atoms found on a variety of commercial polymers, including PVDF, *can* be used effectively for the ATRP grafting of vinyl side chains onto them.[200] Moreover, these graft copolymers may be prepared under conditions of reagent purity similar to those encountered in standard solution free-radical polymerizations, making this technique a commercially attractive option.[*]

The ATRP preparation of graft copolymers from commercial halogenated polymers like PVDF has a number of advantages over the standard free-radical graft copolymerization methods used widely in industry, which rely on the production of free-radicals on the parent polymer chain by exposure to ionizing radiation and/or a free-radical initiator.[202,203] In these reactions, homopolymerization of the comonomer always occurs to some extent, resulting in a product which is a mixture of graft copolymer and homopolymer. Moreover, backbone degradation and gel formation can occur as a result of uncontrolled free-radical production.[196] In the ATRP preparation of graft copolymers, there has been no evidence of homopolymerization,[198,199] and chain degradation reactions are much less probable due to the low concentration of radical species at any given time.

---

[*] A patent on this ATRP technique for the preparation of graft copolymers based on commercial polymers bearing secondary halogen atoms is pending.[201]

Synthesis and Characterization

Synthesis Protocol. Figure 3.4 is a scheme for the ATRP synthesis of PVDF-*g*-POEM. In a typical reaction, PVDF$_{250K}$ (5g) was weighed into a conical flask containing a Teflon stir bar, and the polymer was dissolved in NMP (40 mL) at 50°C. This solution was then cooled to room temperature, after which POEM$_9$ (50 mL), CuCl (0.040 g), and bpy (0.23 g) were added and the conical flask was sealed with a rubber septum. Argon
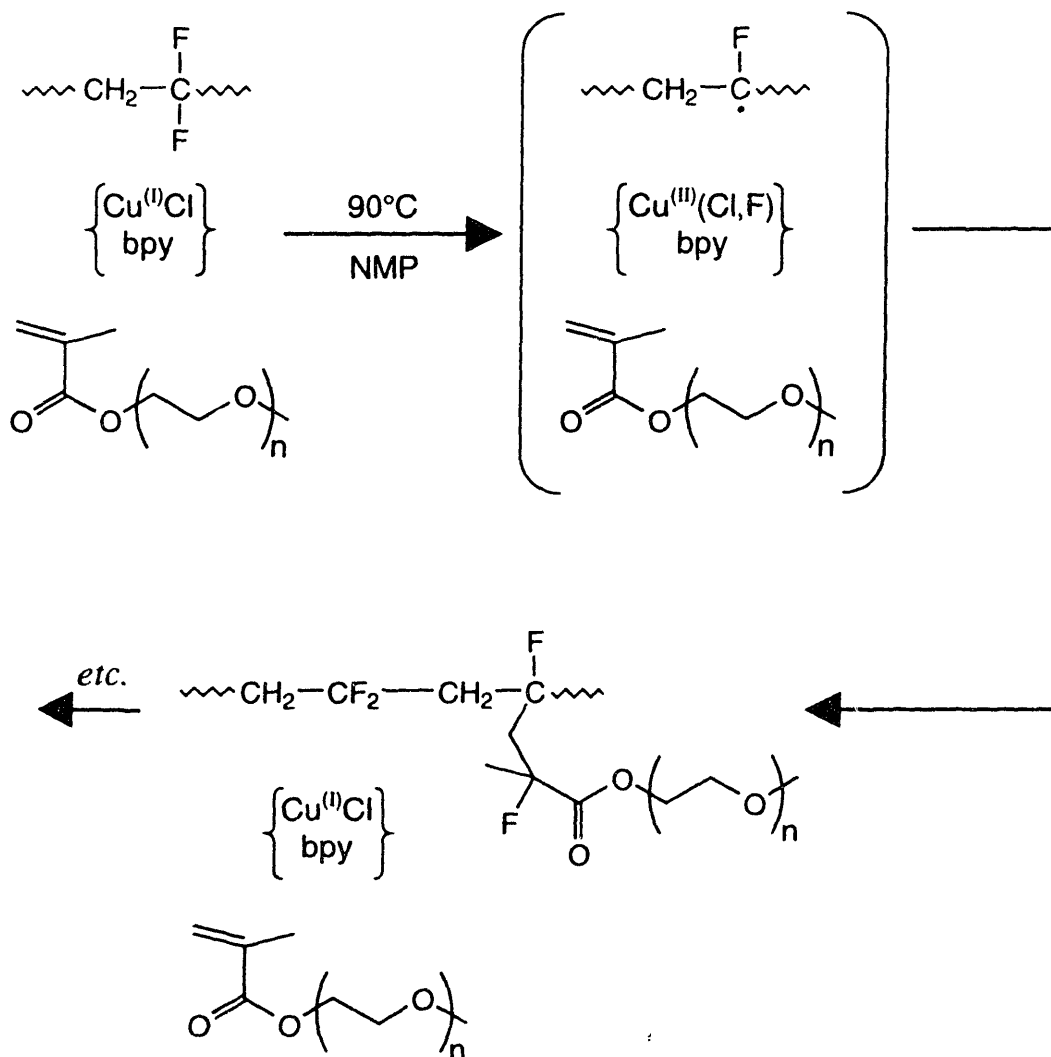
Figure 3.4 Synthesis scheme for PVDF-*g*-POEM

gas was bubbled through the reaction mixture for 15 min while stirring. The reaction vessel was then placed immediately into an oil bath preheated to 90°C, and the reaction was allowed to proceed for 19 h. The graft copolymer was precipitated into a mixture containing 2 parts methanol and 5 parts petroleum ether and recovered by filtration. The polymer was purified by redissolving it in NMP and reprecipitating it 3 times in similar methanol/petroleum ether mixtures. Finally, the graft copolymer, PVDF-g-POEM, was dried in a vacuum oven overnight at room temperature. The details of each synthesis appear in Appendix B.

Characterization. Composition. ^{1}H NMR was performed on 20% solutions of PVDF$_{250K}$ and its POEM-grafted derivatives in deuterated N,N-dimethylformamide (DMF). NMR spectra for PVDF$_{250K}$ and PVDF-g-POEM^b appear in Figure 3.5. The PVDF spectrum exhibits two well-known peaks[204] due to head-to-tail (ht) and head-to-head (hh) bonding arrangements. Grafting of POEM$_9$ to PVDF$_{250K}$ resulted in the appearance of peaks in the region 3.2-4.3 ppm due to the O-CH$_x$ bonding environments in the methacrylate[189] and PEO[190] moieties of POEM. The solvent peaks s_2 and s_3 were subtracted from the spectra using their known intensities relative to solvent peak s_1 obtained by NMR analysis of pure deuterated DMF. The mole fractions of POEM in the copolymers were then calculated as,

$$X_{POEM} = \frac{\frac{1}{37}\left(I_c + I_d + I_e\right)}{\frac{1}{37}\left(I_c + I_d + I_e\right) + \frac{1}{2}\left(I_{a(ht)} + I_{a(hh)}\right)} \tag{3.9}$$
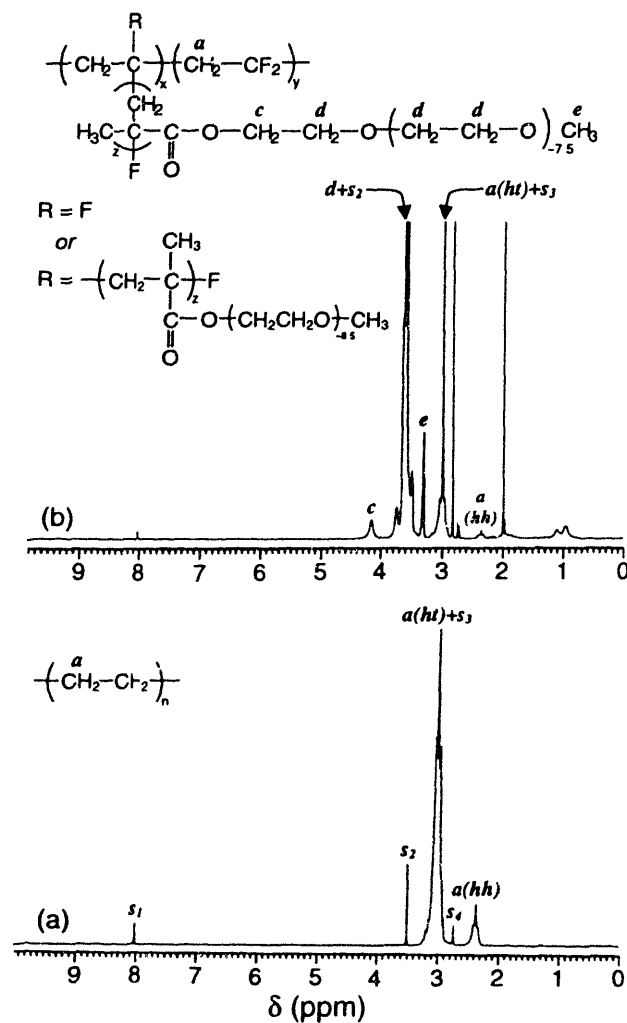
Figure 3.5 NMR spectra for PVDF and PVDF-g-POEM

400 MHz ^{1}H NMR spectra for (a) PVDF$_{250K}$ and (b) PVDF-g-POEM[b]. Resonances labeled s_n are solvent peaks due to deuterated DMF. Resonances labeled ht and hh are due to head-to-tail and head-to-head PVDF repeat units, respectively. One or both of the fluorine atoms on each PVDF repeat unit may act as an initiation point for monomer addition (b, inset chemical structure).

where I_c, I_d, and I_e are the intensities of the resonances labeled c, d, and e in Figure 3.5

and the factor of $\frac{1}{37}$ is due to the 37 O-CH$_x$ protons per POEM$_9$ repeat unit. The mass-

based composition reported in Table 3.1 was then computed using an equation analogous

to Equation 3.4.

Molecular Weight. PVDF$_{250K}$ and PVDF-g-POEM^b were characterized by GPC

in DMF containing 1% lithium nitrate at 30°C, with the molecular weight scale calibrated

using PMMA standards. GPC traces for the two polymers appear in Figure 3.6. The

grafting reaction resulted in a significant molecular weight increase, from a PMMA

standard molecular weight of $\overline{M}_w = 1\,218\,300$ for PVDF$_{250K}$ to $\overline{M}_w = 2\,979\,900$ for

PVDF-g-POEM^b. The molecular weight distribution of the graft copolymer is bimodal.

The GPC trace is virtually unchanged after a 48-h extraction in a large volume of dW, a

good solvent for poly(POEM), indicating that its bimodality is not due to
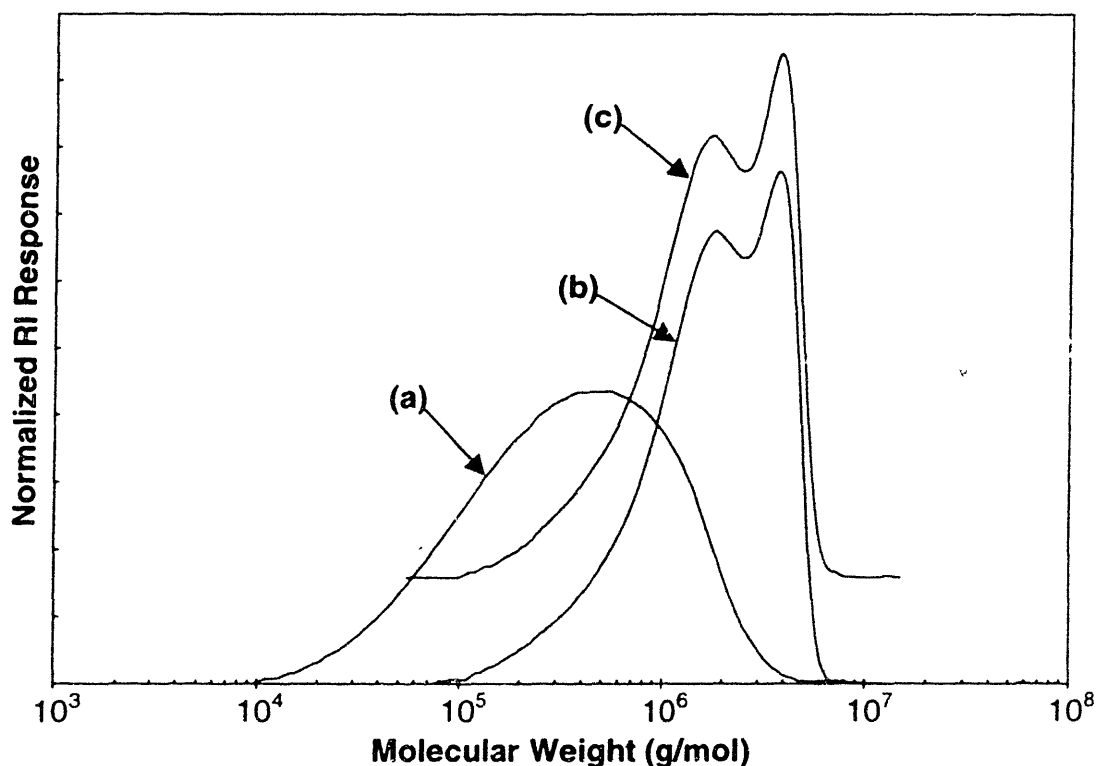
Figure 3.6 GPC traces of PVDF and PVDF-g-POEM
(a) PVDF$_{250K}$, the parent polymer for (b) PVDF-g-POEM^b. Trace (c), offset for clarity, is PVDF-g-POEM^b following a subsequent 48-h extraction in a large volume of water. The molecular weight scale was calibrated using PMMA standards.

homopolymerization of POEM (Fig. 3.6c). Rather, the bimodal distribution is likely a result of radical-radical coupling of chains during polymerization, which has been observed previously in ATRP graft copolymerizations, and which can result in multi-modal molecular weight distributions.[198] While such termination reactions are generally undesirable, we will see in Section 5.3 that they do not compromise the ability of PVDF-g-POEM to surface segregate during membrane fabrication, providing a highly desirable surface chemistry.

Due to the differences in chain flexibility between the PVDF-based graft copolymers and linear PMMA standards and differences between the hydrodynamic radii of linear and branched polymers of equal molecular weight, the PMMA standard molecular weights are not accurate numerical estimates of the true graft copolymer molecular weights. More accurate estimates of the number-average molecular weights of PVDF-g-POEM were obtained from the NMR data using the formula,

$$\overline{M}_{n,copolymer} = \overline{M}_{n,PVDF}\left(1 + x\frac{M_o^{comonomer}}{M_o^{PVDF}}\right) \qquad (3.10)$$

where $\overline{M}_{n,PVDF}$ is the number-average molecular weight of $PVDF_{250K}$ provided by the manufacturer, x is the molar ratio of comonomer units to PVDF repeat units in the copolymer as measured by ^1H NMR, and $M_o^{comonomer}$ and M_o^{PVDF} are the molecular weights of the comonomer and PVDF repeat units, respectively. The molecular weights so calculated appear in Table 3.1.
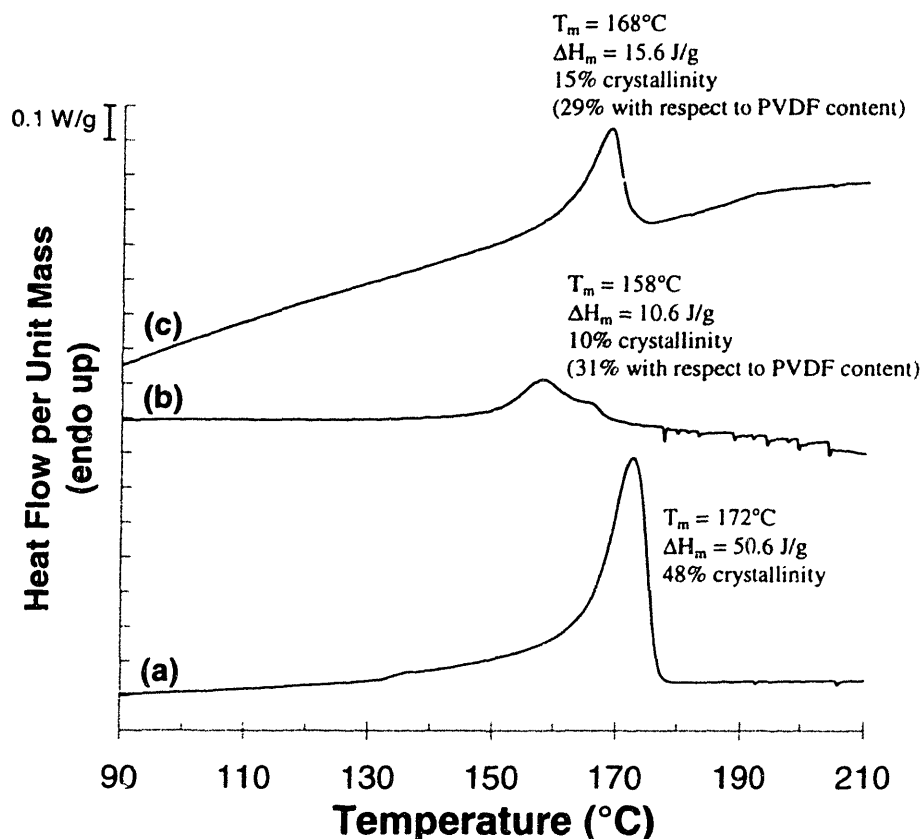
Figure 3.7 DSC thermograms for PVDF and its graft copolymers
DSC thermograms upon heating for (a) pure $PVDF_{250K}$, parent polymer for (b) PVDF-g-POEM[b] and (c) PVDF-g-PMAA.

Crystallinity. Differential scanning calorimetry (DSC) was performed on $PVDF_{250K}$ and PVDF-g-POEM[b] using a Perkin-Elmer (Norwalk, CT) Pyris 1 calorimeter. To achieve a near-equilibrium structure, the samples were preconditioned in the calorimeter by holding at 210°C (above the melting temperature) for 15 min, cooling to 130°C (below the crystallization temperature) at 10°C/min, holding at 130°C for 15 min, and cooling to 50°C at 10°C/min The DSC thermograms appearing in Figure 3.7 were then obtained while heating from 50°C to 230°C at 10°C/min. The results show that

PVDF-g-POEM^b crystallizes, with a depressed melting point compared to PVDF homopolymer and a lower crystalline content, as indicated by its smaller heat of melting. The depressed melting temperature might be expected due to the presence of non-crystallizing POEM units attached to the PVDF backbone.[171] For each polymer, the weight percent crystallinity, with respect to the PVDF content of the polymer, was computed as,[205]

$$W_c = \frac{M_o^{PVDF}}{W_{PVDF}} \cdot \frac{\Delta H_m}{\Delta H_f^\bullet} \tag{3.11}$$

where M_o^{PVDF} is the repeat unit molar mass of PVDF (64 g/mol), W_{PVDF} is the weight fraction PVDF in the polymer from NMR, ΔH_m is the heat of melting observed by DSC [J/g], and $\Delta H_f^\bullet$ is the heat of fusion of PVDF (6700 J/mol[206]).

Morphology and Architecture. Referring to the ATRP synthesis scheme for PVDF-g-POEM in Figure 3.4, consider the situation in which a single POEM monomer has been grafted to the PVDF chain. The tertiary carbon atom bonded to the halogen atom terminating the newly growing POEM side chain, having a radical-stabilizing carbonyl group adjacent to it, is more reactive toward further polymerization than the secondary halogenated carbon atoms on unreacted PVDF repeat units.[195,199,206] However, the concentration of the less reactive, secondary halogenated species, at least initially, is much higher. Thus, it is not clear *a priori* whether POEM will graft to PVDF in the form of long poly(POEM) chains, singly-grafted POEM units, or whether an intermediate architecture will develop.
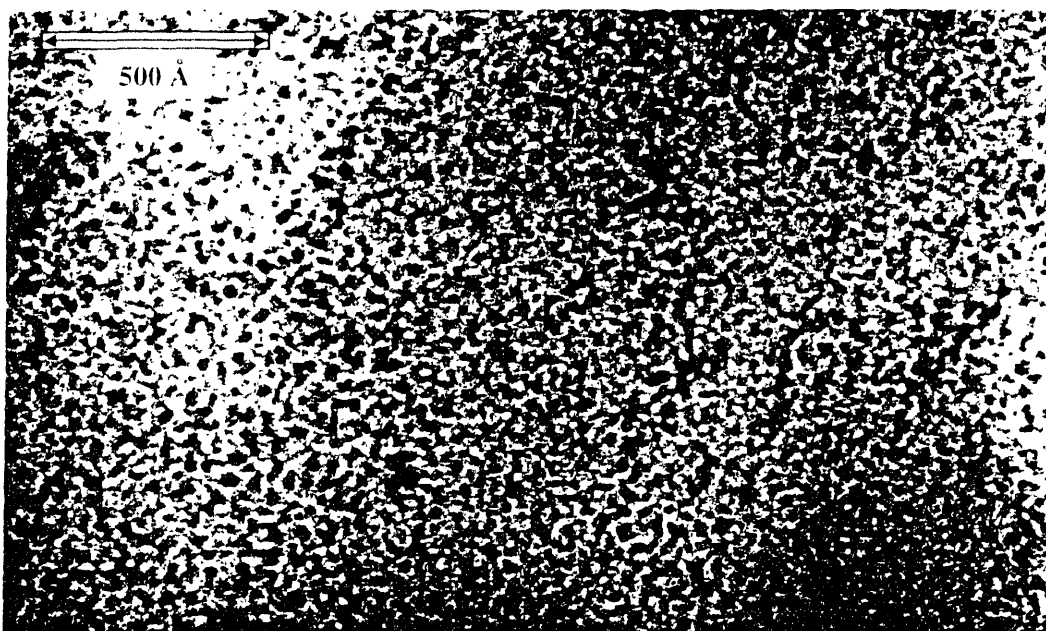
Figure 3.8 TEM image of PVDF-*g*-POEM[b] stained with ruthenium tetroxide
Ruthenium tetroxide stains the ether bonds of POEM, which appears black in the image

To characterize the side chain length, transmission electron microscopy (TEM) was performed on pure PVDF-*g*-POEM[b] using a JEOL 200CX microscope operated at an accelerating voltage of 100 kV. Prior to TEM characterization, a bulk polymer sample was equilibrated in a vacuum oven at 200 C for 12 h. It was then cryomicrotomed into 50-nm thick sections at −55°C using a RMC (Tucson, AZ) MT-XL ultramicrotome. The sections were mounted on copper grids and stained with ruthenium tetroxide for 20 min at room temperature. Ruthenium tetroxide selectively stains the ether oxygen atoms of PEO, and it has been shown not to stain PVDF.[20] Figure 3.8 is an example TEM image of PVDF-*g*-POEM[b], showing an apparently *microphase separated* structure with stained POEM domains appearing dark. The domain size is roughly 20 A, consistent with a

"poly(POEM)" side chain length of only 1-2 POEM units. The morphology is highly defected and completely lacking in long-range order, similar to morphologies observed in other recently-synthesized comb polymers prepared with incompatible backbone / side chain pairs.[208-210] These results offer preliminary evidence that PVDF-g-POEM is characterized by short PEO side chains formed by singly- or nearly singly-grafted POEM units. The size scale of the features observed is very near the resolution limit of the TEM, however.

Note Regarding Thermal Stability. PVDF-g-POEM copolymers were observed to crosslink upon heating above ~80°C, becoming completely insoluble after a period of several hours. This poor thermal stability arises from residual CuCl remaining in the polymer. Due to the abundance of potential initiation sites in PVDF (two per repeat unit), even very low concentrations (ppm) of CuCl remaining after purification by successive precipitations are capable of creating free-radicals on the PVDF chains. In the bulk condition, these can then terminate by transfer to neighboring chains. PVDF-g-POEM is apparently stable indefinitely (at least for 8 months) if refrigerated in the bulk condition or (probably better yet) if stored in solution.

Contamination of products by residual metal catalyst is a problem general to ATRP synthesis. Current work by a number of investigators is directed toward the development of effective and industrially relevant methods for catalyst removal. For example, Matyjaszewski and coworkers[211] have demonstrated the removal of Cu-based ATRP catalysts from reaction mixtures using ion exchange resins. Haddleton, *et al.*[212] and Matyjaszewski, *et al.*[213] have developed heterogeneous ATRP systems employing

surface-immobilized metal catalysts and ligands, respectively. Following polymerization, the catalyst/ligand complex is easily removed from the heterogeneous reaction mixture with its solid support. Liou and coworkers[214] have recently developed a homogeneous reaction system utilizing an ATRP ligand covalently attached to low molecular weight polyethylene (PE). PE is soluble under the reaction conditions, but precipitates from solution at room temperature due to crystallization, taking the catalyst/ligand complex with it.

3.1.5 Synthesis of PVDF-g-PMAA for pH-Responsive Membranes

For the preparation of polymer membranes having pH-responsive separation characteristics (see Section 2.4.2), a polymer having a backbone compatible with PVDF and weak polyacid side chains was desired. The strategy used for the preparation of such a polymer was first to graft copolymerize poly(*tert*-butyl methacrylate) (PtBMA) side chains onto PVDF using ATRP (see Section 3.1.4), then hydrolyze the PtBMA side chains to yield poly(methacrylic acid) (PMAA). It is well-known[215-218] that PtBMA can be selectively and quantitatively hydrolyzed in the presence of TSA to yield PMAA.

Synthesis Protocol. $PVDF_{250K}$ (5 g) was dissolved in NMP (40 mL) at 50°C. The mixture was cooled to room temperature, after which tBMA (50 mL), CuCl (0.041 g), and bpy (0.23 g) were added and the reaction vessel was sealed with a rubber septum. Argon gas was bubbled through the reaction mixture for 15 min while stirring. The reactor was then placed immediately into an oil bath preheated to 90°C, and the reaction was allowed to proceed for 20 h. The graft copolymer was precipitated into a 1:1 water/ethanol mixture. It was then purified by redissolving it in NMP and reprecipitating

it in a similar water/ethanol mixture. The graft copolymer, PVDF-*g*-PtBMA, was recovered by filtration and dried in a vacuum oven overnight.

PVDF-*g*-PtBMA (5.52 g) was cut into chunks ~2 mm in size, which were immersed in anhydrous toluene (300 mL). The polymer swelled significantly in the solvent, although it did not dissolve. TSA (31 g) was added to the reactor, after which the reactor was immediately sealed with a rubber septum and the TSA dissolved by vigorous stirring. Argon gas was then bubbled through the reaction mixture for 15 min, after which the reactor was placed in an oil bath preheated to 85°C. After 7 h, the reaction mixture was poured into excess methanol (a good solvent for TSA). Much of the polymer remained in the form of "chunks," although some of it was finely dispersed. The polymer was recovered by filtration, redissolved in DMF, precipitated in a mixture containing 4 parts hexane and 1 part ethanol, and again recovered by filtration. For further purification, the polymer was stirred overnight in a large volume of THF (in which it swelled but did not dissolve), and precipitated again in a hexane/ethanol mixture. The graft copolymer, PVDF-*g*-PMAA, was finally dried in a vacuum oven overnight at room temperature.

Characterization. Composition. PVDF$_{250K}$, PVDF-*g*-PtBMA, and PVDF-*g*-PMAA were characterized by ^{1}H NMR in deuterated DMF. NMR spectra for the polymers appear in Figure 3.9. Grafting of tBMA to PVDF$_{250K}$ resulted in the appearance of a peak at 1.5 ppm due to the *tert*-butyl protons.[215-219] Despite the heterogeneous nature of the hydrolysis reaction, hydrolysis of the PtBMA side chains to PMAA was quantitative, as indicated by the complete disappearance of the *tert*-butyl

peak. The spectrum for PVDF-g-PMAA also contained a resonance at 12.6 ppm due to the carboxylic acid proton.[218] The compositions of both PVDF-g-PtBMA and PVDF-g-PMAA were calculated from their NMR spectra. In both cases, the solvent resonance s_3 was subtracted using its known intensity relative to solvent peak s_1 established by NMR analysis of pure deuterated DMF. The mole fraction of tBMA in PVDF-g-PtBMA was calculated from Figure 3.9b as,

$$X_{tBMA} = \frac{\dfrac{I_b}{9}}{\dfrac{I_b}{9} + \dfrac{1}{2}\left(I_{a(ht)} + I_{a(hh)}\right)} \tag{3.12}$$

where I_x denotes the intensity of resonance x in Figure 3.9. The mole fraction of MAA in PVDF-g-PMAA was similarly calculated from Figure 3.9c as,

$$X_{MAA} = \frac{I_e}{I_e + \dfrac{1}{2}\left(I_{a(ht)} + I_{a(hh)}\right)} \tag{3.13}$$

The calculated values were $X_{tBMA} = 0.403$ and $X_{MAA} = 0.438$, respectively. The close agreement between the two values provides strong evidence that the hydrolysis reaction was selective and quantitative, and that most of the methacrylic acid units of the hydrolyzed copolymer were protonated. The PVDF-g-PMAA composition reported in Table 3.1 was computed from an average of the two mole fractions above using an equation analogous to Equation 3.4.
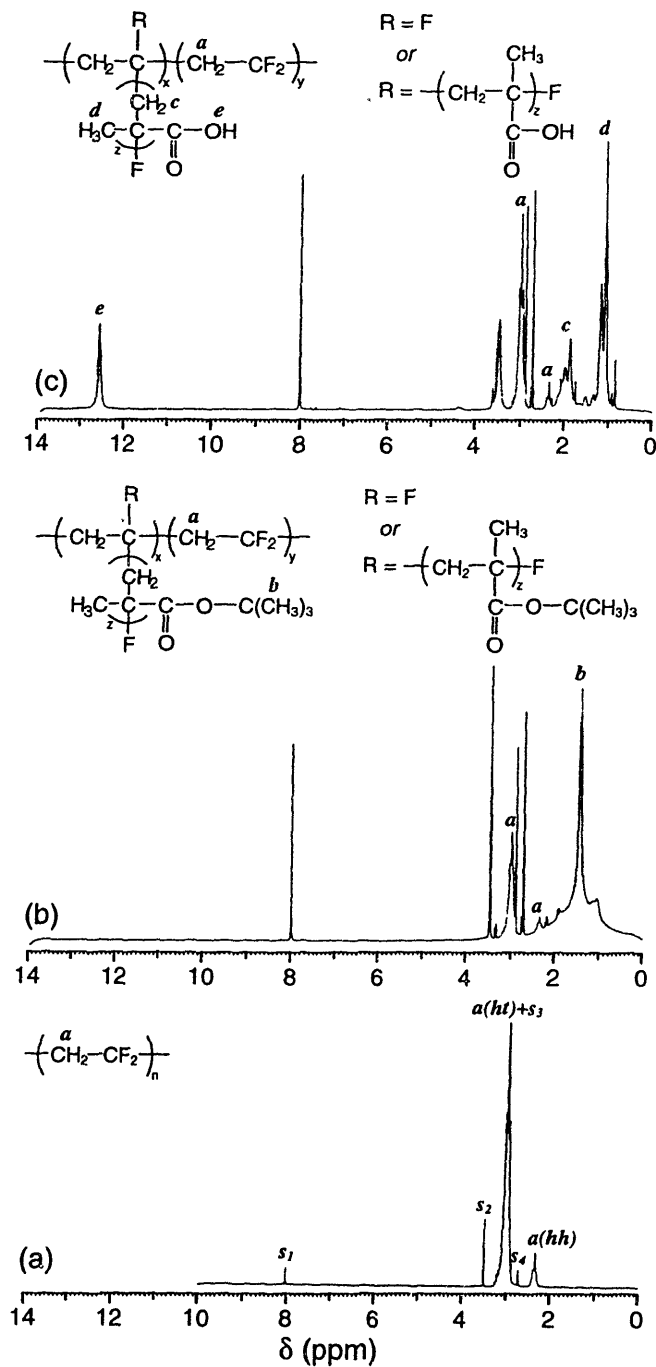
Figure 3.9 NMR spectra for PVDF, PVDF-g-PtBMA, and PVDF-g-PMAA

400 MHz ^{1}H NMR spectra for (a) PVDF$_{250K}$, (b) PVDF-g-PtBMA, and (c) PVDF-g-PMAA. Resonances s_n are solvent peaks due to deuterated DMF. Quantitative hydrolysis of PtBMA to PMAA is confirmed by the disappearance in (c) of the t-butyl peak b and the appearance of the acid proton peak e.

99
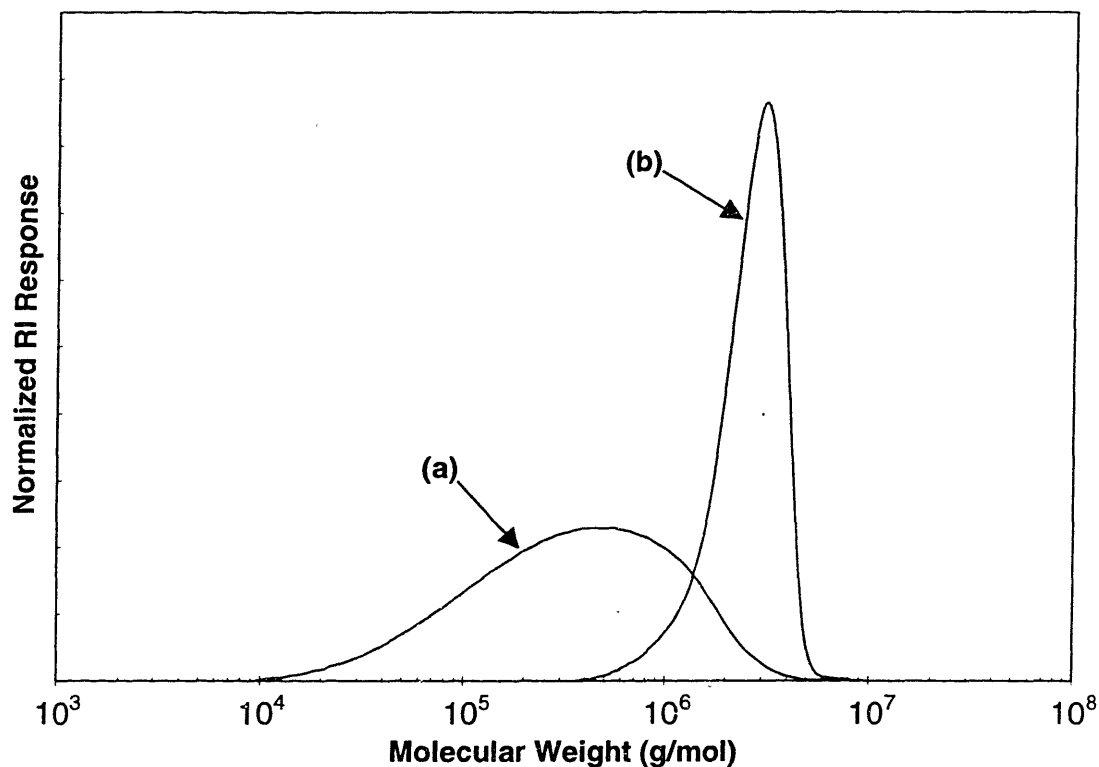
Figure 3.10 GPC traces of PVDF and PVDF-g-PMAA

(a) PVDF$_{250K}$, parent polymer of (b) PVDF-g-PMAA. The molecular weight scale was calibrated using PMMA standards.

Molecular Weight. GPC of PVDF-g-PMAA was conducted in DMF containing

1% lithium nitrate at 30°C, using PMMA standards. GPC traces of PVDF$_{250K}$ and

PVDF-g-PMAA appear in Figure 3.10, where it can be seen that the grafting reaction

results in a significant molecular weight increase. Unlike PVDF-g-POEM, the molecular

weight distribution of PVDF-g-PMAA is monomodal, providing evidence of neither

homopolymerization nor radical-radical coupling reactions. As with PVDF-g-POEM,

above, a more accurate estimate of the number-average molecular weight of PVDF-g-

PMAA was obtained from the NMR data using Equation 3.10. The molecular weight is reported in Table 3.1.

Crystallinity. DSC was conducted on PVDF-*g*-PMAA using the procedure described for PVDF-*g*-POEM[b] in Section 3.1.4. A DSC thermogram of PVDF-*g*-PMAA, exhibiting a clear crystalline melting peak, appears in Figure 3.7. Unlike PVDF-*g*-POEM[b], the melting point of PVDF-*g*-PMAA is not appreciably depressed compared to PVDF homopolymer. This result clearly shows that MAA units, accounting for 49 wt % (42 mol %) of the graft copolymer by NMR, are not grafted singly to the PVDF backbone. Such an architecture, with roughly 4 of every 5 PVDF repeat units having a pendant MAA unit, would not be expected to crystallize. Rather, the observed absence of appreciable melting depression might be expected if the PMAA grafting points along the PVDF backbone are infrequent.[171] Indeed, results presented in Chapter 5 will show that ATRP grafting of MAA onto PVDF results in long PMAA side chains, in contrast to the behavior of the PVDF/POEM system suggested by the TEM results in the previous section. A hypothesis for this apparent difference in polymerization kinetics is that, in the PVDF/POEM system, steric hindrance of the terminal tertiary halogenated carbon atom of the growing side chain by the pendant PEO chain (see Figure 3.4) reduces the reactivity of that site relative to the corresponding site in the PVDF/MAA system.

Thermal Stability. PVDF-*g*-PMAA exhibits the same thermal instability with respect to crosslinking noted for PVDF-*g*-POEM (Section 3.1.4).

3.2 Sample Preparation

3.2.1 Membranes

The casting solution compositions and preparation conditions for all membranes are listed in Table 3.4. A number of membranes were prepared for "exploratory studies." The objective of these studies was to determine the influence of P(MMA-r-POEM) architecture and concentration, as well as various processing parameters, on membrane morphology, surface composition, and static protein adsorption resistance. Once optimal comb polymer attributes and processing conditions had been identified, membranes were prepared for filtration studies designed to quantify the practical benefits achievable through self-organization. The preparation of membranes for filtration studies included the addition of a nonsolvent component (glycerol) to the casting solution for fine control of pore size,[220] as well as steps designed to prevent defect formation during membrane casting.

In Table 3.4, membrane types are named according to the general format, A-B-C-D. The first letter, A, indicates whether the membrane is an "exploratory" membrane (E) or a filtration membrane (F). The number B indicates the bulk concentration of the comb additive in weight percent. The third set of characters, C, specifies the particular additive polymer used or, in the case of pure PVDF membranes, a unique number to distinguish it from other pure PVDF membranes. The number D indicates the temperature of the coagulation bath in degrees Celsius.

Table 3.4 Membrane Casting Solution Compositions and Preparation Conditions

Membrane ID	$\phi_{w,b}$[†]	Casting Solution Composition (wt %)				Casting Temp. (°C)	Gate Size (mil)
		PVDF	Additive	Glycerol	Solvent		
E-00-1-20	Pure PVDF	10.00 (534K)	-	–	90.00 (DMF)	20	-
E-02-9a-20	2% P(MMA-r-POEM₉)[a]	10.00 (534K)	0.20	-	89.80 (DMF)	20	-
E-05-9a-20	5% P(MMA-r-POEM₉)[a]	10.00 (534K)	0.53	-	89.47 (DMF)	20	-
E-10-9a-20	10% P(MMA-r-POEM₉)[a]	10.00 (534K)	1.11	-	88.89 (DMF)	20	-
E-20-9a-20	20% P(MMA-r-POEM₉)[a]	10.00 (534K)	2.50	-	89.47 (DMF)	20	-
E-05-9b-20	5% P(MMA-r-POEM₉)[b]	10.00 (534K)	0.53	-	89.47 (DMF)	20	-
E-05-9c-20	5% P(MMA-r-POEM₉)[c]	10.00 (534K)	0.53	-	89.47 (DMF)	20	-
E-05-9d-20	5% P(MMA-r-POEM₉)[d]	10.00 (534K)	0.53	-	89.47 (DMF)	20	-
E-05-9e-20	5% P(MMA-r-POEM₉)[e]	10.00 (534K)	0.53	-	89.47 (DMF)	20	-
E-05-9f-20	5% P(MMA-r-POEM₉)[f]	10.00 (534K)	0.53	-	89.47 (DMF)	20	-
E-05-9b-90	5% P(MMA-r-POEM₉)[b]	10.00 (534K)	0.53	-	89.47 (DMF)	90	-
E-05-9c-90	5% P(MMA-r-POEM₉)[c]	10.00 (534K)	0.53	-	89.47 (DMF)	90	-
E-05-9d-90	5% P(MMA-r-POEM₉)[d]	10.00 (534K)	0.53	-	89.47 (DMF)	90	-
E-05-9e-90	5% P(MMA-r-POEM₉)[e]	10.00 (534K)	0.53	-	89.47 (DMF)	90	-
E-05-9f-90	5% P(MMA-r-POEM₉)[f]	10.00 (534K)	0.53	-	89.47 (DMF)	90	-
E-05-9g-90	5% P(MMA-r-POEM₉)[g]	10.00 (534K)	0.53	-	89.47 (DMF)	90	-
E-05-9h-90	5% P(MMA-r-POEM₉)[h]	10.00 (534K)	0.53	-	89.47 (DMF)	90	-
E-05-9i-90	5% P(MMA-r-POEM₉)[i]	10.00 (534K)	0.53	-	89.47 (DMF)	90	-
E-05-9j-90	5% P(MMA-r-POEM₉)[j]	10.00 (534K)	0.53	-	87.50 (DMF)	90	-
F-10-9i-90	10% P(MMA-r-POEM₉)[i]	18.00 (534K)	2.00	2.00	78.00 (DMF)	90	20
F-00-1-90[‡]	Pure PVDF	18.00 (534K)	-	1.00	81.00 (DMAc)	90	8
F-10-9k1-90[‡]	10% P(MMA-r-POEM₉)[k]	18.00 (534K)	2.00	1.00	79.00 (DMAc)	90	8
F-00-2-90	Pure PVDF	18.00 (534K)	-	3.00	79.00 (NMP)	90	20
F-10-5-90	10% P(MMA-r-POEM₅)	18.00 (534K)	2.00	2.50	77.50 (NMP)	90	20
F-10-9k2-90	10% P(MMA-r-POEM₉)[k]	18.00 (534K)	2.00	2.50	77.50 (NMP)	90	20
F-10-45-90	10% P(MMA-r-POEM₄₅)	18.00 (534K)	2.00	0.50	79.50 (NMP)	90	20
F-10-MA-90	10% P(MA-r-POEM₉-r-HPC₃M₁₀)	18.00 (534K)	2.00	1.00	79.00 (DMAc)	90	8
F-00-3-90	Pure PVDF	18.00 (534K)	-	1.00	81.00 (DMAc)	90	8
F-10-AT1-90	10% PVDF-g-POEM[a]	18.00 (534K)	2.00	1.00	79.00 (DMAc)	90	8
F-05-AT2-90	5% PVDF-g-POEM[h]	18.00 (534K)	0.95	1.00	80.05 (DMAc)	90	8
F-10-AT2-90	10% PVDF-g-POEM[b]	18.00 (534K)	2.00	1.00	79.00 (DMAc)	90	8
F-00-4-90	Pure PVDF	18.00 (250K)	-	10.00	72.00 (DMAc)	90	8
F-10-PE-90	10% PVDF-g-PMAA	18.00 (250K)	2.00	10.00	70.00 (DMAc)	90	8

[†] $\phi_{w,b}$ = bulk wt % comb additive

[‡] Cast into coagulation baths containing various concentrations of DMAc or CaCl₂ (see Section 4.3.2)

Materials

PVDF₅₃₄ₖ ($\overline{M}_w$ ca. 534 000 g/mol), PVDF₂₅₀ₖ ($\overline{M}_n$ ca. 107 000 g/mol, $\overline{M}_w$ ca. 250 000 g/mol), DMF (reagent grade), NMP (reagent grade), and DMAc (reagent grade) were purchased from Aldrich and used as received. Glycerol was obtained from VWR.

Deionized water (dW) was prepared using a Millipore (Bedford, MA) Milli-Q filtration system and had a resistivity of 18.2 MΩ cm.

Membranes for Exploratory Studies

Exploratory (E-series) membranes were prepared from casting solutions containing $PVDF_{534K}$, comb additive, and solvent according to the following general protocol. The casting solution was cast by pipette onto a glass plate having a raised lip around its edge. The plate was briefly placed on a flat surface to level the solution, then immediately immersed in dW at 20 or 90°C. The membrane was left in the water bath for ~10 min after complete separation from the glass plate and then rinsed in a second bath of dW. Some membranes were subsequently annealed at 90 ± 1°C while immersed in dW. Membranes for morphology and surface composition studies were freeze-dried (Genesis 25LE, Virtis) and held under vacuum at least overnight. Membranes for static protein adsorption studies were stored in dW until use.

Membranes for Surface Regeneration Studies

In Section 5.2, we consider the possibility of "self-healing" membranes, the surface chemistries of which, if chemically damaged during aggressive chemical cleaning procedures or by exposure to aggressive feed species, might be regenerated by surface segregation of residual comb additive in the bulk during a subsequent heat treatment in water. To simulate the effects of multiple acid cleaning procedures or long-term exposure to oxidants in the feed water, wet membranes E-00-1-20, E-05-9a-20, and E-10-9a-20, as well as a sample of pure $P(MMA-r-POEM_9)$[a], were immersed for 30 min in chromic-sulfuric acid (CSA, "Klean-AR," VWR). The membranes were then heat

treated while immersed in water for 12 h at $90 \pm 1°C$. Samples for analysis were cut from these membranes before acid treatment, after acid treatment, and after subsequent heat treatment.

Membranes for Filtration Studies

Membranes for filtration studies (F-series) were prepared from casting solutions containing $PVDF_{534K}$ or $PVDF_{250K}$, comb additive, glycerol, and solvent according to the compositions listed in Table 3.4. For the purposes of some filtration studies, it was desirable to obtain membranes having different compositions but similar pore sizes.
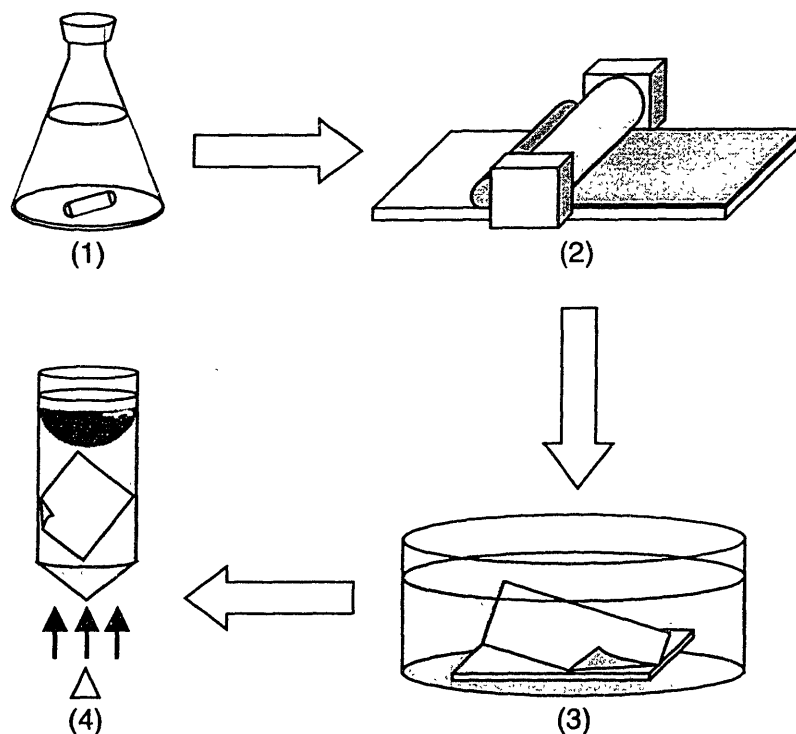
Figure 3.11 Schematic of the lab-scale membrane fabrication process
(1) Casting solution containing polymer(s), solvent, and glycerol is homogenized with a magnetic stirbar and heated at 50-70°C to degas it. The casting solution is passed through a 10 μm glass fiber filter, then (2) spread onto an optical mirror using a casting bar with an 8 or 20-mil gate size. (3) The mirror is immersed in a water bath typically at 90°C. The membrane precipitates and separates from the glass. (4) The membrane may be heat treated while immersed in water, using a wire mesh to prevent the membrane from floating.

Incorporation of glycerol, a "pore forming" component,[53,220] in the casting solutions at concentrations of 0.5-10% by mass enabled fine control of pore size. A nonsolvent for the polymer component(s) of the casting solution, the pore forming component moves the initial composition of the casting solution closer to the binodal[53] (Figure 2.7), resulting in phase separation at earlier times and thus lower overall polymer concentrations. Thus, pore size typically increases with increasing concentration of the pore former.

The principal steps in the lab-scale filtration membrane fabrication process are illustrated in Figure 3.11. To remove any dust particles which might serve as nucleation sites for bubbles or defects during the coagulation step of the casting process, each solution was passed through a 10 μm, binder-free, glass fiber filter (Type APFD Prefilter, Millipore) by means of a stainless steel filter holder (Millipore) pressurized with nitrogen gas. Each solution was degassed by heating it to 50-70°C for at least 4 h until no gas bubbles were visible. It was then cast onto a 3⅜" x 5" first surface optical mirror (Edmund Scientific Co., Barrington, NJ) under a cylindrical casting bar (see machine drawing, Appendix E) having an 8-mil or 20-mil gate size. The optically-smooth surface of the mirror inhibited nucleation of bubbles on its surface during membrane coagulation. Once the solution was cast, the mirror was immediately immersed in a bath of dW at 90°C. The membrane was left in the water bath for ~10 min after complete separation from the mirror, then immersed for 30 min in a second dW bath at 20°C. Some membranes were subsequently autoclaved (Market Forge Sterilmatic, Everett, MA) for 1 h at 121°C while immersed in dW. Wet membranes were placed on a Teflon sheet, and

circles having a diameter of 25 mm were cut from them using a cylindrical die (machine drawing, Appendix E) and a mallet. These circular sections were dried in air at 20°C.

3.2.2 Evaporation Cast Films

Polymer films for XPS studies were prepared on glass coverslips by evaporation casting. Polymers were dissolved in DMAc at a concentration of 0.05 g/mL. DMAc was then evaporated slowly from the resulting solution at room temperature over a period of ~48 h. Finally, the polymer films were held under vacuum for 4 days to remove residual solvent. Due to the low volatility of DMAc and the consequently long evaporation times, the surface compositions of the resulting films were expected to be equilibrium compositions.

3.3 Sample Characterization

3.3.1 X-ray Photoelectron Spectroscopy

Introduction

The near-surface compositions of membranes were determined using XPS. XPS is sensitive to only the first 30-100 Å of the sample surface[221] and, under ideal conditions, enables elemental analysis of polymeric material surfaces with a sensitivity of up to 0.3 percent,[222] as well as determination of the bonding environments present in the near-surface region of the sample.[223-225]

Figure 3.12 is a schematic diagram of the XPS analysis geometry. The sample is irradiated with X-ray photons of energy $h\nu$, some of which excite and eject core-level electrons within the sample. The ejected core electrons, called *photoelectrons*, are

collected and their kinetic energies are recorded. For insulating samples, a charge compensation grid above the sample, which is held at a potential of ~5 eV, supplies electrons to replace the ejected photoelectrons. Neglecting known constants particular to the spectrometer, the kinetic energy of a photoelectron is given by,[221,223,224]

$$KE = h\nu - BE - s \tag{3.14}$$

where $h\nu$ is the energy of the incident photon, BE is the binding energy of the photo-ejected electron, and s is a small correction factor (on the order of a few eV) to account for surface charging, as well as the presence of the charge compensation grid. Since $h\nu$ is
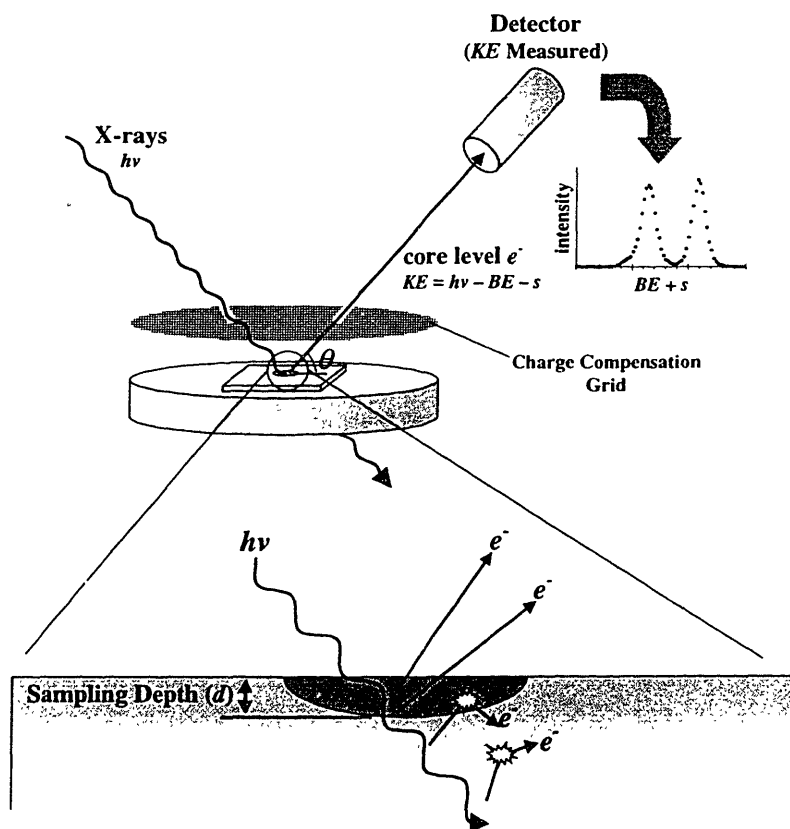
Figure 3.12 Schematic diagram of the XPS analysis geometry

known, measurement of *KE* returns the approximate *BE* of the ejected core electron, which is characteristic of both the element and bonding environment of its origination. The extreme surface sensitivity of XPS results from the fact that only photoelectrons ejected near the surface escape from the sample without undergoing inelastic collisions, so retaining their original *KE* values and contributing to recognizable peaks in the XPS spectrum. The *sampling depth, d,* defined as the depth from which 95% of the detected photoelectrons originate, is a function of the sample material, the photoelectron *KE,* and the photoelectron takeoff angle, θ, and typically ranges between 30 and 100 Å for polymeric samples.[221]

As the value of *s* is generally unknown, XPS data are commonly calibrated based on the photoelectron signal belonging to a known internal reference bonding environment, providing a plot of photoelectron intensity vs. *BE.*[226] A convenient reference environment is the saturated, unfunctionalized C 1s environment. While this environment is present in most polymers, it is also present in the XPS vacuum pump oil, a small amount of which contaminates most samples. Thus, this bonding environment is usually available as an internal reference, and it is conventionally assigned a *BE* of 285.00 eV.[225] All XPS data in this thesis are calibrated in this manner. The *BE* values for a number of elements are listed in Table 3.5.

Table 3.5 XPS Binding Energies for Various Elements

Element	BE (eV)
Au (4f)	86
C (1s)	285
N (1s)	399
O (1s)	531
F (1s)	685

Bonding environment speciation using XPS is accomplished by conducting a high-resolution scan in a small range of BE (~20 eV) centered on the element of interest. For a given element and electron shell, small *chemical shifts* in BE arise due to variations in the magnitude of electrostatic screening which inner shell electrons experience when valence electrons participate in chemical bonds.[221,223] Figure 3.13 is a high-resolution plot of the C 1s region of the XPS spectrum for PVDF. It is readily apparent that the C 1s signal is a sum of two principal peaks due to the $-CH_2-$ and $-CF_2-$ bonding environments, respectively, present in PVDF.[225] The small third peak, assigned a BE of 285.00 eV, arises from hydrocarbon contamination. Quantification of the surface chemistry of a sample is accomplished by curve fitting the high-resolution XPS data with a theoretical model which is a sum of separate Gaussian-Lorentzian sum functions, one for each bonding environment expected.[225] The near-surface molar concentrations of the various bonding environments are then given by the relative areal ratios of the corresponding peaks. The C 1s data for PVDF (Figure 3.13) can be fit with two peaks of equal area, as expected from its stoichiometry.

Experimental Details

The XPS data presented in this thesis were collected on a Surface Science Instruments SSX-100 spectrometer (Mountain View, CA) using monochromatic Al Kα X-rays (hv = 1486.7 eV) with an electron takeoff angle of θ = 45° relative to the sample plane. Charge compensation was provided by a Ni grid mounted 2-3 mm above the sample, which was held at a constant potential of 5 eV. Survey spectra were run in the
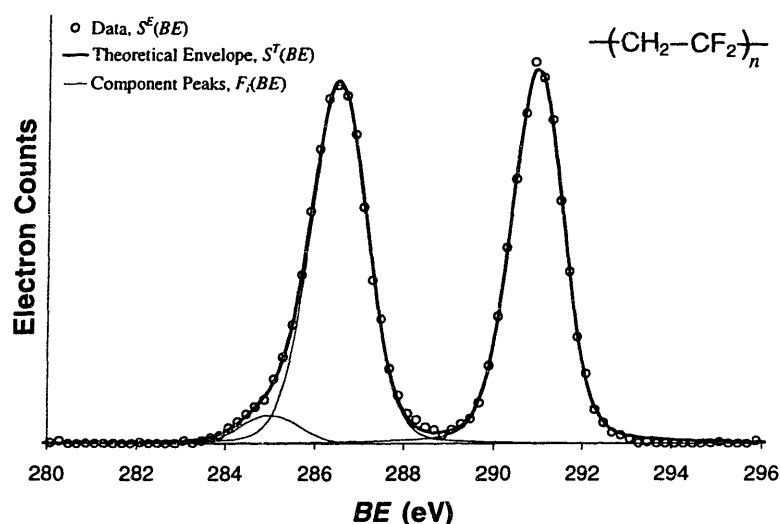
Figure 3.13 Example fit of the C 1s region of the XPS spectrum for PVDF

BE range 0-1000 eV, while high-resolution spectra of the C 1s region were run in the BE

range 277-297 eV. Peak fitting of the high-resolution data was conducted with a linearly

subtracted background and with each peak described by a Gaussian-Lorentzian sum

function,

$$F(BE) = 2A \left\{ \frac{m\sqrt{\ln 2}}{W\sqrt{\pi}} \exp\left[-4\ln 2\left(\frac{BE - BE_o}{W} \right)^2 \right] + \frac{1-m}{\pi W\left[1 + 4\left(\frac{BE - BE_o}{W} \right)^2 \right]} \right\} \quad (3.15)$$

where $F(BE)$ is the intensity at binding energy BE, A is the peak area, BE_o is the peak

center, W is the full-width at half-maximum, and m is the Gaussian-Lorentzian mixing

ratio (1 = pure Gaussian, 0 = pure Lorentzian).

Peak fitting was accomplished using the computer code presented in Appendix F.

This computer code has the advantage over many currently available software packages

that it allows the constraint of peak area ratios to non-integer values other than 1. Peak fitting was conducted using the following general procedure:

1. The structure of the polymer repeat unit(s) and known chemical shifts from the literature were used to determine the number, positions, and area ratios of component peaks to create a theoretical model of the intensity vs. BE envelope.

2. Initial values for E_o, W, m, and A were input for each component. The positions of all component peaks were fixed relative to that of the hydrocarbon peak at 285.00 eV, which was allowed to vary. The area ratios were fixed at their ideal stoichiometric values. The mixing ratio m was constrained between 0.7 and 1.0 for all fits, a range appropriate to the monochromated Al Kα line shape.[225] Good fits were obtained with peak widths W ranging from 1.0 to 1.6 eV.

3. Fitting was conducted by iteratively stepping each of the unconstrained parameters up and down within an appropriate range and with a defined step size, so as to minimize the sum of squared errors,

$$SSE = \sum_{BE} \left[S^T(BE) - S^E(BE) \right]^2 \qquad (3.16)$$

where $S^T(BE)$ and $S^E(BE)$ are the theoretical and experimental photoelectron intensities, respectively, at binding energy BE and $S^T(BE)$ is given by,

$$S^T(BE) = \sum_{i=1}^{N} F_i(BE) \qquad (3.17)$$

where N is the number of peaks in the model spectrum and $F_i(BE)$ is given by Equation 3.15. With BE in units of eV, peak areas A were fit with a step size of 1, while all other parameters were fit with a step size of 0.01.

4. Once the fit had converged subject to the imposed constraints, the relative peak positions E_o were sometimes allowed to float ±0.1 eV, and the constraints on area ratios were sometimes relaxed where appropriate. This refined the fit and allowed for the possibility of non-stoichiometric area ratios. Non-stoichiometric area ratios might be expected, for example, in the case of a polymer repeat unit containing a pendant side chain that is expressed at the sample surface more or less than the polymer backbone.[188]

3.3.2 Contact Angle and Wetting Time Measurements

Water contact angle measurements were performed to assess the relative hydrophilicity and water wettability of polymer membranes. Contact angles were measured using an Advanced Surface Technologies, Inc. VCA2000 video contact angle system in the laboratory of Prof. Michael F. Rubner at MIT. Each sample was raised toward a 1-μL droplet of dW suspended from the tip of a syringe until the droplet was transferred to the sample surface. Advancing contact angles were then measured after adding dW to the droplet in 1-μL increments until its edges were observed to advance over the surface. For spontaneously wettable membranes, the contact angle of a droplet of dW placed on the surface was observed to decrease over time, until the water eventually wetted through the membrane. The "wetting time" of such membranes was defined as the time required for the contact angle of a 1-μL water droplet to reach 0°.

3.3.3 Scanning Electron Microscopy

Field emission scanning electron microscopy (FESEM) was used for the characterization of membrane separation surface and cross-sectional morphologies. Fracture surfaces for cross-sectional imaging were prepared by cracking membranes under liquid nitrogen. To prevent surface charge build-up on the insulating samples, all samples were coated either with ~200 Å of carbon by thermal evaporation (Ladd vacuum evaporator, Ladd Research Industries, Burlington, VT) or with ~50 Å of gold-palladium by sputtering (Pelco SC-7 Auto Sputter Coater). Coated membranes were examined using a JEOL 6320 FESEM, with an accelerating voltage of 1 kV.

Membrane separation surface pore size distributions were constructed directly from digitized FESEM images using the Image-Pro® Plus software package. Once a set of "objects" in an image has been identified, this software package is capable of generating a number of statistics from them, including statistics on the object diameters and areas. The most difficult part of the process is *binarization* of the raw greyscale image to identify the objects (in the case of this thesis, the "objects" are pores). That is, all image pixels inside the pores must be made "black" and all pixels outside the pores must be made "white."

A common method for binarizing images is thresholding.[227] The contrast level of each pixel in a digital greyscale image is defined by an integer value between 0 and 255, where 0 is "black" and 255 is "white." A thresholding algorithm simply sets to 0 any pixels having values below a user-defined threshold value, while all other pixels are set to 255. Thresholding algorithms are thus capable of quickly binarizing images satisfying the following requirements:

a) the "objects" must have a contrast level substantially different from the remainder of the image,

b) interfaces between "object" and "not object" should be relatively sharp, and

c) the image should have a relatively flat background, in terms of contrast.

Thresholding algorithms failing, commercial software packages allow the user to binarize images by the tedious task of manually tracing object edges using a mouse.

Used alone, thresholding was found to be an unsatisfactory method for binarizing images of membrane separation surfaces, due to the fact that most of the images

114

contained regions outside of pores which were actually darker in contrast level than regions inside pores. This circumstance has three probable causes:

1. regions outside the pores may be "shadowed" due to surface topography,

2. pores leading to channels which bend sharply within ~200 Å of the surface may appear bright due to the escape of secondary electrons from the inside surface of the pore channel, and

3. regions outside the pores may appear dark due to lateral passage of pore channels beneath the surface at a distance less than the ejection depth of secondary electrons.

Many of the pores in a typical separation surface image were effectively identified by thesholding, using a threshold greyscale intensity less than ~50. Usually, it was then necessary to identify remaining pores manually. Manual identification was potentially highly subjective, since the identification of pores in the original image, particularly those less than ~20 nm in diameter, was often ambiguous.

It was found that the subjective nature of pore identification could be greatly reduced by the application of a *Sobel filter* to the raw FESEM image using the Image-Pro® Plus software. A *filter* is a mathematical operation performed on an image to produce a modified image. The Sobel filter is a *neighborhood operation*[228] – the greyscale intensity (0-255) of each pixel in the modified image is a function of the intensities of the pixels neighboring the corresponding pixel in the raw image. Consider a neighborhood of pixels numbered 0-8 in the raw image (Figure 3.14):

1	2	3
8	0	4
7	6	5

Figure 3.14 Square neighborhood of 9 pixels in a raw FESEM image

Using the Sobel filter, the greyscale intensity of pixel 0 in the modified image is given by,[229,230]

$$G_0^S = \left(X^2 + Y^2\right)^{1/2} \tag{3.18}$$

where

$$X = \left(G_3 + 2G_4 + G_5\right) - \left(G_1 + 2G_8 + G_7\right) \tag{3.19}$$

and

$$Y = \left(G_1 + 2G_2 + G_3\right) - \left(G_7 + 2G_6 + G_5\right) \tag{3.20}$$

and G_n is the greyscale intensity of pixel n in the raw image. The Sobel filter has the effect of highlighting the gradients in pixel intensity which occur near the edges of pores. The image resulting from application of the Sobel filter to the original provided a relatively objective criterion for identifying pores to be measured. Only those pores which clearly appeared as sharp, continuous "rings" in the Sobel image were selected for measurement. Figure 3.15 displays an example raw image obtained by FESEM, the corresponding Sobel image, and the final binarized image used for statistics compilation.

3.3.4 Bubble Point Measurements

The bubble-point test is a simple, nondestructive method to assess the integrity of a filtration membrane. This test is based on the fact that the minimum pressure required to force a liquid out of a capillary is inversely proportional to the capillary diameter. A membrane is thus wet with a suitable liquid and placed in a holder in such a way that a layer of liquid covers one side of the membrane. A gas pressure is then applied to the opposite side of the membrane. This gas pressure is increased slowly until, at the *bubble*

116
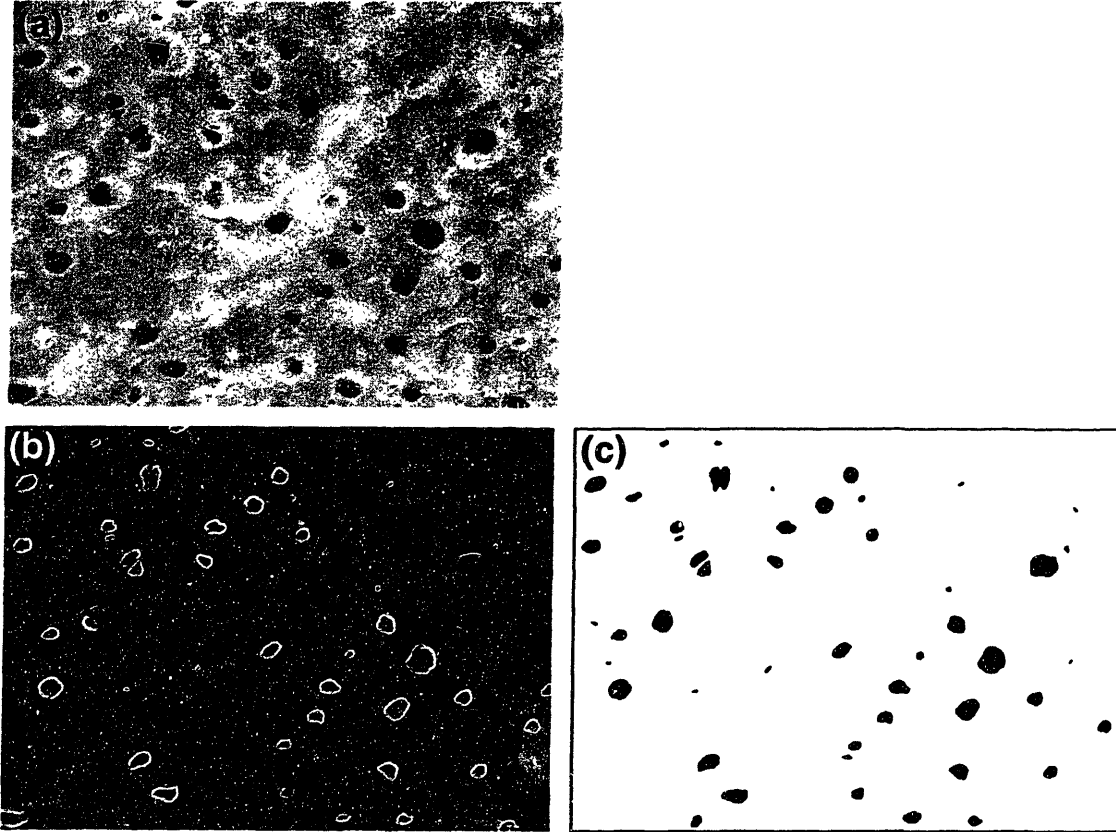
Figure 3.15 Example FESEM raw and processed images of membrane surface
(a) Example FESEM raw image of a membrane surface, (b) the same image after application of a Sobel filter to highlight pore edges, and (c) final binarized image used for computation of pore size and porosity statistics.

point pressure (P_{bp}), liquid is displaced from the largest pore and bubbles appear on the wet side of the membrane. For a straight, cylindrical pore channel, the bubble point pressure is related to the pore diameter (D) by the equation,[42,231]

$$P_{bp} = \frac{4\gamma\cos\theta}{D} \tag{3.21}$$

where γ is the surface tension of the liquid and θ is the solid-liquid contact angle. In reality, the pore channels of membranes prepared by immersion precipitation are neither

straight nor cylindrical, and the use of bubble point measurements to determine actual pore sizes requires a large set of empirical data relating measured bubble point pressures to pore sizes determined using an independent method. Direct observation of pores by FESEM, as described in Section 3.3.3, is better suited to pore size quantification for the purposes of this thesis.

However, bubble point measurements are extremely useful as a rapid method to test membranes for large defects prior to filtration testing. Membranes for use in UF experiments (described in Section 3.3.6) were immersed in methanol for ~30 min. They were then placed in an Amicon 8010 UF cell (described in detail in section 3.3.6) with the separation surface facing down. A short length of Tygon tubing was attached to the outlet of the cell. The cell was then filled with 1-2 mL of methanol and closed. An initial nitrogen pressure of 5 psig was applied to the cell by means of a nitrogen gas cylinder until all of the methanol in the cell was forced through the membrane and into the outlet tubing. The pressure was increased slowly until bubbles were observed in the outlet tubing. The pressure at which the first bubbles appeared, P_{bp}, was recorded. Though bubble point pressures varied with membrane type, membranes were generally deemed to be defect-free for $P_{bp} \geq 20$ psig. The presence of a defect "hole" typically resulted in a bubble point of $P_{bp} < 5$ psig.

3.3.5 Static Protein Adsorption Experiments

Introduction to XPS Techniques for Quantification of Adsorbed Protein

For initial evaluation of protein adsorption resistance, membranes were incubated for a prescribed period in a solution containing bovine serum albumin (BSA). The surface concentration of protein was then assessed by XPS, using one of two general methods. According to one method, the cationic BSA was labeled using anionic colloidal gold, and the surface concentration of the gold label was quantified using XPS. This gold staining technique was originally developed for the staining of proteins on immunoblots,[232] and has been used previously to stain proteins on fouled MF membranes.[101] According to the other method used in this thesis, XPS was simply used to quantify nitrogen occurring naturally in BSA. The first method has the advantage that the level of gold staining can we qualitatively evaluated prior to XPS analysis by visual observation of the intensity of red color produced on the sample. This is useful for rapid determination of protein concentrations and incubation times resulting in good differentiation between the samples. In addition, smaller surface concentrations of BSA should be detectable using the gold staining method, since XPS is roughly 5 times as sensitive to Au 4f electrons as it is to N 1s electrons.[233,234] The second method has the obvious advantage that it is more direct, and complications arising from the possibility of nonspecific background staining of the colloidal gold label are avoided.

Compared to alternative methods for assessing protein adsorption resistance, such as radiocounting of adsorbed radiolabeled protein[235] or spectroscopy of adsorbed and eluted chromophore-labeled protein,[104] the XPS techniques used here have the benefit that

119

they probe protein adsorption solely on or near the membrane separation surface and not on the internal pore channels deep within the membrane. This is vital for the purposes of this thesis, since membrane morphology studies (Section 4.3) will show that the internal surface area available for protein adsorption may vary significantly with membrane composition. For the purposes of exploratory protein adsorption resistance sudies, it was desirable to assess protein adsorption as a function of membrane *surface composition* only.

Membranes Modified with P(MMA-*r*-POEM₉)[a]

As-cast membranes of types E-00-1-20, E-02-9a-20, E-05-9a-20, E-10-9a-20, and E-20-9a-20 (Table 3.4) were first washed with PBS for 1 h, then incubated at room temperature in PBS containing 10.0 g/L BSA (Fraction V, Sigma) for 12 h on a rocking table rotating at 33⅓ rpm. Corresponding control membranes were incubated in PBS containing no BSA. After this static fouling step, all membranes were washed for 5 min in three changes of PBS. Both fouled and control membranes were stained for total protein detection using anionic colloidal gold (pH 4, Zymed Laboratories). The anionic colloidal gold particles bind electrostatically to positively charged groups which exist on BSA at pH 4.[236] Fouled and control membranes were washed for 5 min with two changes of PBS containing 0.3% (w/v) polyoxyethylenesorbitan monolaurate (Tween 20, Zymed Labs) as a blocking agent. They were then incubated in PBS + Tween 20 for 1 h at 37°C and finally washed for 5 min in two changes of PBS + Tween 20 and three changes of dW. Tween 20 is a nonionic surfactant, the purpose of which is to "block" hydrophobic sites on the membrane surface to prevent nonspecific staining by colloidal gold due to the

hydrophobic effect. After the blocking step, fouled and control membranes were incubated in anionic colloidal gold for 4 h on a rocking table at room temperature, then rinsed for 5 min in three changes of dW. Finally, the gold-stained membranes were freeze-dried. Surface coverage of the gold label was quantified using XPS. Survey spectra were run in the *BE* range 0-1000 eV, and the near-surface atomic compositions were determined using numerically integrated peak areas and applying standard sensitivity coefficients.

Membranes Modified with PVDF-*g*-POEM

Membranes of types F-00-3-90, F-05-AT2-90, and F-10-AT2-90 (Table 3.4) were first hydrated by immersion in methanol for 30 min followed by immersion in dW. Membranes were washed with PBS for 1 h, then incubated in PBS containing 10.0 g/L BSA for 24 h at room temperature. After this static fouling step, membranes were washed for 5 min in three changes of PBS followed by three changes of dW. Finally, samples were dried under vacuum at room temperature. The near-surface concentration of nitrogen occurring in BSA was quantified using XPS. Survey spectra were run in the *BE* range 0-1000 eV, and the near-surface atomic compositions were determined using numerically integrated peak areas and applying standard sensitivity coefficients.

3.3.6 Ultrafiltration Experiments

Figure 3.16 is a schematic of the apparatus used for filtration experiments. A 25-mm diameter circular membrane was mounted in an Amicon 8010 stirred, dead-end UF cell (Millipore) having an effective filtration area of 4.1 cm^2. Delivery of feed solution to the cell was provided by a stainless steel dispensing pressure vessel
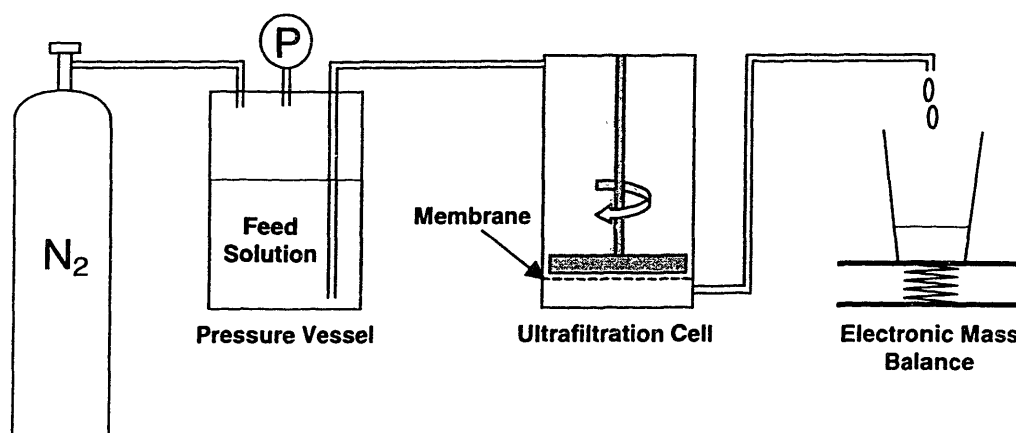
Figure 3.16 Schematic diagram of laboratory filtration apparatus

(Millipore) pressurized by a nitrogen cylinder. To simulate the flow conditions in an actual filtration operation, a stir bar mounted above the membrane worked in conjunction with a speed-adjustable stir plate (VWR) to provide a constant and measured fluid velocity parallel to the membrane surface. Each membrane was prewet with methanol, then immersed in dW for 30 min before it was loaded into the cell.

Fouling Experiments

Membrane fouling resistance was assessed by measurement of the flux of a foulant solution as a function of time at a fixed trans-membrane pressure gradient. Even in the absence of fouling, pressure driven filtration of pure water typically results in a flux which initially decreases with time, eventually stabilizing at a relatively constant value.[86,87,105] The initially decreasing flux is due to compaction of the membrane pore channels under pressure. For assessment of fouling resistance, it is desirable to observe any flux decline due to fouling in isolation from the initial flux decline due to membrane

compaction. Thus, each membrane was pre-compacted by pressure-driven filtration of pure water prior to filtration of the foulant solution.

Each membrane was pre-compacted by filtration of dW at a pressure of 60 psig for 30 min, followed by filtration of dW at a pressure of 40 psig for 60 min. At a pressure of 40 psig, the dW flux was then measured gravimetrically until the mass of permeate eluted during two consecutive 5-min periods differed by less than 2 percent. This constant pure water flux (J_o) was recorded, after which the dW feed solution was exchanged for the foulant solution, a solution of 0.1 g/L BSA in PBS. The foulant solution was pressurized to 40 psig and the flux was measured periodically over a 3-h period. The flux over the final 10 min of the 3-h experiment was recorded as J_f. All of the above compaction and filtration steps were performed at 20°C with a stirring rate of 500 rpm. BSA concentrations in the feed and permeate were measured spectroscopically at 280 nm using a Cary 5E UV/Vis spectrophotometer (Varian Australia Pty Ltd).

pH Response Experiments

Buffered solutions of pH 2-8 were prepared by the addition of prepackaged buffer salts (Hydrion™, Aldrich) to dW. After mounting in the UF cell, the membrane was pre-compacted by filtration of pH 8 buffer at an elevated compaction pressure P_c for 60 min, followed by filtration of pH 8 buffer at the measurement pressure P_m for 30 min. The values of P_c and P_m, listed in Table 3.6, varied based on the membrane type.

Table 3.6 Compaction and Measurement Pressures Used in pH Response Studies

Membrane	P_c (psig)	P_m (psig)
F-00-4-90	70	50
F-10-PE-90	20	5

Following pre-compaction, the pressure vessel was emptied, such that nitrogen gas was delivered directly to the UF cell. The cell was then successively emptied and filled with buffers of various pH, and the flux of each solution was measured gravimetrically at pressure P_m. Each measurement consisted of a 1-min equilibration period, followed by a gravimetric flux measurement over a second 1-min period. To assess the reversibility of the pH response, the trans-membrane flux was first measured during 10 cycles consisting of a pH 8 measurement followed by a pH 2 measurement. Following this test, the pH dependence of the trans-membrane flux was quantified through successive measurements at pH 2-8, in intervals of one pH unit. All of the compaction and filtration steps were performed at 20°C with a stirring speed of 500 rpm.

3.3.7 Atomic Force Microscopy

AFM is a sensitive surface analysis technique which directly measures repulsive forces between atoms on a sample surface and those on a fine silicon nitride probe mounted on a cantilever spring.[237] In this thesis, AFM was used to measure the pH-dependence of the hydrated PMAA layer height on the surfaces of membranes having PVDF-g-PMAA surface segregated. All AFM data was collected by Solar Olugebefola in the Department of Materials Science and Engineering at MIT. The AFM apparatus employed was a Digital Instruments (Santa Barbara, CA) Nanoscope IIIa scanning probe microscope with a pyramidal probe (Digital Instruments) mounted on a V-shaped, silicon nitride cantilever having a spring constant of $k = 0.029$ N/m. The spring constant of the cantilever was determined by measurement of the resonant frequency of the tip as

described by Cleveland, *et al.*,[238] a method that has been shown to be accurate to within 0.002 N/m. The probe was mounted into a commercially available liquid cell (Digital Instruments) for immersion in water.

Membranes containing 10 wt % PVDF-*g*-PMAA (F-10-PE-90) and pure PVDF control membranes (F-00-4-90) were fixed to shallow plastic trays using double-sided tape. A few drops of buffer solution were placed on each membrane. Force-distance information was then obtained by operation of the AFM in "force mode." In this mode, translation of the probe parallel to the sample surface is suspended, and the sample is moved toward and away from the cantilever by the application of a sawtooth voltage to a piezoelectric crystal attached to the sample stage.[239] The vertical deflection (d_z) of the cantilever is monitored by means of a focused laser beam which is reflected from the rear of the cantilever onto a split photodiode.

The supplied AFM software outputs a data file containing the deflection of the cantilever as a function of the displacement (z) of the sample stage on the piezoelectric crystal. This raw data was converted to real force *vs.* separation data using a method described by Ducker, *et al.*,[240] which requires the definition of a position of zero force (F_o) and a position of zero separation (z_o) between the probe and the sample. Zero force is defined where the separation is large, and a change in sample position has no effect on tip deflection. Zero separation is defined as the position of "constant compliance," where the tip deflection becomes a linear function of separation as the tip is driven toward the sample. Force is obtained from the measured tip displacement using the known cantilever spring constant and Hooke's law,

$$F - F_o = k \cdot d_z \qquad\qquad (3.22)$$

3.3.8 Fluorescent Labeling and Fluorescence Microscopy

To evaluate the distribution of the surface-segregated additive polymer throughout the cross-section of a self-organizing membrane, membranes containing 10 wt % PVDF-g-PMAA (F-10-PE-90) and pure PVDF control membranes (F-00-4-90) were stained with acridine orange (AO), a cationic fluorescent molecule which is effective for labeling anionic carboxylic acid groups.[241] Staining solutions of AO (λ_{abs} = 500 nm, λ_{em} = 526 nm,[242] Molecular Probes, Inc., Eugene, OR) were prepared in PBS (0.01 M, pH 7.4) and stored at 4°C in the dark until use.

Membranes were stained using two complementary procedures. According to the first procedure, membranes were immersed in pure PBS for 1 h. Each membrane was then immersed in 50 mL of a staining solution containing 500 nM AO for 3.5 h at room temperature, with gentle stirring. At the end of this 3.5-h period, each membrane was transferred to 50 mL of fresh staining solution. Stirring was then continued for an additional 3.5 h, for a total of 7 h of staining. Finally, each membrane was rinsed in a large volume of pure PBS for 30 min, followed by dW for 1 h.

According to the second procedure, 25-mm diameter membrane discs were immersed in pure PBS for 30 min. Each membrane was then loaded into the UF filtration cell described in Section 3.3.6. The cell was filled with PBS, which was forced through the membrane for 30 min. The cell was then emptied and filled with a staining solution containing 1 µM AO, which was forced through the membrane for 1 h at a pressure resulting in a trans-membrane flux of 20 ± 2 L/m²h. After the staining step, the cell was

emptied and refilled with pure PBS, which was forced through the membrane for 30 min. Finally, each membrane was rinsed in dW for 1 h.

Stained membranes were embedded in paraffin and sectioned by Jason D. Burrill in the MIT Division of Comparative Medicine. Membranes were immersed in three changes of ethanol for 1 h each, followed by two changes of xylene for 1 h each and two changes of paraffin for 1.5 h each. They were then embedded in paraffin wax (Surgipath Formula R, Richmond, IL) and cut into 4-μm sections using a Leica 2125 microtome. The sections were placed on Stat Lab Superfrost Plus glass slides (Lewisville, TX).

The paraffin-embedded sections were imaged using a Zeiss Axiovert 135 fluorescence microscope (Carl Zeiss, Inc., Germany) with an FT 510 filter and a Hamamatsu digital CCD camera (C4742-95-12, Hamamatsu-City, Japan). The fluorescence image intensity was adjusted via an aperture and an electronic gain on the CCD array, both of which were computer-controlled. For each staining condition, identical aperture and CCD gain values were used for the collection of images of blend and control membranes. Some photobleaching of AO was observed. To ensure that all images were comparable, each image was therefore captured exactly 30 s after initial illumination of the section.

4. Implementation of Self-Organization During Membrane Fabrication

4.1 Introduction

This chapter explores the degree of surface segregation of a comb additive polymer obtainable during the preparation of membranes by the standard immersion precipitation process. Various process parameters (*i.e.*, coagulation bath composition and temperature, heat treatment time) are examined with respect to their effects on the surface composition of membranes prepared from self-organizing blends. In addition, elements of the comb polymer architecture (*i.e.*, molecular weight, side chain frequency) are optimized with the objective of achieving maximal surface coverage subject to the requirement of long-term surface stability. These studies are mainly confined to membranes containing P(MMA-*r*-POEM$_9$), due to its high degree of synthetic flexibility with regard to the architectural variables of interest. XPS is used extensively to relate architectural and process variables to membrane surface chemistry at the molecular level. The effects of casting solution and coagulation bath composition on the morphology of self-organizing membranes are explored using FESEM. In Chapter 5, the morphologies and surface chemistries of membranes cast under optimized conditions are related to their performance in practical applications.

4.2 Preparing Tailored Surfaces with Minimal Processing

4.2.1 Processing for Self-Organization

Surface Segregation During Coagulation and Heat Treatment

The surface compositions of membranes were determined by high-resolution analysis of the C 1s regions of their XPS spectra, as described in Section 3.3.1. For membranes containing P(MMA-*r*-POEM), the C 1s region of the XPS spectrum was fit with seven component peaks representing the various carbon bonding environments shown in Figure 4.1. The peak centers of the component peaks, referenced to the saturated, unfunctionalized hydrocarbon peak at 285.00 eV, were constrained ($\pm$0.1 eV) as shown in Table 4.1. These values correspond to values obtained from pure PVDF, PMMA, and PEO homopolymers using high-resolution instrumentation.[225] The areas of the CH_2 and CF_2 peaks were constrained to be equal, as required by stoichiometry, as were those of the C-COO, COO, and COO-C peaks of the methacrylate environment. The ratio of the C-O and COO peak areas was initially constrained to its ideal stoichiometric value, based on the composition of the comb additive from ^{1}H NMR. Once the peak-fitting routine converged, this constraint was released and fitting was
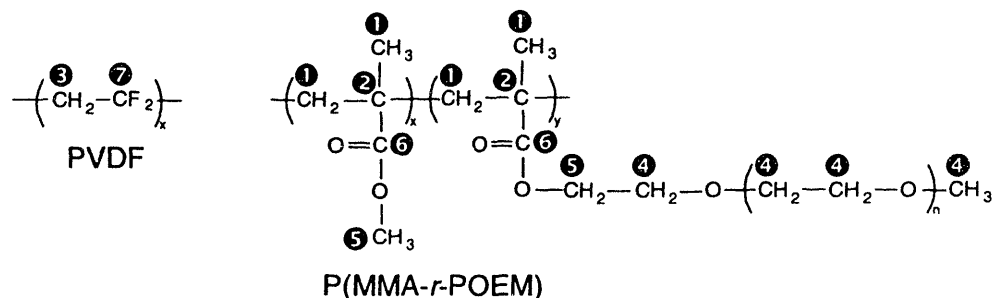
Figure 4.1 Carbon bonding environments present in PVDF and P(MMA-*r*-POEM)

continued in order to allow for the possibility of nonstoichiometric area ratios. Figure 4.2 shows example fitted C 1s envelopes for a pure PVDF membrane, pure P(MMA-r-POEM$_9$)[a], and a membrane containing 10% P(MMA-r-POEM$_9$)[a].

Table 4.1 XPS C 1s Bonding Environments in PVDF and P(MMA-r-POEM)

Carbon Environment (Fig. 4.1)	Carbon Environment Abbreviation	BE_o (eV)
1	HC	285.00
2	C-COO	285.72
3	CH_2 (PVDF)	286.44
4	C-O	286.45
5	COO-C	286.79
6	COO	289.03
7	CF$_2$	290.90

The near-surface mole fraction of P(MMA-r-POEM) was calculated as,

$$n_s = \frac{A_{\underline{C}OO}}{A_{\underline{C}F_2} + A_{\underline{C}OO}}$$

(4.1)

where A_x is the area of the peak for bonding environment x. The near-surface volume fraction of the comb additive was then approximated as,

$$\phi_s = \frac{n_s V_o^{comb}}{n_s V_o^{comb} + (1 - n_s) V_o^{PVDF}}$$

(4.2)

where V_o^x is the molar volume of polymer x per repeat unit. The repeat unit molar volume of the comb copolymer,

$$V_o^{comb} = \frac{\overline{M}_o^{comb}}{\rho_{comb}}$$

(4.3)

was estimated from the weighted averages of the repeat unit molar masses and bulk polymer densities of PMMA and PPOEM homopolymers,

$$\overline{M_o}^{comb} = X_{POEM} M_o^{PPOEM} + (1 - X_{POEM}) M_o^{PMMA} \tag{4.4}$$

and

$$\overline{\rho}_{comb} = W_{POEM} \rho_{PPOEM} + (1 - W_{POEM}) \rho_{PMMA} \tag{4.5}$$

where X_{POEM} and W_{POEM} are the mole fraction and weight fraction, respectively, of POEM in the comb copolymer.* The densities and repeat unit molar masses used in these calculations are given in Table 4.2. Unless otherwise noted, all XPS data presented below are taken from the side of the membrane facing the water bath during the coagulation step of the fabrication process. In practice, solutes are filtered from the feed solution via the dense separation surface on this "water-facing" side, and it is this surface composition that is of greatest practical interest with respect to fouling resistance. Component peak area percentages for all fitted XPS data are tabulated in Appendix C.

Table 4.2 Bulk Densities and Repeat Unit Molar Masses

	M_o (g/mol)	ρ (g/cm^3)‡
PMMA	100	1.19
PPOEM	300, 475, 2080†	1.08
PVDF	64	1.74

† for PPOEM$_5$, PPOEM$_9$, and PPOEM$_{45}$, respectively
‡ obtained from the manufacturer (Aldrich)

* The P(MMA-r-POEM) repeat unit molar volumes obtained using this simple estimation method differ by less than 3% from values obtained using the group contribution methods of van Krevelen.[243]

132
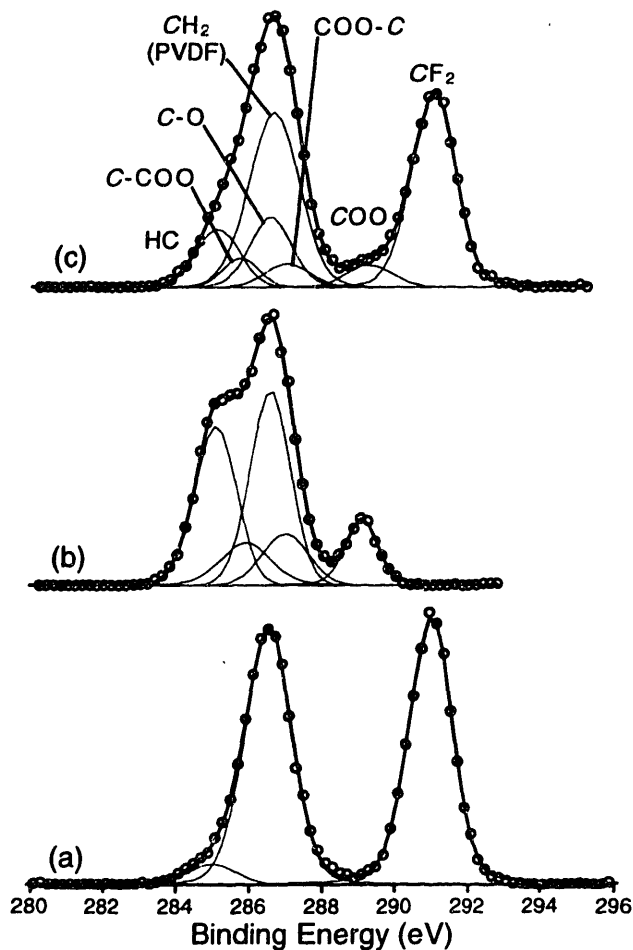
Figure 4.2 Fitted C 1s envelopes
(a) Pure PVDF membrane, (b) pure P(MMA-r-POEM9)[a], and (c) as-cast membrane E-10-9a-20, containing 10 wt % P(MMA-r-POEM9)[a] and cast at 20°C.

Figure 4.3 is a plot of near-surface concentration of P(MMA-r-POEM9)[a] versus bulk concentration (both as volume fractions) for unannealed membranes cast at 20°C, and for membranes cast at 20°C and subsequently annealed for 4 h, 12 h, and 24 h at 90°C while immersed in water. The solid line denotes the condition in which the bulk and surface compositions are equal $(\phi_s = \phi_b)$. Significant surface segregation of the comb additive is observed during the coagulation step of the immersion precipitation
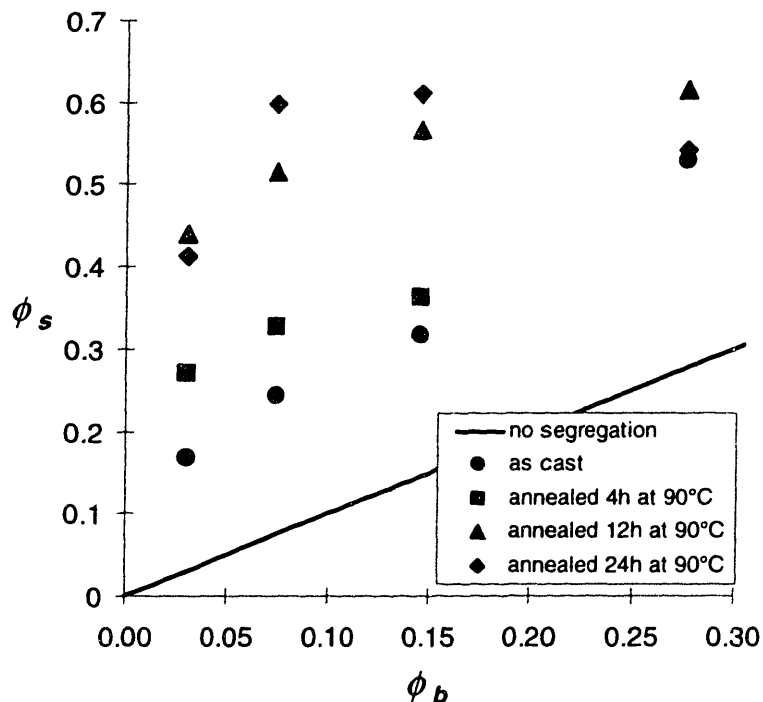
Figure 4.3 Near-surface membrane composition versus bulk composition
Near-surface concentration of P(MMA-r-POEM9)[a] versus bulk concentration (vol. fraction) for unannealed membranes E-xx-9a-20 cast at 20°C and for membranes cast at 20°C and subsequently heat treated for 4, 12, and 24 h at 90°C while immersed in water (for details, see Appendix C, Table C.1).

process. Moreover, the comb surface coverage is substantially enhanced by subsequent heat treatment in water. In fact, an integrated near-surface coverage of nearly 45 vol % is achieved by heat treatment of a membrane with a bulk concentration of only 3 volume percent. Thus, substantial surface segregation of P(MMA-r-POEM) is achieved during both the coagulation and heat treatment steps of the conventional immersion precipitation process for fabricating polymer membranes.

The 45° photoelectron takeoff angle used in these XPS experiments integrates contributions from a sampling depth of ~60 Å (see Appendix D). Thus, the actual

134

surface fraction of the comb additive is likely higher than that measured using XPS. The fact that the near-surface compositions of annealed membranes (Figure 4.3) appear to reach a limiting value of ~60 vol % P(MMA-r-POEM$_9$)[a] suggests that this integrated value might correspond to nearly complete surface coverage of the comb additive. Quantitative support for this hypothesis is provided in Appendix D.

The ratio $A_{C\text{-}O}/A_{COO}$ for membranes containing P(MMA-r-POEM$_9$)[a] had a mean value of 2.77 (see Appendix C, Table C.1), somewhat less than the stoichiometric value of 2.98. This suggests a surface depletion of the PEO side chains of the comb relative to its PMMA backbone. Orientation of the PEO side chains away from the *dry* surface examined by XPS might be expected, since the PEO side chains have a high surface energy compared to both the PMMA backbone and PVDF. A similar observation has been made by other researchers,[188] who studied the near-surface compositions of pure P(MMA-r-POEM) copolymers using XPS.

Influence of Coagulation Bath Temperature

The data presented in the previous paragraphs demonstrate that significant surface localization of an amphiphilic comb additive can be achieved during the coagulation step of the standard immersion precipitation process, requiring no post-coagulation processing steps. Moreover, an even greater surface coverage was realized with the use of a conventional heat treatment step in water. For the greatest benefit, however, heat treatments on the order of 12 h in duration were necessary for membranes incorporating a comb additive of fairly low molecular weight (~14K based on PS standards). From the above results, it is clear that the thermodynamically stable surface composition

135

(apparently ~60 vol % comb additive by XPS) was not achieved during membrane coagulation.

As surface localization of the comb additive during coagulation occurs by diffusion of the two polymer components prior to gelation, it is reasonable to expect that by increasing the kinetics of polymer diffusion, $e.g.$, by increasing the coagulation bath temperature, higher comb surface concentrations might be achieved. The influence of coagulation bath temperature on surface composition is shown in Figure 4.4. Here, membranes containing 5 wt % (7.5 vol %) P(MMA-r-POEM$_9$)^d were (a) coagulated in a water bath at 20°C, (b) coagulated in a water bath at 20°C and subsequently heat treated
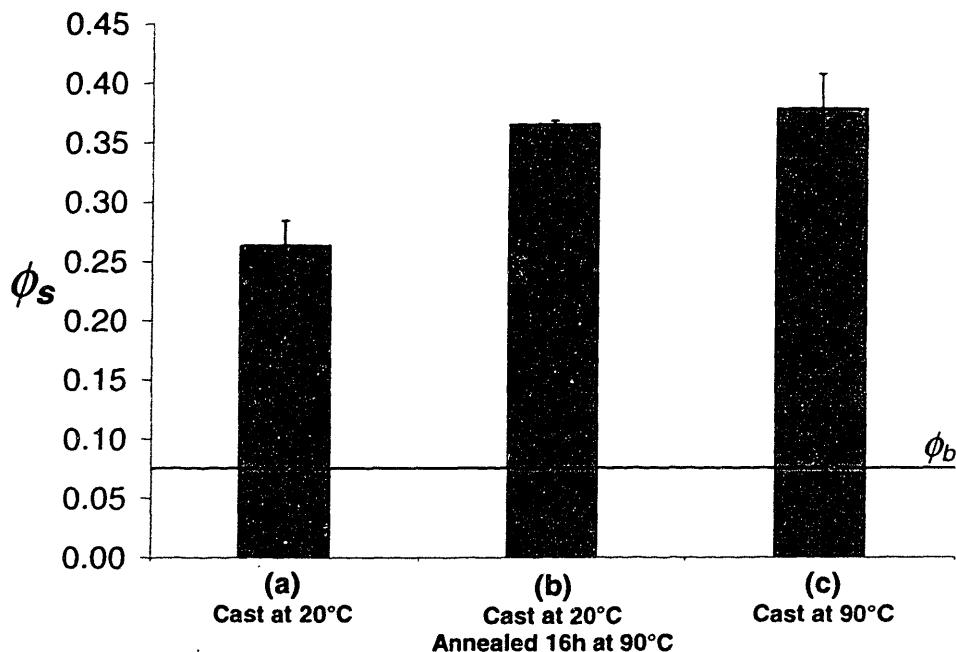
Figure 4.4 Dependence of near-surface composition on processing conditions
Near-surface concentration (vol. fraction) of P(MMA-r-POEM$_9$)^d for (a) as-cast membrane E-05-9d-20, (b) membrane E-05-9d-20 after a subsequent 16 h heat treatment in water at 90°C, and (c) as-cast membrane E-05-9d-90. For reference, the bulk comb concentration (ϕ_b, vol. fraction) is indicated by the solid line. An unannealed membrane cast into a 90°C water bath has the same surface composition as a membrane cast into a 20°C bath and subsequently heat treated for 16 h. For details of the XPS fits, see Appendix C, Table C.2.

for 16 h in water at 90°C, and (c) coagulated in a water bath at 90°C. Simply casting a membrane at 90°C results in the same level of surface segregation obtained by casting at 20°C and heat treating for 16 h. Thus, with proper selection of coagulation bath temperature, it is possible to achieve substantial surface localization of the comb additive using a *single-step* fabrication process.

4.2.2 Comb Polymer Design for Self-Organization

Comb Polymer Composition

The various driving forces for surface localization of P(MMA-*r*-POEM) are all dependent on its composition. The enthalpic driving force is dependent on the fraction of POEM, which creates energetically favorable EO/H$_2$O contacts. The entropic driving forces are dependent on the concentration of EO/H$_2$O contacts, as well as the POEM chain end density. To evaluate the effect of comb composition on membrane surface composition, membranes modified with combs having POEM contents ranging from ~30 to ~50 wt % were cast using the three processing routes discussed in Section 4.2.2. The near-surface compositions of these membranes, each of which had a bulk composition of 5 wt % comb, are plotted in Figure 4.5. Near-surface compositions were obtained by XPS, as described in Section 4.2.1.

For membranes cast at 20°C, both unannealed and subsequently annealed, there is no significant variation in the membrane surface composition with the composition of the comb additive over this range of comb compositions. For membranes cast at 90°C, a statistically significant increase is seen in the near-surface concentration of P(MMA-*r*-POEM), which occurs for comb compositions of $\geq$40 wt % POEM. In fact, the benefit of

137
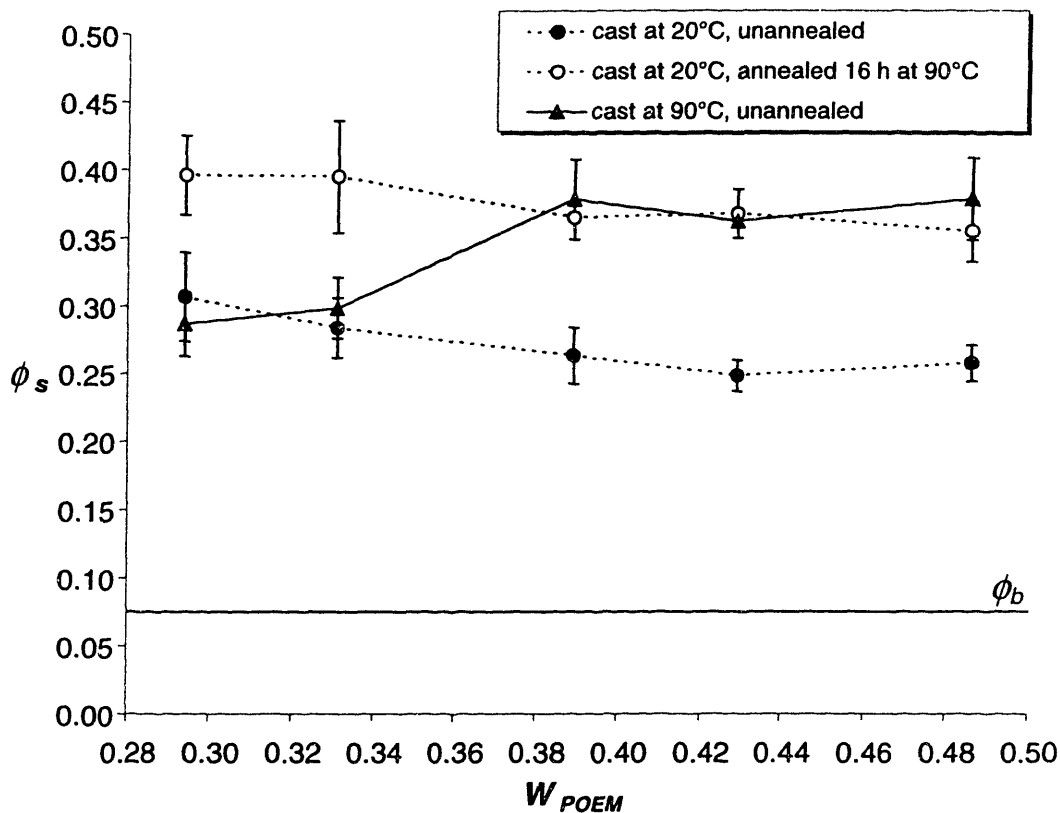
Figure 4.5 Variation of surface composition with P(MMA-r-POEM) composition
Surface comb concentration (vol. fraction) versus comb composition in wt % POEM for
unannealed and annealed membranes E-05-9(b,c,d,e,f)-20 and for membranes E-05-9(b,c,d,e,f)-
90 (for details, see Appendix C, Table C.2). The bulk comb concentration (ϕ_b, vol. fraction) is
indicated for reference.

casting membranes into a hot coagulation bath relative to casting them at room
temperature is realized only at comb compositions of at least $W_{POEM} = {\sim}0.40$.

Aside from the level of surface segregation achieved during coagulation, other
criteria of interest include fouling resistance and water insolubility. Of course, at a given
near-surface concentration of the additive, fouling resistance is expected to increase with
increasing POEM content. However, the potential for water solubility also increases with
increasing POEM content. Water solubility is undesirable, since it might result in long-

term instability of the surface chemistry. The water solubilities of the various polymers used in this thesis are noted in Table 3.1. These were determined by stirring roughly 50 mg of polymer in 20 mL of water overnight.

P(MMA-r-POEM) combs having PS-standard weight-average molecular weights of 10 000 to 20 000 g/mol are water insoluble for POEM contents up to 40 percent by weight. It is interesting to note that the water solubility of combs P(MMA-r-POEM$_9$)[e] and P(MMA-r-POEM$_9$)[f] does not appear to significantly affect the surface composition achieved during coagulation. For higher molecular weights ($\geq$ 60 000 g/mol based on PS standards), combs having POEM contents of up to ~50 wt % are water insoluble. In the following section, the influence of comb molecular weight on the degree of surface segregation achieved during coagulation is considered. To achieve water insolubility for combs of low molecular weight ($<$ 20 000 g/mol based on PS standards) while maximizing the degree of surface segregation attained, combs containing roughly 40 wt % POEM were used in this study.

Comb Polymer Molecular Weight

Section 2.6.2 put forth an expected kinetic mechanism for surface segregation of the amphiphilic comb during the coagulation step. This mechanism was based on the responses of the two polymers in the casting solution to the chemical potential gradients imposed on them by the creation of a steep water concentration gradient at the interface between the cast film and the water bath. The extent of comb surface localization due to this mechanism was expected to *increase* with comb molecular weight.
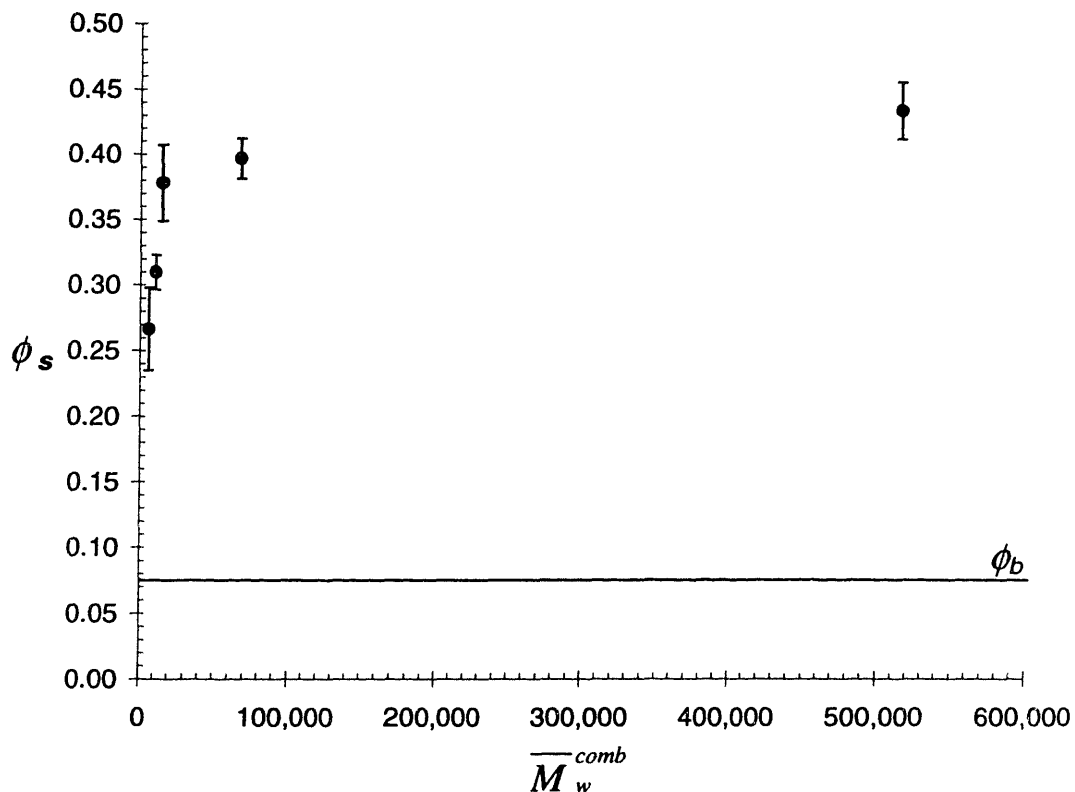
Figure 4.6 Effect on surface composition of P(MMA-r-POEM) molecular weight
Surface comb concentration (vol. fraction) versus comb molecular weight (based on PS standards) for membranes E-05-9(g,h,d,i,j)-90 (for details, see Appendix C, Table C.3). The bulk comb concentration (ϕ_b, vol. fraction) is indicated for reference.

To evaluate the importance of comb molecular weight for surface segregation during coagulation, membranes containing 5 wt % of P(MMA-r-POEM) combs having similar compositions but different molecular weights were cast into a water bath at 90°C. Figure 4.6 is a plot of near-surface membrane composition, determined by XPS, as a function of comb molecular weight. The degree of surface localization of the comb during membrane coagulation clearly increases with increasing comb molecular weight,

140

particularly in the range of molecular weights between ~6000 and ~60 000, based on PS standards.

As proposed in Section 2.6.2, this result is due to the fact that the mobility of the comb additive polymer decreases with increasing comb molecular weight according to Equation 2.6. Thus, as both polymers are transported down their chemical potential gradients (into the casting solution) during membrane coagulation, the additive polymer is transported more slowly with increasing molecular weight, and is "left behind" in greater proportion at the membrane surface. The results in Figure 4.6 validate the proposed kinetic mechanism for comb surface segregation, and also have important
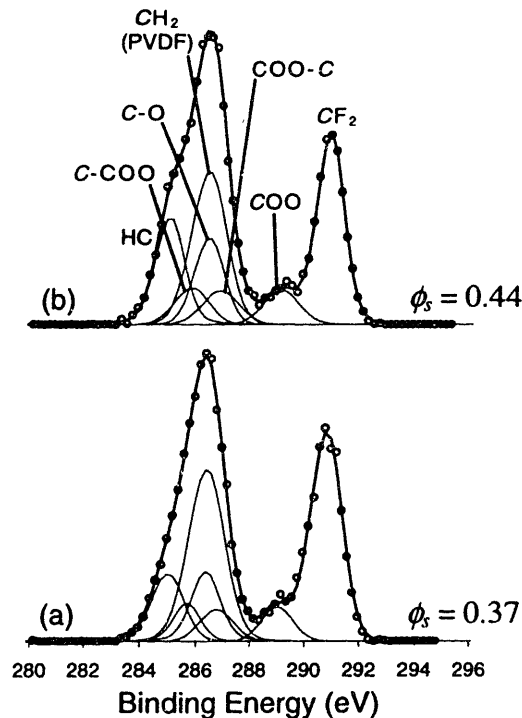
Figure 4.7 C 1s XPS spectra for membranes before and after 24-h UF with water
Fitted C 1s XPS spectra for membranes F-10-9i-90, containing 10 wt % P(MMA-r-POEM₉)ⁱ, (a) in the as-cast condition and (b) after filtration of dW for 24 h at a pressure of 40 psig (for details, see Appendix C, Table C.4). The calculated near-surface comb concentration (vol. fraction) is indicated for each membrane.

141

practical implications. In particular, the stability of the surface-localized polymer with respect to extraction should increase with its molecular weight, since the number of entanglements per chain increases linearly with molecular weight.[244] In this respect, surface segregation during immersion precipitation can be contrasted with surface segregation in polymer melts, which typically requires diffusion of the surface-active species from the bulk and hence is limited to relatively low molecular weight additives.

4.2.3 Surface Stability

As discussed in Sections 2.6.1 and 2.6.2, an important motivation for the preparation of self-organizing membranes using amphiphilic, macromolecular additives is the need for surface chemistries combining hydrophilicity with long-term surface stability in an aqueous environment. The previous section demonstrated that surface localization of high molecular weight comb additives capable of providing highly entangled surfaces is possible, and in fact favored, using the standard immersion precipitation process. Figures 4.7 and 4.8 are C1s XPS results for membranes before and after UF of dW for 24 h and storage in dW for 32 months, respectively. Near-surface comb concentrations were calculated from the XPS spectra according to the method described in Section 4.2.1. Neither system shows any evidence for comb extraction from the membrane surface. It is of interest to note that the membrane stored in water for 32 months contained a comb additive, P(MMA-r-POEM9)[a], which is marginally *water soluble*. The long-term surface stability of this membrane in an aqueous environment is a testament to the robust nature of surfaces composed of entangled macromolecular additives.
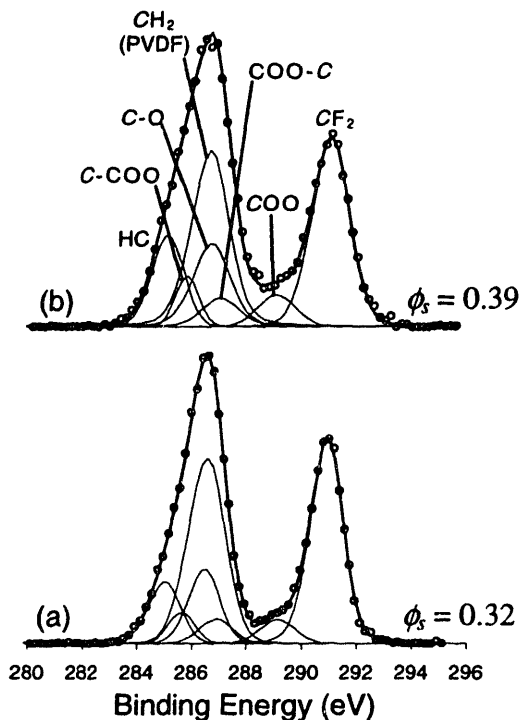
Figure 4.8 C 1s XPS spectra for membranes before and after 32-mo. storage in water
Fitted C 1s XPS spectra for membranes E-10-9a-20, containing 10 wt % P(MMA-r-POEM$_9$)[a], (a) in the as-cast condition and (b) after continuous storage in dW for 32 months (for details, see Appendix C, Table C.4). The calculated near-surface comb concentration (vol. fraction) is indicated for each membrane.

4.2.4 3-Dimensional Nature of the Modified Surface

A significant potential advantage of self-organization with respect to other membrane surface modification techniques is the ability to provide robust, chemically tailored layers on the internal pore channel surfaces, as well as the separation surface. To evaluate this possibility, membranes having bulk compositions of 10 wt % PVDF-g-PMAA were stained with AO, a cationic fluorescent dye which binds to the carboxylic acid groups of PMAA. Evidence in Section 5.4 will show that, under the staining conditions used (pH 7.4), PMAA is negatively charged.

143

Figures 4.9 (a) and (b) are 20x fluorescence micrographs of the cross-sections of a pure PVDF membrane and a 10% PVDF-g-PMAA membrane, respectively, stained by forced permeation of a dye solution under pressure. These images were captured under identical imaging conditions, and all contrast is due to fluorescence of the dye. A very
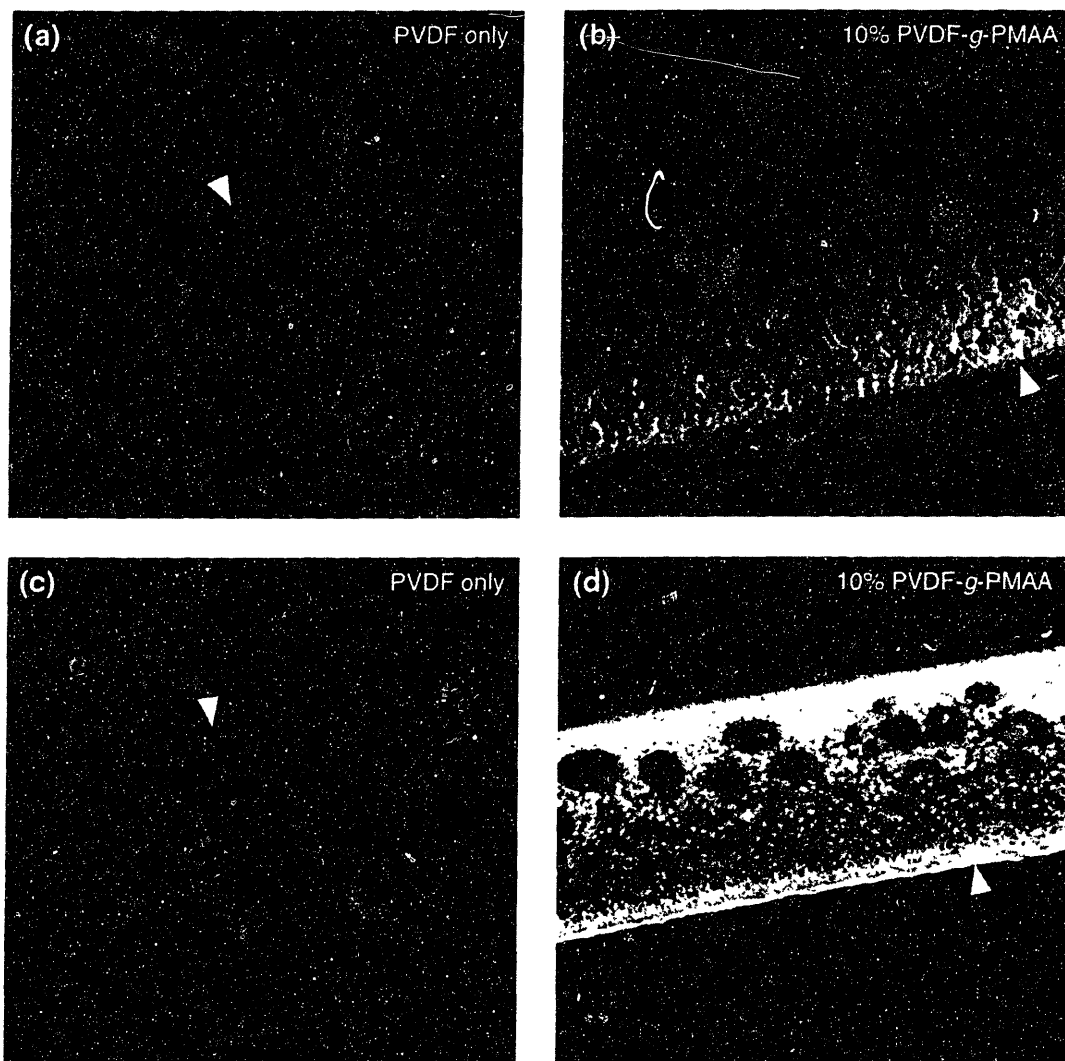
Figure 4.9 Fluorescence micrographs of AO-stained membranes
(a) and (b) are membranes F-00-4-90 and F-10-PE-90, respectively, autoclaved for 1 h at 121°C and stained by filtration of a 1 μM AO solution for 1 h. (c) and (d) are the same membranes stained by immersion in a stirred 500 nM AO solution for 7 h. All images are at 20x magnification. Arrows indicate the membrane separation surfaces. All contrast is due to fluorescence of AO.

small fluorescence intensity is apparent on the PVDF-only membrane (a) due to nonspecific background staining of the dye. The blend membrane (b) exhibits comparatively strong fluorescence due to the presence of carboxylic acid groups at the surface. This fluorescence is observed throughout the membrane cross-section, indicative of internal pore channel coverage.

The fluorescence in (b) appears to exhibit a gradient from the separation surface to the opposite surface, being most intense near the separation surface. However, it is not possible to conclude that this indicates a higher surface concentration of PVDF-*g*-PMAA near the separation surface. During the staining procedure, the separation surface of the membrane was adjacent to a well-mixed solution of the dye, and the concentration of dye remaining in the staining solution would be expected to decrease with distance into the membrane. These conditions may have caused the binding of more dye in the region of the separation surface. This conjecture is supported by Figures 4.9 (c) and (d), a pure PVDF and blend membrane stained by simply immersing the membranes in gently stirred dye solutions for 7 h. The blend membrane (d) is substantially more intensely stained than the pure PVDF membrane (c), but exhibits a depletion of dye in the center region of the cross-section. This depletion is probably due to the fact that the exterior surfaces of the membrane were exposed to a well-mixed dye solution, while diffusion of dye into the membrane center was comparatively limited. The regions near the separation surface and the opposite exterior surface of (d) appear roughly equivalent in terms of fluorescence intensity. XPS analyses of the separation surface and the opposite surface, detailed in

Section 5.3.1, indicate near-surface compositions of 29 and 39 wt % PMAA, respectively (compared to the bulk composition of 5 wt % PMAA – see Appendix C, Table C.9).

The major conclusion to be drawn from these experiments is that self-organization results in the chemical modification of internal pore channels throughout the membrane cross-section, in addition to the separation surface. In contrast, spraying and dip coating methods, as well as grafting techniques which rely on line-of-sight processes for initiation site generation, typically impart the desired surface chemistry to the region of the separation surface only (see Section 2.4.1). This is an important distinction with respect to the surface modification of membranes for fouling resistance, since foulant accumulation takes place on internal pore channel surfaces, as well as the separation surface.[90,92]

The results of this experiment may also have important ramifications for the use of polymer membranes to remove specific species (e.g., toxic metals) from feed water streams by chemical binding. Indeed, this experiment has demonstrated the surface segregation of a *functional* polymer additive capable of binding a target species (AO) and removing it from water during filtration. The capability of self-organization to modify membrane surfaces throughout the membrane cross-section is important in such an application, since this enables the utilization of maximal surface area for binding of the target species. Indeed, the ratio of internal surface area to separation surface area for UF membranes can easily be as high as 8000:1 (see Section 6.2.2). The potential use of functional, self-organizing polymer membranes to remove specific heavy metals from water is considered in Section 6.2.2.

146

4.3 Influence of Amphiphilic Comb on Membrane Morphology

4.3.1 Separation Surface Morphology

To evaluate the influence of an amphiphilic comb additive polymer on the morphology of the separation surface, membranes E-00-1-20 and E-xx-9a-20 (Table 3.4) were studied by FESEM. The casting solutions used to prepare these membranes were
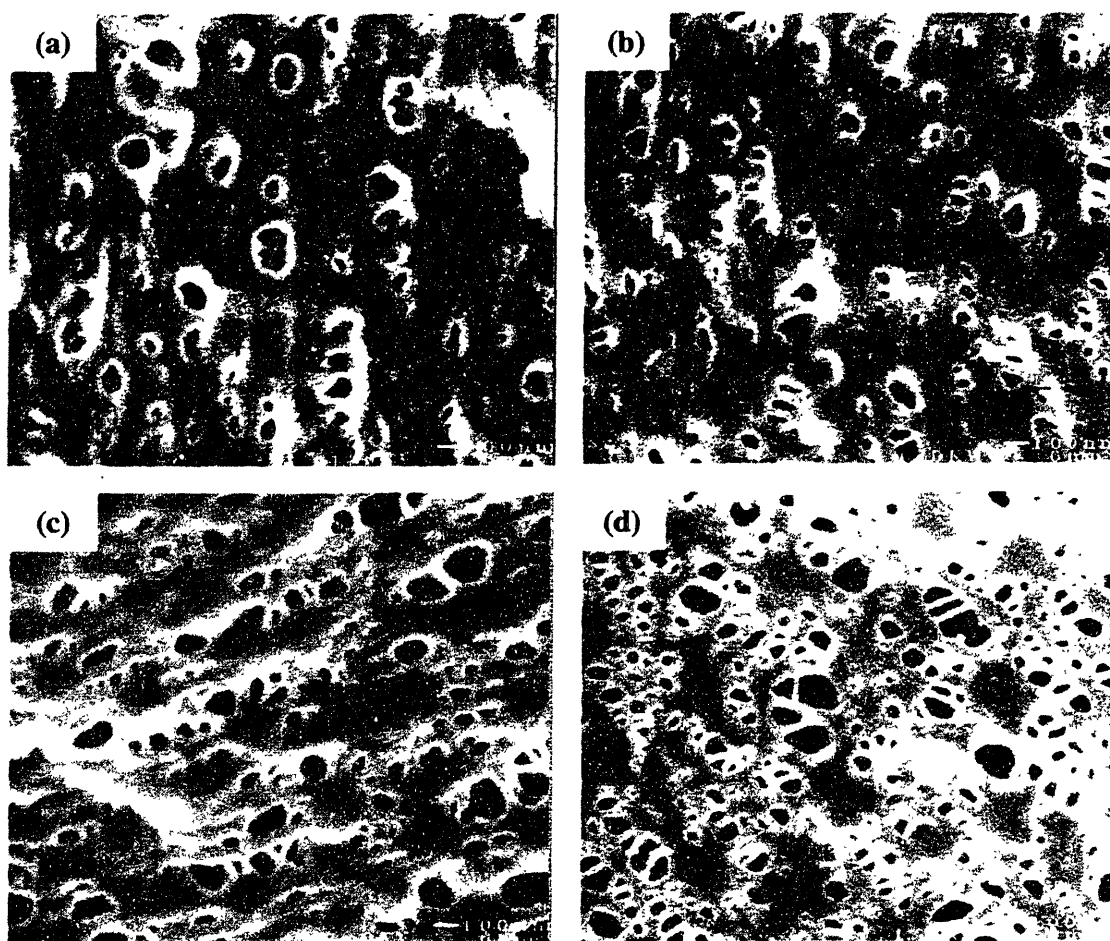
Figure 4.10 Surface morphologies of membranes containing P(MMA-r-POEM)
Example FESEM micrographs of the separation surfaces of membranes E-xx-9a-20, with bulk compositions of (a) 0%, (b) 5%, (c) 10%, and (d) 20% by mass P(MMA-r-POEM9)[a]. Qualitatively, the observed increase in membrane porosity with increasing comb content (see Table 4.3) is readily discernible.

identical in every way except for their P(MMA-r-POEM$_9$)[a] contents, which varied

between 0 and 20 wt % of the total polymer. Micrographs a-d in Figure 4.10 are example

FESEM images obtained at a magnification of 50,000x from membranes containing 0, 5,

10, and 20 wt % comb additive, respectively. For each composition, three randomly

selected images were binarized as described in Section 3.3.3. Magnifications greater than

50,000x failed to resolve any smaller pores. Thus, this magnification was used for

statistical averaging of pore sizes. Statistics generated from the binarized images are

summarized in Table 4.3, where $\overline{D}$ is the mean pore diameter, σ_D is the standard

deviation of pore diameters, D_{mode} is the 5-nm bin of pore diameters occurring most

frequently, D_{max} is the maximum observed pore diameter, and ε is the membrane

porosity, defined as the total area enclosed by pore inlets per unit area of membrane

separation surface.

Table 4.3 Summary of Pore Size Distribution Statistics for Membranes E-xx-9a-20

$\phi_{w,b}$	ϕ_b	$\overline{D}$ (nm)	σ_D (nm)	D_{mode} (nm)	D_{max} (nm)	ε
0.00	0.000	45	29	30-35	138	0.036
0.02	0.030	42	26	20-25	158	0.020
0.05	0.075	37	23	20-25	128	0.038
0.10	0.146	48	36	25-30	253	0.078
0.20	0.277	40	25	20-35	240	0.092

The morphology of the separation surface appears unaffected by the addition of

P(MMA-r-POEM$_9$)[a] up to a bulk composition of 5 percent by mass. Membranes

containing 10 wt % or more of the amphiphilic additive were characterized by

significantly increased porosities, as well as the appearance of a few pores roughly twice

as large as the largest pores observed in samples containing smaller amounts of the comb. However, no significant trends in the mean and standard deviation of pore diameters were observed as the membrane composition was varied.

The increase in separation surface porosity with increasing concentration of P(MMA-r-POEM$_9$)[a] is comparable to that observed by other researchers[131] in membranes prepared from PVDF/PMMA blends. This morphological change is a result of an increase in the rate of transport of water into the cast film with increasing content of the amphiphilic additive polymer, leading to liquid-liquid phase separation at lower overall polymer concentrations and enhancement of the conditions for instantaneous demixing, as discussed in Sections 2.3.2 and 2.5. The observed ~2x increase in ε with the addition of 10 wt % comb polymer is highly significant, as it suggests that substantially higher pure water fluxes might be obtainable with membranes containing 10% or more of the additive polymer, compared to pure PVDF membranes. Indeed, we will find in Section 5.1.2 that, when membranes are used to filter a foulant solution, the flux benefit realized by higher porosities in membranes prepared from self-organizing blends is as important as the benefit due to increased fouling resistance.

4.3.2 Substructure Morphology

Effect of the Amphiphilic Additive Polymer

The previous section examined the effect of the amphiphilic comb additive on the morphology of the membrane separation surface. The morphology of the substructure is also important, as it strongly influences the permeability and mechanical properties of the
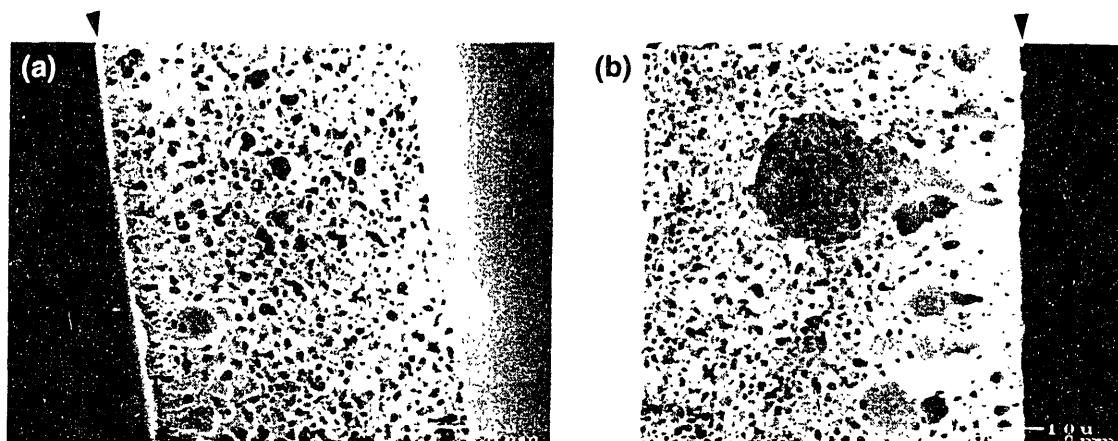
Figure 4.11 Substructure morphologies of membranes cast into pure water baths
Cross-sectional FESEM images of membranes cast into pure water coagulation baths at 90°C. (a) pure PVDF membrane F-00-1-90 and (b) membrane F-10-9k1-90, containing 10 wt % P(MMA-r-POEM₉)ᵏ. Arrows indicate the separation surface.

membrane. Thus, it is necessary to understand the effect of the amphiphilic comb on the substructure morphology as well.

Cross-sectional FESEM micrographs of a pure PVDF membrane and a membrane containing 10 wt % $P(MMA-r-POEM_9)^k$ appear in Figure 4.11. The casting solutions contained equal amounts PVDF (18 wt %) and glycerol (1 wt %) as a pore former, and were cast under identical conditions (in pure dW at 90°C). While both membranes exhibit macrovoid formation, the macrovoids are larger and more numerous in the membrane containing the amphiphilic comb. This result is expected based on previous experimental observations and modeling of macrovoid formation reviewed in Section 2.3.2, and based on previous work on membranes containing small-molecule and macromolecular additives discussed in Section 2.5. The presence of the amphiphilic additive in the casting solution increases the affinity of the casting solution and

precipitant, enhancing the conditions for instantaneous demixing and associated macrovoid formation.

Control of the Substructure Morphologies of Self-Organizing Membranes

The presence of large macrovoids typically results in increased membrane permeability, and substructure morphologies like that shown in Figure 4.11b are therefore often desirable in moderate-pressure UF applications.[48] However, macrovoid formation can result in separation surface pore sizes and mechanical properties unsuitable for high-pressure applications.[52,55,68] Thus, the ability to control and suppress macrovoid formation in self-organizing polymer membranes, with a minimal sacrifice in terms of surface segregation, is desirable.

Perhaps the most common method of reducing or suppressing macrovoid formation is addition of solvent to the coagulation bath.[48,52] This decreases the activities of both the solvent in the casting solution and the water in the coagulation bath,[48] reducing the water-solvent exchange rate at the interface and enhancing the conditions for delayed demixing. However, addition of solvent to the coagulation bath also dilutes the unfavorable contacts between the matrix polymer and water that are responsible for important enthalpic and entropic (hydrophobic effect) driving forces for surface segregation of the additive. Further, it reduces the magnitudes of the interfacial chemical potential gradients for both polymers, and would therefore tend to negate the kinetic mechanism for surface segregation shown to be important in Section 4.2.2. Thus, use of this method might be expected to entail a significant reduction in the level of surface segregation obtained during membrane coagulation.

A second method for reducing membrane porosity and reducing or suppressing macrovoid formation is the addition of an inorganic salt to the coagulation bath. Again, the presence of the salt reduces the activity of the water in the bath upon contact with the casting solution, thereby decreasing the rate of diffusion of water into the cast film. Unlike the presence of solvent in the coagulation bath, however, the salt does not reduce the rate of diffusion of solvent *out* of the cast film. Thus, in their studies of cellulose acetate RO membranes coagulated in aqueous baths containing a number of inorganic salts as well as sucrose, Frommer *et al.*[245] found that solute concentrations in the range of 1 N to 4 N resulted in decreased specific pore volumes as well as substantial reductions in membrane thickness relative to membranes cast in pure water, due to the change in the relative exchange rates of water and solvent. Moreover, these effects appeared to be mainly dependent on the activity of the water in the coagulation bath, and relatively insensitive to the nature of the solute. Based on Monte Carlo simulations of polymer membranes coagulated in aqueous salt solutions, Termonia[77] concluded that a salt poorly miscible with the polymer solvent is most effective in preventing macrovoid formation. In summary, the mechanism of macrovoid suppression by salt in the coagulation bath is probably enhancement of the conditions for delayed demixing due to decreased water activity, combined with increased overall compaction of the cast film prior to gelation as a result of the enhanced rate of solvent transport out of the film relative to water transport into it.

Like solvent, the addition of salt to the precipitation medium might be expected to have a deleterious effect on the level of comb surface segregation achieved during

membrane coagulation. The addition of an inorganic salt to an aqueous PEO solution is well known to reduce the solubility of PEO and, at sufficiently high salt concentrations, to precipitate it from solution.[246-249] This so-called "salting out" effect arises from salt-PEO complexation as well as the ability of salts to compete with PEO for water contacts,[247,248] and would tend to negate the driving forces for segregation of the PEO-bearing comb to the water surface.

The inorganic salts vary widely in their capacity to "salt out" PEO. The PEO-water system exhibits a lower critical solution temperature (LCST) type phase diagram, such that a homogeneous solution at room temperature phase separates upon heating above a critical temperature.[179,250,251] Thus, a good measure of the effectiveness of a salt in competing with PEO for water contacts is its ability to depress the theta-temperature of a given PEO-water system.[247,248] Boucher and Hines[248] studied theta-temperature depression by 18 different salts in aqueous solutions containing 20 000 g/mol PEO. LiCl and the Group II chlorides were found to be remarkably ineffective in "salting out" PEO compared to the other salts studied, depressing the theta-point by only ~10°C relative to the salt-free theta-temperature of 96°C at concentrations of 2 N (roughly 20 wt %). Thus, with proper salt selection, one might achieve morphological control with minimal effect on the surface segregation behavior of a PEO-bearing comb. In any case, unlike solvent addition to the coagulant bath, salt addition would not be expected to reduce the nonsolvent power of the coagulation bath with respect to the matrix component. This is an important distinction with regard to the kinetic mechanism for surface segregation of the comb.
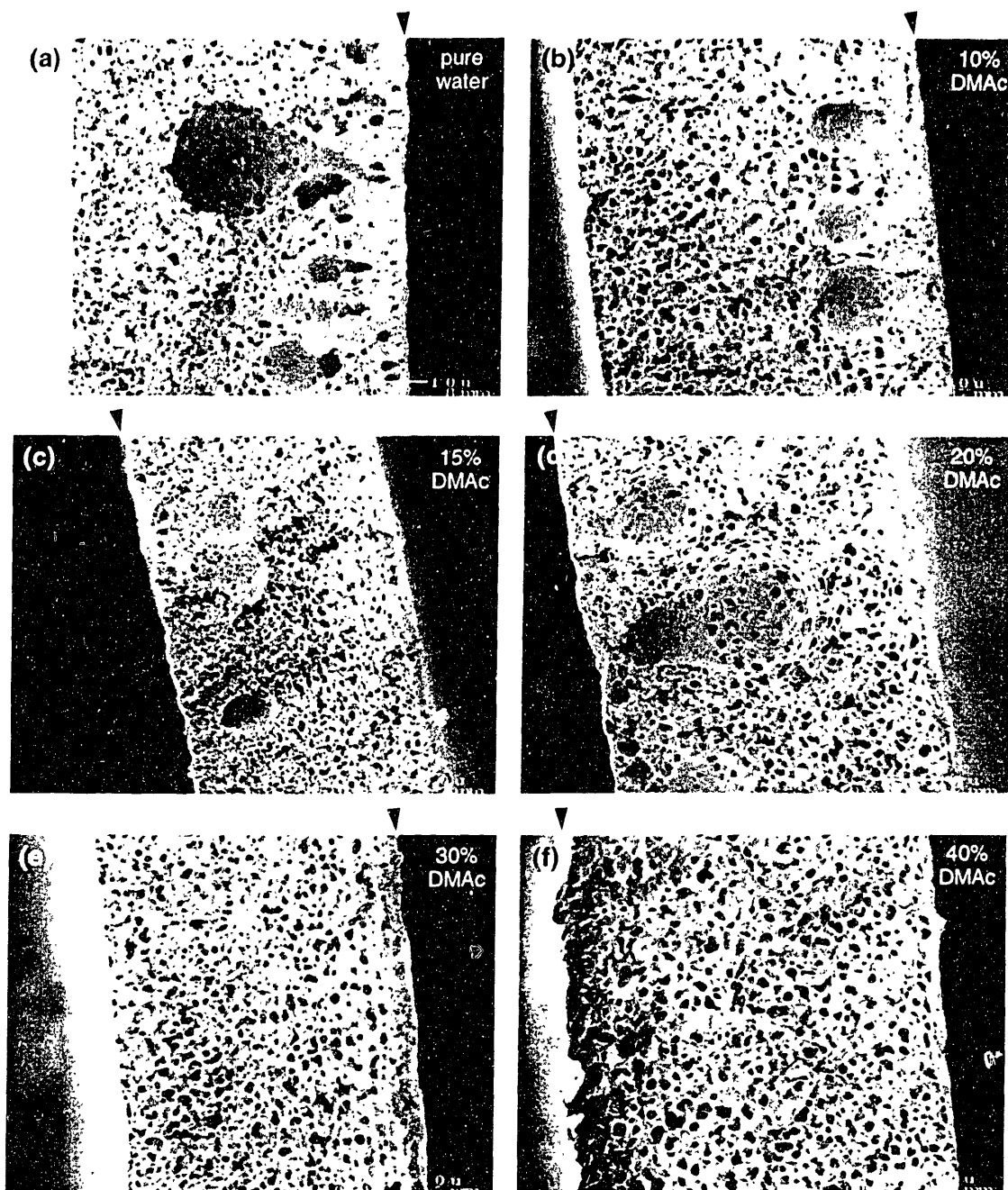
Figure 4.12 Morphologies of membranes cast in baths containing DMAc

Cross-sectional FESEM images of membranes F-10-9k1-90, containing 10 wt % P(MMA-r-POEM-)F, cast into 90 'C coagulation baths containing various concentrations of DMAc Bath compositions are (a) pure water, (b) 10 wt % DMAc, (c) 15 wt % DMAc, (d) 20 wt % DMAc, (e) 30 wt % DMAc, and (f) 40 wt % DMAc. Arrows indicate the separation surface.

154

To assess the effects on substructure morphology of solvent and salt addition to the coagulation bath, a casting solution containing 18 wt % PVDF, 2 wt % P(MMA-r-POEM$_9$)^k, and 1 wt % glycerol was cast into aqueous baths at 90°C containing various amounts of DMAc or CaCl$_2$. CaCl$_2$ was chosen as the candidate salt because it is highly soluble in water but only sparingly soluble in DMAc, and because it is relatively ineffective in "salting out" PEO. Cross-sectional FESEM micrographs of membranes cast into baths containing DMAc are shown in Figure 4.12. Strong macrovoid formation occurs with coagulation baths containing up to 20 wt % DMAc. Membranes cast into baths containing 30 wt % DMAc are characterized by a thickening of the dense surface layer and the complete absence of macrovoids. Such a morphology might be suitable for high-pressure filtration applications. Further addition of DMAc to the coagulation bath produces membranes with thicker surface layers, as well as increased surface roughness due to reduced interfacial tension between the bath and the cast film.[55]

Cross-sectional micrographs of membranes cast into coagulation baths containing CaCl$_2$ appear in Figure 4.13. The progression from macrovoid-containing membranes to thick-skinned, macrovoid-free membranes with increasing salt concentration appears entirely analogous to that observed for coagulation baths containing DMAc, with complete macrovoid suppression occurring at greater than or equal to ~15 wt % CaCl$_2$. The membranes appear to become thinner with increasing salt concentration, due to an increase in the rate of solvent transport relative to the rate of water transport across the interface between the casting solution and the coagulation bath. The addition of 30 wt % CaCl$_2$ to the coagulation bath results in the formation of a nearly dense film.
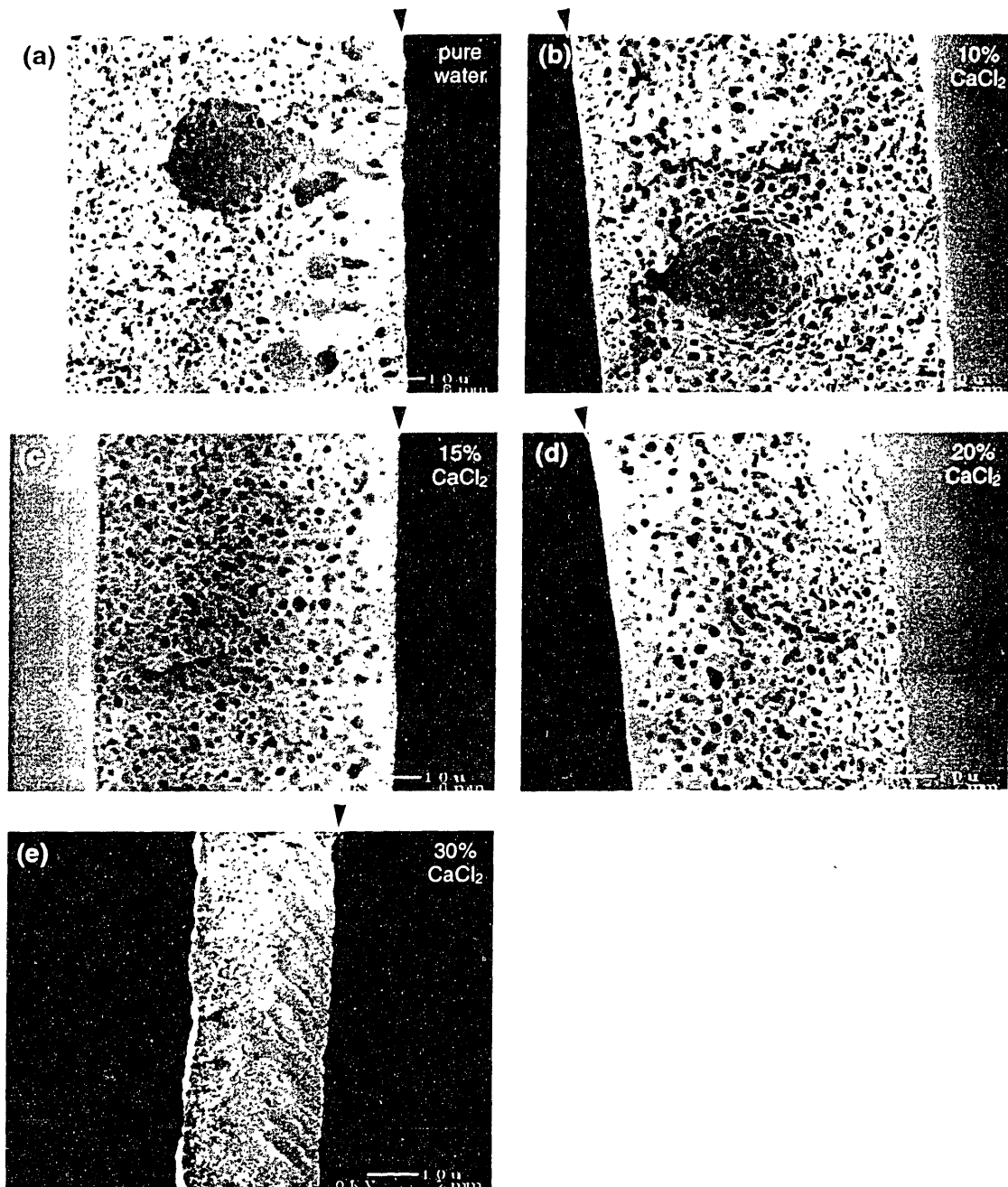
Figure 4.13 Morphologies of membranes cast in baths containing CaCl₂
Cross-sectional FESEM images of membranes F-10-9k1-90, containing 10 wt % P(MMA-r-POEM₉)ᵏ, cast into 90°C coagulation baths containing various concentrations of CaCl₂. Bath compositions are (a) pure water, (b) 10 wt % CaCl₂, (c) 15 wt % CaCl₂, (d) 20 wt % CaCl₂, and (e) 30 wt % CaCl₂. Arrows indicate the separation surface.

The effect of bath composition on final surface composition as determined by XPS is shown in Figure 4.14. Open symbols denote membranes having macrovoids, while closed symbols denote membranes in which macrovoid formation is suppressed. As expected, addition of DMAc to the coagulation bath results in decreased surface segregation of the P(MMA-r-POEM). In fact, the accomplishment of macrovoid suppression using this method entails a comb surface concentration reduction of ~10 volume percent. By contrast, addition of up to 20 wt % CaCl$_2$ to the coagulation bath, well more than required for the suppression of macrovoid formation, results in no significant reduction in the surface concentration of P(MMA-r-POEM). Thus, addition of a properly selected salt to the coagulation bath appears to be a better method than solvent addition for the control of substructure morphology in self-organizing membranes.

Although the boundary for solid-liquid demixing lies closer to the solvent-polymer axis of the PVDF phase diagram than the liquid-liquid binodal (Figure 2.7), none of the micrographs in Figures 4.12 and 4.13 exhibit the spheroidal structures characteristic of membranes in which solid-liquid demixing is an important process.[69,83] Instead, cellular morphologies are observed, indicating complete domination by liquid-liquid demixing. As discussed in Section 2.3.2, this is not surprising given the rapid kinetics of liquid-liquid demixing relative to solid-liquid demixing. If anything, we may have expected to observe crystallization-dominated morphologies in the membranes coagulated slowly in baths containing high concentrations of solvent.[69,83] In addition,

none of the membranes containing P(MMA-r-POEM) exhibit morphological features indicative of large-scale phase separation of the two polymer components.
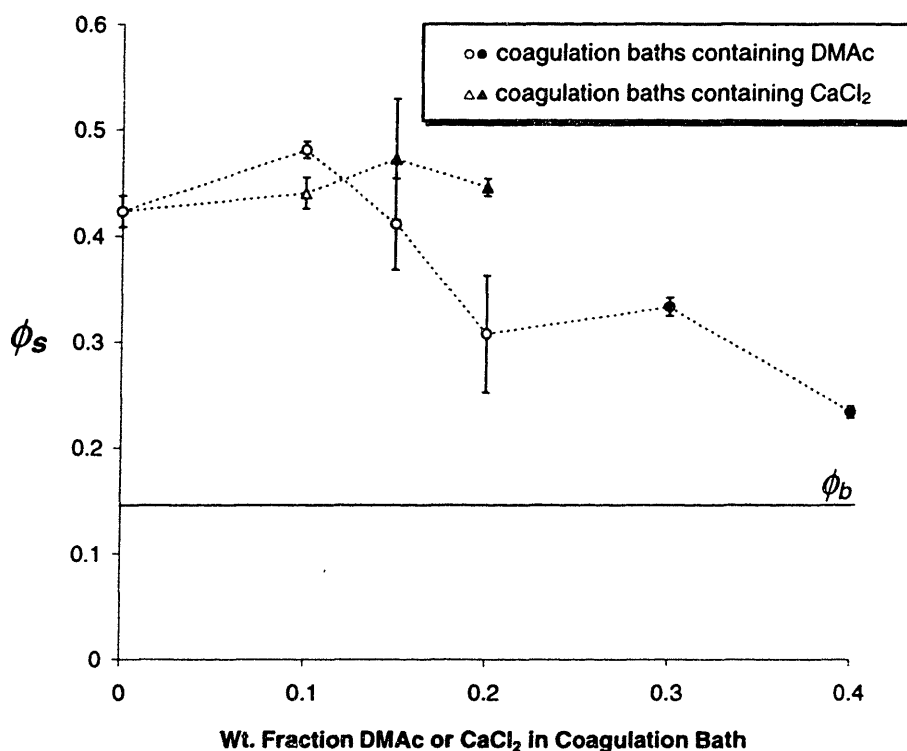
Figure 4.14 Effect of coagulation bath additives on membrane surface composition
Near-surface concentration (vol. fraction) of P(MMA-r-POEM$_9$)[k] versus concentration of DMAc or CaCl$_2$ in the coagulation bath for membranes F-10-9k1-90 cast into 90°C coagulation baths (for details, see Appendix C, Table C.5). Open symbols denote membranes having macrovoids, while closed symbols denote membranes in which macrovoid formation is suppressed (see Figs. 4.12 and 4.13). For reference, the bulk comb concentration (ϕ_b, vol. fraction) is indicated by the solid line.

5. Performance of Self-Organizing Membranes

5.1 Foul-Resistant Membranes

5.1.1 Static Fouling Resistance

To evaluate the influence of near-surface P(MMA-r-POEM) concentration on protein adsorption resistance, membranes having various bulk concentrations of P(MMA-r-POEM$_9$)[a] were fouled by immersion in a 10.0 g/L BSA solution for 12 h. These membranes, along with control membranes which had not been exposed to BSA, were then stained for protein detection using anionic colloidal gold, as described in Section 3.3.5. After colloidal gold staining, the level of protein fouling of membranes was first assessed visually by the intensity of the red color produced, with deep red indicating heavy fouling and pink indicating less fouling. Some control membranes appeared a very light pink in color, indicating a low level of nonspecific background staining of colloidal gold.

XPS analysis was performed on the separation surfaces of both fouled and control gold-labeled membranes to determine the near-surface gold concentration. The near-surface atomic compositions were obtained by integration of the following peaks in the XPS survey spectra: Au 4f (86 eV), C 1s (285 eV), O 1s (531 eV), and F 1s (685 eV). No other elements were detected in the spectra. Background staining was accounted for by subtracting the gold concentration detected on each control membrane from that detected on the corresponding fouled membrane. Figure 5.1 is a plot of background-subtracted, near-surface gold concentration as a function of the near-surface
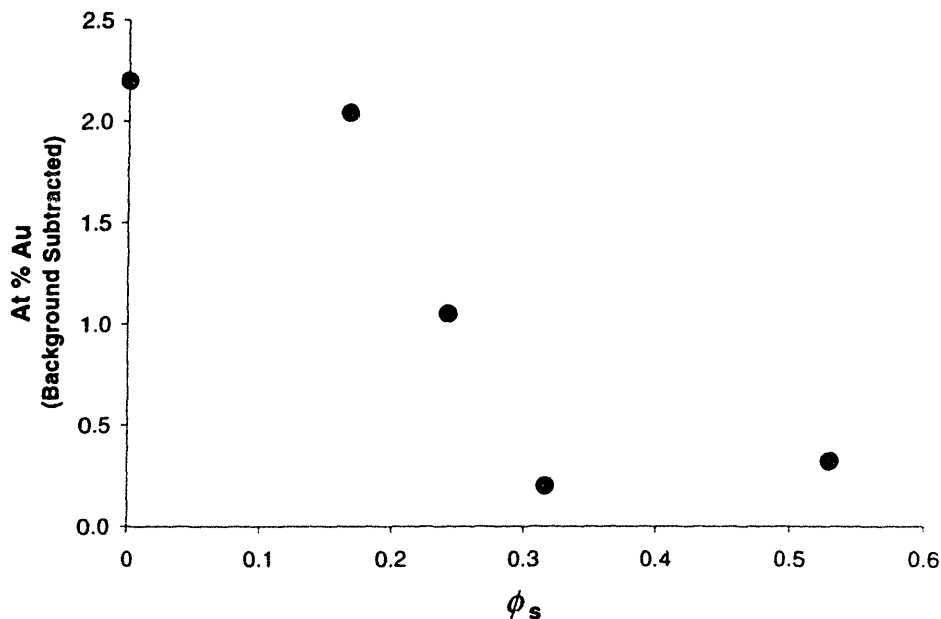
Figure 5.1 Effect of P(MMA-r-POEM₉) surface concentration on protein adsorption
Background-subtracted near-surface gold concentration (atom %) versus surface concentration P(MMA-r-POEM₉)[a] (vol. fraction, as measured by XPS) for as-cast membranes E-xx-9a-20 fouled by immersion in a 10 g/L BSA solution for 12 h and stained for total protein detection using anionic colloidal gold. Membranes having ϕ_s greater than ~0.3 exhibit nearly complete resistance to static BSA adsorption.

concentration of P(MMA-r-POEM₉)[a] obtained by XPS (see Section 4.2.1). According to the measured concentrations of the gold label, membranes having near-surface compositions of greater than ~30 wt % comb exhibit nearly complete resistance to BSA adsorption in this static experiment.

5.1.2 Fouling Resistance in Ultrafiltration

Membrane Design and Fabrication

Based on the results presented in the previous section and in Chapter 4, a series of membranes optimized for protein adsorption resistance was prepared with the objective of assessing the fouling resistance of self-organizing membranes in an UF experiment.

The UF experiment, described in detail in Section 3.3.6, was designed to simulate the operating conditions of an industrial filtration process. According to Figure 5.1, resistance to BSA adsorption is strongly enhanced for near-surface compositions of greater than ~30 wt % P(MMA-r-POEM$_9$) as measured by XPS. The results in Chapter 4 indicate that stable near-surface comb concentrations well above this value can be achieved in a single processing step by casting membranes containing a sufficiently high molecular weight comb ($\geq$ ~60 000 g/mol based on PS standards) at a bulk concentration of $\phi_b = 0.10$ into a 90°C water bath. Membranes for UF fouling experiments were prepared according to these molecular design and processing criteria.

An architectural parameter that has not yet been considered is the PEO *side chain length* of the comb. A second objective of the UF experiments was to determine the influence of side chain length on fouling resistance, if any. Thus, membranes containing comb additives having similar compositions but different side chain lengths were prepared. These comb polymers are schematically illustrated in Figure 5.2. Statistically, P(MMA-r-POEM$_5$) had roughly one 4-5 unit PEO side chain on every fourth backbone segment, P(MMA-r-POEM$_9$)^k had roughly one 8-9 unit PEO side chain on every sixth backbone segment, and P(MMA-r-POEM$_{45}$) had roughly one 45-unit PEO side chain on every thirtieth backbone segment.

P(MMA-*r*-POEM₅)

50.9 wt % (25.7 mol %) POEM₅
33.9 wt % EO

P(MMA-*r*-POEM₉)ᵏ

50.7 wt % (17.8 mol %) POEM₉
40.0 wt % EO

P(MMA-*r*-POEM₄₅)

41.2 wt % (3.3 mol %) POEM₉
39.2 wt % EO
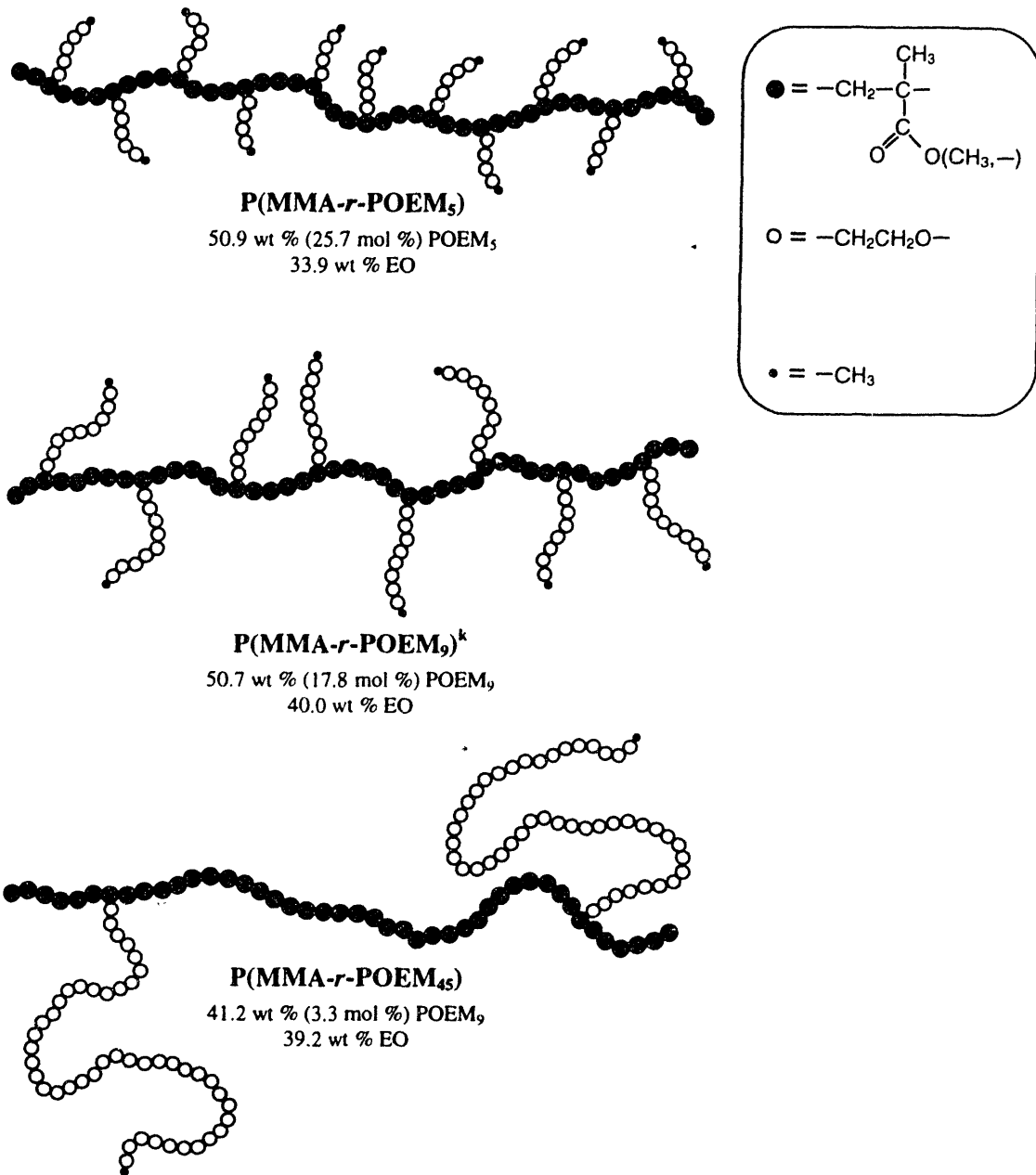
Figure 5.2 Illustration of P(MMA-*r*-POEM) combs with different tooth lengths

162

Membrane Surface Composition and Morphology

The integrated near-surface compositions of membranes containing combs with 5-unit, 9-unit, and 45-unit side chains were 50, 54, and 47 vol % comb, respectively, as measured by XPS (for details of the fits, see Appendix C, Table C.6). Thus, significant and roughly equivalent levels of comb surface segregation occurred in these membranes during coagulation in water at 90°C. As expected, the near-surface comb concentrations were substantially higher than the criterion for nearly complete static BSA adsorption resistance identified in Section 5.1.1.

FESEM micrographs of the separation surfaces of a pure PVDF membrane and membranes containing each of the comb additives appear in Figure 5.3. The separation surfaces of all of the membranes, including the pure PVDF membrane, exhibit a distinctly *nodular* morphology, with polymer nodules roughly 200 nm in diameter. These are not spherulites, since the cross-sectional morphologies of the membranes (Figure 5.4) are cellular in nature. Indeed, solid-liquid phase separation leading to spherulitic structures would not be expected under the fast precipitation conditions used in the preparation of these membranes.[69,83] Rather, the nodular structures are probably a result of top-layer liquid-liquid phase separation by spinodal decomposition. Spinodal decompostion of the surface layer of the casting solution may occur if rapid solvent-coagulant exchange brings the top-layer composition deeply into the 2-phase region of the phase diagram on a time scale shorter than the induction time for nucleation and growth.[53]
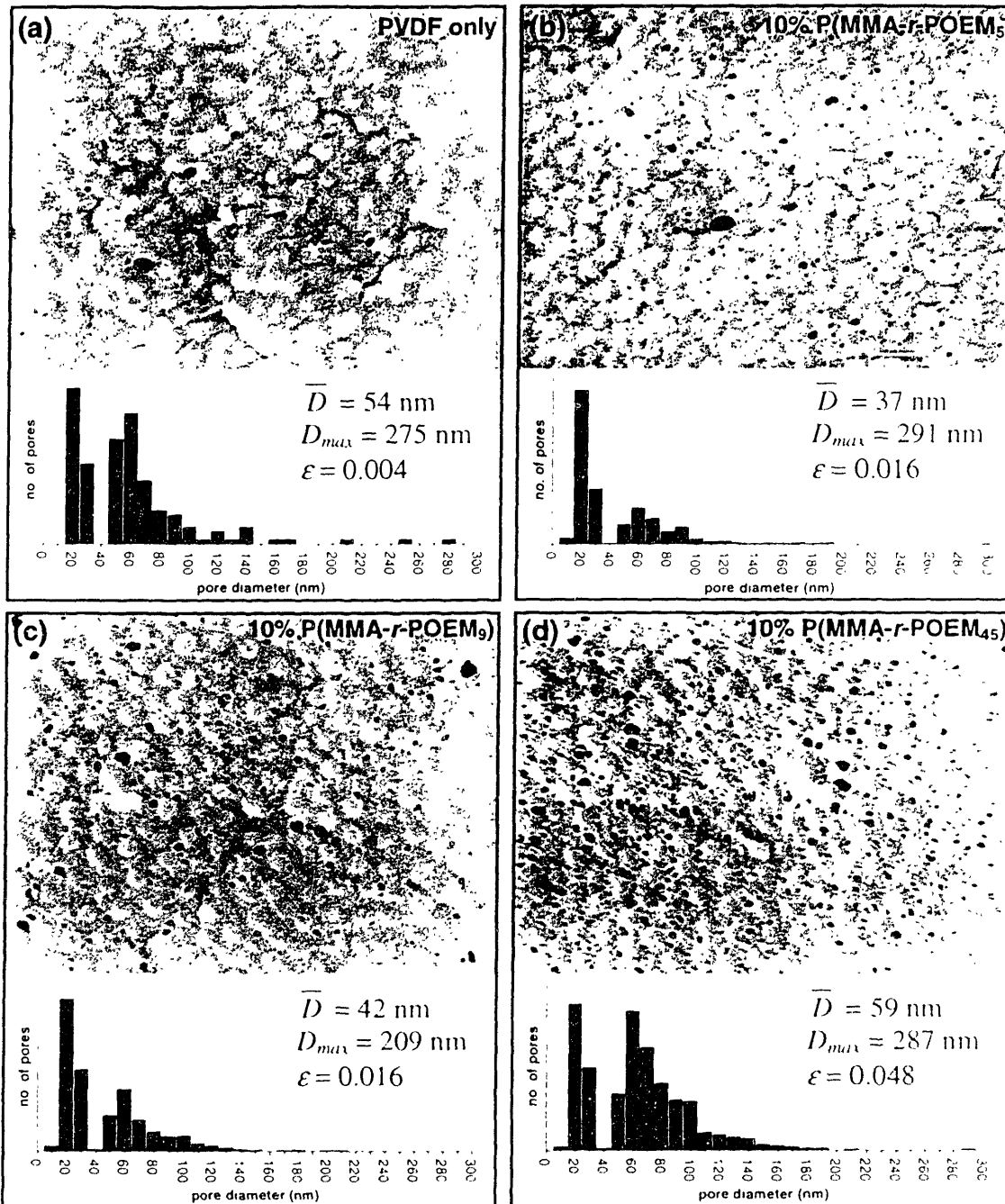
Figure 5.3 Separation surface morphology as a function of comb tooth length
FESEM micrographs of the separation surfaces of membranes having bulk compositions of
(a) pure PVDF (F-00-2-90), (b) 10 wt % P(MMA-*r*-POEM₅) (F-10-5-90), (c) 10 wt % P(MMA-*r*-
POEM₉)ᵏ, (F-10-9k2-90), and (d) 10 wt % P(MMA-*r*-POEM₄₅) (F-10-45-90) All membranes were
coagulated in pure dW at 90°C. Pore diameter histograms and pore statistics for each sample
type appear below the corresponding micrograph.

164

Nodular separation surface morphologies are commonly observed in UF membranes,[52,53,252] which are typically prepared using solvent-coagulant pairs with high mixing enthalpies.[47] The nodular structures have been compared to structures observed upon spinodal decomposition of concentrated polymer solutions by thermal quenching.[253,254] Dilatometric measurements and electron microscopy studies performed on such systems indicate that the fast spinodal demixing process is followed by a slower process during which the polymer-rich phase coarsens to produce the final morphology.[254] The characteristic size of the regularly spaced nodules is related to the fastest-growing wavelength of the initial concentration fluctuations.[53,254] Factors that favor rapid quenching and the consequent nodular separation surface morphology in polymer membranes include the choice of solvent-coagulant pairs with large mixing enthalpies, high casting temperatures, high polymer concentrations in the casting solution, and the presence of a water-soluble polymer in the casting solution (see Section 2.5).[53]

A histogram of pore diameters for each membrane type, along with pore size and porosity statistics, appears below the corresponding micrograph in Figure 5.3. Statistics for each membrane were compiled from 2-5 randomly selected micrographs. In preparing the membranes, a tendency toward larger pores with the addition of P(MMA-r-POEM) was observed, which increased with increasing PEO side chain length. This effect was offset, however, by adjustment of the glycerol concentration in the casting solution (see Table 3.4 and Section 3.2.1). Thus, as shown in Figure 5.3, the membranes used for filtration studies had similar pore size distributions. As observed and discussed in Section 4.3.1, addition of P(MMA-r-POEM) results in a substantial increase in

separation surface porosity (ε). This increase in porosity was particularly notable for the comb with 45-unit PEO side chains, the addition of which resulted in a porosity over an order of magnitude greater than that of a pure PVDF membrane with roughly the same average and maximum pore size. The cross-sections of the various membranes appear similar and feature large macrovoids, as shown in Figure 5.4.

Ultrafiltration Performance

Figure 5.5 is a plot of normalized flux (J/J_o) as a function of time for pure PVDF membranes and modified membranes during filtration of a 0.1 g/L BSA solution. Each data point is an average of data taken from two different membranes. Protein fouling of the pure PVDF membranes resulted in a rapid decline of the flux to less than 20% of the initial pure water flux (J_o) within 40 min. Membranes modified with the comb additives exhibited substantially less dramatic flux declines. In fact, membranes modified with the comb having the longest side chains (45 PEO units) had an average normalized flux over 4 times that of the pure PVDF membranes after 3 h of filtration of the protein solution. The BSA rejection coefficients for the membranes are plotted in the inset of Figure 5.5. The rejection coefficient is defined as,

$$R_{BSA} = 1 - \frac{C_{BSA}^{permeate}}{C_{BSA}^{feed}} \tag{5.1}$$

where $C_{BSA}^{permeate}$ and C_{BSA}^{feed} are the BSA concentrations in the permeate and feed streams, respectively, measured by UV/Vis spectroscopy immediately following the 3-h filtration experiment. All membranes retained BSA to some extent, indicating that they had similar separation characteristics with respect to this protein, which, under the filtration

166

conditions, fills a prolate ellipsoid ("cigar-shaped") volume with minor and major axes of 42 and 141 Å, respectively.[255] The fact that R_{BSA} was significantly less than one for all membranes indicates that these filtration experiments were *through-pore* fouling experiments, which probed the fouling resistance of the internal pore channels as well as the external separation surface.
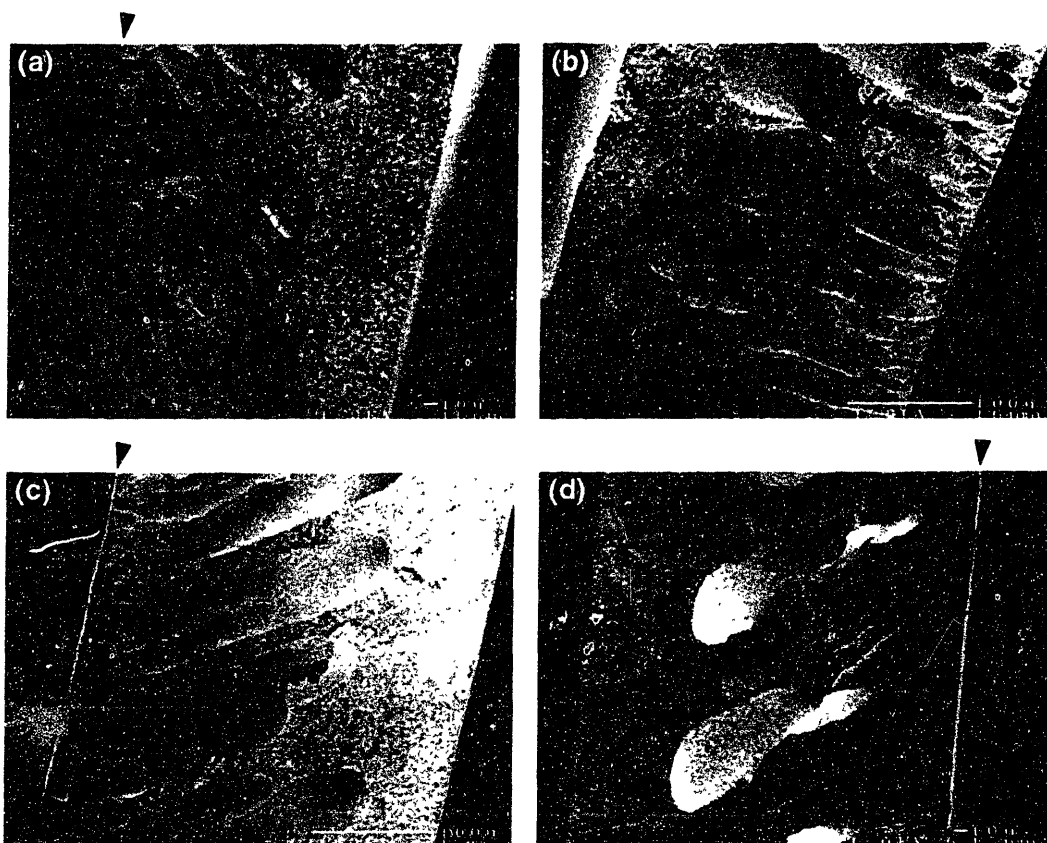
Figure 5.4 Substructure morphology as a function of comb tooth length
Cross-sectional FESEM micrographs of the membranes appearing in Fig. 5.3: (a) pure PVDF (F-00-2-90), (b) 10 wt % P(MMA-r-POEM5) (F-10-5-90), (c) 10 wt % P(MMA-r-POEM0)k, (F-10-9k2-90), and (d) 10 wt % P(MMA-r-POEM45) (F-10-45-90). The separation surface of each membrane is indicated by an arrow.
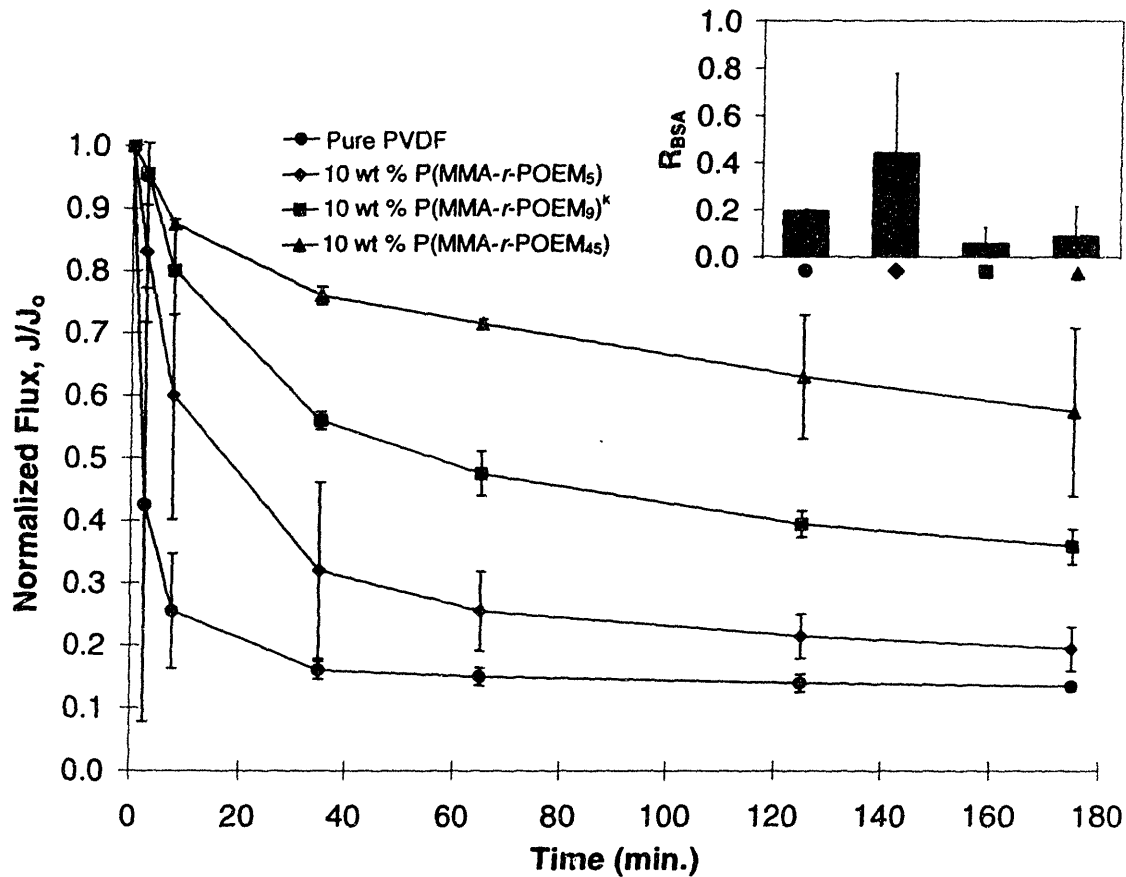
Figure 5.5 Normalized flux of BSA solution through PVDF and blend membranes
Flux of a 0.1 g/L BSA solution (J) divided by initial pure water flux (J_o) as a function of time for pure PVDF membranes and for membranes containing P(MMA-r-POEM) comb additives having different side chain lengths. The membranes were F-00-2-90 (●), F-10-5-90 (◆), F-10-9k2-90 (■), and F-10-45-90 (▲). *Inset:* BSA rejection coefficients for the same membranes.
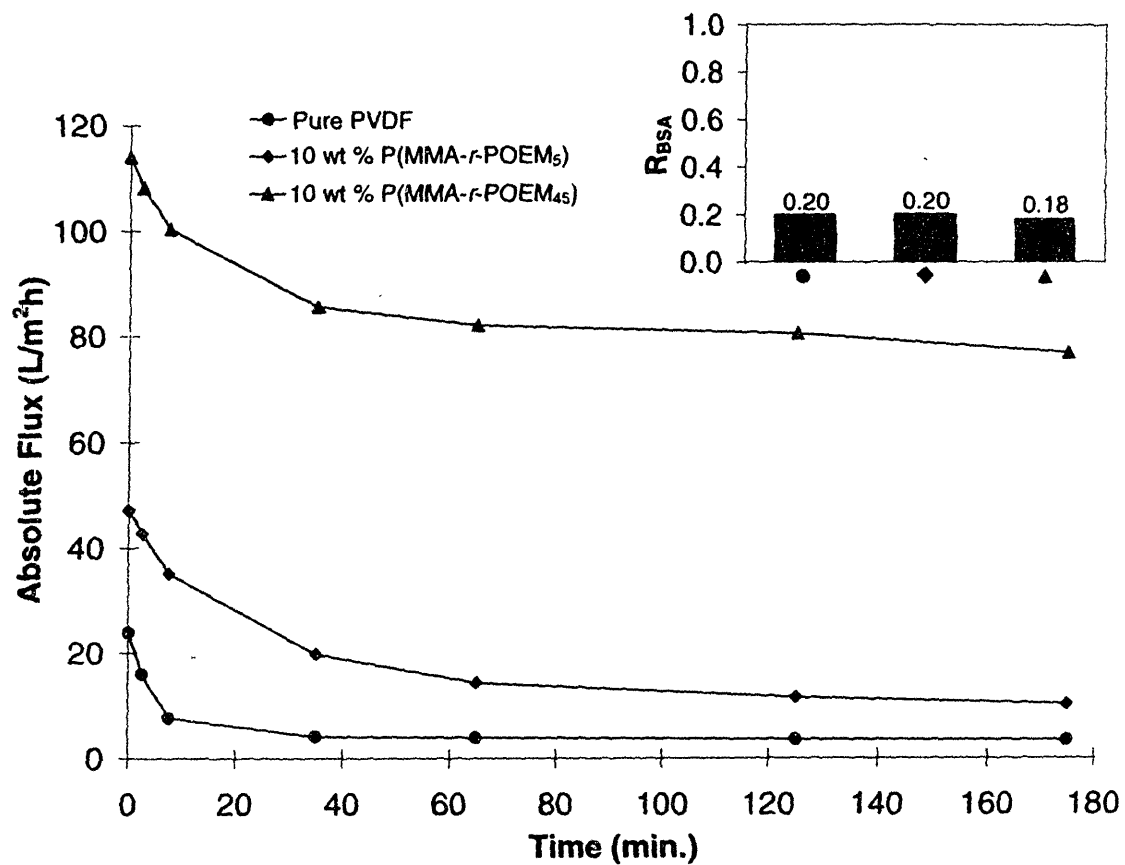
Figure 5.6 Absolute flux of BSA solution through PVDF and blend membranes
Flux of a 0.1 g/L BSA solution through a PVDF membrane and membranes containing P(MMA-*r*-POEM) comb additives having different side chain lengths. The membranes were F-00-2-90 (●), F-10-5-90 (◆), and F-10-45-90 (▲). *Inset:* BSA rejection coefficients for the same membranes.

The data in Figure 5.5 indicate a significant increase in fouling resistance with increasing PEO side chain length, at constant overall PEO content of the comb. This observation is consistent with the results of previous studies of protein adsorption onto surfaces modified with end-grafted PEO.[174,176,256,257] For example, Hlady, et al.[257] studied albumin and IgG adsorption onto silica surfaces modified with end-grafted PEO of molecular weight 750-14,000 g/mol. While all PEO-modified surfaces adsorbed substantially less protein than unmodified silica, surfaces modified with 1900 g/mol PEO adsorbed roughly an order of magnitude less protein than surfaces modified with 750 g/mol PEO. However, further increases in PEO molecular weight above 1900 g/mol resulted in only slight enhancements in protein adsorption resistance. In their study of albumin and fibrinogen adsorption onto poly(ethylene terephthalate) films modified with end-grafted PEO, Gombotz, et al.[176] similarly observed decreasing protein adsorption with increasing PEO molecular weight up to 3500 g/mol, with only slight reductions in adsorption with further molecular weight increases. In the latter study, the trend to higher protein resistance with higher PEO molecular weight occurred in spite of a significant measured decrease in the total amount of grafted PEO with increasing molecular weight.

In Figure 5.5, each flux value has been normalized by the initial pure water flux in order to compare the various membranes on the basis of flux reductions due to fouling alone. In Figure 5.6, the same data for selected membranes has been plotted in terms of *absolute flux* (J). The three flux curves in Figure 5.6 were obtained from individual membranes, all of which had nearly identical BSA rejection coefficients (see Fig. 5.6, inset) of 0.18-0.20. These results demonstrate the practical significance of the observed

increase in separation surface porosity with addition of the comb additives, namely,

higher pure water fluxes. Hence, a self-organizing membrane with a bulk composition of

10 wt % P(MMA-r-POEM$_{45}$) has an initial pure water flux nearly 5 times higher than a

pure PVDF membrane having the same separation characteristics with respect to BSA,

and an absolute flux over 22 times higher than the PVDF-only membrane after 3 h of

filtration of the concentrated foulant solution. The numerical results of the filtration

studies described above are tabulated in Table 5.1 for comparison with the results of

previous surface modification studies similarly tabulated in Appendix A.

Table 5.1 Summary of Ultrafiltration Data

Membrane	Bulk Composition	ϕ_s *	R_{BSA}	J_o (L/m^2h)	J_f (L/m^2h)	‡ J_f/J_o	†† $J_o{}^M/J_o{}^C$	‡‡ $J_f{}^M/J_f{}^C$
F-00-2-90	pure PVDF	-	0.20 (0.20)†	31.78 (23.91)	4.22 (3.42)	0.13 (0.14)	-	-
F-10-5-90	10 wt % P(MMA-r-POEM$_5$)	0.50	0.44 (0.20)	48.23 (47.16)	9.38 (10.18)	0.19 (0.22)	1.52 (1.97)	2.22 (2.98)
F-10-9k2-90	10 wt % P(MMA-r-POEM$_9$)^k	0.54	0.06	90.61	32.21	0.36	2.85	7.63
F-10-45-90	10 wt % P(MMA-r-POEM$_{45}$)	0.47	0.09 (0.18)	166.15 (113.99)	90.42 (76.59)	0.57 (0.67)	5.23 (4.77)	21.43 (22.39)

* For details, see Appendix C, Table C.6.

† Values without parenthesis are averages; values inside parenthesis are for an individual membrane of each type having a BSA rejection coefficient of ~0.20.

‡ Final flux of BSA solution divided by initial pure water flux.

†† $J_o{}^C$ = initial pure water flux for pure PVDF membrane; $J_o{}^M$ = initial pure water flux for blend membrane.

‡‡ $J_f{}^C$ = final flux of BSA solution for pure PVDF membrane; $J_f{}^M$ = final flux of BSA solution for blend membrane.

Comparison with Other Surface Modification Approaches

In setting forth the criteria for success of any anti-fouling surface modification (Table 1.1, Section 2.6.1), we stated that the ideal surface modification technique would enhance membrane performance by (a) imparting resistance to flux decline caused by adsorption of foulants from the feed solution, while (b) causing no reduction in pure water permeability (and, if possible, enhancing it). To capture the first of these criteria quantitatively, we define the "flux decline ratio,"

$$R_{f,d} = \frac{J_f^M / J_o^M}{J_f^C / J_o^C} \tag{5.2}$$

where symbols for the various fluxes (J's) are defined in Section 2.4.1. $R_{f,d}$ compares the fouling resistance of a surface-modified membrane with that of the corresponding unmodified membrane. The second criterion is captured simply by the ratio of the pure water flux through the modified membrane to that through the unmodified membrane $\left(J_o^M / J_o^C\right)$. The ratio of fluxes through the fouled modified membrane vs. the fouled unmodified membrane $\left(J_f^M / J_f^C\right)$ is simply the product of these two performance metrics.

In Figure 5.7, the values of these two metrics are plotted simultaneously for all past surface modification studies summarized in Appendix A for which both are available. The grey-shaded region of the plot, in which the values of both metrics are greater than one, is the most desirable region in terms of membrane performance. This region represents the space in which the modified membrane is both more fouling resistant and more permeable to pure water than the corresponding unmodified membrane. Although the data from past work were obtained using a variety of base

172

membranes and surface modification techniques, they superpose remarkably well, showing a clear inverse relationship between the two performance metrics. Surface-modified membranes have often exhibited enhanced pure water permeability compared to unmodified controls, due to increased hydrophilicity. However, grafted or coated surface layers of sufficient density to impart significant fouling resistance occlude the membrane pores, resulting in reduced pure water permeability.
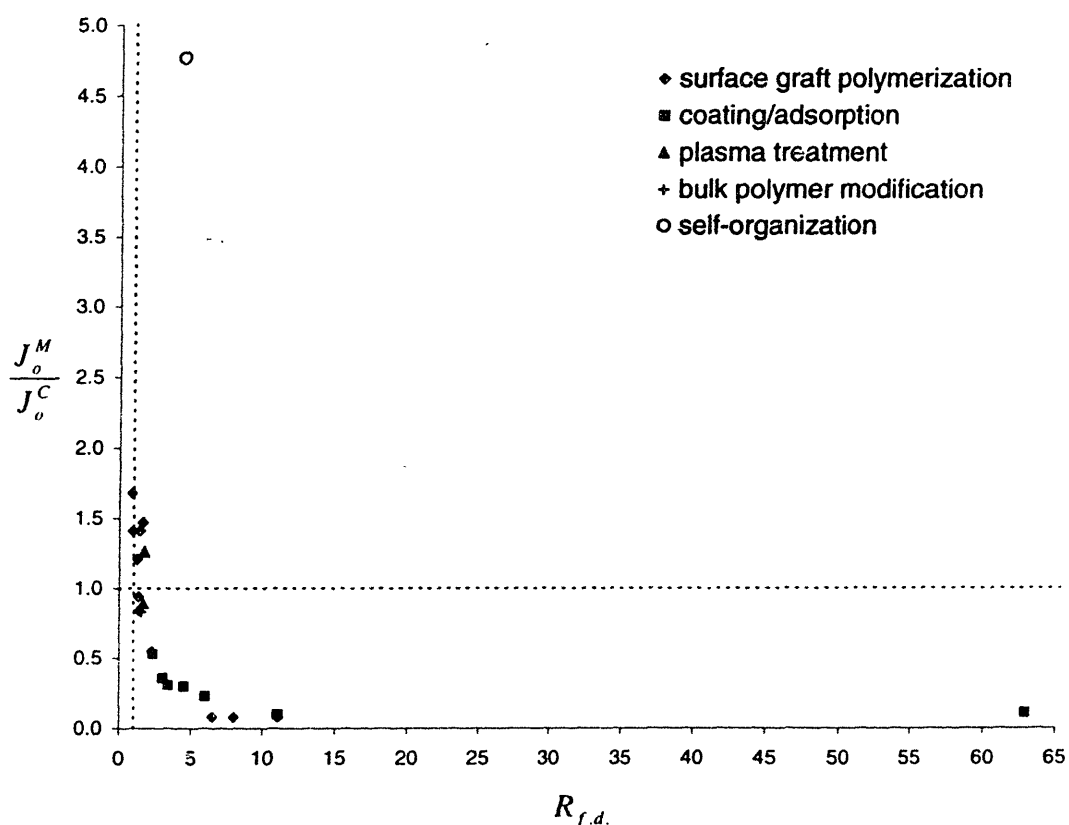
Figure 5.7 Comparison of self-organization to other surface modification methods
Black symbols are data from previous surface modification studies reviewed in Appendix A. The self-organizing membrane (white symbol) is membrane F-10-45-90, having a bulk composition of 10 wt % P(MMA-r-POEM$_{45}$). For this membrane $R_{fd.}$ was computed using averaged flux values from two separate membranes, while J_o^M/J_o^C was computed using initial fluxes from a membrane of each type having nearly equivalent separation characteristics with respect to BSA (see Table 5.1).

A self-organizing membrane with a bulk composition of 10 wt % P(MMA-*r*-POEM$_{45}$) (white symbol) has comparable fouling resistance to membranes modified using other techniques. Significantly, however, the pure water permeability of the self-organizing membrane is substantially higher than that of an unmodified membrane with equivalent separation characteristics. Thus, the increased porosity achieved through addition of the amphiphilic comb offers an opportunity to escape the traditional inverse relationship between fouling resistance and pure water permeability, enhancing both properties simultaneously.

5.2 Self-Healing Membranes

5.2.1 Introduction

In Section 2.4.1, we discussed the limitations of surface layers constructed by surface graft polymerization and, particularly, coating and adsorption methods with respect to long-term stability. We discussed in Section 2.6.2 the possibility of using self-organizing polymer blends to construct self-healing membranes, exploiting the residual amphiphilic additive left in the bulk after membrane fabrication. That is, a tailored, surface-segregated polymer layer degraded by repeated chemical cleanings or long-term exposure to aggressive species in the feed stream might be regenerated simply by heat treating the membrane in water, allowing sufficient diffusion to restore the equilibrium, additive-rich surface composition. Indeed, it was shown in Section 4.2.1 that substantial surface segregation of P(MMA-*r*-POEM) can be achieved by heat treating membranes in water at 90°C for periods of ~12 h.

This section explores the possibility of using heat treatment to reconstruct P(MMA-r-POEM) surface layers damaged by exposure to acid. In an attempt to simulate the effects of long-term acid exposure in a reasonable period of laboratory time, wet membranes containing P(MMA-r-POEM9)[a] (membranes E-xx-9a-20, Table 3.4) were treated for a short time (30 min) with pure, concentrated CSA, as described in Section 3.2.1. This particular acid was chosen because it produced well-characterized surfaces, the chemistries of which could be readily identified by XPS. Following acid treatment, membranes were annealed for 12 h in an attempt to regenerate their surface chemistries. Section 5.2.2 investigates the effects on membrane surface chemistry of the acid treatment and subsequent heat treatment. Section 5.2.3 relates these surface chemistries to static protein fouling resistance.

5.2.2 Surface Composition

XPS spectra obtained before and after acid treatment from a pure PVDF membrane (E-00-1-20), pure P(MMA-r-POEM9)[a], and membranes containing 5 wt % of the comb additive (E-05-9a-20) are displayed in Figure 5.8. A spectrum obtained from the 5% comb membrane after exposure to acid and subsequent heat treatment in water is also shown. The surface chemistry of the pure PVDF membrane was unchanged by immersion in acid. To fit the XPS spectrum for the pure comb polymer after acid treatment, it was necessary to shift the position of the COO peak to 289.41 eV, up approximately 0.4 eV from its position prior to acid treatment. A reaction which is facile in concentrated acid and which would result in such a shift is partial hydrolysis of the methacrylate ester group, followed by attack of the acid group so generated on the
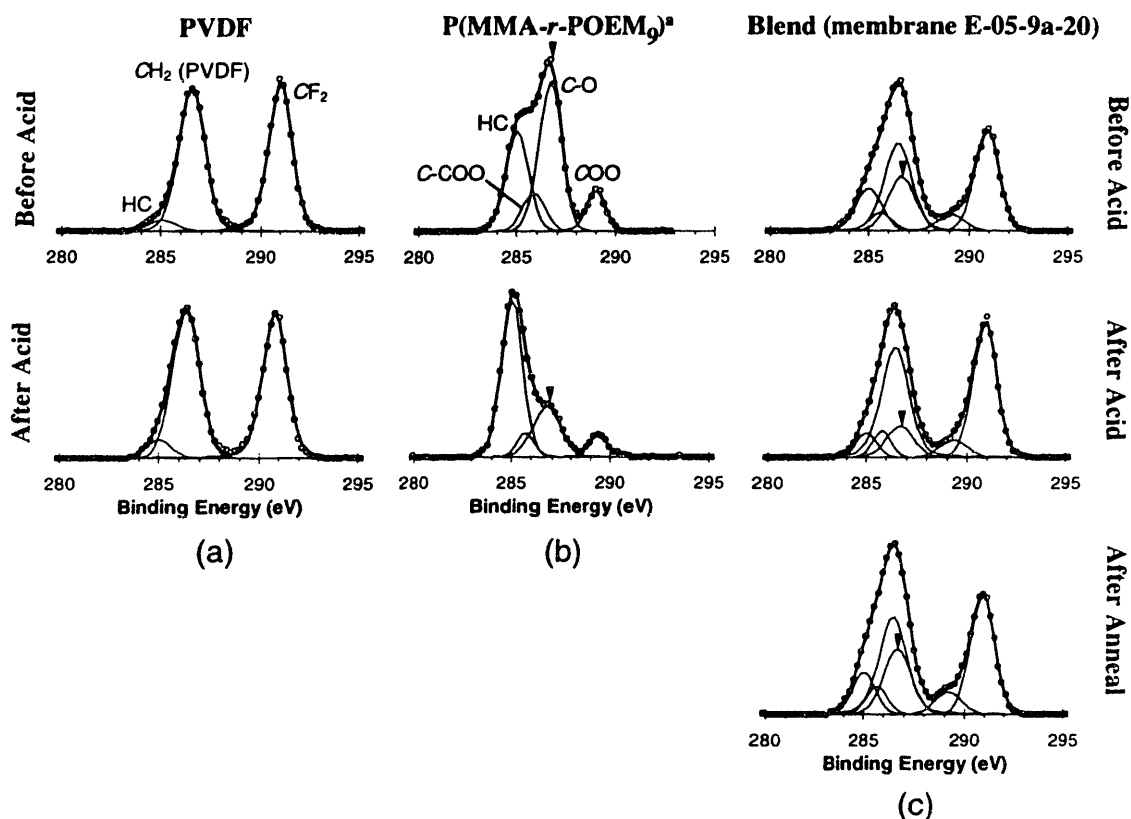
Figure 5.8 Fitted C 1s XPS spectra for samples used in surface regeneration study
High-resolution C 1s XPS data and fitted peaks for (a) pure PVDF membrane before and after acid treatment; (b) pure P(MMA-r-POEM9)[a] before and after acid treatment; and (c) membrane E-05-9a-20 (ϕ_b = 0.075) before and after acid treatment, and after subsequent heat treatment for 12 h in water at 90°C. Triangular arrows indicate the component peaks due to the C-O bonding environment. (For details of the fits, see Appendix C, Figure C.7.)

carbonyl of its adjacent ester to form the anhydride (Figure 5.9).[258] The anhydride carbonyl has been assigned a position of 289.4 eV using high-resolution equipment.[225]

In any case, due to the apparent change in the chemistry of the carbonyl after acid exposure, it was not possible to distinguish between the COO-C and C-O environments using the assumption of equal COO-C and C-O peak areas. Thus, XPS spectra for the regeneration study were fit with a single C-O peak with the position constrained at

286.62 ± 0.15 eV. The COO peak was allowed to shift up to 289.41 eV for acid-treated samples. With these exceptions, fitting of the C 1s XPS spectra was conducted as described in Section 4.2.1. Component peak area percentages for the pure comb and 5% blend samples are tabulated in Appendix C, Table C.7.
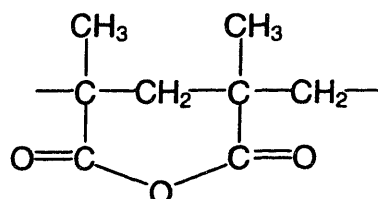
Figure 5.9 Possible product formed on exposure of P(MMA-r-POEM) to CSA

Acid treatment of the pure comb sample resulted in a significant reduction of the relative number of carbon atoms having a C-O bonding environment (component peak denoted with an arrow in Figure 5.3). This is probably due to hydrolysis of the PEO side chains to yield soluble fragments, as well as the change in the carbonyl bonding environment noted above. The peak area ratios $A_{\underline{C}OO}/A_{\underline{C}F_2}$, $A_{\underline{C}-O}/A_{\underline{C}F_2}$, and $A_{\underline{C}-O}/A_{\underline{C}OO}$ for 5 wt % membranes before acid immersion, after acid immersion, and after subsequent heat treatment are listed in Table 5.2.

Table 5.2 C 1s Peak Area Ratios for Membranes Used in Regeneration Study

History	$A_{\underline{C}OO}/A_{\underline{C}F_2}$	$A_{\underline{C}-O}/A_{\underline{C}F_2}$	$A_{\underline{C}-O}/A_{\underline{C}OO}$
as cast	0.17	0.58	3.42
30 min in acid	0.14	0.25	1.77
30 min in acid + 12 h anneal	0.20	0.62	3.12

Acid treatment resulted in a slight reduction in the area of the COO peak relative to that of the CF$_2$ peak and a substantial reduction in the relative area of the C-O peak. These observations are consistent with hydrolysis of the PEO side chains upon immersion in acid, leaving most of the backbone of the comb additive intact. Subsequent heat treatment resulted in enhancement of the $A_{\underline{C}OO}/A_{\underline{C}F_2}$ and $A_{\underline{C}-O}/A_{\underline{C}F_2}$ ratios to values slightly greater than their initial, pre-acid treatment values. These results demonstrate the regenerative capability afforded by the use of an amphiphilic, surface-segregating additive polymer in the membrane composition.

5.2.3 Static Fouling Resistance

To assess the effectiveness of surface regeneration with respect to fouling resistance, membranes having bulk compositions of 5 and 10 wt % P(MMA-r-POEM$_9$)[a] (membranes E-05-9a-20 and E-10-9a-20, Table 3.4) were fouled by static BSA adsorption and stained for BSA detection using anionic colloidal gold, as described in Sections 3.3.5 and 5.1.1. Figure 5.10 shows the background-subtracted, near-surface gold concentrations for membranes containing 5 and 10 wt % P(MMA-r-POEM$_9$)[a] in the as-cast (at 20°C) condition, after acid exposure, and after acid exposure and subsequent heat treatment for 12 h in water at 90°C.

The data indicate a dramatic reduction in protein resistance for both membrane compositions after acid treatment, followed by substantial, though not complete, recovery of protein resistance after heat treatment. It is of interest to note that the membrane with the initially greater near-surface concentration of P(MMA-r-POEM) is significantly *less* protein resistant after acid exposure. This observation indicates that the methacrylate
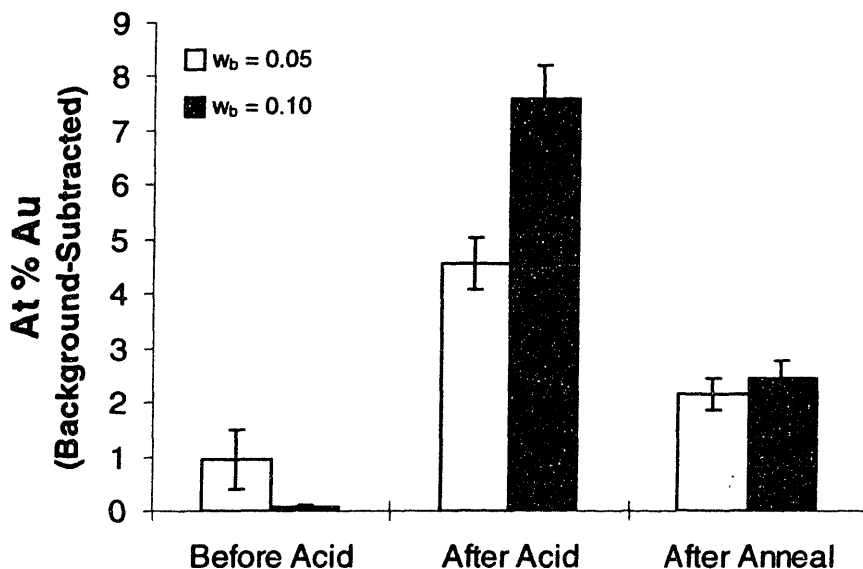
Figure 5.10 Static fouling resistance of membranes with regenerative surfaces
Background-subtracted, near-surface gold concentrations (atom %) for as-cast (at 20°C), acid-treated, and acid-treated and subsequently annealed membranes fouled with BSA and stained for protein detection using anionic colloidal gold. (□) Membrane E-05-9a-20, with a bulk composition of 5 wt % P(MMA-r-POEM$_9$)[a]; and (■) membrane E-10-9a-20, with a bulk composition of 10 wt % P(MMA-r-POEM$_9$)[a].

backbone remaining after acid hydrolysis of the comb side chains is more susceptible to protein adsorption than PVDF. This is not surprising, since PVDF, due to its extreme hydrophobicity, has been shown to adsorb BSA less readily than many polymers of intermediate polymer/water interfacial energy, including PMMA.[259] It is likely that, with further annealing in water, the hydrolyzed comb species would eventually be fully displaced by the more hydrophilic combs from the membrane bulk, providing more complete recovery of protein adsorption resistance.

5.3 Spontaneously Wettable Membranes

5.3.1 Characterization of Membranes Containing PVDF Graft Copolymers

In Sections 5.3 and 5.4, we explore the properties of self-organizing membranes prepared by the addition to the casting solution of amphiphilic graft copolymer derivatives of PVDF prepared by ATRP. These membranes were cast according to the principles identified in Chapter 4 as optimal for the preparation of membranes containing P(MMA-r-POEM). All of the PVDF copolymer additives used were of high molecular weight (>150 000 g/mol according to ^{1}H NMR – see Section 3.1). In fact, in the case of membranes containing PVDF-g-PMAA, the molecular weight of the additive was higher than that of the PVDF matrix. In all cases, membranes were cast into 90°C coagulation baths in order to increase the kinetics of surface segregation. As will be shown in the following paragraphs, the application of these principles resulted in significant surface localization of the additive polymers, with no need for post-coagulation heat treatment.

Membranes Containing PVDF-g-POEM

Surface Composition. For membranes containing PVDF-g-POEM, the C 1s region of the XPS spectrum was fit with six component peaks representing the carbon bonding environments shown in Figure 5.11. The peak centers of the component peaks were constrained (±0.1 eV) as shown in Table 5.3, according to previously determined peak positions for pure PVDF, PMMA, and PEO homopolymers.[225] The areas of the CH_2 and CF_2 peaks were constrained to be equal, according to stoichiometry, as were the areas of the C-COO and COO peaks of the methacrylate environment. The ratio of the C-O and COO peak areas was constrained to its stoichiometric value of 18.04.

$$-\left(CH_2-CF_2\right)_x$$
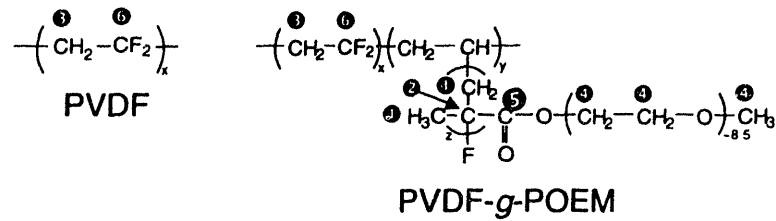
PVDF

PVDF-g-POEM

Figure 5.11 Carbon bonding environments present in PVDF and PVDF-g-POEM

Table 5.3 XPS C 1s Bonding Environments in PVDF and PVDF-g-POEM

Carbon Environment (Fig. 4.1)	Carbon Environment Abbreviation	BE_o (eV)
1	HC	285.00
2	C-COO	285.72
3	CH$_2$ (PVDF)	286.44
4	C-O	286.50
5	COO	289.03
6	CF$_2$	290.90

Figure 5.12 shows fitted C 1s envelopes for (a) a pure PVDF membrane, (b) an evaporation-cast film of pure PVDF-g-POEM[b], and (c,d) membranes having bulk compositions of 5 and 10 wt % PVDF-g-POEM[b], respectively. For membranes containing PVDF graft copolymer additives, the backbones of which are indistinguishable from the matrix by XPS, near-surface compositions will be reported in terms of the weight fraction of the comonomer. The near-surface mole fraction of POEM for membranes containing PVDF-g-POEM was calculated from XPS as,

$$n_s^{POEM} = \frac{A_{\underline{C}OO}}{A_{\underline{C}F_2} + A_{\underline{C}OO}} \tag{5.3}$$

where A_x is the area of the peak for bonding environment x. The near-surface weight fraction of POEM was then computed as,

$$\phi_{w,s}^{POEM} = \frac{n_s^{POEM} M_o^{PPOEM}}{n_s^{POEM} M_o^{PPOEM} + (1 - n_s^{POEM}) M_o^{PVDF}} \qquad (5.4)$$

where M_o^{PPOEM} and M_o^{PVDF} are the repeat unit molar masses of poly(POEM$_9$) (475 g/mol) and PVDF (64 g/mol).
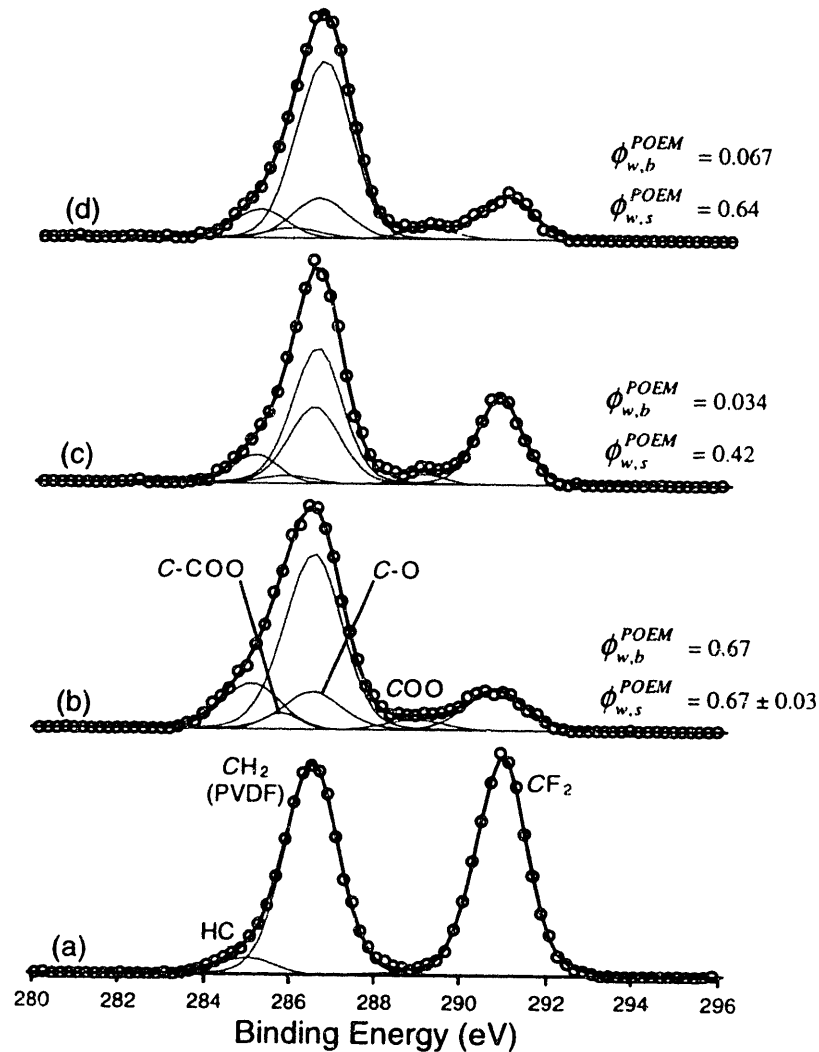
Figure 5.12 **Fitted C 1s envelopes for PVDF, PVDF-g-POEM, and blend membranes** (a) Pure PVDF membrane, (b) evaporation cast film of pure PVDF-g-POEM[b], (c) membrane F-05-AT2-90, containing 5 wt % PVDF-g-POEM[b], and (d) membrane F-05-AT2-90, containing 10 wt % PVDF-g-POEM[b]. For (b), (c), and (d), the computed bulk and surface compositions are noted in terms of weight fraction of POEM. For (b), the surface composition is an average from two samples. (For details of the fits, see Appendix C, Table C.8.)
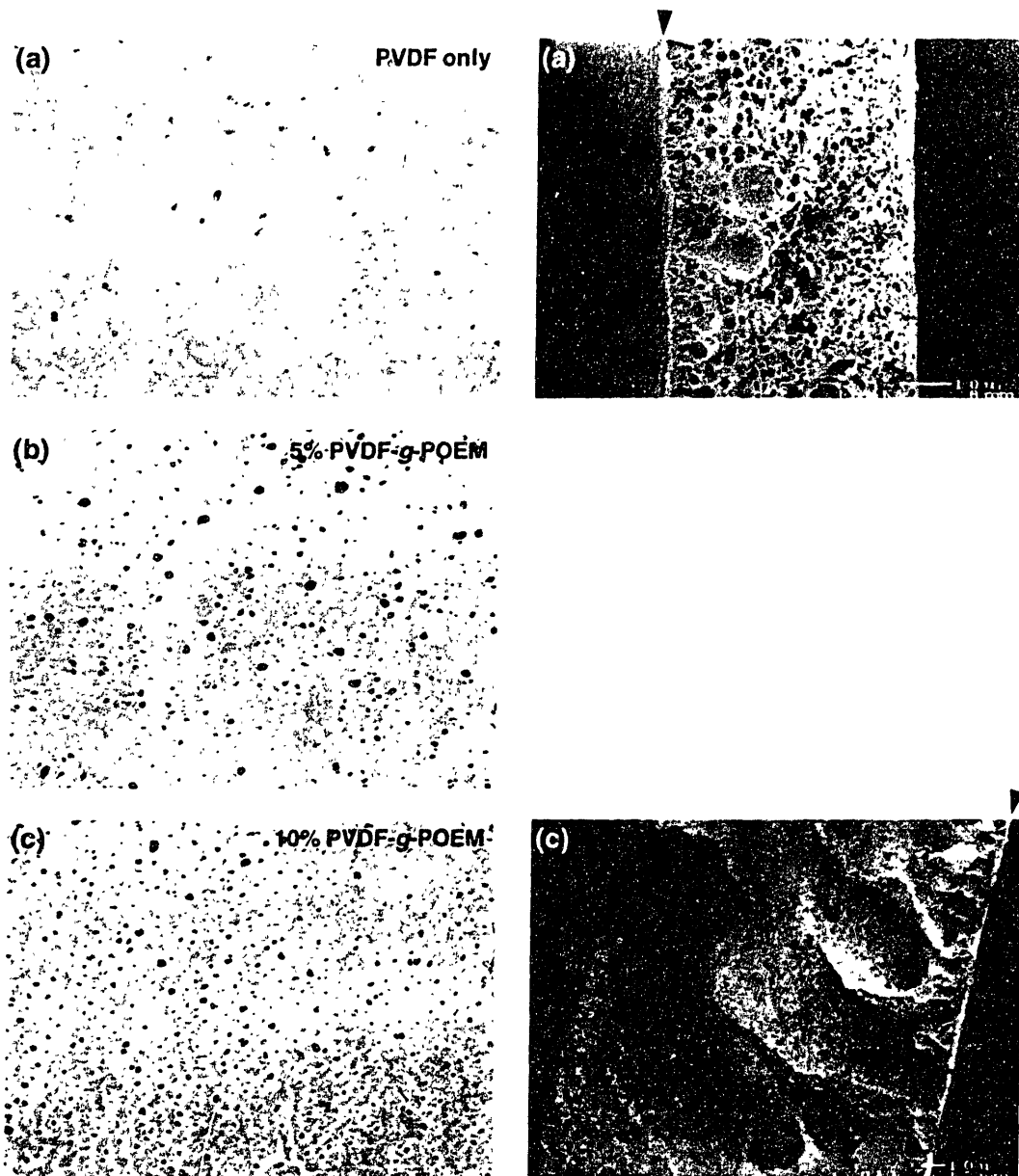
Figure 5.13 Morphology of membranes containing PVDF-g-POEM

FESEM images of the separation surfaces (left) and cross-sections (right) of membranes cast into a dW bath at 90°C. (a) Pure PVDF membrane F-00-3-90, (b) membrane F-05-AT2-90, containing 5 wt % PVDF-g-POEM[b], and (c) membrane F-10-AT2-90, containing 10 wt % PVDF-g-POEM[b]. Arrows indicate the separation surfaces in cross-sectional images.

183

Bulk compositions $\phi_{w,b}^{POEM}$ and near-surface compositions $\phi_{w,s}^{POEM}$ of the pure

PVDF-g-POEM films and example membranes appear next to the corresponding XPS

spectra in Figure 5.12. The pure comb films were cast by evaporation as described in

Section 3.2.2. Due to the long evaporation time, the near-surface composition of the

films, which equals the bulk composition of the copolymer determined by ^{1}H NMR, is

expected to be an equilibrium composition. The near-surface compositions of the

membranes indicate substantial surface segregation of PVDF-g-POEM during

coagulation at 90°C, such that a membrane containing 10 wt % of the comb additive

(6.7 wt % POEM) has a near-surface POEM concentration roughly identical to the pure

copolymer.

Morphology. FESEM micrographs of the separation surfaces and cross-sections

of membranes cast under identical conditions but having different bulk fractions of

PVDF-g-POEM are shown in Figure 5.13. All membranes, including PVDF-only

samples, exhibit nodular separation surface morphologies indicating top-layer liquid-

liquid phase separation by spinodal decomposition (see Section 5.1.2). As with P(MMA-

r-POEM), addition of PVDF-g-POEM to the casting solution results in significantly

higher separation surface porosities compared to PVDF-only membranes, as well as

increased macrovoid formation. Current work by Ariya Akthakul in the laboratory of

Prof. A. M. Mayes at MIT has shown that macrovoid formation in membranes prepared

from PVDF / PVDF-g-POEM blends can be completely suppressed by addition of $CaCl_2$

to the coagulation bath (as suggested by the results in Section 4.3.2), while retaining

substantial surface coverage of the amphiphilic copolymer and high surface porosities

relative to pure PVDF membranes. None of the micrographs in Figure 5.13 provide any evidence of large-scale phase separation of PVDF and PVDF-g-POEM.
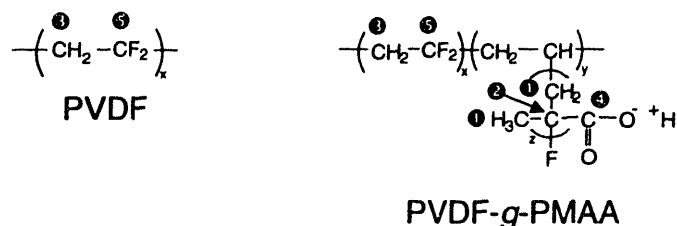
Figure 5.14 Carbon bonding environments present in PVDF and PVDF-g-PMAA

Membranes Containing PVDF-g-PMAA

Surface Composition. The C 1s regions of the XPS spectra for membranes containing PVDF-g-PMAA were fit with five component peaks representing the bonding environments indicated in Figure 5.14. These peaks were centered (±0.1 eV) as shown in Table 5.4, according to previously determined peak positions for PVDF and PMAA homopolymers.[225] The areas of the CH_2 and CF_2 peaks of PVDF were constrained to be equal, as were the areas of the C-COOH and COOH peaks.

Table 5.4 XPS C 1s Bonding Environments in PVDF and PVDF-g-PMAA

Carbon Environment (Fig. 4.1)	Carbon Environment Abbreviation	BE_o (eV)
1	HC	285.00
2	C-COOH	285.80
3	CH_2 (PVDF)	286.44
4	COOH	289.33
5	CF_2	290.90

Figure 5.15 shows fitted C 1s envelopes for (a) a pure PVDF membrane, (b) a pure PVDF-g-PMAA film evaporation cast from DMAc, and (c) an as-cast membrane
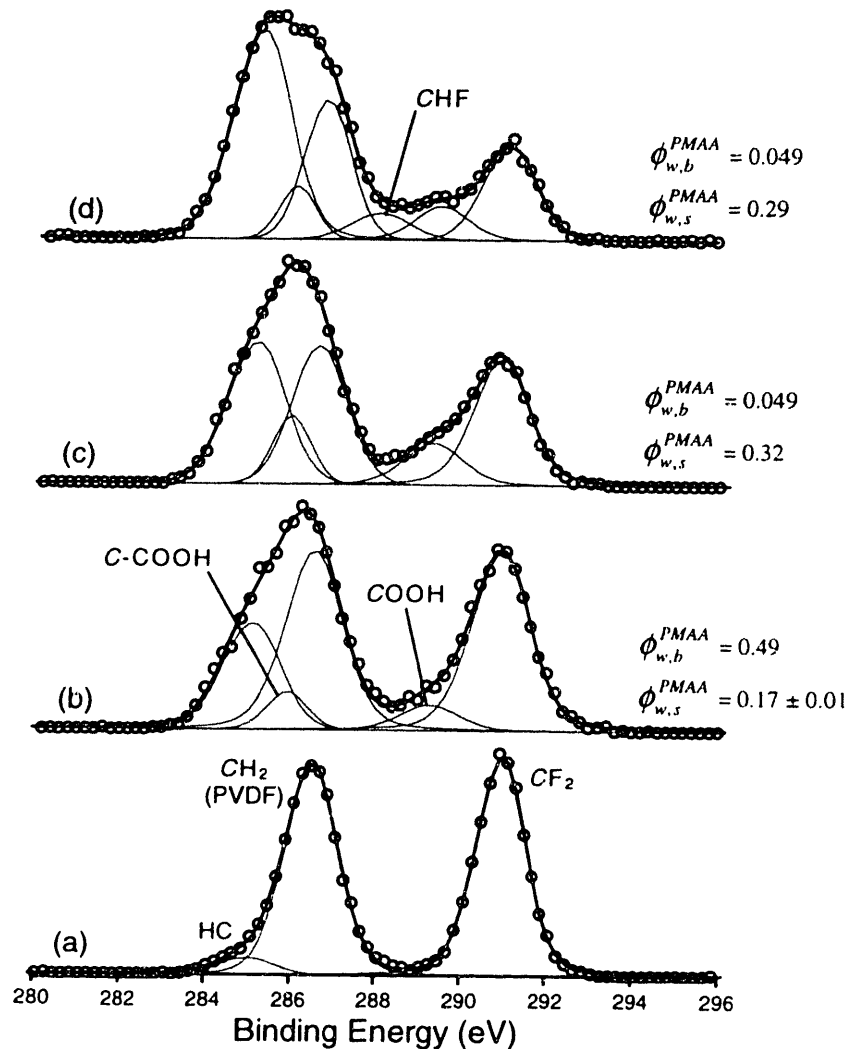
Figure 5.15 Fitted C 1s envelopes for PVDF, PVDF-g-PMAA, and blend membranes (a) Pure PVDF membrane, (b) evaporation cast film of pure PVDF-g-PMAA, (c) membrane F-10-PE-90, containing 10 wt % PVDF-g-PMAA, and (d) the same membrane after autoclaving for 1 h at 121°C while immersed in dW. For (b), (c), and (d), the computed bulk and surface compositions are noted in terms of weight fraction of PMAA. For (b), the surface composition is an average from two samples. (For details of the fits, see Appendix C, Table C.9.)

with a bulk composition of 10 wt % PVDF-g-PMAA. The near-surface mole fraction of PMAA was calculated from the XPS fits as,

$$n_s^{PMAA} = \frac{A_{\underline{C}OOH}}{A_{\underline{C}H_2(PVDF)} + A_{\underline{C}OOH}}.$$ (5.5)

The near-surface weight fraction of PMAA was then computed using an equation analogous to Equation 5.4, with $M_o^{PMAA} = 86$ g/mol. Bulk and near-surface compositions for each sample appear in Figure 5.15.

The near-surface concentration of PMAA in the pure comb films, which were evaporation cast under the same slow conditions used in the preparation of the PVDF-g-POEM films, was significantly lower than its bulk concentration as measured by ^{1}H NMR. This result suggests that PMAA is grafted onto PVDF in the form of long side chains capable of strong orientation away from the air surface to maximize exposure of the low-energy fluorinated backbone. The near-surface composition of the as-cast membrane (c) indicates substantial surface localization of PVDF-g-PMAA as well as surface expression of PMAA, such that the near-surface PMAA concentration is over 6 times the bulk concentration.

For reasons described in Section 5.4.1, evaluation of the pH-responsive properties of membranes modified with PVDF-g-PMAA required post-coagulation heat treatment by autoclaving for 1 h in water at 121°C. Figure 5.15(d) is the fitted C 1s envelope for a membrane containing 10 wt % of the copolymer additive after this autoclaving treatment. After autoclaving, satisfactory fitting of the XPS data required the introduction of an additional peak centered at 287.8-288.0 eV, which corresponds to the C 1s binding energy of the CHF bonding environment of poly(vinyl fluoride).[225] Moreover, post-autoclaving spectra were well fit using the peak area constraint that,

$$A_{\underline{C}F_2} + A_{\underline{C}HF} = A_{\underline{C}H_2(PVDF)}.$$

<div align="right">(5.6)</div>

This change in surface chemistry can be explained by thermal crosslinking of PVDF-*g*-PMAA (probably involving PVDF homopolymer as well) due to a small amount of residual CuCl remaining in the graft copolymer, as discussed in Section 3.1. Such a cross-linking reaction would be expected to convert doubly-fluorinated carbon atoms to singly-fluorinated ones, roughly conforming to Equation 5.6. As shown in Figure 5.15, the surface compositions of as-cast and autoclaved membranes, as calculated using Equation 5.4, are similar. Surface segregation of PVDF-*g*-PMAA during heat treatment in water at 121°C would not be expected, due to the comparatively high melting point of PVDF-*g*-PMAA (see Section 3.1.5) and to its propensity to cross-link upon heating.

Morphology. FESEM micrographs of the separation surfaces and cross-sections of autoclaved pure PVDF and 10% PVDF-*g*-PMAA membranes appear in Figure 5.16. The familiar increase in separation surface porosity with addition of the amphiphilic additive is readily apparent. Thus, this effect is not related to POEM in particular. As discussed in Section 4.3.1, such an effect would likely be observed with the addition of any amphiphilic additive of sufficient hydrophilicity. In this case, a simultaneous increase in pore size is clearly observed. Presumably, this could be offset by adjustment of the casting conditions (*e.g.*, polymer or glycerol concentration in the casting solution, composition of the coagulation bath). No nodular structures indicative of spinodal decomposition are observed in the separation surfaces. This is likely due to the faster diffusion kinetics of the low molecular weight $PVDF_{250K}$ used to prepare these membranes relative to the $PVDF_{534K}$ used in the preparation of other membranes in this thesis. The higher mobility of $PVDF_{250K}$ may have allowed nucleation and growth to

occur prior to deep quenching of the casting solution composition.[53] Neither the

separation surface nor the cross-sectional images provide any evidence for large-scale

phase separation of the two polymer components in the blend membrane.
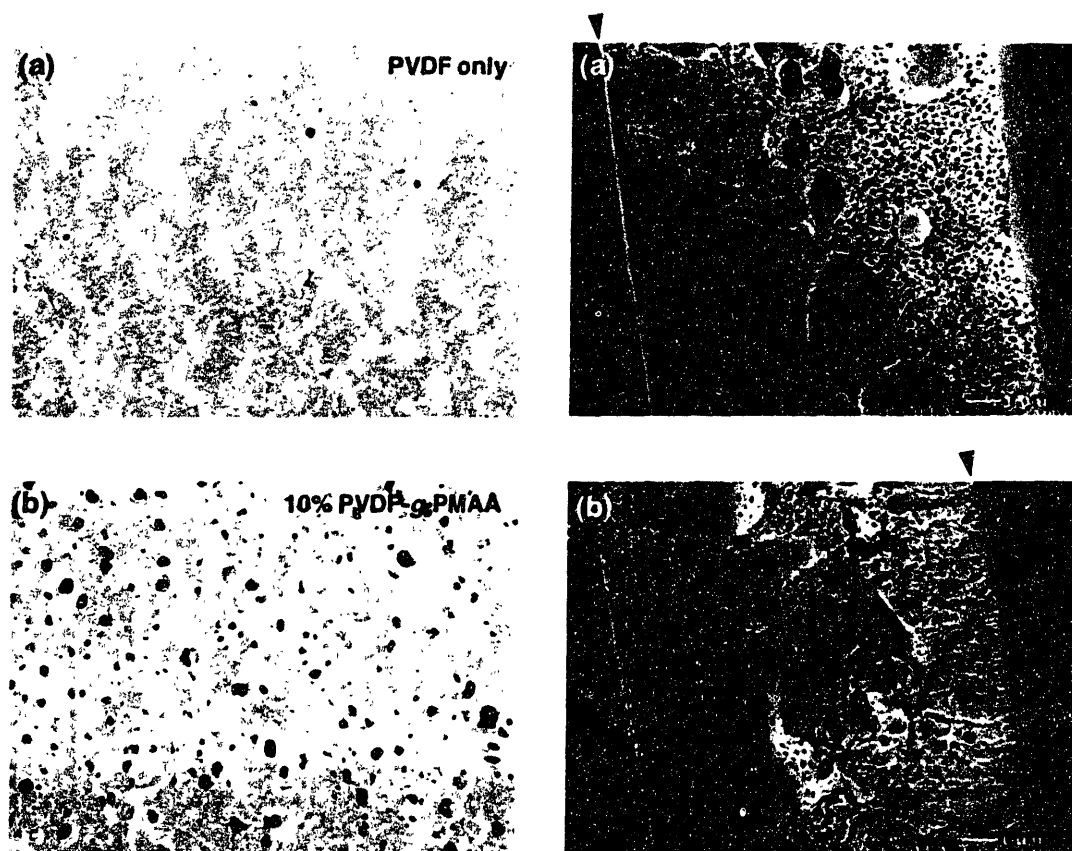
Figure 5.16 Morphology of membranes containing PVDF-g-PMAA
FESEM images of the separation surfaces (left) and cross-sections (right) of membranes cast into a dW bath at 90°C. (a) Pure PVDF membrane F-00-4-90, and (b) membrane F-10-PE-90, containing 10 wt % PVDF-g-PMAA. Both membranes were autoclaved for 1 h at 121°C in water. Arrows indicate the separation surfaces in cross-sectional images.
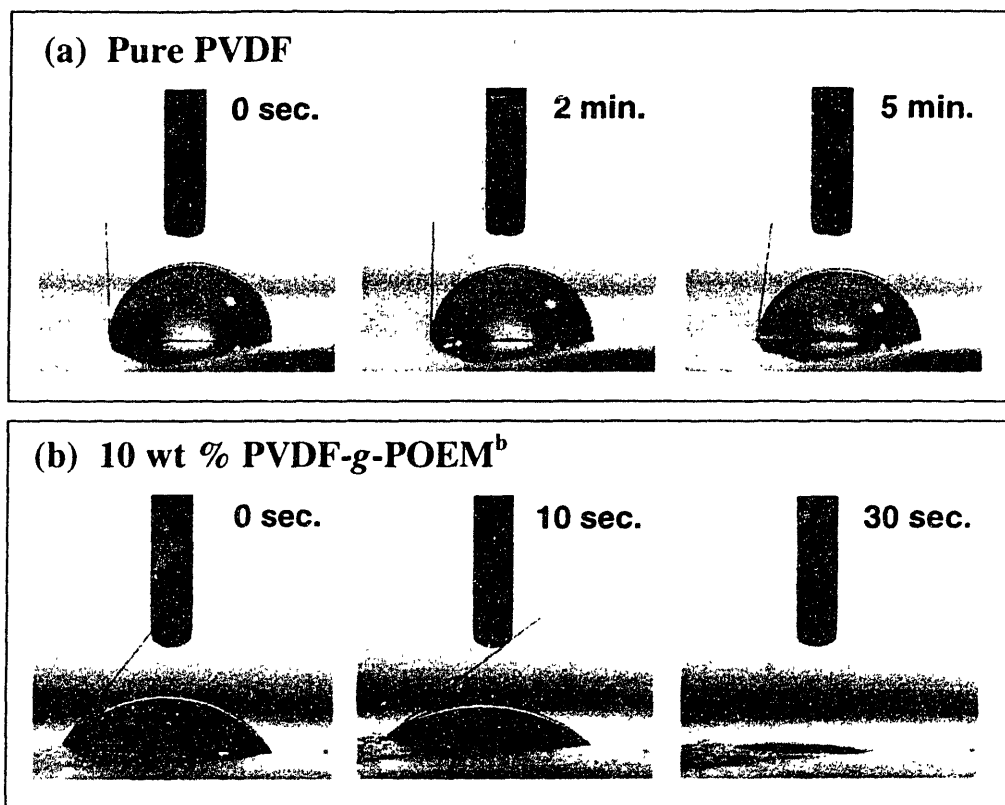
Figure 5.17 Images of water droplets on nonwettable and wettable membranes
Images of 1 µL water droplets at various times on (a) pure PVDF membrane F-00-3-90 and (b) membrane F-10-AT2-90, having a bulk composition of 10 wt % PVDF-g-POEM[b]. The contact angle of a water droplet on the hydrophobic PVDF membrane changes very little over time, until the droplet finally evaporates without wetting the membrane. The contact angle of a droplet on the surface-modified membrane decreases to zero over time.

5.3.2 Wettability Assessment

Pure PVDF membranes do not wet spontaneously with water, due to their extreme hydrophobicity. This fact has important practical consequences, as it means that a dry PVDF membrane (much cheaper to transport than a wet one) must be prewet prior to use with an alcohol, which can then be exchanged with water. Moreover, hydrophobic membranes typically require higher operating pressures than hydrophilic membranes

having the same separation characteristics.[87] Much commercial effort has thus been expended to render PVDF membranes spontaneously wettable by water.[42] This can be achieved, for example, by surface graft polymerization using a hydrophilic monomer or by sulfonation of PVDF.[87,88,110]

In the laboratory, the wetting behavior of a membrane can be observed in a controlled manner by measuring the time evolution of the contact angle formed between the surface and a droplet of water placed on it. A droplet of water placed on a pure PVDF membrane assumes a high contact angle, which changes very little over time until the drop finally evaporates. In contrast, a water droplet placed on a self-organizing membrane having a sufficient near-surface fraction of PVDF-g-POEM[b] assumes a moderate initial contact angle (>50°) which decreases to zero over time, and the droplet ultimately wets through the membrane (see Figure 5.17). We term this behavior *spontaneous wetting*.

In this thesis, the wettability of a membrane was assessed based on the initial advancing contact angle (θ_{adv}) of a 1 μL droplet of dW placed on its surface, as well as the time required for the contact angle of the droplet to reach 0°. These values are reported in Table 5.5. It should be noted that the advancing contact angle is only a very qualitative indicator of surface chemistry. The contact angle may be significantly affected by surface topography as well as chemistry,[132] and, as electron microscopy results in previous sections have shown, the surface morphologies of the membranes listed in Table 5.5 vary widely.

191

Table 5.5 Wetting Properties of Various Membranes

Membrane	Bulk Composition	Comonomer Content (wt %) Bulk	Comonomer Content (wt %) Surface*	θ_{adv} initial	Wetting Behavior
F-00-3-90	pure PVDF	0	0	89.9 ± 4.1	nonwetting
F-10-9k2-90	10 wt % P(MMA-r-POEM$_9$)^k	5.1	22**	83.3 ± 3.9	nonwetting
F-10-MA-90	10% P(MA-r-POEM$_9$-r-HPOEM$_{10}$)	4.1	9.5†	85.2 ± 3.2	immersion wetting††
F-10-AT1-90	10 wt % PVDF-g-POEM^a	4.4	27	76.5 ± 3.7	partial wetting‡
F-05-AT2-90	5 wt % PVDF-g-POEM^b	3.4	42	60.4 ± 2.3	wetting, 147 ± 83 s‡‡
F-10-AT2-90	10 wt % PVDF-g-POEM^b	6.7	64	53.5 ± 7.0	wetting, 16 ± 10 s‡‡
F-10-PE-90	10 wt % PVDF-g-PMAA	4.9	29	75.6 ± 1.0	partial wetting‡

* For details of the XPS fits, see Appendix C, Tables C.6, C.8, C.9, and C.10.

** Computed from a near-surface mole fraction of POEM estimated as $X_{POEM} \cdot n_s$, where X_{POEM} is the mole fraction of POEM in the pure comb additive by NMR (Eqn. 3.1) and n_s is the near-surface mole fraction of comb obtained from XPS (Eqn. 4.1).

† Computed from a combined near-surface mole fraction of POEM$_9$ and HPOEM$_{10}$ estimated as $X_{(POEM+HPOEM)} \cdot n_s$, where $X_{(POEM+HPOEM)}$ is the composition of the pure comb additive by NMR (Eqn. 3.5) and n_s is the near-surface mole fraction of the comb obtained by XPS. XPS was performed as described in Section 4.2.1, with n_s given by Eqn. 4.1 (see Appendix C, Table C.10 for details of the XPS fit).

†† Defined as complete translucence of a previously dry membrane after immersion in dW for 15 min.

‡ Defined as partial translucence of a previously dry membrane after immersion in dW for 12 h.

‡‡ Spontaneous wetting; time required for a 1 µL droplet of dW placed on the membrane surface to reach a contact angle of 0°.

Most notable for their wetting behavior are self-organizing membranes prepared from blends containing PVDF-g-POEM^b. A membrane containing only 5 wt % of this additive (corresponding to a bulk POEM concentration of only 3.4 wt %) is spontaneously wettable on a time scale of 2-3 minutes. The time needed for complete wetting can be reduced to just a few seconds with the incorporation of 10 wt % PVDF-g-POEM^b. The delayed wetting behavior of membranes modified with PVDF-g-POEM^b indicates local surface reorganization to express POEM upon contact with water. Membranes containing 10 wt % PVDF-g-POEM^a (which has a lower POEM content than PVDF-g-POEM^b), PVDF-g-PMAA, or P(MA-r-POEM$_9$-r-HPOEM$_{10}$) do not spontaneously wet. When immersed in water for several hours, however, these membranes (or some regions of them) become translucent indicating wetting. Pure

PVDF membranes and membranes containing 10 wt % P(MMA-r-POEM$_9$)[k] show no such behavior.

It is of interest to note the difference in wetting behavior between the nonwetting membranes containing P(MMA-r-POEM$_9$)[k] and the wetting or partially-wetting membranes containing P(MA-r-POEM$_9$-r-HPOEM$_{10}$), PVDF-g-POEM[a], and PVDF-g-PMAA. All of these additives had roughly equivalent contents of hydrophilic comonomer (40-51 wt %), and all of the membranes contained equal weight fractions of additive polymer and were cast under identical conditions. A few hypotheses can be advanced which might explain the differences in wetting behavior of the various membranes and the nonwettability of membranes modified with P(MMA-r-POEM).

First, an advantage of the PVDF graft polymerization route for the preparation of amphiphilic additives is that high POEM contents (at least 67 wt %) are achievable without water solubility, enabling delivery of high POEM concentrations to the surface. This fact almost certainly contributes to the spontaneous spreading of water droplets placed on membranes modified with PVDF-g-POEM[b]. Moreover, the data in Table 5.5 indicate that the PVDF-based combs are more efficient in the delivery of hydrophilic side chains to the surface than P(MMA-r-POEM$_9$)[k].

A second hypothesis for the nonwettability of self-organizing membranes containing P(MMA-r-POEM) is arrived at through consideration of the interactions between the side chains and backbone of the amphiphilic additive polymers. PEO and PMMA are miscible, having a small negative interaction parameter (χ) as measured experimentally by a variety of methods.[260-265] According to XPS measurements performed in this thesis (see Section 4.2.1 and Appendix D), the surface monolayer of

self-organizing membranes containing P(MMA-*r*-POEM) may have a composition approaching 100% comb. Thus, on the hydrated membrane surface, one might expect that there will be an equilibrium between EO-water contacts and favorable EO-MMA contacts. Such an equilibrium would be expected to oppose the spreading of a water droplet on the dry membrane surface. In contrast, PVDF has not been shown to be miscible with PEO or PMAA, and the PVDF backbones of the graft copolymers are crystalline. Unlike P(MMA-*r*-POEM), the thermodynamics and crystallinity of the PVDF-based combs might be expected to favor rejection of the hydrophilic side chains from the hydrated membrane surface. Thus, the wettability of surfaces modified using comb copolymers bearing hydrophilic side chains might depend partly on the interactions between the side chains and the membrane surface.

The phase behavior of PMA/PEO homopolymer blends has not been well studied. However, Pedemonte and Burgisi[266] inferred a small negative enthalpy of mixing from the measured enthalpies of solution of PMA, PEO, and their blends in a common solvent, suggesting that the two polymers are miscible. Thus, the above hypothesis may not explain the observed difference in wetting behavior between membranes modified with P(MMA-*r*-POEM) and those modified with P(MA-*r*-POEM$_9$-*r*-HPOEM$_{10}$), which were wet completely upon immersion in water despite the relatively low level of terpolymer comb surface segregation achieved.

A third hypothesis for the nonwettability of membranes containing P(MMA-*r*-POEM) can be arrived at through consideration of the kinetics of local reorganization of the comb to express the hydrophilic side chains upon contact with water. The glass transition temperatures of PVDF and PMA homopolymers are -40°C[170] and 6°C,[267]

respectively, compared with the PMMA T_g of 105°C.[206] Thus, the backbone of P(MA-r-POEM$_9$-r-HPOEM$_{10}$) and the amorphous regions of the PVDF-based comb backbones are highly mobile at room temperature, compared with the backbone of P(MMA-r-POEM). This mobility may facilitate rearrangement in the near-surface region. P(MMA-r-POEM) is known to undergo surface rearrangement in contact with water, as evidenced by contact angle hysteresis.[185] However, the depth at which this rearrangement occurs is unknown. Amphiphilic combs having low-T_g backbones may be capable of rearrangement at greater depths.

It is currently not known whether the terminal –OH groups of HPOEM play a role in the wettability of membranes modified with the PMA terpolymer comb. In their studies of POEM- and HPOEM-grafted PAN membranes, Ulbricht, et $al.$[104] observed slightly lower water contact angles on HPOEM-grafted membranes. Evaluation of the importance of the hypotheses put forth above would require further study, employing comb additives having similar architectures but composed of backbone/side chain pairs of varying compatibility and T_g.

5.3.3 Static Fouling Resistance of Spontaneously Wettable Membranes

Spontaneously wettable membranes containing PVDF-g-POEM^b were fouled by immersion in a 10.0 g/L BSA solution for 24 h. The relative amount of BSA adsorbed on each membrane was then determined by XPS measurement of the near-surface concentration of nitrogen occurring in BSA. The near-surface atomic compositions were obtained by integration of the following peaks in the XPS survey spectra: C 1s (285 eV), N 1s (399 eV), O 1s (531 eV), and F 1s (685 eV).
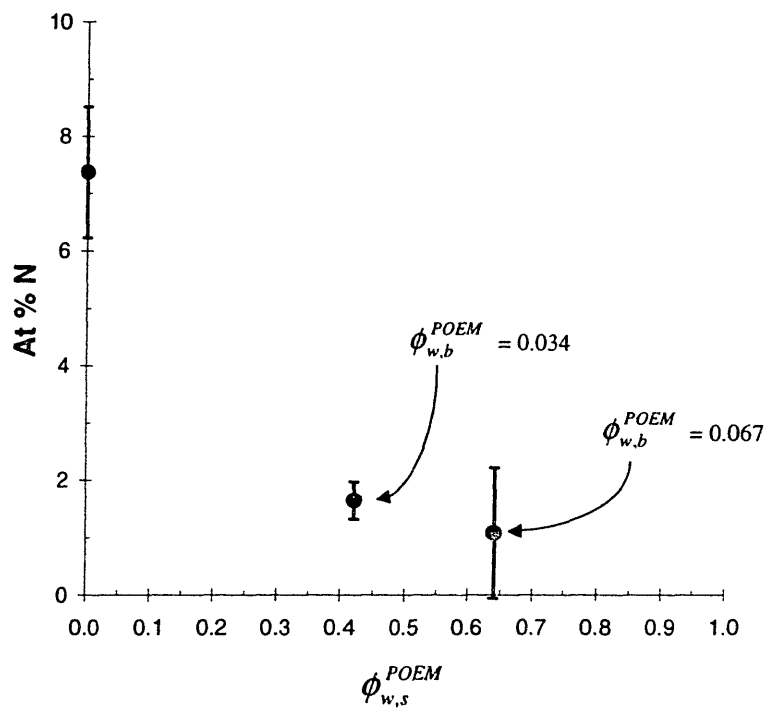
Figure 5.18 Static protein adsorption of spontaneously wettable membranes
Near-surface nitrogen concentration (atom %) versus surface concentration PVDF-g-POEM[b] (vol. fraction, as measured by XPS) for as-cast membranes F-xx-AT2-90 fouled by immersion in a 10 g/L BSA solution for 24 h. Bulk POEM weight fractions $\phi_{w,b}^{POEM}$ are shown next to each data point for the blend membranes.

Figure 5.18 is a plot of near-surface nitrogen concentration as a function of surface composition. Like self-organizing membranes containing P(MMA-r-POEM) (see Section 5.1), membranes modified through surface segregation of PVDF-g-POEM are highly resistant to BSA adsorption compared to pure PVDF membranes. In fact, membranes with a bulk composition of only 3.4 wt % POEM adsorb BSA at a level less than 25% that of PVDF-only membranes. Future work might profitably explore the fouling resistance of membranes containing PVDF-g-POEM polymers, perhaps with longer PEO chain lengths, in filtration experiments. Based on the assumption that fouling resistance is related to wettability, such membranes might be expected to display excellent anti-fouling properties.

5.4 pH-Responsive Membranes

5.4.1 Introduction

In the following paragraphs, it is shown that self-organizing membranes having surface-localized PVDF-g-PMAA are pH-responsive, in that their pores can be opened and closed reversibly simply by changing the pH of the feed solution, thereby changing the conformation of the weak polyacid side chains expressed at the surface (see Section 2.4.2). The pH-responsive behavior of membranes containing PVDF-g-PMAA will be demonstrated by measuring their permeability, along with the permeability of PVDF-only control membranes, to buffer solutions of various pH. At high pH, where the PMAA side chains are dissociated and extended, we expect to observe relatively low buffer fluxes through the surface-modified membranes. At low pH, where the side chains are protonated and assume a more collapsed conformation, we expect to observe high fluxes. The permeability of membranes fabricated from neutral PVDF only would not be expected to display pH-dependence based on such a mechanism.

In fact, as-cast PVDF-only membranes prepared using 90°C coagulation baths *were* observed to exhibit pH-dependent permeabilities mirroring, at least initially, the general rule expected for the modified membranes. However, this pH behavior was not reversible. In an experiment during which the trans-membrane flux was monitored as the pH was alternated between pH 2 and pH 8, the pH-dependence of the flux through an as-cast PVDF-only membrane was observed to decrease rapidly over 3-5 cycles, in a manner that was poorly reproducible between different membranes. As will be shown below, this behavior is quite different from that of membranes modified with PVDF-g-PMAA,

which, in the same experiment, retain their pH-response over many cycles without any sign of irreversibility. Moreover, the pH-dependent behavior of PVDF-only membranes was observed to vanish almost completely if they were autoclaved for 1 h at 121°C while immersed in water. This fact suggests that their pH-dependent filtration behavior may be a result of pH-dependent swelling of amorphous PVDF. Heat treatment of the membranes at 121°C ($>0.7 \cdot T_m$) may facilitate crystallization of PVDF quenched into the amorphous state during coagulation. In any case, in order to evaluate pH-responsiveness due to the presence of PVDF-g-PMAA alone, both self-organizing and PVDF-only membranes were autoclaved prior to filtration testing. As discussed in Section 5.3.1, this heat treatment did not substantially change the near-surface PMAA concentration of the self-organizing membranes, the surfaces of which were highly enriched in PMAA in the as-cast conditon.

5.4.2 pH-Dependence of the Pure Water Flux

Figure 5.19 is a plot showing the pH dependence of the flux of buffer solutions through autoclaved membranes having surface-localized PVDF-g-PMAA ($\phi_{w,s}^{PMAA} = 0.29$). The data points for the blend are averages of data taken from three different membranes. The self-organizing membranes exhibit a flux variation of well over an order of magnitude, from a flux of 506.5 L/m^{2}h at pH 2 to 29.0 L/m^{2}h at pH 8. An autoclaved pure PVDF membrane exhibits very little flux variation with pH. The solid lines in Figure 5.19 are best-fit symmetric functions of the form,

$$J = C - D\left[\frac{B^{x-A} - B^{-(x-A)}}{B^{x-A} + B^{-(x-A)}}\right] \tag{5.7}$$
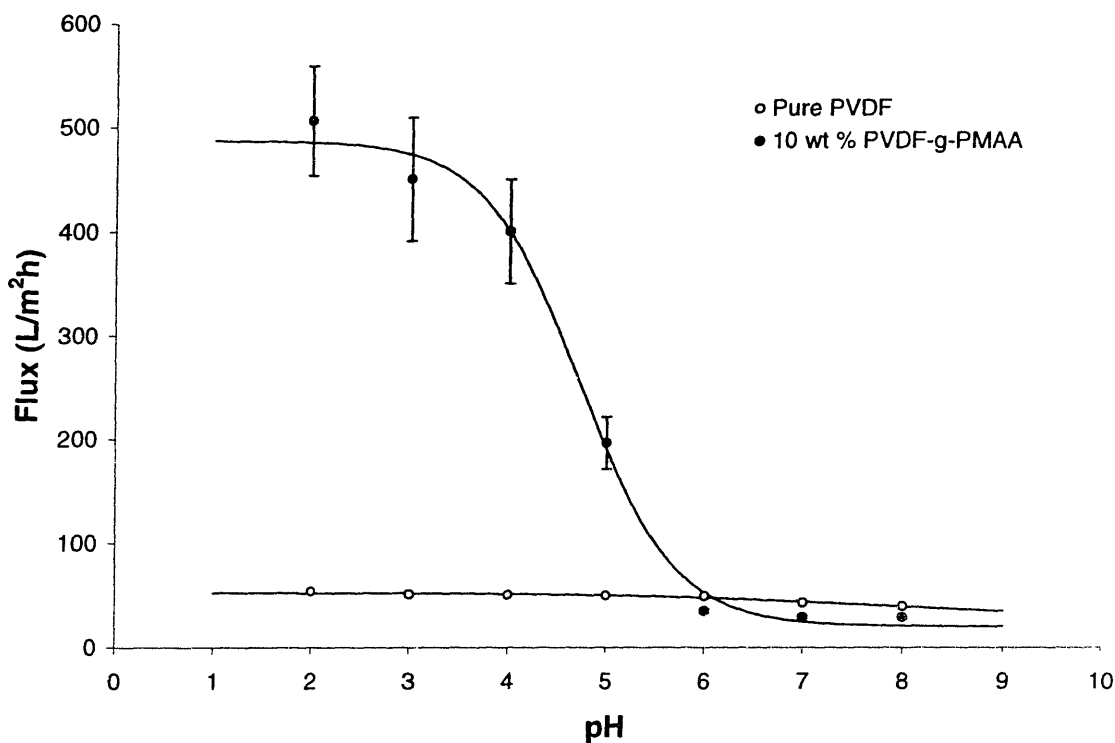
Figure 5.19 pH-dependence of flux through self-organizing ER membrane
Buffer solution flux versus pH for a pure PVDF membrane (F-00-4-90) and membranes
F-10-PE-90, having a bulk composition of 10 wt % PVDF-g-PMAA, after autoclaving for
1 h in water at 121°C. The lines are a guide to the eye.

where x is the feed solution pH and A, B, C, and D are fitting parameters. The purpose of

this fit was not to suggest a particular functional form for the data, but rather to obtain an

estimate of the apparent pK_a, given by the pH at the inflection point (the parameter A).

The location of the inflection point at pH ~4.7 is comparable to results obtained by other

researchers from membranes modified by surface graft polymerization of PMAA.[113,116]
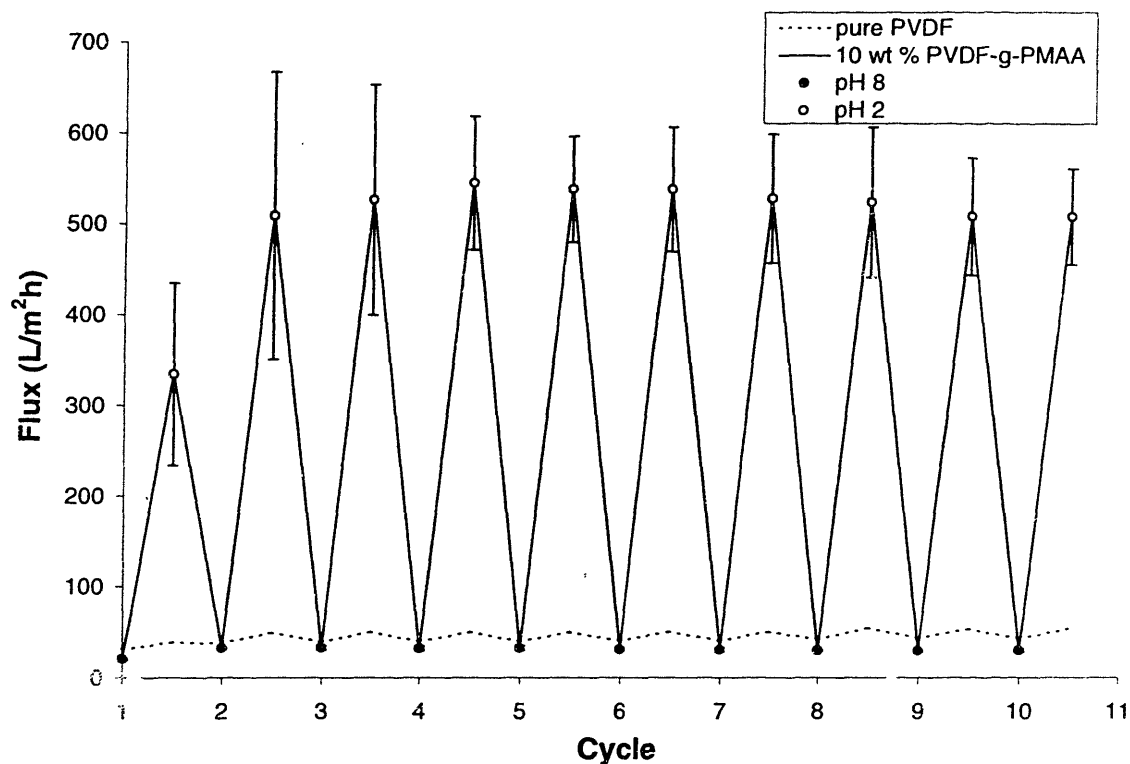
Figure 5.20 Reversibility of pH-responsive flux

Flux of buffer solution through an autoclaved pure PVDF membrane (F-00-4-90) and autoclaved membranes F-10-PE-90, having a bulk composition of 10 wt % PVDF-*g*-PMAA, as the pH of the feed was alternated between 8 and 2. Each half-cycle consisted of a 1-min filtration period for equilibration, followed by a gravimetric flux measurement taken over a second 1-min period.

Figure 5.20 shows the flux response of these self-organizing, environmentally responsive membranes as the pH of the feed solution was alternated between pH 8 and pH 2 over a 40-min period. Again, the data points for the blend are averages of data collected from three separate membranes. After 1-2 equilibration cycles, during which reorganization of the membrane surface to express the PMAA side chains of the graft copolymer additive may have occurred, the flux response is completely reversible over this time period. Each half-cycle consisted of a 1-min filtration period for equilibration,

200

followed by a flux measurement over a second 1-min period. Although no quantitative evaluation of the rapidity of the flux response was attempted, the flux was observed to change substantially within a few seconds following exchange of the filtration buffers.

5.4.3 pH-Dependence of the Surface PMAA Layer Height

The pH-dependent variation of the PMAA surface layer height on membranes containing PVDF-g-PMAA was estimated from AFM force-distance measurements conducted on membranes immersed in buffer solutions. Collection of the AFM data was performed by Solar Olugebefola in the research group of Prof. A. Mayes at MIT. These measurements were performed and analyzed following a method used by Iwata, et al.[98] to measure the thicknesses of surface graft polymerized poly(acrylic acid) (PAA) layers on polycarbonate track-etch membranes.

Figure 5.21 shows force-distance curves for the self-organizing membranes obtained in buffer solutions at (a) pH 2 and (b) pH 8. At large separation distances, the AFM tip is not deflected by interaction with the surface, and the deflection force is zero. As the tip approaches the surface, the force increases monotonically as the tip compresses the PMAA layer, until the slope of the force-distance curve finally becomes constant. In this region, termed the *region of constant compliance* by Ducker, et al.,[240] the tip and surface are assumed to be in "close contact." For an AFM probe approaching a rigid surface, the constant slope of this region of the force-distance curve is simply the spring constant of the cantilever. For measurements on hydrated polymer membranes, the slope of the force-distance curve in the region of constant compliance was generally somewhat

less than the spring constant of the cantilever due to the compliance of the swollen polymer surface.

The width of the transition region of the force-distance curve, between the regions of zero force and constant compliance, provides a rough measure of the PMAA layer height. Qualitatively, this width is clearly larger at pH 8 than at pH 2. The layer height may be quantified by plotting the ratio of an increment of the force, ΔF, to a decrement of the distance, Δz, as a function of the separation distance, z-z_o (see Figure 5.21). The layer height is then estimated as the distance, H, between the inflection points. To objectively qᵤ tify the layer height H, the numerical derivatives of the force-distance profiles were fit with a function of the form,

$$\frac{\Delta F}{\Delta z} = \left(\frac{\Delta F}{\Delta z}\right)_C - \left[\left(\frac{\Delta F}{\Delta z}\right)_C - \left(\frac{\Delta F}{\Delta z}\right)_0\right] \tanh\left\{\frac{4[(z - z_o) - z_m]}{H}\right\} \qquad (5.8)$$

where $(\Delta F/\Delta z)_C$ and $(\Delta F/\Delta z)_0$ are the $\Delta F/\Delta z$ ratios in the regions of constant compliance and zero force, respectively, and z_m is the middle position of the PMAA layer. Example fits of this type are shown in Figure 5.21. Average values of H obtained from 3-10 measurements at nine separate spots on membranes at pH 2 and pH 8 are shown in Figure 5.22. The mean layer heights are 14 nm and 51 nm at pH 2 and pH 8, respectively.
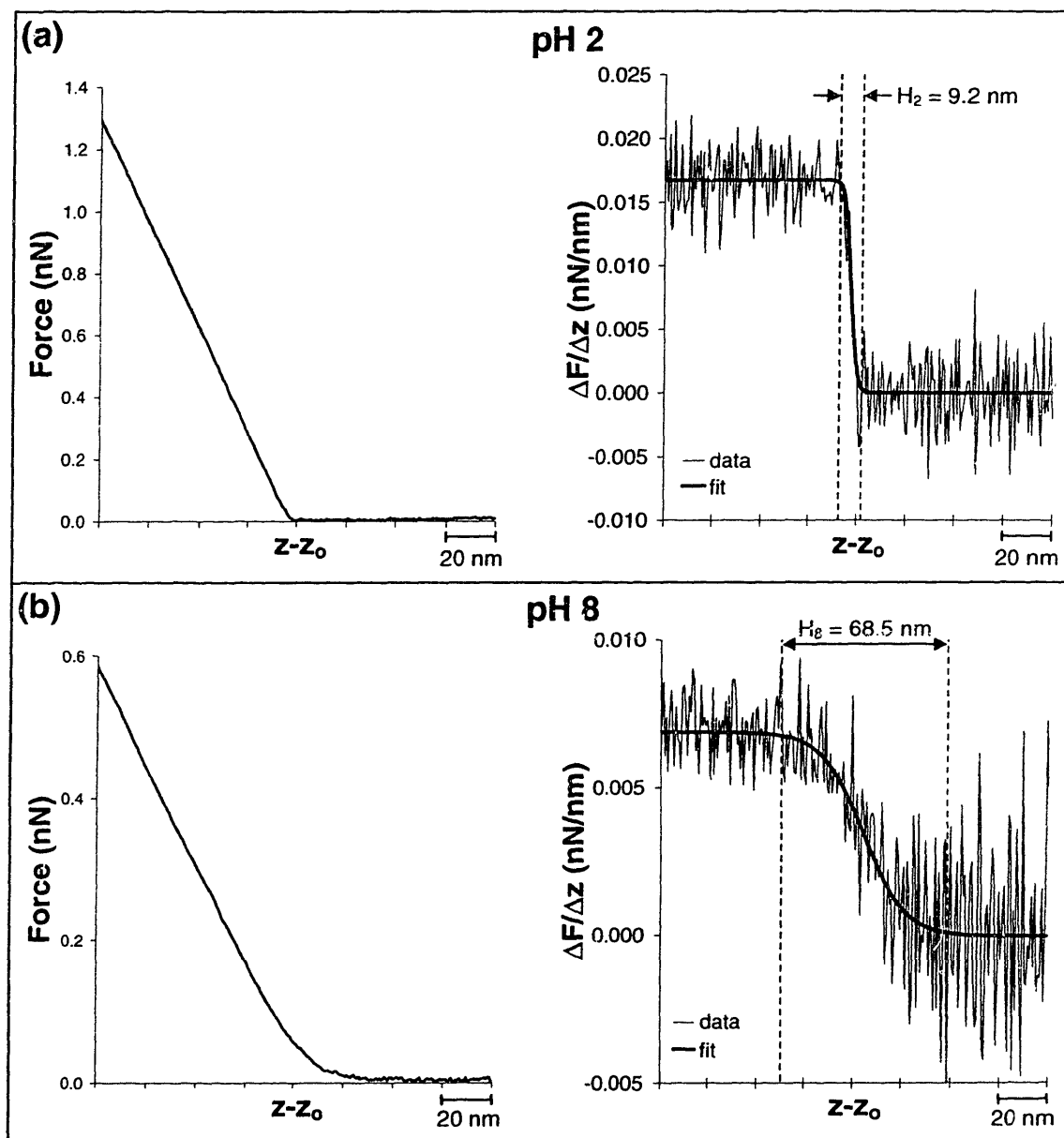
Figure 5.21 Analytical method for estimating layer heights from AFM force curves
Example *in situ* AFM force curves and their numerical derivatives for membranes F-10-PE-90, containing 10 wt % PVDF-*g*-PMAA, immersed in (a) pH 2 and (b) pH 8 buffers.
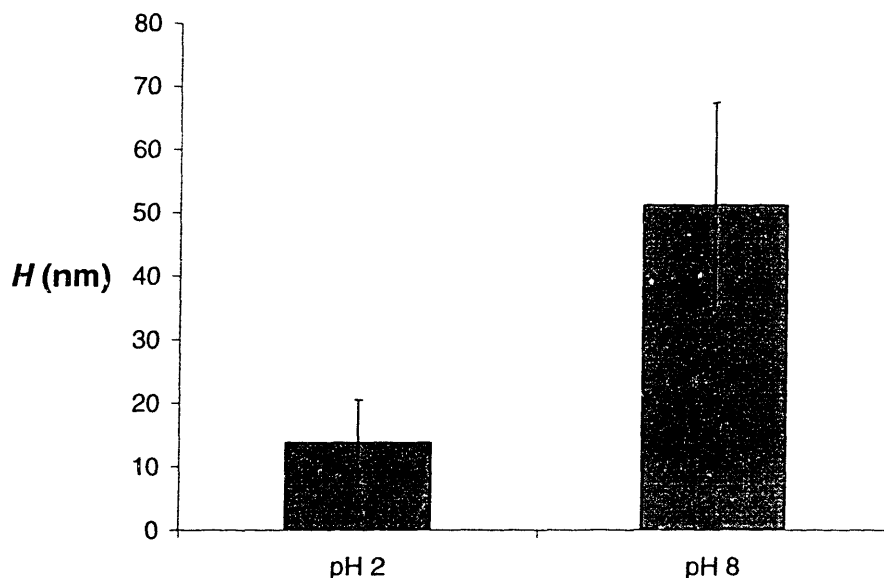
Figure 5.22 PMAA layer heights at pH 2 and pH 8

PMAA layer heights for membranes F-10-PE-90, containing 10 wt % PVDF-g-PMAA, obtained from *in situ* AFM force curves. Each value is an average of the layer heights estimated from nine spots on the membrane surface using the analytical method illustrated in Figure 5.21. The average layer heights are 14 nm and 51 nm at pH 2 and pH 8, respectively.

The average PMAA side chain length of PVDF-g-PMAA can be very roughly estimated using the AFM data. Assuming the PMAA chain conformation at pH 8 can be approximated as a fully extended, all-trans chain having a length of 2.5 Å per repeat unit, the measured layer height at pH 8 (~500 Å) is consistent with a PMAA side chain degree of polymerization of ~200 MAA units. In pH 2 buffer, PMAA should be nearly neutral and in a good solvent. Thus, its dimension might be approximated by the Flory radius,[244]

$$R_F = N^{\frac{3}{5}} a \qquad (5.9)$$

where N is the degree of polymerization and a is the statistical segment length. Substituting the values $N = 200$ and $a = 5$ Å, we obtain $R_F = 120$ Å, a value in fair

agreement with the pH 2 layer height obtained by AFM. Thus, it appears that the AFM measurements at pH 8 and pH 2 are both reasonably consistent with a PMAA degree of polymerization of ~200. Given the substantial statistical error in the AFM measurements and the simplistic assumptions made with regard to the PMAA chain conformations, this value is expected to be only an extremely rough estimate of the PMAA side chain length. More importantly, this analysis shows that the results of the AFM measurements conducted at pH 2 and pH 8 are consistent with each other in supporting the proposed mechanism of pore size control due to reversible conformational changes of surface-localized PMAA chains.

5.4.4 Relationship Between Flux and PMAA Layer Height

Table 5.6 is a comparison of the flux measurements and AFM results reported in Sections 5.4.2 and 5.4.3 to a previous study by Iwata, et al.,[98] of pH-responsive PAA-grafted polycarbonate membranes having comparable pore size. Under one set of grafting conditions, these authors obtained a modified membrane having a maximum PAA graft layer height (H_{closed}) comparable to the PMAA layer height of our self-organizing membrane at pH 8, as measured by a similar AFM technique. Despite the uncertainties involved in both studies and the large pore size distribution of the self-organizing membrane, the ratios between the "open" and "closed" water fluxes agree within a factor of 2. This suggests that the pH-responsive water permeabilities of membranes modified by self-organization and surface graft polymerization are due to the same mechanism.

Table 5.6 Comparison of Results for Self-Organizing and Grafted ER Membranes

Membrane	$\overline{D}$ (nm)	σ_D (nm)	H_{closed} (nm)	J_{open}/J_{closed}
F-10-PE-90 (this thesis)	204	117	51	17.5[†]
Iwata, et al.[98] (membrane "M-1")	200	~0	~50	~30[‡]

[†] J_{open} = flux of pH 2 buffer; J_{closed} = flux of pH 8 buffer.
[‡] J_{open} = approximate flux of pH 2.5 buffer; J_{closed} = approximate flux of pH 7.4 buffer.

Based on the hypothesis that the observed flux variations with pH result from conformational changes of PMAA side chains expressed at the membrane surface, it is possible to arrive at a very rough prediction of the ratio of the "open" (pH 2) and "closed" (pH 8) pore diameters, D_2/D_8, based on the flux measurements reported in Section 5.4.2. Assuming laminar flow, the flux through a set of cylindrical pores is given by the well-known Hagen-Poiseulle equation,[268]

$$J = \frac{n\pi\left(\dfrac{D}{2}\right)^4 (\Delta P)}{8\eta L}$$

(5.10)

where n is the number of pores per unit area, D is the pore diameter, ΔP is the pressure drop, η is the fluid viscosity, and L is the length of the pore channels. The dependence of the flux on the 4th power of the pore diameter means that slight changes in the pore size can result in large flux variations. Based on the flux measurements and Equation 5.10, the ratio of the "open" and "closed" pore diameters is,

$$\frac{D_2}{D_8} = \left(\frac{J_2}{J_8}\right)^{\frac{1}{4}} = \left(\frac{506.5}{29.0}\right)^{\frac{1}{4}} = \underline{2.04}.$$

(5.11)

From the FESEM estimate of the mean pore diameter and the AFM measurements of Section 5.4.3, we obtain an estimate of the same ratio,

$$\frac{D_2}{D_8} \approx \frac{\overline{D} - 2H_2}{\overline{D} - 2H_8} = \frac{204 - 2(14)}{204 - 2(51)} = \underline{\underline{1.73}}.$$
(5.12)

Thus, the estimate of D_2/D_8 obtained from the flux measurements agrees fairly well with the estimate obtained from the AFM measurements. The above analysis is laden with assumptions. We have modeled the separation surface pore channels as cylinders and assumed laminar flow. Moreover, we have represented a large distribution of pore sizes in the hydrated membrane using the mean pore size obtained from the *dry* membrane. Still, the results of the analysis do not contradict the conclusion indicated by the AFM measurements, that the observed pH-dependent filtration behavior is due to reversible conformational changes of the surface-localized PMAA side chains of the graft copolymer additive.

5.4.5 Summary

In conclusion, it should be noted that post-coagulation autoclaving of self-organizing membranes containing PVDF-*g*-PMAA is *not* necessary for the achievement of pH-responsive behavior. This treatment was simply used to avoid ambiguity due to the transient pH-dependent behavior of as-cast PVDF-only controls. Figure 5.23 is a plot showing the pH-dependent flux of an as-cast membrane containing 10 wt % PVDF-*g*-PMAA. Thus, through self-organization, it is possible to prepare a membrane capable of responding "intelligently" to its environment *in a single processing step*.
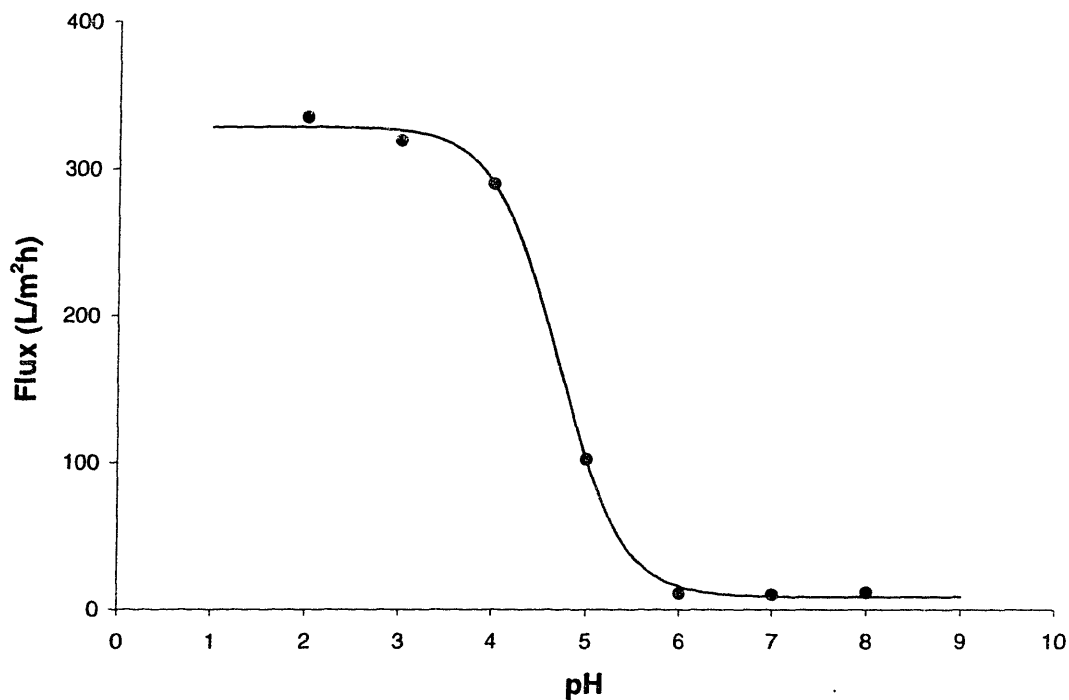
Figure 5.23 pH-dependence of flux through as-cast ER membrane
Buffer solution flux versus pH for membrane F-10-PE-90, having a bulk composition of
10 wt % PVDF-g-PMAA, in the as-cast condition.

Fabrication of ER membranes by surface graft polymerization (see review, Section 2.4.2) typically requires much "trial-and-error" experimentation to optimize the length and density of graft chains, which are kinetically limited and difficult to control. Thus, a further advantage of the self-organization approach lies in the fact that the length and "grafting" density of the environmentally-responsive chains should be controllable simply and systematically through architectural adjustment of the amphiphilic additive polymer. Synthesis routes for the preparation of pH-responsive comb additives having easily-adjusted architectures will be proposed in Section 6.2.1.

6. Conclusions and Future Work

6.1 Self-Organization: Effective, Economical, and Versatile

This thesis has explored the preparation of water filtration membranes having tailored surface chemistries from polymer blends, composed of a commercial membrane-forming polymer and a small proportion (5-10%) of an amphiphilic additive polymer, which self-organize during processing to express the additive component preferentially at the surface. This self-organization process occurs during the coagulation and (optionally) aqueous heat treatment steps of the conventional immersion precipitation process used most commonly for the fabrication of such membranes. With the use of heated coagulation baths, high surface concentrations of the amphiphilic additive (approaching 100%) can be obtained without the need for heat treatment, providing a *single-step* surface modification technique.

The surface modification agents used in this work are amphiphilic, comb-shaped polymers. The backbones of these polymers are designed for compatibility with the matrix polymer, while the side chains impart hydrophilicity and other desired surface properties. The comb architecture is uniquely suited to take advantage of the thermodynamic driving forces for surface segregation that exist during membrane coagulation in water. Due to the amphiphilic nature of the comb additive polymers and the kinetics of the immersion precipitation process, which actually *favors* the surface segregation of higher molecular weight combs, the water-insoluble, highly entangled surface layers produced by this self-organization technique exhibit excellent long-term

stability in water, exhibiting no change in surface chemistry over a period of at least 32 months of aqueous storage. Other advantages of the comb architecture include the availability of a wide range of engineered surface chemistries at low cost. Comb polymers having a large variety of backbone and side chain chemistries can be produced inexpensively using free-radical methods amenable to routine commercial production methods. Besides traditional solution free-radical techniques, this thesis has explored a novel ATRP technique by which a wide range of vinyl monomers can be grafted directly onto PVDF to create PVDF-compatible comb polymers. This technique is expected to be commercially relevant, requiring a single synthesis step and having no unusual requirements with respect to reagent purity. The advantages and disadvantages of the various comb additive polymers used in this thesis work are summarized in Table 6.1. Other flexible and commercially relevant synthesis routes to amphiphilic comb polymers will be proposed in Section 6.2.

Self-organization has been used to prepare PVDF membranes having a number of desirable surface properties. Surface segregation of P(MMA-r-POEM) and PVDF-g-POEM comb polymers provides substantial resistance to protein fouling. Significantly, and unlike coating and grafting methods used commonly for membrane surface modification, the self-organization approach results in *higher membrane porosities* relative to PVDF-only membranes. Thus, due to the combined benefits of fouling resistance and increased porosity, an optimized PVDF membrane with a bulk composition of 10 wt % P(MMA-r-POEM) is over 20 times as permeable as a PVDF-only membrane with equivalent separation characteristics after 3 h of filtration of a

Table 6.1 Comparison of Comb Additive Polymers Used in this Thesis Work

Additive Polymer	Advantages	Disadvantages
P(MMA-r-POEM)	• Very economical synthesis (cheaper than the PVDF matrix) • Facile control of side chain frequency and length through selection of monomer ratio and PEO chain length of POEM • Damaged surface layers may be regenerated by surface segregation of residual additive from the bulk upon simple heat treatment of the membrane in water	• Composition limited to $\leq$ ~50 wt % POEM, due to the requirement of water insolubility • Though it imparts substantially enhanced fouling resistance, does not impart sensible wettability to membranes (substitution of methyl acrylate for the backbone MMA results in enhanced wettability, however) • Diffuses *away* from the membrane surface during heat treatment in air, due to its high surface energy relative to PVDF • Incorporation of ~10 wt % of a (meth)acrylate-based additive polymer may compromise chemical stability of membranes in some extreme applications
PVDF-g-POEM	• Remains water-insoluble, even with incorporation of ~70 wt % POEM • Highly efficient delivery of POEM to membrane surface, compared to P(MMA-r-POEM) (see Table 5.5) • Imparts spontaneous wettability, as well as protein fouling resistance, to membranes • Crystallinity increases surface stability and prevents high-energy additive from diffusing away from surface during heating in air at T<T_m (~160°C) • Thermal crosslinking of the membrane surface layer using residual transition metal catalyst (see Section 5.3.1) may further increase surface stability • Membranes containing PVDF-based additive polymers may exhibit better thermal/chemical stability in extreme applications than membranes containing (meth)acrylate-based additives	• More expensive synthesis than (meth)acrylate-based additives • Poor thermal stability when stored in bulk condition, due to residual transition metal catalyst. OK if stored in solution • Possible extractables issue in some applications due to residual catalyst • Crystallinity prevents regeneration of damaged surface layers through aqueous heat treatment
PVDF-g-PMAA	• Provides pH-responsive separation characteristics • Provides enhanced wettability, though not as effectively as PVDF-g-POEM (at least for the composition tested – see Table 5.5) • Advantages due to crystallinity, crosslinking capability, and chemical resistance of backbone (see PVDF-g-POEM, above)	• More expensive synthesis than (meth)acrylate-based additives • Difficult to control PMAA side chain length and frequency • MAA not expected to perform as well as POEM in terms of protein fouling resistance • Possible thermal stability and extractables issues due to residual metal catalyst (see PVDF-g-POEM, above) • Crystallinity prevents regeneration of damaged surface layers through aqueous heat treatment

foulant protein solution. Moreover, a PVDF membrane containing as little as 5 wt %
PVDF-g-POEM (corresponding to only 3.4 wt % POEM) is spontaneously wettable by
water.

Using the ATRP synthesis technique, PVDF-based comb polymers having weak
polyacid (PMAA) side chains can be prepared. When localized at the membrane surface
by self-organization, the PMAA side chains of these combs change their conformation
reversibly according to the local pH. Thus, with no post-coagulation processing,
"intelligent" membranes can be produced, the separation characteristics of which can be
adjusted *in situ* by variation of a feed solution characteristic.

Membranes prepared by self-organization employing various comb additives
exhibit anti-fouling, wetting, and pH-responsive characteristics comparable to
membranes prepared previously by coating and grafting techniques. Work in this thesis
has identified three important performance advantages of self-organization over these
commonly-used methods for membrane surface modification. First, as mentioned above,
self-organization tends to increase, rather than decrease, the porosity of the separation
surface, eliminating a classical trade-off between fouling resistance and pure water
permeability. Second, self-organization modifies the internal pore channels of the
membrane, as well as the separation surface. This may have important consequences
with respect to resistance to the adsorption of through-pore foulants. Moreover, in
Section 6.2.2, we will see how the ability to tailor surface chemistry throughout the
membrane thickness may enable the preparation of "chemical filters" capable of
selectively binding target species in the feed solution. Finally, self-organization has the

advantage of providing *self-healing* membranes capable of regenerating damaged surface layers upon heat treatment in water, by surface segregation of residual additive polymer from the bulk.

Table 6.2 Market Prices of Acrylic and PVDF Resins

Polymer	Price[269] (US$/lb. for prime resin as of July 20, 2000)
general acrylic	0.82-0.87[†]
PVDF	7.20-7.60[‡]

[†] for annual volume of 2-5 million lbs.
[‡] for annual volume of 200,000 lbs.

In summary, the self-organization approach described in this thesis appears capable of providing all of the beneficial surface properties commonly obtained using grafting techniques, as well as the additional benefits described above, without the need for post-coagulation processing steps. Thus, the added cost for tailored surface properties is simply the difference in price between the small amount of comb polymer added to the casting solution and the matrix polymer it replaces. The economic importance of this fact can be appreciated by comparing the market prices of PVDF and, for example, acrylic resins (Table 6.2). PVDF, one of the most important commercial membrane polymers, is a relatively expensive material. By contrast, comb polymers like P(MMA-r-POEM) can be synthesized using methods routinely employed in the production of acrylic resins. Thus, it is quite possible that membranes with tailored surface properties, such as enhanced fouling resistance, can be produced at prices equal to *or lower than* PVDF-only membranes.

6.2 Issues for Future Work

6.2.1 Alternative Synthesis Routes for Comb Additive Materials

In setting out the objectives of this thesis (Chapter 1; Section 2.6), it was noted that a goal of any general surface modification technique should be a high degree of flexibility in the choice of surface chemistry. Herein, we have demonstrated an economical, highly flexible ATRP synthesis route enabling the graft copolymerization of PVDF (as well as other halogenated polymers[200]) with any vinyl monomer polymerizable by ATRP.

While branched additive polymers prepared by this method are clearly capable of imparting desirable properties to self-organizing membranes, this synthesis technique has some disadvantages. Very low concentrations of residual transition metal catalyst in these copolymers result in poor thermal stability with respect to crosslinking, due to the fact that every PVDF repeat unit is a potential free-radical initiation site in the presence of catalyst.* As discussed in Section 3.1.4, ongoing work in several laboratories is directed toward the development of economical methods to remove residual catalyst, which is a problem general to ATRP synthesis techniques. Perhaps more importantly from a design point of view, control of the side chain length and frequency using this synthesis route is difficult due to the abundance of potential initiation sites on the parent

---

* This might actually be used to advantage in some membrane applications. Simple aqueous, post-coagulation heat treatment of a membrane containing a PVDF-based graft copolymer prepared by ATRP having residual transition metal catalyst results in crosslinking of the graft copolymer backbone and matrix PVDF (see Section 5.3.1). This would be expected to increase the stability of the surface. Thus, for example, it might be possible to prepare stable surfaces using water-soluble polymer additives.

PVDF. In the preparation of environmentally responsive membranes by self-organization, in particular, side chain length and frequency are expected to be important optimization parameters. Finally, the application of self-organization as a general surface modification technique will require flexibility in the selection of backbone chemistries for compatibility with matrix materials other than PVDF. In this section, we briefly describe two alternative synthesis routes for the preparation of comb additive polymers. Both are economical, entirely free-radical routes, and both allow for a high degree of flexibility in terms of backbone chemistry, side chain chemistry, and architecture.

Figure 6.1 is a synthesis scheme illustrating an ATRP-based method for the preparation of comb polymers having a poly[methyl (meth)acrylate] backbone and vinyl side chains. Methyl (meth)acrylate is first copolymerized with a halogenated vinyl monomer such as 2-bromoethyl acrylate using a standard free-radical method to yield a random copolymer I. The pendant halogen atoms are then used as initiation sites for the ATRP graft copolymerization of a vinyl monomer to obtain the product II. The side chain frequency is simply controlled by the monomer ratio used in the synthesis of the prepolymer I. The side chain length is then controlled by choice of the appropriate stoichiometric excess of the vinyl monomer in the preparation of II. Using this method, the preparation of a comb with poly[(meth)acrylic acid] side chains of controlled length and frequency can be accomplished by the ATRP graft copolymerization of tB(M)A, followed by its hydrolysis with TSA in a third step (see Section 3.1.5). Characterization of the side chain length and frequency is accomplished simply by ^{1}H NMR determination

of the concentration of bromomethyl protons in **I** and the concentration of side chain repeat units in **II**.

$R_1 = H, CH_3$
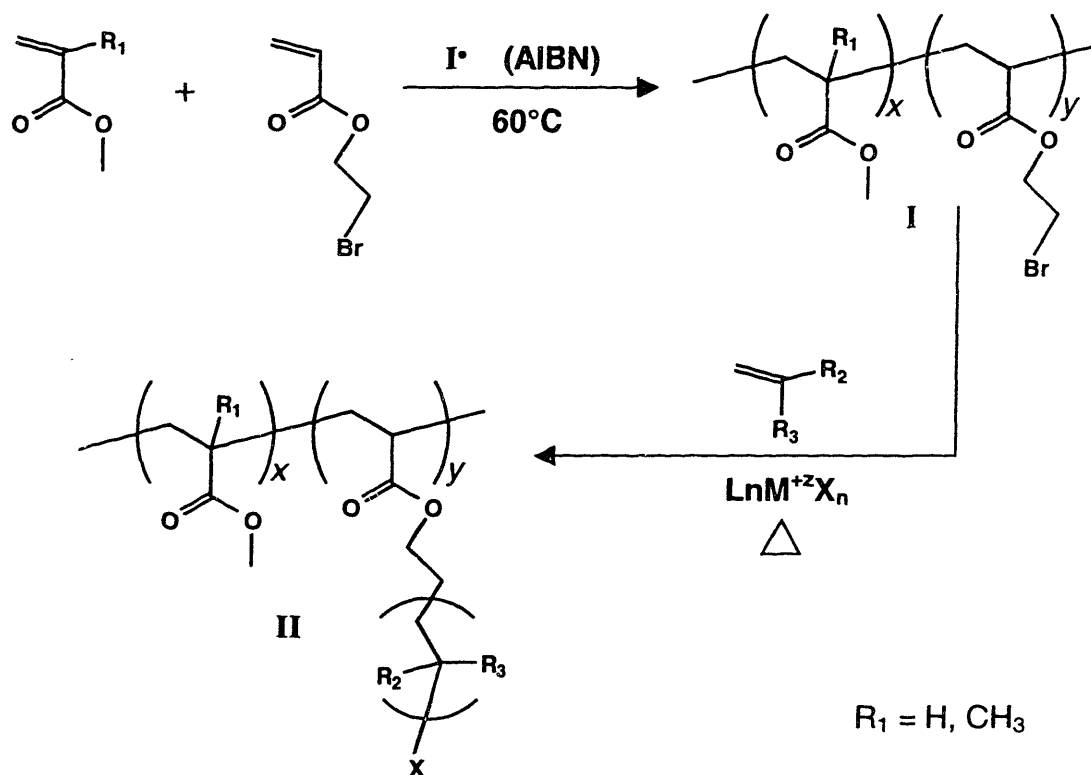
Figure 6.1 General ATRP synthesis route to comb polymer with PM(M)A backbone
In step 1, methyl (meth)acrylate is copolymerized with 2-bromoethyl acrylate free-radically to obtain a brominated prepolymer. In step 2, the pendant Br atoms are used as initiation sites for the ATRP polymerization of a vinyl monomer. The resulting polymer has a poly[methyl (meth)acrylate] backbone and side chains made up of any vinyl monomer(s) polymerizable by ATRP.
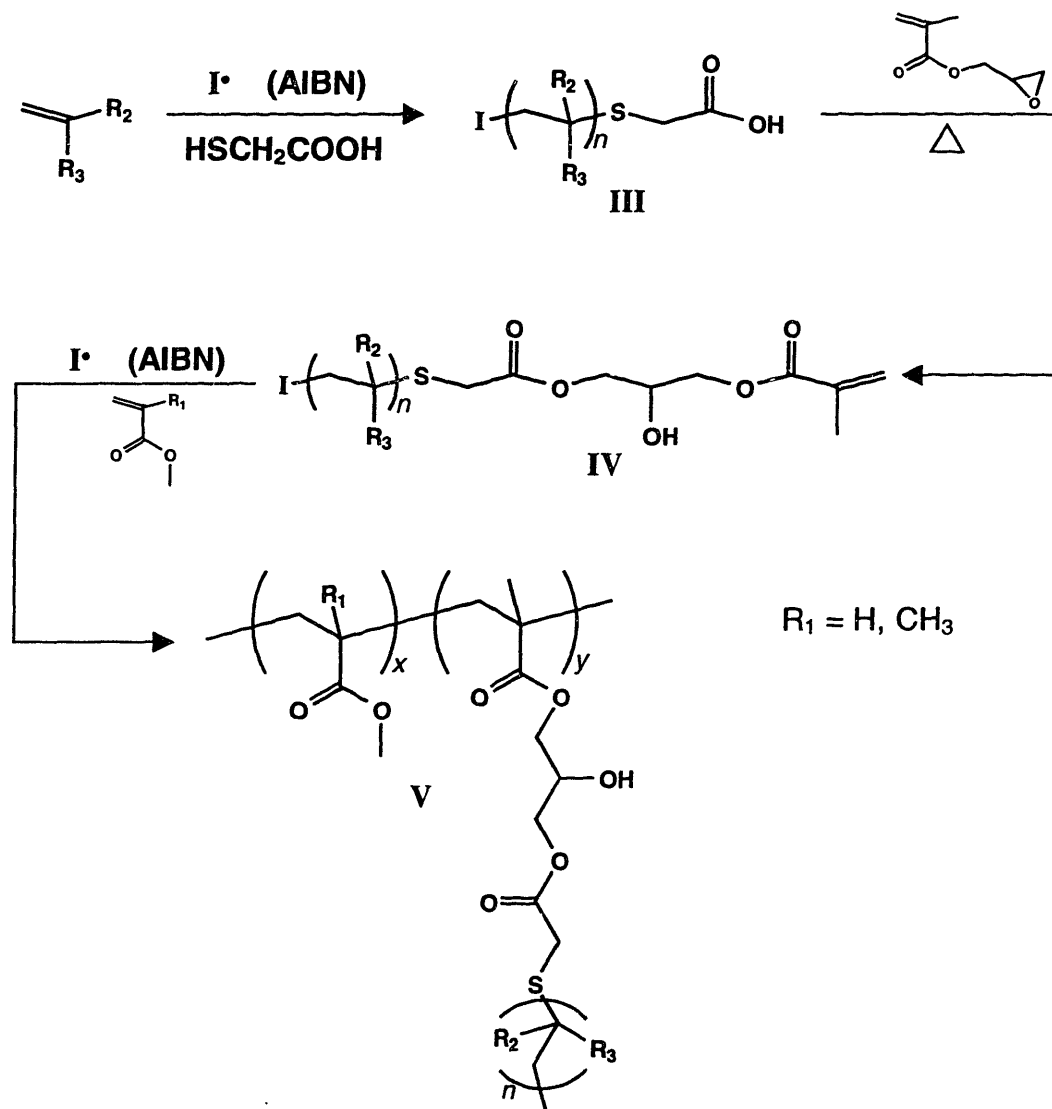
Figure 6.2 Standard free-radical route to comb polymer with PM(M)A backbone

$R_1 = H, CH_3$

Figure 6.2 illustrates a standard free-radical route for the preparation of similar comb polymers. This method has been used in the laboratory of Prof. A. M. Mayes at MIT to prepare PMMA-g-PMAA analogues, and is based on routes used previously in the preparation of comb polymer dispersants for the commercial production of PMMA latexes.[270,271] Bulk polymerization of a vinyl monomer is initiated by AIBN in the presence of a measured quantity of thioglycolic acid (TGA), a chain transfer agent. The polymerization is allowed to proceed for on the order of 1 h at 60°C. Chain transfer to TGA results in the termination of each prepolymer chain **III** with a carboxyl group. The prepolymer is purified by successive precipitations and dried, after which it is reacted with excess glycidyl methacrylate (GMA) at 140°C in xylene in the presence of small amounts of hydroquinone and N,N-dimethyllaurylamine to inhibit thermal polymerization of GMA. Reaction of the prepolymer carboxyl groups with GMA yields a macromonomer **IV** with a terminal methacrylate group. After purification and vacuum drying at room temperature (to avoid thermal polymerization), the macromonomer is copolymerized with methyl (meth)acrylate using a standard free-radical method to obtain the comb polymer **V**. Using this method, the side chain length is controlled by selection of the TGA/monomer ratio in the preparation of the carboxylated prepolymer **III**,[270] and the side chain frequency is determined by the monomer mixture in the random copolymerization to obtain **V**. Again, a graft copolymer with P(M)AA side chains may be synthesized by preparing the carboxylated prepolymer using tB(M)A, then selectively hydrolyzing the *tert*-butyl groups of the graft copolymer with TSA as a final step.

It should be noted that both of the above synthesis strategies enable the selection of virtually any vinyl monomer for the comb polymer backbone, which will be important for engineering compatibility with matrix polymers other than PVDF. Of course, many other synthetic routes to comb polymers exist. Current work in the laboratory of Prof. A. M. Mayes at MIT is focused on the development of ATRP synthetic methods for the preparation of comb polymers with PSf backbones. PSf-based materials will enable the preparation of self-organizing membranes from PSf, another important material for water treatment UF, NF, and RO membranes.

6.2.2 Additional Applications for Self-Organizing Polymer Membranes

Removal of Toxic Metals from Water

As discussed in Section 4.2.4, the surface modification of immersion precipitation membranes by self-organization offers an unprecedented ability to economically provide robust, chemically tailored layers on *all internal surfaces* of the 3-dimensional membrane, in addition to the external surfaces more easily accessible to coating and line-of-sight grafting methods. The large internal surface area now available for economical chemical modification may enable the use of MF and UF membranes as *chemical* separators, as well as physical ones. In fact, the data in Section 4.2.4 are a simple demonstration of the use of a membrane as a chemical separator capable of specifically binding a dissolved anionic dye during filtration. One potential application of such a membrane is the removal of heavy metals from water. The following paragraphs outline a proposed method for the preparation of a self-organizing UF membrane capable of specifically binding mercury(II) and consider the expected performance of such a membrane in realistic water treatment scenarios.

Figure 6.3 is a proposed synthesis scheme for the preparation of a PM(M)A-based comb additive polymer with side chains capable of selectively chelating Hg^{2+}. The first step is the preparation of a prepolymer, such as **VI**, having PS side chains. POEM may optionally be incorporated to provide increased hydrophilicity for surface segregation, if necessary. Such a prepolymer might be prepared by the ATRP graft copolymerization of PVDF with styrene, or by either of the general synthesis methods outlined in Section 6.2.1. Functionalization of the PS-bearing prepolymer with mercury-selective thiazoline groups might then be achieved using a procedure following Sugii, *et al.*,[272] who prepared crosslinked PS beads functionalized with this group. A standard Friedel-Crafts acylation reaction[273] is used for the addition of chloroacetyl chloride to the PS rings to obtain **VII**. Thermal reaction of the functionalized rings with *N,N*-dimethylthiourea yields the final mercury-chelating comb **VIII**.

Thiazoline-functionalized PS resins used as column adsorbents have been shown to be highly effective and selective in the isolation of Hg^{2+} from both fresh and saline aqueous solutions.[272] At the appropriate pH, maximum Hg^{2+} uptake was achieved within a few minutes, a realistic time scale with respect to an UF operation. Once bound, the mercury can then be eluted from the adsorbent simply by washing with 0.1 M hydrochloric acid containing 5% thiourea. Moreover, thiazoline-functionalized polystyrenes were found to be highly hydrophilic, absorbing greater than their own weight of water upon immersion. Thus, a comb bearing thiazoline-functionalized PS side chains might be expected to surface segregate during membrane fabrication using the molecular and process design guidelines established in this thesis.
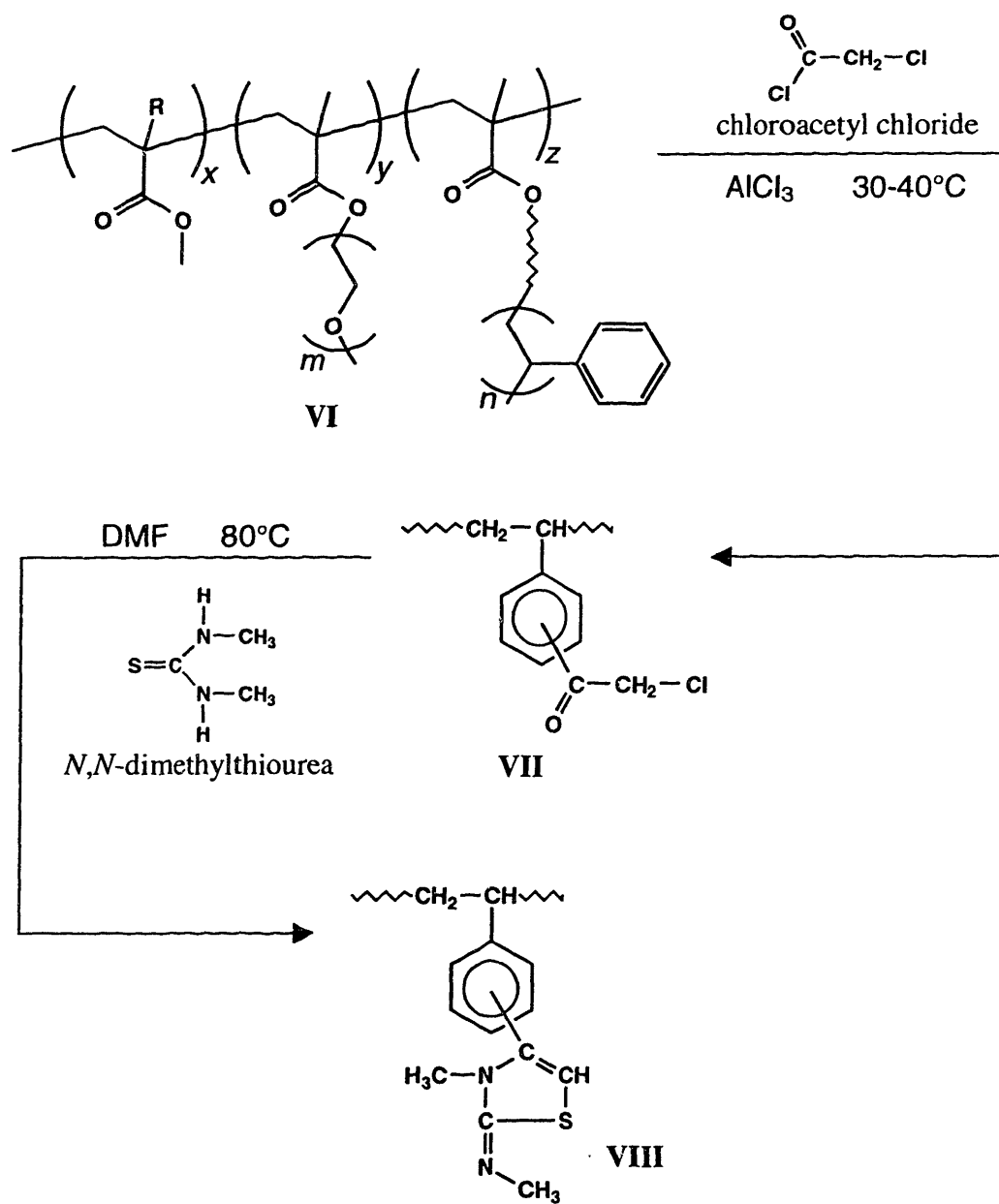
Figure 6.3 Synthesis scheme for a mercury-chelating comb

Aqueous, mercury-containing waste streams are produced by a number of industrial activities, including chloralkali production, oil refining, and pulp and paper, paint, pharmaceutical, and battery manufacturing.[274,275] Mercury is toxic to humans in extremely small quantities and readily accumulates in the food chain.[276,277] Thus, its environmental discharge is increasingly regulated, and cost-effective methods for removing low levels of mercury from water are needed.[275,278] Hg(II), the most water-soluble of the common mercury contaminant species,[275] is an important component of chloralkali and other wastewater streams.[274,278,279]

Based on data available in the literature and the experience accumulated in this thesis, it is possible to arrive at a rough estimate of the expected performance of a UF process utilizing self-organizing, Hg(II)-chelating membranes in the context of a realistic wastewater treatment scenario. First, it is necessary to obtain an estimate of the loading capacity of such a membrane per unit membrane area. Figure 6.4 illustrates a simple model used here to arrive at such an estimate. The comb additive polymer has side chains of average degree of polymerization n_{sc} spaced along the backbone with an average of n_b backbone segments between joints. Each side chain unit is capable of binding a single Hg^{2+} ion. All internal and external surfaces of the membrane are made up of comb polymer backbone units (black) and matrix polymer units (white). A fraction $1/n_b$ of the backbone units are joints to which side chains are attached. For simplicity, we make the approximation that the matrix polymer, comb backbone, and comb side chains are of equal statistical segment length, a.
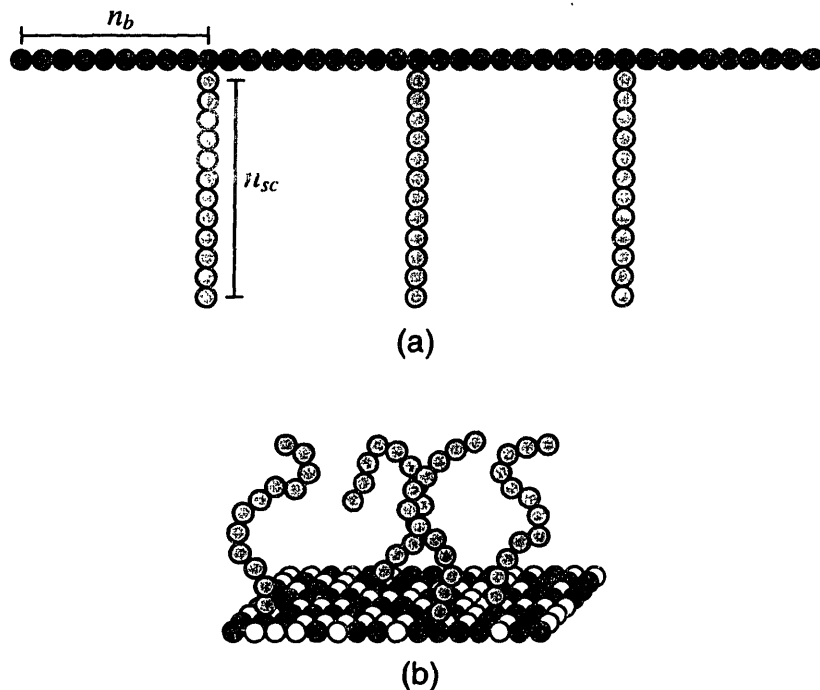
Figure 6.4 Diagrams illustrating a model for estimating membrane binding capacity
The comb additive polymer (a) is comprised of side chains of average degree of polymerization n_{sc}, each structural unit of which is capable of binding one Hg atom, spaced along the backbone with an average of n_b backbone units between joints. The membrane surface (b) is composed of matrix polymer units (white) and comb backbone units (black). Some backbone units have Hg-chelating side chains (grey) attached.

For each comb side chain of n_{sc} units "grafted" to the surface, there are n_b comb backbone units and a number of matrix polymer units, n_m, in the surface monolayer. The molar binding capacity for Hg^{2+} per unit membrane mass is then given by,

$$C_{sp}^m = \frac{A_{sp}}{N_{AV}} \cdot \frac{n_{sc}}{(n_b + n_m)a^2} \qquad (6.1)$$

where A_{sp} is the specific internal surface area of the membrane $[L^2/M]$ and N_{AV} is Avogadro's number. Combining with Equation 6.1 expressions for the fraction of comb polymer in the surface monolayer,

$$\phi_0 = \frac{n_b + n_{sc}}{n_m + n_b + n_{sc}} \tag{6.2}$$

and the fraction of side chain units in the comb polymer,

$$X_{sc} = \frac{n_{sc}}{n_b + n_{sc}} \tag{6.3}$$

we obtain,

$$C_{sp}^M = \frac{A_{sp}}{N_{AV} a^2} \cdot \frac{\phi_0 X_s}{1 - \phi_0 X_s}. \tag{6.4}$$

It should be noted that this estimate assumes that all comb side chains originating from joints in the surface layer are accessible for Hg^{2+} chelation. This is considered to be a good assumption in light of recent work by Irvine, *et al.*,[186,280] who studied RGD peptide presentation on the hydrated surfaces of films composed of P(MMA-*r*-POEM) and a second P(MMA-*r*-POEM) polymer having RGD covalently bonded at its side chain ends. Fluorescence labeling experiments performed on these blends indicated that comb molecules at the film surface take on a *quasi-2-dimensional conformation*, arranging themselves in a "pancake"-like fashion for maximal exposure of the hydrophilic side chains, resulting in extremely high RGD presentation efficiency. The hypothesis of quasi-2D confinement of comb polymers near surfaces has been further supported by SCF calculations.[186,280]

The specific internal surface areas of polymer membranes can be determined using a variety of sorption/desorption measurement techniques,[281-283] and UF membranes having specific surface areas as high as ~80 m^2/g have been prepared by standard immersion precipitation methods.[283] Assuming that a membrane designed for mercury

chelation would be optimized to attain a high specific surface area, we take $A_{sp} = 70 \text{ m}^2/\text{g}$.

As shown in this thesis (see Appendix D), $\phi_0 = 0.7$ is a conservative estimate of the surface fraction of comb obtainable by self-organization. Using a reasonable comb composition of $X_s = 0.5$ and a monomer size of $a = 6 \text{ Å}$, we obtain via Equation 6.4 an estimate of the specific Hg^{2+} binding capacity for a self-organizing membrane, $C_{sp}^M = 175 \text{ μmol/g}$. 25-mm filtration discs of membrane type F-00-2-90 (Table 3.4) were weighed and found to have a mass of $48.9 \pm 1.6 \text{ mg}$, or roughly 100 g/m^2. Thus, an estimate of the Hg^{2+} binding capacity per unit membrane area is $C_{sp}^A = 17.5 \text{ mmol/m}^2$.

The per-mass specific binding capacity estimated above is roughly an order of magnitude smaller than the measured capacities of mercury(II)-selective resins which have been prepared by a variety of methods.[272,274] Many mercury-containing waste streams are characterized by extremely low Hg concentrations, however, and the capabilities of many mercury removal systems are therefore not limited by capacity.[275] For example, Hg^{2+} concentrations ranging from 8 to 38 μmol/L have been found in several chloroalkali industry waste streams.[274,278,279] A commercially-available, moderate-size UF system has 224 modules, each with a membrane filtration area of 55 square meters.[4] We consider the use of a system of this size, having the above estimated Hg^{2+} specific binding capacity, for the treatment of a waste stream having a Hg^{2+} concentration of 25 μmol/L. Assuming that 80% of the maximum binding capacity is utilized, and that the system is regenerated once every 12 h by removal of bound mercury, such a system would produce clean permeate at a rate of,

$$(224)(55m^2) \cdot \frac{(0.80)(0.0175mol)}{1m^2} \cdot \frac{1L}{25(10^{-6})mol} \cdot \frac{1}{12h} = 575\,000 \text{ L/h}.$$

This is about 25% of the nominal production rate of an UF system of this size used for general surface water treatment.[4] Operation at the full nominal production rate would require membrane regeneration every 3 h. Thus, the economics of such a process would depend heavily on the design of efficient methods for membrane regeneration. For example, regeneration might be combined with periodic backwash operations.

Metal-chelating membranes would seem more attractive for use in conjunction with new *polymer enhanced ultrafiltration* (PEUF) processes for heavy-metal extraction. These processes are based on complexation of heavy metals by various water-soluble polymers, which are then removed from the feed stream by UF.[284-286] PEUF processes are expected to compare favorably with conventional adsorption technologies in terms of cost, due to low energy requirements and high efficiencies afforded by the single-phase nature of the metal ion separation process.[284,285] In pilot scale PEUF systems, mercury retentions as high as 0.98 have been accomplished, but retention has been shown to decrease linearly with increasing mercury concentration above a critical ratio of mercury concentration to polymer concentration in the feed stream.[285] Cheaply-fabricated, metal-chelating membranes prepared by the self-organization method described in this thesis might be useful as the membrane components of PEUF systems. These membranes would increase metal retention and function as a "safety net" against fluctuations in metal concentration, as well as other feed stream characteristics,[285] which might occasionally allow permeation of the metal in a standard PEUF system. The presence of the water-

soluble polymer as the primary binding agent would result in very infrequent membrane regeneration requirements.

UF employing metal-chelating membranes might similarly be useful as a low-cost safety backup and finishing step for the chemical precipitation processes used most commonly for heavy metal removal from industrial wastewater streams.[275] These processes already employ filtration steps for removal of the insoluble, metal-containing precipitate. Mercury precipitation processes have a typical lower limit treatment capability of 0.05-0.10 μmol/L.[275] Operating at its full nominal production rate, the 224-module UF system considered above would need to be regenerated only once every 30-60 days if used to remove residual Hg^{2+} at this concentration from the post-precipitation stream.

Barrier Devices and Scaffolds for Biomedical Applications

With proper process parameter selection, the immersion precipitation process used to prepare filtration membranes can easily be used to produce porous articles having pores on the size scale of biological cells. The combination of the simplicity of this process with the unprecedented ability of self-organization to chemically tailor all internal and external membrane surfaces, independent of the bulk material, makes immersion precipitation membranes attractive candidates for biological implant materials. Previous work by Irvine, *et al.* examined blends of PLLA with P(MMA-*r*-POEM)[186] and poly(lactide)-*g*-POEM[287] comb polymers whose side chain ends could be derivatized with cell-regulating peptides. Heat treatment of films prepared from these blends drove surface segregation of the hydrophilic comb, which was shown to provide

protein resistance and cell-regulating properties. Building on the work of Irvine and coworkers as well as work in this thesis, current research in the laboratories of Profs. A. Mayes and L. Griffith at MIT is directed toward the development of self-organizing PLLA-based membranes containing amphiphilic comb additives with poly(caprolactone urethane) and PLLA backbones. These membranes are expected to be useful as bioinert or bioregulating, biodegradable surgical barrier materials and scaffolds.

Advanced Reverse Osmosis Membranes

Results presented in Section 3.1.4 suggested that PVDF-*g*-POEM microphase separates on an unusually small length scale of ~2 nm. Current work in the MIT laboratory of Prof. Mayes is focused on the preparation of self-organizing, PVDF-based membranes having nonporous or nearly nonporous separation surfaces composed almost entirely of PVDF-*g*-POEM. These membranes are envisioned as advanced RO membranes, the separation mechanism of which will be water transport through the hydrophilic POEM domains. Though permeable to water, these domains are expected to be impermeable to salts due to their small size. "Advanced" RO membranes so prepared would bring to RO the desirable mechanical properties and chemical resistance of PVDF. PVDF-based RO membranes would thus be expected to have notable advantages over conventional cellulosic and polyamide membranes which, as discussed in Section 2.2.2, are susceptible to various forms of chemical attack. In addition, the self-organizing PVDF-based RO membranes should be inexpensive to produce, compared with thin-film composite membranes.[288]

228

List of Symbols and Acronyms

a	Statistical segment length
a_D	Thickness of near-surface comb depletion layer
A	Peak area for XPS fitting
A_x	Area of XPS component peak for bonding environment x
A_{sp}	Specific internal surface area of membrane [L^2/M]
AA	Acrylic acid
ads	Adsorbed onto
AFM	Atomic force microscopy
AIBN	2,2'-azobisisobutyronitrile
AO	Acridine orange
ATRP	Atom transfer radical polymerization
AWS	Accessible water supply
BE	Photoelectron binding energy
BE_o	Peak center for XPS fitting
BγGl	Bovine γ-globulin
β-LG	β-lactoglobulin
bl	Blended with
bpy	4,4'-dimethyl-2,2'-dipyridyl
BSA	Bovine serum albumin
χ_{ij}	Flory-Huggins interaction parameter for components i and j
c_i	Concentration of component i
C_{BSA}^x	Concentration of BSA in stream x
C_{sp}^A	Molar metal ion binding capacity per unit membrane area
C_{sp}^M	Molar metal ion binding capacity per unit membrane mass
CSA	Chromic-sulfuric acid
ct	Coated with
CyC	Cytochrome C
d	XPS sampling depth
d_z	Vertical deflection of AFM cantilever
d-PS	Deuterated polystyrene
D	Diffusion coefficient
D	Pore diameter
D_n	Pore diameter at pH n
$\overline{D}$	Mean pore diameter
D_{max}	Maximum observed pore diameter
D_{mode}	5-nm bin of pore diameters occurring most frequently
DMAc	N,N-dimethylacetamide
DMF	N,N-dimethylformamide
dW	Deionized water
ε	Membrane porosity (pore area per unit separation surface area)

EO	A single ethylene oxide ($-CH_2-CH_2-O-$) repeat unit of PEO
ER	Environmentally responsive
$F_i(BE)$	Photoelectron intensity at binding energy BE for XPS peak i
FESEM	Field emission scanning electron microscopy
ϕ_0	Fraction of comb additive polymer in surface monolayer
ϕ_b	Bulk volume fraction of comb additive polymer
ϕ_s	Near-surface volume fraction of comb additive polymer
$\phi_{w,b}$	Bulk weight fraction of comb additive polymer
$\phi_{w,b}^{PMAA}$	Bulk weight fraction of PMAA
$\phi_{w,b}^{POEM}$	Bulk weight fraction of POEM
$\phi_{w,s}^{PMAA}$	Near-surface weight fraction of PMAA
$\phi_{w,s}^{POEM}$	Near-surface weight fraction of POEl 1
F	AFM measured force
F_o	AFM measured force at position of "zero force"
γ	Surface tension
G_n	Greyscale intensity of pixel n in a raw FESEM image
G_0^S	Greyscale pixel intensity obtained by application of the Sobel filter
GMA	Glycidyl methacrylate
GPC	Gel permeation chromatography
gr	Grafted with
η	Viscosity
$h\nu$	Energy of a photon
hh	Head-to-head bonding arrangement in PVDF
ht	Head-to-tail bonding arrangement in PVDF
H	PMAA surface layer height
H_n	PMAA surface layer height at pH n
ΔH_m	Heat of melting as measured by DSC [J/g]
ΔH_f^*	Heat of fusion [J/mol]
HPOEM	Poly(ethylene glycol) methacrylate
i_x	Intensity of NMR resonance x
$\vec{J}_i$	Flux of component i
J_n	Flux of water at pH n
J_o	Pure water flux
J_f	Final flux of foulant solution
J_o^C	Initial trans-membrane flux of pure water for control membrane
J_o^M	Initial trans-membrane flux of pure water for modified membrane
J_f^C	Final trans-membrane flux of foulant solution for control membrane
J_f^M	Final trans-membrane flux of foulant solution for modified membrane
k	Hooke's law spring constant
KE	Photoelectron kinetic energy
λ_i	Photoelectron mean free path for core level photoelectron i

230

λ_{abs}	Longest-wavelength fluorescence adsorption maximum
λ_{em}	Wavelength of the fluorescence emission maximum
L	Pore channel length
LCST	Lower critical solution temperature
Ln	Organic ligand in ATRP
LYS	Lysozyme
μ_i	Chemical potential of component i
m	Gaussian-Lorentzian mixing ratio for XPS fitting
M	Polymer molecular weight
M_o^x	Repeat unit or monomer molecular weight of x
$\overline{M}_w$	Weight-average molecular weight
MA	Methyl acrylate
MAA	Methacrylic acid
MF	Microfiltration
MMA	Methyl methacrylate
mpb	Modified bulk polymer chemically
MSF	Multi-stage flash distillation
N	Number of peaks in XPS model spectrum
N	Degree of polymerization
n_b	Backbone average degree of polymerization between side chains
n_m	Number of matrix polymer units per comb side chain in surface monolayer
n_s	Near-surface mole fraction of comb additive polymer
n_s^{PMAA}	Near-surface mole fraction of PMAA
n_s^{POEM}	Near-surface mole fraction of POEM
n_{sc}	Side chain average degree of polymerization
N_{AV}	Avogadro's number
NF	Nanofiltration
NMP	1-methyl-2-pyrrolidinone
NMR	Nuclear magnetic resonance
NVP	N-vinyl-pyrrolidone
P_{bp}	Bubble point pressure
P_c	Compaction pressure
P_m	Measurement pressure
ΔP	Pressure drop
PAm	Polyamide
PAN	Polyacrylonitrile
PAS	Poly(arylsulfone)
PBS	Phosphate buffered saline
PCL	Poly(ε-caprolactone)
PDMS	Poly(dimethylsiloxane)
PE	Polyethylene
PEI	Poly(ether imide)
PEG	Poly(ethylene glycol), or PEO of low molecular weight

PEO	Poly(ethylene oxide)
PES	Poly(ethersulfone)
PEUF	Polymer enhanced ultrafiltration
PLLA	Poly(L-Lactide)
PMA	Poly(methyl acrylate)
PMAA	Poly(methacrylic acid)
PMMA	Poly(methyl methacrylate)
$POEM_n$	Poly(oxyethylene methacrylate) having nominally n EO repeat units
PS	Polystyrene
PSA	Porcine serum albumin
PSf	Polysulfone
PtBMA	Poly(*tert*-butyl methacrylate)
PVC	Poly(vinyl chloride)
PVDF	Poly(vinylidene fluoride)
$PVDF_{nK}$	Poly(vinylidene fluoride) having $\overline{M}_w = 1000n$ g/mol
PVP	Poly(vinyl pyrrolidone)
ρ_x	Density of x
R_{BSA}	BSA rejection coefficient
R_F	Flory radius
$R_{f.d.}$	Flux decline ratio
RGD	Arginine-glycine-aspartic acid
RO	Reverse osmosis
σ_D	Standard deviation of pore diameter
s	XPS correction factor for surface charging
S_i	XPS signal
$S_E(BE)$	Experimental XPS photoelectron intensity at binding energy BE
$S_T(BE)$	Theoretical XPS photoelectron intensity at binding energy BE
SCF	Self-consistent mean-field
SEM	Scanning electron microscopy
SSE	Sum of squared errors
θ	Solid-liquid contact angle
θ	Photoelectron take-off angle
θ_{adv}	Advancing contact angle
T_m	Melting point
tBMA	*tert*-butyl methacrylate
TGA	Thioglycolic acid
THF	Tetrahydrofuran
TSA	p-toluenesulfonic acid monohydrate
UF	Ultrafiltration
V_o^x	molar volume of polymer x per structural repeat unit
w_i	Value of exponential XPS weighting function
W	Full-width at half-maximum for XPS fitting
W_c	Weight percent crystallinity with respect to PVDF content of polymer

W_{POEM}	Weight fraction of POEM
x	Molar ratio of comonomer units to PVDF units in graft copolymer
X_{POEM}	Mole fraction POEM
X_{sc}	Fraction of side chain repeat units in comb polymer
XPS	X-ray photoelectron spectroscopy
z	Depth below sample surface
z	Displacement of AFM sample stage
z_0	Zero position of AFM sample stage
z_m	Middle position of PMAA surface layer

Bibliography

1. J. A. Howell; "Overview of membranes;" *The Membrane Alternative: Energy Implications for Industry*; J. A. Howell, Ed.; Elsevier Applied Science: London, 1990, pp 1-8.

2. P. Aptel and C. A. Buckley; "Categories of membrane operations;" *Water Treatment Membrane Processes*; J. Mallevialle, P. E. Odendaal and M. R. Wiesner, Ed.; McGraw-Hill Book Company: New York, 1996, pp 2.1-2.24.

3. H. Strathmann; "Synthetic membranes and their preparation;" *Synthetic Membranes: Science, Engineering and Applications*; P. M. Bungay, H. K. Lonsdale and M. N. DePinho, Ed.; Kluwer Academic Publishers: Dordrecht, The Netherlands, 1983, pp 1-37.

4. C. Anselme and E. P. Jacobs; "Ultrafiltration;" *Water Treatment Membrane Processes*; J. Mallevialle, P. E. Odendaal and M. R. Wiesner, Ed.; McGraw-Hill Book Company: New York, 1996, pp 10.1-10.88.

5. I. Cabasso, E. Klein and J. K. Smith; "Polysulfone hollow fibers. II. Morphology;" *Journal of Applied Polymer Science* **1977**, *21*, 165-180.

6. J. R. Fried; *Polymer Science and Technology*; Prentice Hall: Upper Saddle River, NJ, 1995.

7. T. M. Missimer; *Water Supply Development for Membrane Water Treatment Facilities*; Lewis Publishers: Boca Raton, 1994.

8. C. A. Buckley and Q. E. Hurt; "Membrane applications: A contaminant-based perspective;" *Water Treatment Membrane Processes*; J. Mallevialle, P. E. Odendaal and M. R. Wiesner, Ed.; McGraw-Hill Book Company: New York, 1996, pp 3.1-3.24.

9. S. L. Postel, G. C. Daily and P. R. Ehrlich; "Human appropriation of renewable fresh water;" *Science* **1996**, *271*, 785-788.

10. S. L. Postel; "Dividing the waters;" *Technology Review* **1997**, *April*, 54-62.

11. S. L. Postel; *Last oasis: Facing water scarcity*; W. W. Norton & Company: New York, 1997.

12. United Nations; *Long-Range World Population Projections: Two Centuries of Population Growth, 1950-2150*; United Nations: New York, 1992.

13. S. L. Postel, J. I. Morrison and P. H. Gleick; "Allocating fresh water to aquatic ecosystems: The case of the Colorado River delta;" *Water International* **1998**, *23*, 119-125.

14. P. H. Gleick; "Water and conflict: Fresh water resources and international security;" *International Security* **1993**, *18*, 79-112.

15. M. Mulder; "The use of membrane processes in environmental problems. An introduction;" *Membrane Processes in Separation and Purification*; J. G. Crespo and K. W. Boddeker, Ed.; Kluwer Academic Publishers: Dordrecht, The Netherlands, 1994, pp 229-262.

16. T. Richardson and R. Trussell; "Taking the plunge;" *Civil Engineering* **1997**, *67*, 42-45.

17. A. Benedek; "Development and commercialization of new technologies for large scale water and wastewater treatment;" *The 1999 Membrane Technology/ Separations Planning Conference proceedings: as presented at the Seventeenth Annual Membrane Technology/Separations Planning Conference, Dec. 6 and 7, 1999, Newton, Massachusetts*, Business Communications Co., Inc.: Norwalk, CT, 2000.

18. A. T. Caetano; "Existing industrial membrane applications: Results and perspectives;" *Membrane Technology: Applications to Industrial Wastewater Treatment*; A. T. Caetano, M. N. DePinho, E. Drioli and H. Muntau, Ed.; Kluwer Academic Publishers: Dordrecht, The Netherlands, 1995, pp 47-62.

19. P. Aptel; "Membrane pressure driven processes in water treatment;" *Membrane Processes in Separation and Purification*; J. G. Crespo and K. W. Boddeker, Ed.; Kluwer Academic Publishers: Dordrecht, The Netherlands, 1994, pp 263-281.

20. H. Strathmann; "Membrane separation processes in advanced waste water treatment;" *Pure and Applied Chemistry* **1976**, *46*, 213-220.

21. M. Williams, R. Deshmukh and D. Bhattacharyya; "Separation of hazardous organics by reverse osmosis membranes;" *Environmental Progress* **1990**, *9*, 118-125.

22. N. Wade; "Desalination technologies compared;" *The Membrane Alternative: Energy Implications for Industry*; J. A. Howell, Ed.; Elsevier Applied Science: London, 1990, pp 19-29.

23. J. D. Birkett; "Desalination technology/industry update;" *The 1999 Membrane Technology/Separations Planning Conference proceedings: as presented at the Seventeenth Annual Membrane Technology/Separations Planning Conference, Dec. 6 and 7, 1999, Newton, Massachusetts*, Business Communications Co., Inc.: Norwalk, CT, 2000.

24. C. H. Deutsch; "Satisfying an age-old thirst;" *The New York Times* **1999**, *May 16*, BU 5.

25. J. Mallevialle, P. E. Odendaal and M. R. Wiesner; "The emergence of membranes in water and wastewater treatment;" *Water Treatment Membrane Processes*; J. Mallevialle, P. E. Odendaal and M. R. Wiesner, Ed.; McGraw-Hill Book Company: New York, 1996, pp 1.1-1.10.

26. J. Cross; "Membrane processes: Versatile technology for cutting costs and protecting the environment;" *Filtration and Separation* **1992**, *29*, 386-390.

27. F. I. H. M. Oesterholt and B. A. Bult; "Improving municipal waste water quality by effluent polishing: A pilot scale experiment at Winterswijk, The Netherlands;" *Water Science and Technology* **1993**, *27*, 277-286.

28. K. D. Pickering and M. R. Wiesner; "Cost model for low-pressure membrane filtration;" *Journal of Environmental Engineering - American Society of Civil Engineers* **1993**, *119*, 772-797.

29. M. R. Wiesner and P. Aptel; "Mass transport and permeate flux and fouling in pressure-driven processes;" *Water Treatment Membrane Processes*; J. Mallevialle, P. E. Odendaal and M. R. Wiesner, Ed.; McGraw-Hill Book Company: New York, 1996, pp 4.1-4.30.

30. S. Loeb and S. Sourirajan; "Sea water demineralization by means of an osmotic membrane;" *Advances in Chemistry Series* **1962**, *38*, 117-132.

31. H. Yamagishi, J. V. Crivello and J. Belfort; "Development of a novel photochemical technique for modifying poly(arylsulfone) ultrafiltration membranes;" *Journal of Membrane Science* **1995**, *105*, 237-247.

32. P. Aimar, M. Meireles, P. Bacchin and V. Sanchez; "Fouling and concentration polarisation in ultrafiltration and microfiltration;" *Membrane Processes in Separation and Purification*; J. G. Crespo and K. W. Boddeker, Ed.; Kluwer Academic Publishers: Dordrecht, The Netherlands, 1994, pp 27-57.

33. P. Aptel and M. Clifton; "Ultrafiltration;" *Synthetic Membranes: Science, Engineering and Applications*; P. M. Bungay, H. K. Lonsdale and M. N. DePinho, Ed.; Kluwer Academic Publishers: Dordrecht, The Netherlands, 1983, pp 249-305.

34. N. Sanders and J. Hubble; "The effect of membrane fouling and cleaning on rejection of low molecular weight tracer in ultrafiltration;" *Effective Membrane Processes - New Perspectives*; R. Paterson, Ed.; Mechanical Engineering Publications Limited: London, 1993, pp 35-48.

35. H. Bauser, H. Chmiel, N. Stroh and E. Walitza; "Control of concentration polarization and fouling of membranes in medical, food and biotechnical applications;" *Journal of Membrane Science* **1986**, *27*, 195-202.

36. J. Hiddink, D. Kloosterboer and S. Bruin; "Evaluation of static mixers as convection promoters in the ultrafiltration of dairy liquids;" *Desalination* **1980**, *35*, 149-167.

37. S. N. Gaeta; "The industrial development of polymeric membranes and membrane modules for reverse osmosis and ultrafiltration;" *Membrane Technology: Applications to Industrial Wastewater Treatment*; A. T. Caetano, M. N. De Pinho, E. Drioli and H. Muntau, Ed.; Kluwer Academic Publishers: Dordrecht, The Netherlands, 1995, pp 25-45.

38. J. S. Taylor and E. P. Jacobs; "Reverse osmosis and nanofiltration;" *Water Treatment Membrane Processes*; J. Mallevialle, P. E. Odendaal and M. R. Wiesner, Ed.; McGraw-Hill Book Company: New York, 1996, pp 9.1-9.70.

39. T. N. Eisenberg and E. J. Middlebrooks; *Reverse Osmosis Treatment of Drinking Water*; Butterworths: Stoneham, MA, 1986.

40. P. E. Barker, K. Poland, A. Till and R. M. Alsop; "The development of a diafiltration cascade system for the fractionation of a dextran hydrolysate;" *Chemical Engineering Research & Design* **1989**, *67*, 262-266.

41. J. A. Koehler, M. Ulbricht and G. Belfort; "Intermolecular forces between proteins and polymer films with relevance to filtration;" *Langmuir* **1997**, *13*, 4162-4171.

237

42. R. W. Baker; *Membrane Technology and Applications*; McGraw-Hill: New York, 2000.

43. L. Yilmaz and A. J. McHugh; "Modelling of asymmetric membrane formation. I. Critique of evaporation models and development of a diffusion equation formalism for the quench period;" *Journal of Membrane Science* **1986**, *28*, 287-310.

44. E. R. Watson, G. V. Rowley and C. R. Wunderlich; *Method and Apparatus for Continuous Fabrication of Desalination Membrane*; US Patent #3,432,585 (1969).

45. S. P. Nunes, M. L. Sforca and K.-V. Peinemann; "Dense hydrophilic composite membranes for ultrafiltration;" *Journal of Membrane Science* **1995**, *106*, 49-56.

46. R. E. Kesting; *Synthetic Polymeric Membranes*; McGraw-Hill Book Company: New York, 1971.

47. H. Strathmann and K. Kock; "The formation mechanism of phase inversion membranes;" *Desalination* **1977**, *21*, 241-255.

48. H. Strathmann, K. Kock, P. Amar and R. W. Baker; "The formation mechanism of asymmetric membranes;" *Desalination* **1975**, *16*, 179-203.

49. A. J. Reuvers, J. W. A. van den Berg and C. A. Smolders; "Formation of membranes by means of immersion precipitation. Part I. A model to describe mass transfer during immersion precipitation;" *Journal of Membrane Science* **1987**, *34*, 45-65.

50. J. E. Anderson and R. Ullman; "Mathematical analysis of factors influencing the skin thickness of asymmetric reverse osmosis membranes;" *Journal of Applied Physics* **1973**, *44*, 4303-4311.

51. R. M. Boom, H. W. W. Rolevink, T. van den Boomgaard and C. A. Smolders; "Microscopic structures in phase inversion membranes: The use of polymer blends for membrane formation by immersion precipitation;" *Makromolekulare Chemie, Macromolecular Symposia* **1993**, *69*, 133-140.

52. C. A. Smolders, A. J. Reuvers, R. M. Boom and I. M. Wienk; "Microstructures in phase inversion membranes. Part 1. Formation of macrovoids;" *Journal of Membrane Science* **1992**, *73*, 259-275.

53. R. M. Boom, I. M. Wienk, T. van den Boomgaard and C. A. Smolders; "Microstructures in phase inversion membranes. Part 2. The role of a polymeric additive;" *Journal of Membrane Science* **1992**, *73*, 277-292.

54. C. Stropnik, L. Germic and B. Zerjal; "Morphology variety and formation mechanisms of polymeric membranes prepared by wet phase inversion;" *Journal of Applied Polymer Science* **1996**, *61*, 1821-1830.

55. F.-C. Lin, D.-M. Wang, C.-L. Lai and J.-Y. Lai; "Effect of surfactants on the structure of PMMA membranes;" *Journal of Membrane Science* **1997**, *123*, 281-291.

56. S.-G. Li, T. van den Boomgaard, C. A. Smolders and H. Strathmann; "Physical gelation of amorphous polymers in a mixture of solvent and nonsolvent;" *Macromolecules* **1996**, *29*, 2053-2059.

57. H. Strathmann, P. Scheible and R. W. Baker; "A rationale for the preparation of Loeb-Sourirajan-type cellulose acetate membranes;" *Journal of Applied Polymer Science* **1971**, *15*, 811-828.

58. M. A. Frommer, I. Feiner, O. Kedem and R. Bloch; "The mechanism for formation of 'skinned' membranes. II. Equilibrium properties and osmotic flows determining membrane structure;" *Desalination* **1970**, *7*, 393-402.

59. H. K. Lonsdale; "Properties of cellulose acetate membranes;" *Desalination by Reverse Osmosis*; U. Merten, Ed.; M.I.T. Press: Cambridge, MA, 1966, pp 93-160.

60. L.-P. Cheng, D.-J. Lin, C.-H. Shih, A.-H. Dwan and C. C. Gryte; "PVDF membrane formation by diffusion-induced phase separation - Morphology prediction based on phase behavior and mass transfer modeling;" *Journal of Polymer Science. Part B: Polymer Physics* **1999**, *37*, 2079-2092.

61. L. P. Cheng, Y. S. Soh, A. H. Dwan and C. C. Gryte; "An improved model for mass-transfer during the formation of polymeric membranes by the immersion-precipitation process;" *Journal of Polymer Science. Part B: Polymer Physics* **1994**, *32*, 1413-1425.

62. P. Radovanovic, S. W. Thiel and S.-T. Hwang; "Formation of asymmetric polysulfone membranes by immersion precipitation. Part I. Modelling mass transport during gelation;" *Journal of Membrane Science* **1992**, *65*, 213-229.

63. P. Radovanovic, S. W. Thiel and S.-T. Hwang; "Formation of asymmetric polysulfone membranes by immersion precipitation. Part II. The effects of casting solution and gelation bath compositions on membrane structure and skin formation;" *Journal of Membrane Science* **1992**, *65*, 231-246.

64. C. S. Tsay and A. J. McHugh; "Mass transfer modeling of asymmetric membrane formation by phase inversion;" *Journal of Polymer Science. Part B: Polymer Physics* **1990**, *28*, 1327-1365.

65. A. J. Reuvers and C. A. Smolders; "Formation of membranes by means of immersion precipitation. Part II. The mechanism of formation of membranes prepared from the system cellulose acetate-acetone-water;" *Journal of Membrane Science* **1987**, *34*, 67-86.

66. C. Cohen, G. B. Tanny and S. Prager; "Diffusion-controlled formation of porous structures in ternary polymer systems;" *Journal of Polymer Science: Polymer Physics Edition* **1979**, *17*, 477-489.

67. Y. Termonia; "Monte Carlo diffusion model of polymer coagulation;" *Physical Review Letters* **1994**, *72*, 3678-3681.

68. Y. Termonia; "Fundamentals of polymer coagulation;" *Journal of Polymer Science. Part B: Polymer Physics* **1995**, *33*, 279-288.

69. T.-H. Young, L.-P. Cheng, D.-J. Lin, L. Fane and W.-Y. Chuang; "Mechanisms of PVDF membrane formation by immersion-precipitation in soft (1-octanol) and harsh (water) nonsolvents;" *Polymer* **1999**, *40*, 5315-5323.

70. L. Yilmaz and A. J. McHugh; "Analysis of nonsolvent-solvent-polymer phase diagrams and their relevance to membrane formation modeling;" *Journal of Applied Polymer Science* **1986**, *31*, 997-1018.

71. F. W. Altena and C. A. Smolders; "Calculation of liquid-liquid phase separation in a ternary system of a polymer in a mixture of a solvent and a nonsolvent;" *Macromolecules* **1982**, *15*, 1491-1497.

72. H. Tompa; "Phase relationships in polymer solutions;" *Transactions of the Faraday Society* **1949**, *45*, 1142-1152.

73. P. van de Witte, P. J. Dijkstra, J. W. A. van den Berg and J. Feijen; "Metastable liquid-liquid and solid-liquid phase boundaries in polymer-solvent-nonsolvent systems;" *Journal of Polymer Science. Part B: Polymer Physics* **1997**, *35*, 763-770.

74. C. Castellari and S. Ottani; "Preparation of reverse osmosis membranes. A numerical analysis of asymmetric membrane formation by solvent evaporation from cellulose acetate casting solutions;" *Journal of Membrane Science* **1981**, *9*, 29-41.

75. M. Ataka and K. Sasaki; "Gravimetric analysis of membrane casting. I. Cellulose acetate-acetone binary casting solutions;" *Journal of Membrane Science* **1982**, *11*, 11-25.

76. M. N. Sarbolouki; "Preparation of the skinned membranes without evaporation step;" *Journal of Polymer Science, Polymer Letters Edition* **1973**, *11*, 753-754.

77. Y. Termonia; "Molecular modeling of phase-inversion membranes: Effect of additives in the coagulant;" *Journal of Membrane Science* **1995**, *104*, 173-180.

78. M. A. Frommer and D. Lancet; "The mechanism of membrane formation: Membrane structures and their relation to preparation conditions;" *Reverse Osmosis Membrane Research*; H. K. Lonsdale and H. E. Podall, Ed.; Plenum Press: New York, 1972, pp 85-110.

79. M. A. Frommer and R. M. Messalum; "Mechanism of membrane formation. VI. Convective flows and large void formation during membrane precipitation;" *Industrial and Engineering Chemistry Product Research and Development* **1973**, *12*, 328-333.

80. I. M. Wienk, R. M. Boom, M. A. M. Beerlage, A. M. W. Bulte, C. A. Smolders and H. Strathmann; "Recent advances in the formation of phase inversion membranes made from amorphous or semi-crystalline polymers;" *Journal of Membrane Science* **1996**, *113*, 361-371.

81. J. G. Wijmans, H. J. J. Rutten and C. A. Smolders; "Phase separation phenomena in solutions of poly(2,6-dimethyl-1,4-phenyleneoxide) in mixtures of trichloroethylene, 1-octanol, and methanol: relationship to membrane formation;" *Journal of Polymer Science: Polymer Physics Edition* **1985**, *23*, 1941-1955.

82. T. H. Young, D. J. Lin, J. J. Gau, W. Y. Chuang and L. P. Cheng; "Morphology of crystalline nylon-610 membranes prepared by the immersion precipitation process: Competition between crystallization and liquid-liquid phase separation;" *Polymer* **1999**, *40*, 5011-5021.

83. H. Matsuyama, M. Teramoto, R. Nakatani and T. Maki; "Membrane formation via phase separation induced by penetration of nonsolvent from vapor phase. II. Membrane morphology;" *Journal of Applied Polymer Science* **1999**, *74*, 171-178.

84. H. Iwata and T. Matsuda; "Preparation and properties of novel environment-sensitive membranes prepared by graft polymerization onto a porous membrane;" *Journal of Membrane Science* **1988**, *38*, 185-199.

85. T. Kanamori, K. Sakai, M. Fukuda and Y. Yamashita; "Preferable structure of poly(ethylene glycol) for grafting onto a cellulosic membrane to increase hemocompatibility without reduction in solute permeability of the membrane;" *Journal of Applied Polymer Science* **1995**, *55*, 1601-1605.

86. H. Chen and G. Belfort; "Surface modification of poly(ether sulfone) ultrafiltration membranes by low-temperature plasma-induced graft polymerization;" *Journal of Applied Polymer Science* **1999**, *72*, 1699-1711.

87. J. Pieracci, J. V. Crivello and G. Belfort; "Photochemical modification of 10 kDa polyethersulfone ultrafiltration membranes for reduction of biofouling;" *Journal of Membrane Science* **1999**, *156*, 223-240.

88. F. F. Stengaard; "Preparation of asymmetric microfiltration membranes and modification of their properties by chemical treatment;" *Journal of Membrane Science* **1988**, *36*, 257-275.

89. P. W. Kramer, Y.-S. Yeh and H. Yasuda; "Low temperature plasma for the preparation of separation membranes;" *Journal of Membrane Science* **1989**, *46*, 1-28.

90. S. T. Kelly and A. L. Zydney; "Mechanisms for BSA fouling during microfiltration;" *Journal of Membrane Science* **1995**, *107*, 115-127.

91. L. E. S. Brink, S. J. G. Elbers, T. Robbertsen and P. Both; "The anti-fouling action of polymers preadsorbed on ultrafiltration and microfiltration membranes;" *Journal of Membrane Science* **1993**, *76*, 281-291.

92. J. M. Sheldon, I. M. Reed and C. R. Hawes; "The fine structure of ultrafiltration membranes. 2. Protein fouled membranes;" *Journal of Membrane Science* **1991**, *62*, 87-102.

93. K. J. Kim, A. G. Fane and C. J. D. Fell; "The performance of ultrafiltration membranes pretreated by polymers;" *Desalination* **1988**, *70*, 229-249.

94. V. Chen, A. G. Fane and C. J. D. Fell; "The use of anionic surfactants for reducing fouling of ultrafiltration membranes: Their effects and optimization;" *Journal of Membrane Science* **1992**, *67*, 249-261.

95. A. G. Fane, C. J. D. Fell and K. J. Kim; "The effect of surfactant pretreatment on the ultrafiltration of proteins;" *Desalination* **1985**, *53*, 37-55.

96. S. Belfer, Y. Purinson and O. Kedem; "Surface modification of commercial polyamide reverse osmosis membranes by radical grafting: An ATR-FTIR study;" *Acta Polymerica* **1998**, *49*, 574-582.

97. S. Belfer, Y. Purinson and O. Kedem; "Reducing fouling of RO membranes by redox-initiated graft polymerization;" *Desalination* **1998**, *119*, 189.

98. H. Iwata, I. Hirata and Y. Ikada; "Atomic force microscopic analysis of a porous membrane with pH-sensitive molecular valves;" *Macromolecules* **1998**, *31*, 3671-3678.

99. Y. Ito, Y. Ochiai, Y. S. Park and Y. Imanishi; "pH-sensitive gating by conformational change of a polypeptide brush grafted onto a porous polymer membrane;" *Journal of the American Chemical Society* **1997**, *119*, 1619-1623.

100. M. Ulbricht and G. Belfort; "Surface modification of ultrafiltration membranes by low temperature plasma. II. Graft polymerization onto polyacrylonitrile and polysulfone;" *Journal of Membrane Science* **1996**, *111*, 193-215.

101. S. Akhtar, C. Hawes, L. Dudley, I. Reed and P. Stratford; "Coatings reduce the fouling of microfiltration membranes;" *Journal of Membrane Science* **1995**, *107*, 209-218.

102. H. Iwata, M. I. Ivanchenko and Y. Miyaki; "Preparation of anti-oil stained membrane by grafting polyethylene glycol macromer onto polysulfone membrane;" *Journal of Applied Polymer Science* **1994**, *54*, 125-128.

103. V. Thom, M. Ulbricht and G. Jonsson; "Photochemical grafting of poly(ethylene glycol)s yielding low-protein-adsorbing UF membranes;" *Acta Polytechnica Scandinavica. Chemical Technology Series* **1997**, *247*, 35-50.

104. M. Ulbricht, H. Matuschewski, A. Oechel and H.-G. Hicke; "Photo-induced graft polymerization surface modifications for the preparation of hydrophilic low-protein-adsorbing ultrafiltration membranes;" *Journal of Membrane Science* **1996**, *115*, 31-47.

105. H. Yamagishi, J. V. Crivello and G. Belfort; "Evaluation of photochemically modified poly(arylsulfone) ultrafiltration membranes;" *Journal of Membrane Science* **1995**, *105*, 249-259.

106. S. Mok, D. J. Worsfold, A. Fouda and T. Matsuura; "Surface modification of polyethersulfone hollow-fiber membranes by γ-ray irradiation;" *Journal of Applied Polymer Science* **1994**, *51*, 193-199.

107. J. Hautojarvi, K. Kontturi, J. H. Nasman, B. L. Svarfvar, P. Viinikka and M. Vuoristo; "Characterization of graft-modified porous polymer membranes;" *Industrial and Engineering Chemistry Research* **1996**, *35*, 450-457.

108. G. Ellinghorst, A. Niemoller and D. Vierkotten; "Radiation initiated grafting of polymer films - An alternative technique to prepare membranes for various separation problems;" *Radiation Physics and Chemistry* **1983**, *22*, 635-642.

109. T. Peng and Y.-L. Cheng; "pH-responsive permeability of PE-g-PMAA membranes;" *Journal of Applied Polymer Science* **2000**, *76*, 778-786.

110. S. Munari, A. Bottino and G. Capannelli; "Casting and performance of polyvinylidene fluoride based membranes;" *Journal of Membrane Science* **1983**, *16*, 181-193.

111. A. Nabe, E. Staude and G. Belfort; "Surface modification of polysulfone ultrafiltration membranes and fouling by BSA solutions;" *Journal of Membrane Science* **1997**, *133*, 57-72.

112. M. Ulbricht and G. Belfort; "Surface modification of ultrafiltration membranes by low temperature plasma. I. Treatment of polyacrylonitrile;" *Journal of Applied Polymer Science* **1995**, *56*, 325-343.

113. Y. Ito, M. Inaba, D.-J. Chung and Y. Imanishi; "Control of water permeation by pH and ionic strength through a porous membrane having poly(carboxylic acid) surface-grafted;" *Macromolecules* **1992**, *25*, 7313-7316.

114. Y. Ito, S. Kotera, M. Inaba, K. Kono and Y. Imanishi; "Control of pore size of polycarbonate membrane with straight pores by poly(acrylic acid) grafts;" *Polymer* **1990**, *31*, 2157-2161.

115. Y. Okahata, H. Noguchi and T. Seki; "Functional capsule membranes. 26. Permeability control of polymer-grafted capsule membranes responding to ambient pH changes;" *Macromolecules* **1987**, *20*, 15-21.

116. Y. Osada, K. Honda and M. Ohta; "Control of water permeability by mechanochemical contraction of poly(methacrylic acid)-grafted membranes;" *Journal of Membrane Science* **1986**, *27*, 327-338.

117. Y. Okahata, K. Ozaki and T. Seki; "pH-Sensitive permeability control of polymer-grafted nylon capsule membranes;" *Journal of the Chemical Society, Chemical Communications* **1984**, 519-521.

118. R. Israels, D. Gersappe, M. Fasolka, V. A. Roberts and A. C. Balazs; "pH-controlled gating in polymer brushes;" *Macromolecules* **1994**, *27*, 6679-6682.

119. K. Ishihara, M. Kobayashi, N. Ishimaru and I. Shinohara; "Glucose induced permeation control of insulin through a complex membrane consisting of immobilized glucose oxidase and poly(amine);" *Polymer Journal* **1984**, *16*, 625-631.

120. Y. S. Park, Y. Ito and Y. Imanishi; "Photocontrolled gating by polymer brushes grafted on porous glass filter;" *Macromolecules* **1998**, *31*, 2606-2610.

121. Y. Okahata, H. Noguchi and T. Seki; "Functional capsule membranes. 23. Thermoselective permeation from a polymer-grafted capsule membrane;" *Macromolecules* **1986**, *19*, 493-494.

122. T. Uragami, Y. Naito and M. Sugihara; "Studies on synthesis and permeability of special polymer membranes. 39. Permeation characteristics and structure of polymer blend membranes from poly(vinylidene fluoride) and poly(ethylene glycol);" *Polymer Bulletin* **1981**, *4*, 617-622.

123. I. Cabasso, E. Klein and J. K. Smith; "Polysulfone hollow fibers. I. Spinning and properties;" *Journal of Applied Polymer Science* **1976**, *20*, 2377-2394.

124. T. A. Tweddle, O. Kutowy, W. L. Thayer and S. Sourirajan; "Polysulphone ultrafiltration membranes;" *Industrial and Engineering Chemistry Product Research and Development* **1983**, *22*, 320-326.

125. P. Aptel, N. Abidine, F. Ivaldi and J. P. LaFaille; "Polysulphone hollow fibers - Effect of spinning conditions on ultrafiltration properties;" *Journal of Membrane Science* **1985**, *22*, 199-215.

126. L. Y. Lafreniere, F. D. F. Talbot, T. Matsuura and S. Sourirajan; "Effect of poly(vinyl pyrrolidone) additive on the performance of polyethersulphone ultrafiltration membranes;" *Industrial and Engineering Chemistry Research* **1987**, *26*, 2385-2389.

127. R. M. Boom, T. Vandenboomgaard and C. A. Smolders; "Mass-transfer and thermodynamics during immersion precipitation for a 2-polymer system - Evaluation with the system PES-PVP-NMP-water;" *Journal of Membrane Science* **1994**, *90*, 231-249.

128. R. M. Boom, T. Vandenboomgaard and C. A. Smolders; "Equilibrium thermodynamics of a quaternary membrane-forming system with 2 polymers. 1. Calculations;" *Macromolecules* **1994**, *27*, 2034-2040.

129. R. M. Boom, H. W. Reinders, H. H. W. Rolevink, T. Vandenboomgaard and C. A. Smolders; "Equilibrium thermodynamics of a quaternary membrane-forming system with 2 polymers. 2. Experiments;" *Macromolecules* **1994**, *27*, 2041-2044.

130. I. M. Wienk, F. Scholtenhuis, T. Vandenboomgaard and C. A. Smolders; "Spinning of hollow-fiber ultrafiltration membranes from a polymer blend;" *Journal of Membrane Science* **1995**, *106*, 233-243.

131. S. P. Nunes and K.-V. Peinemann; "Ultrafiltration membranes from PVDF/PMMA blends;" *Journal of Membrane Science* **1992**, *73*, 25-35.

132. M. Morra, E. Occhiello and F. Garbassi; "Knowledge about polymer surfaces from contact angle measurements;" *Advances in Colloid and Interface Science* **1990**, *32*, 79-116.

133. A. M. Mayes, J. F. Hester and D. G. Walton; *Polymer Articles, Including Membranes, Having Hydrophilic Surfaces and Method for their Preparation*; International Patent Application No. PCT/US97/16488.

134. A. M. Mayes and S. K. Kumar; "Tailored polymer surfaces;" *MRS Bulletin* **1997**, *22*, 43-47.

135. F. Garbassi, M. Morra and E. Occhiello; "Bulk modifications;" *Polymer Surfaces: From Physics to Technology*; John Wiley & Sons: New York, 1994, pp 274-298.

136. D. T. Wu and G. H. Fredrickson; "Effect of architecture in the surface segregation of polymer blends;" *Macromolecules* **1996**, *29*, 7919-7930.

137. A. Yethiraj; "Entropic and enthalpic surface segregation from blends of branched and linear polymers;" *Physical Review Letters* **1995**, *74*, 2018-2021.

138. R. A. L. Jones, E. J. Kramer, M. H. Rafailovich, J. Sokolov and S. A. Schwartz; "Surface enrichment in an isotopic polymer blend;" *Physical Review Letters* **1989**, *62*, 280-283.

139. J. Sokolov, M. H. Rafailovich, R. A. L. Jones and E. J. Kramer; "Enrichment depth profiles in polymer blends measured by forward recoil spectrometry;" *Applied Physics Letters* **1989**, *54*, 590-592.

140. R. J. Composto, R. S. Stein, E. J. Kramer, R. A. L. Jones, A. Mansour, A. Karim and G. P. Felcher; "Surface enrichment in polymer blends - A neutron reflection test;" *Physica B* **1989**, *156*, 434-436.

141. R. A. L. Jones, L. J. Norton, E. J. Kramer, R. J. Composto, R. S. Stein, T. P. Russell, A. Mansour, A. Karim, G. P. Felcher, M. H. Rafailovich, J. Sokolov, X. Zhao and S. A. Schwarz; "The form of the enriched surface layer in polymer blends;" *Europhysics Letters* **1990**, *12*, 41-46.

142. A. Hariharan, S. K. Kumar and T. P. Russell; "Reversal of the isotopic effect in the surface behavior of binary polymer blends;" *Journal of Chemical Physics* **1993**, *98*, 4163-4173.

143. P. P. Hong, F. J. Boerio and S. D. Smith; "Surface segregation in blends of polystyrene and deuterated polystyrene;" *Macromolecules* **1993**, *26*, 1460-1464.

144. P. P. Hong, F. J. Boerio and S. D. Smith; "Effect of annealing time, film thickness, and molecular weight on surface enrichment in blends of polystyrene and deuterated polystyrene;" *Macromolecules* **1994**, *27*, 596-605.

145. R. A. L. Jones, L. J. Norton, E. J. Kramer, F. S. Bates and P. Wiltzius; "Surface-directed spinodal decomposition;" *Physical Review Letters* **1991**, *66*, 1326-1329.

146. L. J. Norton, E. J. Kramer, R. A. L. Jones, F. S. Bates, H. R. Brown, G. P. Felcher and R. Kleb; "Resonantly enhanced neutron intensity in a surface segregated polymer blend;" *Journal de Physique II* **1994**, *4*, 367-376.

147. D. H. K. Pan and W. M. Prest; "Surfaces of polymer blends - X-ray photoelectron spectroscopy studies of polystyrene/poly(vinylmethylether) blends;" *Journal of Applied Physics* **1985**, *58*, 2861-2870.

148. Q. S. Bhatia, D. H. Pan and J. T. Koberstein; "Preferential surface adsorption in miscible blends of polystyrene and poly(vinylmethylether);" *Macromolecules* **1988**, 2166-2175.

149. J. Israelachvili; *Intermolecular and surface forces*; Academic Press Limited: London, 1992.

150. D. N. Theodorou; "Microscopic structure and thermodynamic properties of bulk copolymers and surface-active polymers at interfaces. 2. Results for some representative chain architectures;" *Macromolecules* **1988**, *21*, 1422-1436.

151. R. G. Winkler, T. Matsuda and D. Y. Yoon; "Stochastic dynamics simulations of polymethylene melts confined between solid surfaces;" *Journal of Chemical Physics* **1993**, *98*, 729-736.

152. S. Affrossman, M. Hartshorne, R. Jerome, R. A. Pethrick, S. Petitjean and M. R. Vilar; "Surface concentration of chain ends in polystyrene determined by static secondary ion mass spectroscopy;" *Macromolecules* **1993**, *26*, 6251-6254.

153. D. T. Wu, G. H. Fredrickson, J.-P. Carton, A. Ajdari and L. Leibler; "Distribution of chain ends at the surface of a polymer melt: compensation effects and surface tension;" *Journal of Polymer Science. Part B: Polymer Physics* **1995**, *33*, 2373-2389.

154. A. Hariharan, S. K. Kumar and T. P. Russell; "A lattice model for the surface segregation of polymer chains due to molecular weight effects;" *Macromolecules* **1990**, *23*, 3584-3592.

245

155. I. Hopkinson, F. T. Kiff, R. W. Richards, S. Affrossman, M. Hartshorne, R. A. Pethrick, H. Munro and J. R. P. Webster; "Investigation of surface enrichment in isotopic mixtures of poly(methyl methacrylate);" *Macromolecules* **1995**, *28*, 627-635.

156. T. F. Schaub, G. J. Kellogg, A. M. Mayes, R. Kulasekere, J. F. Ankner and H. Kaiser; "Surface modification via chain end segregation in polymer blends;" *Macromolecules* **1996**, *29*, 3982-3990.

157. D. G. Walton and A. M. Mayes; "Entropically driven segregation in blends of branched and linear polymers;" *Physical Review E* **1996**, *54*, 2811-2815.

158. U. Steiner, J. Klein, E. Eiser, A. Budkowski and L. J. Fetters; "Complete wetting from polymer mixtures;" *Science* **1992**, *258*, 1126-1129.

159. D. G. Walton, P. P. Soo, A. M. Mayes, S. J. S. Allgor, J. T. Fujii, L. G. Griffith, J. F. Ankner, H. Kaiser, J. Johansson, G. D. Smith, J. G. Barker and S. K. Satija; "Creation of stable poly(ethylene oxide) surfaces on poly(methyl methacrylate) using blends of branched and linear polymers;" *Macromolecules* **1997**, *30*, 6947-6956.

160. W. Kauzmann; *Advances in Protein Chemistry* **1959**, *14*, 1-63.

161. C. Tanford; *The Hydrophobic Effect*; John Wiley & Sons: New York, 1980.

162. J. Israelachvili and H. Wennerstrom; "Role of hydration and water structure in biological and colloidal interactions;" *Nature* **1996**, *379*, 219-225.

163. S. Wu; *Polymer Interface and Adhesion*; Marcel Dekker: New York, 1982.

164. R. A. L. Jones and E. J. Kramer; "The surface composition of miscible polymer blends;" *Polymer* **1993**, *34*, 115-118.

165. R. L. Schmitt, J. A. Gardella, Jr. and L. Salvati, Jr.; "Studies of surface composition and morphology in polymers. 2. Bisphenol-A polycarbonate and poly(dimethylsiloxane) blends;" *Macromolecules* **1986**, *19*, 648-651.

166. M. J. Owen and T. C. Kendrick; "Surface activity of polystyrene-polysiloxane-polystyrene ABA block copolymers;" *Macromolecules* **1970**, *3*, 458-461.

167. I. Yilgor and J. E. McGrath; "Polysiloxane containing polymers - A survey of recent developments;" *Advances in Polymer Science* **1988**, *86*, 1-86.

168. M. M. Coleman and J. Zarian; "Fourier-transform infrared studies of polymer blends. II. Poly(ε-caprolactone)-poly(vinyl chloride) system;" *Journal of Polymer Science, Polymer Physics Edition* **1979**, *17*, 837-850.

169. M. B. Clark, Jr., C. A. Burkhardt and J. A. Gardella, Jr.; "Surface studies of polymer blends. 3. An ESCA, IR, and DSC study of poly(epsilon-caprolactone) poly(vinyl chloride) homopolymer blends;" *Macromolecules* **1989**, *22*, 4495-4501.

170. G. Teyssedre, A. Bernes and C. Lacabanne; "Influence of the crystalline phase on the molecular mobility of PVDF;" *Journal of Polymer Science. Part B - Polymer Physics* **1993**, *31*, 2027-2034.

171. P. J. Flory; *Principles of Polymer Chemistry*; Cornell University Press: Ithaca, NY, 1953.

172. S. Zalipsky and J. M. Harris; "Introduction to chemistry and biological applications of poly(ethylene glycol);" *Poly(ethylene glycol): Chemistry and Biological Applications*; J. M. Harris and S. Zalipsky, Ed.; American Chemical Society: Washington, D.C., 1997, pp 1-13.

173. D. L. Elbert and J. A. Hubbell; "Surface treatments of polymers for biocompatibility;" *Annual Review of Materials Science* **1996**, *26*, 365-394.

174. S. W. Kim; "Nonthrombogenic treatments and strategies;" *Biomaterials Science: An Introduction to Materials in Medicine*; B. D. Ratner, A. S. Hoffman, F. J. Schoen and J. E. Lemons, Ed.; Academic Press: San Diego, CA, 1996, pp 297-308.

175. J. M. Harris; "Introduction to biotechnical and biomedical applications of poly(ethylene glycol);" *Poly(ethylene glycol) Chemistry: Biotechnical and Biomedical Applications*; J. M. Harris, Ed.; Plenum Press: New York, 1992, pp 1-14.

176. W. R. Gombotz, W. Guanghui, T. A. Horbett and A. S. Hoffman; "Protein adsorption to poly(ethylene oxide) surfaces;" *Journal of Biomedical Materials Research* **1991**, *25*, 1547-1562.

177. S. I. Jeon, J. H. Lee, J. D. Andrade and P. G. de Gennes; "Protein-surface interactions in the presence of polyethylene oxide;" *Journal of Colloid and Interface Science* **1991**, *142*, 149-166.

178. J. H. Lee, H. B. Lee and J. D. Andrade; "Blood compatibility of polyethylene oxide surfaces;" *Progress in Polymer Science* **1995**, *20*, 1043-1079.

179. R. Kjellander and E. Florin; "Water structure and changes in thermal stability of the system poly(ethylene oxide)-water;" *Journal of the Chemical Society - Faraday Transactions I* **1981**, *77*, 2053-2077.

180. D. J. Irvine, A. M. Mayes, S. K. Satija, J. G. Barker, S. J. Sofia-Allgor and L. G. Griffith; "Comparison of tethered star and linear poly(ethylene oxide) for control of biomaterials surface properties;" *Journal of Biomedical Materials Research* **1998**, *40*, 498-509.

181. R. E. Bernstein, C. A. Cruz, D. R. Paul and J. W. Barlow; "LCST behavior in polymer blends;" *Macromolecules* **1977**, *10*, 681-686.

182. H. Tomura, H. Saito and T. Inoue; "Light scattering analysis of upper critical solution temperature behavior in a poly(vinylidene fluoride)/poly(methyl methacrylate) blend;" *Macromolecules* **1992**, *25*, 1611-1614.

183. B. R. Hahn, O. Herrmann-Schonherr and J. H. Wendorff; "Evidence for a crystal-amorphous interphase in PVDF and PVDF/PMMA blends;" *Polymer* **1987**, *28*, 201-208.

184. W. Ullmann and J. H. Wendorff; "Mechanical properties of blends of poly(methyl methacrylate) and poly(vinylidene fluoride);" *Composites Science and Technology* **1985**, *23*, 97-112.

185. P. Banerjee, D. J. Irvine, A. M. Mayes and L. G. Griffith; "Polymer latexes for cell-resistant and cell-interactive surfaces;" *Journal of Biomedical Materials Research* **2000**, *50*, 331-339.

186. D. J. Irvine; *Spatially Controlled Presentation of Biochemical Ligands on Biomaterial Surfaces Using Comb Polymers*, Ph.D. Thesis, Massachusetts Institute of Technology. 2000.

187. G. Odian; "Ionic chain polymerization;" *Principles of Polymerization*; John Wiley & Sons, Inc.: New York, 1991, pp 356-451.

188. A. G. Shard, M. C. Davies, S. J. B. Tendler, C. V. Nicholas, M. D. Purbrick and J. F. Watts; "Surface characterization of methyl methacrylate-poly(ethylene glycol) methacrylate copolymers by secondary ion mass spectrometry and X-ray photoelectron spectroscopy;" *Macromolecules* **1995**, *28*, 7855-7b59.

189. Q.-T. Pham, R. Petiaud, M.-F. Llauro and H. Waton; *Proton and Carbon NMR Spectra of Polymers*; John Wiley & Sons: Chichester, U.K., 1984; Vol. 3, pp 478-479.

190. Q.-T. Pham and R. Petiaud; *Proton and Carbon NMR Spectra of Polymers*; Editions SCM: Paris, 1980; Vol. 1, pp 138-139.

191. H. E. Gottlieb, V. Kotlyar and A. Nudelman; "NMR chemical shifts of common laboratory solvents as trace impurities;" *Journal of Organic Chemistry* **1997**, *62*, 7512-7515.

192. J.-S. Wang and K. Matyjaszewski; "Controlled/'living' radical polymerization. Atom transfer radical polymerization in the presence of transition-metal complexes;" *Journal of the American Chemical Society* **1995**, *117*, 5614-5615.

193. M. Sawamoto and M. Kamigaito; "Living radical polymerization based on transition metal complexes;" *Trends in polymer science* **1996**, *4*, 371-377.

194. K. Matyjaszewski and T. Grimaud; "Controlled/'living' radical polymerization of methyl methacrylate by atom transfer radical polymerization;" *Macromolecules* **1997**, *30*, 2216-2218.

195. T. E. Patten and K. Matyjaszewski; "Atom transfer radical polymerization and the synthesis of polymeric materials;" *Advanced Materials* **1998**, *10*, 901-915.

196. X.-S. Wang, N. Luo and S.-K. Ying; "Synthesis of EPDM-g-PMMA through atom transfer radical polymerization;" *Polymer* **1999**, *40*, 4515-4520.

197. G. Odian; "Radical chain polymerization;" *Principles of Polymerization*; John Wiley & Sons, Inc.: New York, 1991, pp 198-334.

198. K. L. Beers, S. G. Gaynor and K. Matyjaszewski; "The synthesis of densely grafted copolymers by atom transfer radical polymerization;" *Macromolecules* **1998**, *31*, 9413-9415.

199. H.-J. Paik, S. G. Gaynor and K. Matyjaszewski; "Synthesis and characterization of graft copolymers of poly(vinyl chloride) with styrene and (meth)acrylates by atom transfer radical polymerization;" *Macromolecular Rapid Communications* **1998**, *19*, 47-52.

200. J. F. Hester, P. Banerjee, A. Akthakul, R. A. Mickiewicz and A. M. Mayes; "Amphiphilic graft copolymers based on commercial halogenated polymers;" *Macromolecules, In submission.*

201. P. Banerjee, J. F. Hester, A. Akthakul and A. M. Mayes; *Graft Copolymers, Methods for Grafting Vinyl Species, Including Hydrophilic Species, Onto Halogenated Polymers, and Articles Thereof*; Provisional US Patent Application.

202. G. X. Xu and S. G. Lin; "Functional modification of polypropylene;" *Journal of Macromolecular Science - Reviews in Macromolecular Chemistry and Physics* **1994**, *C34*, 555-606.

203. A. K. Mukherjee and B. D. Gupta; "Graft co-polymerization of vinyl monomers onto polypropylene;" *Journal of Macromolecular Science - Chemistry* **1983**, *A19*, 1069-1099.

204. Q.-T. Pham, R. Petiaud, M.-F. Llauro and H. Waton; *Proton and Carbon NMR Spectra of Polymers*; John Wiley & Sons: Chichester, U.K., 1984; Vol. 3, pp 674-675.

205. F. W. Billmeyer, Jr.; *Textbook of Polymer Science*; John Wiley & Sons: New York, 1984.

206. J. Brandrup, E. H. Immergut, E. A. Grulke and Ed.; *Polymer Handbook*; John Wiley & Sons: New York, 1999.

207. L. C. Sawyer and D. T. Grubb; *Polymer Microscopy*; Chapman and Hall: London, 1987.

208. M. Xenidou, F. L. Beyer, N. Hadjichristidis, S. P. Gido and N. B. Tan; "Morphology of model graft copolymers with randomly placed trifunctional and tetrafunctional branch points;" *Macromolecules* **1998**, *31*, 7659-7667.

209. F. L. Beyer, S. P. Gido, C. Buschl, H. Iatrou, D. Uhrig, J. W. Mays, M. Y. Chang, B. A. Garetz, N. P. Balsara, N. B. Tan and N. Hadjichristidis; "Graft copolymers with regularly spaced, tetrafunctional branch points: Morphology and grain structure;" *Macromolecules* **2000**, *33*, 2039-2048.

210. M. Baumert, J. Heinemann, R. Thomann and R. Mulhaupt; "Highly branched polyethylene graft copolymers prepared by means of migratory insertion polymerization combined with TEMPO-mediated controlled radical polymerization;" *Macromolecular Rapid Communications* **2000**, *21*, 271-276.

211. K. Matyjaszewski, T. Pintauer and S. Gaynor; "Removal of copper-based catalyst in atom transfer radical polymerization using ion exchange resins;" *Macromolecules* **2000**, *33*, 1476-1478.

212. D. M. Haddleton, D. J. Duncalf, D. Kukulj and A. P. Radigue; "3-Aminopropyl silica supported living radical polymerization of methyl methacrylate: Dichlorotris(triphenylphosphine)ruthenium(II) mediated atom transfer polymerization;" *Macromolecules* **1999**, *32*, 4769-4775.

213. G. Kickelbick, H.-J. Paik. and K. Matyjaszewski; "Immobilization of the copper catalyst in atom transfer radical polymerization;" *Macromolecules* **1999**, *32*, 2941-2947.

214. S. Liou, J. T. Rademacher, D. Malaba, M. E. Pallack and W. J. Brittain; "Atom transfer radical polymerization of methyl methacrylate with polyethylene-functionalized ligands;" *Macromolecules* **2000**, *33*, 4295-4296.

215. T. E. Long, R. D. Allen and J. E. McGrath; "Synthesis and characterization of block copolymers containing acid and ionomeric functionalities;" *Chemical Reactions on Polymers*; J. L. Benham and J. F. Kinstle, Ed.; American Chemical Society: Washington, D.C., 1988, pp 258-275.

216. S. K. Kwon, W. J. Choi, Y. H. Kim and S. K. Choi; "Synthesis of amphiphilic poly(alkyl methacrylate-b-methacrylic acid) by group transfer polymerization and selective hydrolysis;" *Bulletin of the Korean Chemical Society* **1992**, *13*, 479-482.

217. A. Shefer, A. J. Grodzinsky, K. L. Prime and J. P. Busnel; "Free-radical telomerization of tert-butyl acrylate in the presence of bis(4-aminophenyl) disulfide as a useful route to amino-terminated telomers of poly(acrilic acid);" *Macromolecules* **1993**, *26*, 2240-2245.

218. S. P. Rannard, N. C. Billingham, S. P. Armes and J. Mykytiuk; "Synthesis of monodisperse block copolymers containing methacrylic acid segments by group-transfer polymerization: Choice of protecting group and catalyst;" *European Polymer Journal* **1993**, *29*, 407-414.

219. M. Kubo, W. C. Mollberg, A. B. Padias and H. K. Hall, Jr.; "Solubilization of peptides in water and hexane - Synthesis of peptide-terminated poly(tert-butyl acrylate) and poly(acrilic acid) via living anionic polymerization;" *Macromolecules* **1995**, *28*, 838-843.

220. W. D. Benzinger and D. N. Robinson; *Porous Polyvinylidene Fluoride Polymer Membrane and Process for Its Preparation*; US Patent #4,384,047 (1983).

221. E. Desimoni and P. G. Zambonin; "Spectroscopies for surface characterization;" *Surface Characterization of Advanced Polymers*; L. Sabbatini and P. G. Zambonin, Ed.; VCH Publishers, Inc.: New York, 1993, pp 1-45.

222. M. P. Seah and D. Briggs; "A perspective on the analysis of surfaces and interfaces;" *Practical Surface Analysis by Auger and X-ray Photoelectron Spectroscopy*; D. Briggs and M. P. Seah, Ed.; John Wiley & Sons: New York, 1983, pp 1-15.

223. A. F. Orchard; "Basic principles of photoelectron spectroscopy;" *Handbook of X-ray and Ultraviolet Photoelectron Spectroscopy*; D. Briggs, Ed.; Heyden & Son Ltd.: Suffolk, U.K., 1977, pp 1-78.

224. D. Briggs; *Surface Analysis of Polymers by XPS and Static SIMS*; Cambridge University Press: Cambridge, U.K., 1998.

225. B. Beamson and D. Briggs; *High-Resolution XPS of Organic Polymers: The Scienta ESCA300 Database*; John Wiley & Sons: Chichester, U.K., 1992.

226. D. T. Clark; "ESCA applied to organic and polymeric systems;" *Handbook of X-ray and Ultraviolet Photoelectron Spectroscopy*; D. Briggs, Ed.; Heyden & Son Ltd.: Suffolk, U.K., 1977, pp 211-248.

227. J. C. Russ; "Discrimination and thresholding;" *Computer-Assisted Microscopy: The Measurement and Analysis of Images*; Plenum Press: New York, 1990, pp 99-128.

228. J. C. Russ; "Image processing;" *Computer-Assisted Microscopy: The Measurement and Analysis of Images*; Plenum Press: New York, 1990, pp 33-69.

229. J. C. Russ; "Segmentation of edges and lines;" *Computer-Assisted Microscopy: The Measurement and Analysis of Images*; Plenum Press: New York, 1990, pp 71-98.

230. Media Cybernetics; *Image-Pro Plus Version 1.3 for Windows: Reference Guide*; Media Cybernetics, L.P.: Silver Spring, MD, 1994, pp 1-25.

231. T. H. Meltzer; *Filtration in the Pharmaceutical Industry*; Marcel Dekker: New York, 1987.

232. D. E. Garfin and G. Bers; "Basic aspects of protein blotting;" *Protein Blotting: Methodology, Research and Diagnostic Applications*; B. A. Baldo, E. R. Tovey and N. S. W. St. Leonards, Ed.; Karger: Basel, 1989, pp 5-42.

233. J. H. Scofield; "Hartree-Slater subshell photoionization cross-sections at 1254 and 1487 eV;" *Journal of Electron Spectroscopy and Related Phenomena* **1976**, *8*, 129-137.

234. I. Elliott, C. Doyle and J. D. Andrade; "Calculated core-level sensitivity factors for quantitative XPS using an HP5950B spectrometer;" *Journal of Electron Spectroscopy and Related Phenomena* **1983**, *28*, 303-316.

235. J.-B. Lhoest, E. Detrait, P. van den Bosch de Aguilar and P. Bertrand; "Fibronectin adsorption, conformation, and orientation on polystyrene substrates studied by radiolabeling, XPS, and ToF SIMS;" *Journal of Biomedical Materials Research* **1998**, *41*, 95-103.

236. M. Moeremans, G. Daneels and J. DeMey; "Sensitive colloidal metal (gold or silver) staining of protein blots on nitrocellulose membranes;" *Analytical Biochemistry* **1985**, *145*, 315-321.

237. R. Wiesendanger; *Scanning Probe Microscopy and Spectroscopy: Methods and Applications*; Cambridge University Press: Cambridge, 1994.

238. J. P. Cleveland, S. Manne, D. Bocek and P. K. Hansma; "A nondestructive method for determining the spring constant of cantilevers for scanning force microscopy;" *Review of Scientific Instruments* **1993**, *64*, 403-405.

239. S. Biggs; "Non-equilibrium interaction forces between adsorbed polymer layers;" *Journal of the Chemical Society, Faraday Transactions* **1996**, *92*, 2783-2790.

240. W. A. Ducker, T. J. Senden and R. M. Pashley; "Measurement of forces in liquids using a force microscope;" *Langmuir* **1992**, *8*, 1831-1836.

241. J. T. Stewart, J. R. Lang and I. L. Honigberg; "Flow injection analysis of carboxylic acid drugs using cationic dyes and on-line ion-pair extraction;" *Journal of Liquid Chromatography* **1988**, *11*, 3353-3373.

242. R. D. Haugland; *Handbook of Fluorescent Probes and Research Chemicals*; Molecular Probes, Inc.: Eugene, OR, 1996.

243. D. W. van Krevelen; *Properties of Polymers: Their Correlation with Chemical Structure, Their Numerical Estimation and Prediction from Group Contributions*; Elsevier: New York, 1990.

244. P.-G. de Gennes; *Scaling Concepts in Polymer Physics*; Cornell University Press: Ithaca, NY, 1979.

245. M. A. Frommer, R. Matz and U. Rosenthal; "Mechanism of formation of reverse osmosis membranes;" *Industrial and Engineering Chemistry Product Research and Development* **1971**, *10*, 193-196.

246. F. E. Bailey, Jr. and J. V. Koleske; "Configuration and hydrodynamic properties of the polyoxyethylene chain in solution;" *Nonionic Surfactants*; M. J. Schick, Ed.; Marcel Dekker, Inc.: New York, 1967, pp 794-822.

247. D. H. Napper; "Steric stabilization and the Hofmeister series;" *Journal of Colloid and Interface Science* **1970**, *33*, 384-392.

248. E. A. Boucher and P. M. Hines; "Effects of inorganic salts on the properties of aqueous poly(ethylene oxide) solutions;" *Journal of Polymer Science. Polymer Physics Edition* **1976**, *14*, 2241-2251.

249. P. Molyneux; *Water-Soluble Synthetic Polymers: Properties and Behavior*; CRC Press, Inc.: Boca Raton, FL, 1984; Vol. 2.

250. S. Saeki, N. Kuwahara, M. Nakata and M. Kaneko; "Upper and lower critical solution temperatures in poly(ethylene glycol) solutions;" *Polymer* **1976**, *17*, 685-689.

251. G. Karlstrom; "A new model for upper and lower critical solution temperatures in poly(ethylene oxide) solutions;" *Journal of Physical Chemistry* **1985**, *89*, 4962-4964.

252. L. Broens, F. W. Altena, C. A. Smolders and D. M. Koenhen; "Asymmetric membrane formation as a result of phase separation phenomena;" *Desalination* **1980**, *32*, 33-45.

253. J. J. van Aartsen; "Theoretical observations on spinodal decomposition of polymer solutions;" *European Polymer Journal* **1970**, *6*, 919-924.

254. C. A. Smolders, J. J. van Aartsen and A. Steenbergen; "Liquid-liquid phase separation in concentrated solutions of non-crystallizable polymers by spinodal decomposition;" *Kolloid-Zeitschrift & Zeitschrift fur Polymere* **1971**, *243*, 14-20.

255. T. Peters, Jr.; "Serum albumin;" *Advances in Protein Chemistry*; C. B. Anfinsen, J. T. Edsall and F. M. Richards, Ed.; Academic Press, Inc.: New York, 1985; Vol. 37, pp 161-245.

256. K. P. Antonsen and A. S. Hoffman; "Water structure of PEG solutions by differential scanning calorimetry measurements;" *Poly(ethylene glycol) Chemistry: Biotechnical and Biomedical Applications*; J. M. Harris, Ed.; Plenum Press: New York, 1992, pp 15-28.

257. V. Hlady, R. A. Van Wagenen and J. D. Andrade; "Total internal reflection intrinsic fluorescence (TIRIF) spectroscopy applied to protein adsorption;" *Surface and Interfacial Aspects of Biomedical Polymers*; J. D. Andrade, Ed.; Plenum Press: New York, 1985; Vol. 2, pp 81-119.

258. H. J. Griesser and G. F. Meijs; *Journal of Bioactive and Compatible Polymers* **1990**, *5*, 179-193.

259. K. Nakamae; "Polymeric materials for oculistics;" *Biomedical Applications of Polymeric Materials*; T. Tsuruta, T. Hayashi, K. Kataoka, K. Ishihara and Y. Kimura, Ed.; CRC Press: Boca Raton, FL, 1993, pp 257-272.

260. S. A. Liberman, A. S. Gomes and E. M. Macchi; "Compatibility in poly(ethylene oxide)-poly(methyl methacrylate) blends;" *Journal of Polymer Science: Polymer Chemistry Edition* **1984**, *22*, 2809-2815.

261. E. Martuscelli, M. Pracella and W. P. Yue; "Influence of composition and molecular mass on the morphology, crystallization and melting behavior of poly(ethylene oxide)/poly(methyl methacrylate) blends;" *Polymer* **1984**, *25*, 1097-1106.

262. G. C. Alfonso and T. P. Russell; "Kinetics of crystallization in semicrystalline/amorphous polymer mixtures;" *Macromolecules* **1986**, *19*, 1143-1152.

263. H. Ito, T. P. Russell and G. D. Wignall; "Interactions in mixtures of poly(ethylene oxide) and poly(methyl methacrylate);" *Macromolecules* **1987**, *20*, 2213-2220.

264. A. Brunacci, J. Yin, E. Pedemonte and A. Turturro; "A study on polymer-polymer interactions through mixing calorimetry;" *Thermochimica Acta* **1993**, *227*, 117-124.

265. J. A. Pomposo, R. de Juana, A. Mugica, M. Cortazar and M. A. Gomez; "Binary poly(ethylene oxide)/poly(methyl methacrylate-co-ethyl methacrylate) blends: Miscibility predictions from model compound mixtures vs. experimental phase behavior;" *Macromolecules* **1996**, *29*, 7038-7046.

266. E. Pedemonte and G. Burgisi; "Thermodynamics of poly(ethylene oxide)-poly(methyl acrylate) blends: Prediction of miscibility based on the Prigogine-Flory theory;" *Polymer* **1994**, *25*, 3719-3721.

267. R. W. Novak; "Acrylic ester polymers;" *Kirk-Othmer Encyclopedia of Chemical Technology*; J. I. Kroschwitz and M. Howe-Grant, Ed.; John Wiley & Sons: New York, 1991; Vol. 1, pp 314-343.

268. D. J. Tritton; *Physical Fluid Dynamics*; Clarenden Press: Oxford, 1988.

269. *Plastics News* **2000**, *12 (July 20)*, 83.

270. K. Ito, N. Usami and Y. Yamashita; "Synthesis of methyl methacrylate-stearyl methacrylate graft copolymers and characterization by inverse gas chromatography;" *Macromolecules* **1980**, *13*, 216-221.

271. D. J. Walbridge; "The design and synthesis of dispersants for dispersion polymerization in organic media;" *Dispersion Polymerization in Organic Media*; K. E. J. Barrett, Ed.; John Wiley & Sons: London, U.K., 1975, pp 45-114.

272. A. Sugii, N. Ogawa and H. Hashizume; "Preparation and properties of macroreticular resins containing thiazole and thiazoline groups;" *Talanta* **1980**, *27*, 627-631.

273. G. M. Loudon; *Organic Chemistry*; The Benjamin/Cummings Publishing Company: Menlo Park, CA, 1995.

274. M. K. Sreedhar and T. S. Anirudhan; "Preparation of an adsorbent by graft polymerization of acrylamide onto coconut husk for mercury(II) removal from

aqueous solution and chloralkali industry wastewater;" *Journal of Applied Polymer Science* **2000**, *75*, 1261-1269.

275. S. M. Wilhelm; "Generation and disposal of petroleum processing waste that contains mercury;" *Environmental Progress* **1999**, *18*, 130-143.

276. R. N. Yong, A. M. O. Mohamed and B. P. Warkentin; *Principles of Contaminant Transport in Soils*; Elsevier: New York, 1992.

277. D. Porcella; "Mercury in the environment: Biogeochemistry;" *Mercury Pollution, Integration and Synthesis*; C. Watras and J. Huckabee, Ed.; Lewis Publishers: Boca Raton, FL, 1994, pp 3-19.

278. H. von Canstein, Y. Li, K. N. Timmis, W.-D. Deckwer and I. Wagner-Dobler; "Removal of mercury from chloralkali electrolysis wastewater by a mercury-resistant Pseudomonas Putida strain;" *Applied and Environmental Microbiology* **1999**, *65*, 5279-5284.

279. K. Selvaraj, V. Chandramohan and S. Pattabhi; "Removal of Hg(II) from aqueous solution and chlor-alkali industry wastewater using photofilm waste sludge;" *Journal of Scientific & Industrial Research* **1998**, *57*, 271-278.

280. D. J. Irvine, A. M. Mayes and L. G. Griffith; "Nanoscale clustering of RGD peptides at surfaces using comb polymers. 1. Synthesis and characterization of comb thin films;" *Biomacromolecules, In submission.*

281. L. Zeman and G. Tkacik; "Pore volume distribution in ultrafiltration membranes;" *Materials Science of Synthetic Membranes*; D. R. Lloyd, Ed.; American Chemical Society: Washington, D.C., 1985, pp 339-350.

282. M. Ulbricht and A. Papra; "Polyacrylonitrile enzyme ultrafiltration membranes prepared by adsorption, cross-linking, and covalent binding;" *Enzyme and Microbial Technology* **1997**, *20*, 61-68.

283. M. Ulbricht and H.-G. Hicke; "Photomodifizierung von ultrafiltrationsmembranen, 1. Photochemische modifizierungen von polyacrylnitril-ultrafiltrationsmembranen mit arylaziden;" *Die Angewandte Makromolekulare Chemie* **1993**, *210*, 69-95.

284. Y. Uludag, H. O. Ozbelge and L. Yilmaz; "Removal of mercury from aqueous solutions via polymer-enhanced ultrafiltration;" *Journal of Membrane Science* **1997**, *129*, 93-99.

285. J. Muslehiddinoglu, Y. Uludag, H. O. Ozbelge and L. Yilmaz; "Effect of operating parameters on selective separation of heavy metals from binary mixtures via polymer enhanced ultrafiltration;" *Journal of Membrane Science* **1998**, *140*, 251-266.

286. J. Muslehiddinoglu, Y. Uludag, H. O. Ozbelge and L. Yilmaz; "Determination of heavy metal concentration in feed and permeate streams of polymer enhanced ultrafiltration process;" *Talanta* **1998**, *46*, 1557-1565.

287. A. M. Mayes, D. J. Irvine and L. G. Griffith; "Tailoring polymer surfaces for controlled cell behavior;" *Materials Research Society Symposia Proceedings, Vol. 530*; Materials Research Society, 1998, pp 73-84.

288. L. Lien; "Using membrane technology to minimize wastewater;" *Pollution Engineering* **1998**, *May*, 44-47.

289. D. Briggs; "Applications of XPS in polymer technology;" *Practical Surface Analysis*; D. Briggs and M. P. Seah, Ed.; John Wiley & Sons: Chichester, U.K., 1983, pp 359-396.

290. C. J. Jalbert, J. T. Koberstein, R. Balaji and Q. Bhatia; "Surface depletion of end groups in amine-terminated poly(dimethylsiloxane);" *Macromolecules* **1994**, *27*, 2409-2413.

291. D. T. Clark and H. R. Thomas; "Application of ESCA to polymer chemistry. XVI. Electron mean free paths as a function of kinetic energy in polymeric films determined by means of ESCA;" *Journal of Polymer Science. Polymer Chemistry Edition* **1977**, *15*, 2843-2867.

292. R. F. Roberts, D. L. Allara, C. A. Pryde, D. N. E. Buchanan and N. D. Hobbins; "Mean free path for inelastic scattering of 1.2 keV electrons in thin poly(methylmethacrylate) films;" *Surface and Interface Analysis* **1980**, *2*, 5.

293. D. Briggs; "X-ray photoelectron spectroscopy as an analytical technique;" *Handbook of X-ray and Ultraviolet Photoelectron Spectroscopy*; D. Briggs, Ed.; Heyden & Son Ltd.: Suffolk, U.K., 1977, pp 153-182.

294. S. H. Anastasiadis and T. P. Russell; "The morphology of symmetric diblock copolymers as revealed by neutron reflectivity;" *Journal of Chemical Physics* **1990**, *92*, 5677-5691.

295. T. P. Russell; "X-ray and neutron reflectivity for the investigation of polymers;" *Materials Science Reports* **1990**, *5*, 171-271.

296. W. H. Press, S. A. Teukolsky, W. T. Vetterling and B. P. Flannery; *Numerical Recipes in Fortran 77*; Cambridge University Press: Cambridge, 1992.

Appendix A. Review of Quantitative Literature on Surface Modification for Fouling Resistance

The following table is a quantitative review of key performance metrics from literature in which surface modification was performed on polymer membranes for the purpose of enhancing their fouling resistance. In each case, filtration tests were undertaken to compare the fouling resistance of the modified membrane to that of an unmodified control. These tests generally involved measurement of the trans-membrane flux of pure water, followed by measurement of the trans-membrane flux of a foulant solution after a fixed period of foulant solution filtration. This table summarizes the surface modification methods used, the filtration experiments performed, and the key results in terms of trans-membrane flux metrics discussed in Section 2.4.1. For comments on the information and abbreviations, see Section 2.4.1 and the notes at the end of the table.

Table A.1 Key Results of Past Fouling Studies on Surface-Modified Membranes

Ref.	Control Membrane[a]	Modification[b]	Foulant[c]	End Criterion[d]	J_f^C/J_o^C [†]	J_f^M/J_o^M [††]	J_o^M/J_o^C [‡]	J_f^M/J_f^C [‡‡]
87	PES	gr N-vinyl-2-pyrrolidinone	10 g/L BSA	10 mL of permeate collected	0.40	0.54	0.94	1.28
87	PES	gr N-vinylformamide	10 g/L BSA	10 mL of permeate collected	0.40	0.54	0.84	1.16
87	PES	gr N-vinylcaprolactam	10 g/L BSA	10 mL of permeate collected	0.40	0.50	1.21	1.53
86	PES	gr N-vinyl-2-pyrrolidinone	10 g/L BSA	10 mL of permeate collected	0.32	0.52	1.47	2.48
100	PSf	gr 2-hydroxyethyl methacrylate	1 g/L BSA	25 mL of permeate collected	0.29	0.27	1.41	1.32
100	PSf	gr 2-hydroxyethyl methacrylate	1 g/L LYS	25 mL of permeate collected	0.23	0.33	1.41	2.00
104	PAN	gr polyoxyethylene methacrylate	1.0 g/L BSA	30-min static exposure to foulant solution, followed by flux measurement	0.08	0.52	0.08	0.51
104	PAN	gr polyoxyethylene methacrylate	1.0 g/L CyC	30-min static exposure	0.06	0.66	0.08	0.90

Ref.	Control Membrane[a]	Modification[b]	Foulant[c]	End Criterion[d]	J_f^C/J_o^C [†]	J_f^M/J_o^M [††]	J_o^M/J_o^C [‡]	J_f^M/J_f^C [‡‡]
104	PAN	gr polyoxyethylene methacrylate	1.0 g/L BγGl	30-min static exposure	0.06	0.48	0.08	0.71
105	PAS	gr 2-hydroxyethyl methacrylate	1.0 g/L BSA	3-h duration	0.54	0.47	1.68	1.45
106	PES	gr poly(ethylene glycol)	500 ppm PSA	20-h duration	~0.27	~0.61	0.55	~1.22
88	PVDF	gr proprietary hydrophilic polymers/monomers	Skim milk	1-h duration	-	-	-	~3
102	PSf	gr polyoxyethylene diacrylate	0.3% olive oil	24-h static exposure to foulant solution, followed by 5-min flux measurement	"0"	~0.41	-	-
108	PVDF	gr N-vinyl pyrrolidone	Pure water only	Immediate measurement of water flux	-	-	~4	-
45	PVDF	ct polyether-b-polyamide copolymer	6 wt % oil	100 mL of permeate collected	<0.007	0.44	0.11	>7.0
91	PSf	ads poly(vinyl methylether)	1 g/L β-LG	2-h duration	~0.10	~0.34	~0.31	~1.05
91	PSf	ads methylcellulose	1 g/L β-LG	2-h duration	~0.08	~0.36	~0.30	~1.35
94	PSf	ads sodium di-2-ethylhexyl sulfosuccinate nonionic surfactant	1 g/L BSA	6-h duration	-	-	0.90	1.17
93	PSf	ads methylcellulose	1 g/L BSA	24-h duration	0.03	0.18	0.23	1.40
93	PSf	ads polyvinylalcohol	1 g/L BSA	24-h duration	0.03	0.33	0.10	1.21
93	PSf	ads polyvinylpyrrolidone	1 g/L BSA	24-h duration	0.03	0.09	0.36	1.20
93	PSf	ads nonyl phenol polyethoxylate nonionic surfactant	1 g/L BSA	24-h duration	0.03	0.07	0.53	1.37
95	PAm	ads nonyl phenol polyethoxylate nonionic surfactant	1 g/L BSA	3-h duration	-	-	-	1.38

Ref.	Control Membrane[a]	Modification[b]	Foulant[c]	End Criterion[d]	J_f^C/J_o^C [†]	J_f^M/J_o^M [††]	J_o^M/J_o^C [‡]	J_f^M/J_f^C [‡‡]
95	P(AN-co-VC)	ads nonyl phenol polyethoxylate nonionic surfactant	1 g/L BSA	3-h duration	-	-	-	1.20
131	PVDF	bl with 9.5 wt % poly(methyl methacrylate)	Pure water only	Immediate measurement of water flux	-	-	80.8	-
86	PES	Plasma treatment to create peroxide groups on surface	10 g/L BSA	10 mL of permeate collected	0.32	0.55	1.26	2.30
100	PSf	Plasma treatment	1 g/L BSA	25 mL of permeate collected	0.43	0.72	0.89	1.49
111	PSf	mbp with -SO₃H groups	0.07 g/L BSA	Flux constant for 10 min	0.60	0.91	0.83	1.13
110	PVDF	mbp by sulfonation (2% sulfonic group content)	20% cutting oil	1-h duration	-	-	-	47.8
This Thesis*	PVDF	bl with 10 wt % P(MMA-r-POEM₄₅) (self-organization)	0.1 g/L BSA	3-h duration	0.13*	0.57*	4.77*	22.39*

[a] Refers to the base membrane type used for comparison. PSf = polysulfone; PAS = poly(arylsulfone); PES = poly(ethersulfone); PVDF = poly(vinylidene fluoride); PAm = polyamide; PAN = polyacrylonitrile; P(AN-co-VC) = poly(acrylonitrile-co-vinyl chloride).

[b] Refers to the type of modification performed on the control membrane to obtain the modified membrane. gr = grafted onto base membrane; ct = coated onto base membrane; ads = adsorbed onto base membrane from aqueous solution; bl = blended base polymer with second polymer; mpb = modified bulk polymer chemically.

[c] Refers to foulant used in filtration study. BSA = bovine serum albumin; PSA = porcine serum albumin; LYS = lysozyme; CyC = cytochrome C; BγGl = bovine γ-globulin; β-LG = β-lactoglobulin.

[d] Refers to criterion used to determine end of filtration experiment.

[†] J_o^C = initial pure water flux for control membrane; J_f^C = flux of foulant solution through control membrane at end of filtration experiment.

[††] J_o^M = initial pure water flux for modified membrane; J_f^M = flux of foulant solution through modified membrane at end of filtration experiment.

[‡] Ratio of initial pure water fluxes for modified and control membranes.

[‡‡] Ratio of final foulant solution fluxes for modified and control membranes.

* Asterisks indicate data presented in this thesis.

Appendix B. Synthesis Details

B.1 Details of P(MMA-r-POEM) Syntheses

The details of all P(MMA-r-POEM) syntheses are presented in Table B.1. Except where indicated below, all reactions were performed for 12-16 h at 60-65°C using 10% (v/v) monomer solutions in ethyl acetate. The synthesis protocols for a few of the P(MMA-r-POEM) copolymers were somewhat different than the general free-radical procedure described in Section 3.1.2. These differences are detailed below.

Table B.1 Free-Radical P(MMA-r-POEM) Synthesis Details

polymer	Target Composition (wt % POEM)	MMA (g)	POEM (g)	$\frac{[M]}{[AIBN]}$	AIBN (g)	Composition (wt % POEM)	$\overline{M}_w$ (g/mol)
P(MMA-r-POEM$_9$)^b	30	14	6	20	1.251	29.4	18 600
P(MMA-r-POEM$_9$)^c	35	13	7	20	1.186	33.1	41 300
P(MMA-r-POEM$_9$)^d	40	12	8	20	1.121	38.9	15 200
P(MMA-r-POEM$_9$)^e	45	11	9	20	1.056	42.9	14 500
P(MMA-r-POEM$_9$)^f	50	10	10	20	0.991	48.6	14 800
P(MMA-r-POEM$_9$)^g	40	6	4	10	1.122	38.4	6 100
P(MMA-r-POEM$_9$)^h	40	6	4	40	0.281	40.2	10 800
P(MMA-r-POEM$_9$)^i	40	18	12	400	0.084	38.9	67 700
P(MMA-r-POEM$_9$)^j	40	18	12	13 465	0.0025	36.3	515 800
P(MMA-r-POEM$_5$)	50	15	15	400	0.082	50.9	155 000
P(MMA-r-POEM$_9$)^k	50	15	15	400	0.074	50.7	63 300
P(MMA-r-POEM$_{45}$)	50	15	15	400	0.065	41.2	73 800

P(MMA-r-POEM$_9$)$^{b-f}$

These copolymers were synthesized as 10% (v/v) monomer solutions in toluene (reagent grade, VWR), rather than ethyl acetate.

P(MMA-r-POEM$_9$)^j

In order to prepare a copolymer of high molecular weight, the reaction was performed with a high monomer concentration (30% monomer in ethyl acetate), using a very high [M]/[AIBN] ratio (see Table B.1). To prevent side reactions and/or autoacceleration, the reaction was stopped after 2 h at ~40% conversion.

P(MMA-r-POEM$_{45}$)

For the synthesis of this polymer, an alternative protocol was found to be convenient due to the condition of the POEM$_{45}$ monomer, which was purchased as a 50% solution in water. Reagent-grade THF (Aldrich), which is miscible with water, was used as the reaction medium instead of ethyl acetate. MMA (15 g) and 30 g of the POEM$_{45}$/water

solution were weighed into a reactor containing 700 mL of THF, and the reaction was otherwise carried out according to the general free-radical procedure outlined in Section 3.1.2.

B.2 Details of PVDF-*g*-POEM Syntheses

Table B.2 PVDF-*g*-POEM Synthesis Details

polymer	PVDF (g)	POEM₉ (mL)	NMP (mL)	CuCl (g)	bpy (g)	Temp. (°C)	Time (h)	Composition (wt % POEM₉)	$\overline{M}_w$ [†] (g/mol)
PVDF-*g*-POEM[a]	5	5	30	0.066	0.15	85	60	43.5	189 400
PVDF-*g*-POEM[b]	5	50	40	0.040	0.23	90	19	66.9	323 200

[†] Calculated from ^{1}H NMR

262

Appendix C. Tabulated Component Peak Areas from XPS Fits

Table C.1 C 1s Component Peak Areas as Percentages of Total Area (Fig. 4.3)

Membrane ID	$\phi_{w,b}$	ϕ_b	Casting Temp. (°C)	Anneal Time (h)	HC	$\underline{C}$-COO	CH_2 (PVDF)	C-O	COO-$\underline{C}$	COO	CF_2
E-02-9a-20	0.02	0.030	20	-	12.45	1.94	38.16	5.42	1.94	1.94	38.16
E-02-9a-20	0.02	0.030	20	4	13.55	3.18	34.00	8.92	3.18	3.18	34.00
E-02-9a-20	0.02	0.030	20	12	41.14	3.70	18.58	10.62	3.70	3.70	18.58
E-02-9a-20	0.02	0.030	20	24	29.42	4.10	23.09	12.08	4.10	4.10	23.09
E-05-9a-20	0.05	0.075	20	-	9.98	2.98	36.83	7.42	2.98	2.98	36.83
E-05-9a-20	0.05	0.075	20	4	12.63	3.92	31.97	11.68	3.92	3.92	31.97
E-05-9a-20	0.05	0.075	20	12	32.47	5.10	18.96	14.31	5.10	5.10	18.96
E-05-9a-20	0.05	0.075	20	24	27.38	6.61	17.61	17.56	6.61	6.61	17.61
E-10-9a-20	0.10	0.146	20	-	9.45	3.94	33.65	11.42	3.94	3.94	33.65
E-10-9a-20	0.10	0.146	20	4	14.90	4.38	30.51	10.94	4.38	4.38	30.51
E-10-9a-20	0.10	0.146	20	12	32.71	5.90	17.81	13.99	5.90	5.90	17.81
E-10-9a-20	0.10	0.146	20	24	27.38	6.77	17.11	18.10	6.77	6.77	17.11
E-20-9a-20	0.20	0.277	20	-	18.69	6.26	22.01	18.49	6.26	6.26	22.01
E-20-9a-20	0.20	0.277	20	12	32.63	6.22	15.49	17.73	6.22	6.22	15.49
E-20-9a-20	0.20	0.277	20	24	17.13	6.56	21.94	19.30	6.56	6.56	21.94

Table C.2 C 1s Component Peak Areas as Percentages of Total Area (Figs. 4.4, 4.5)

Membrane ID	W_{POEM}	ϕ_b	Casting Temp. (°C)	Anneal Time (h)	HC	C-COO	CH₂ (PVDF)	C-O	COO-C	COO	CF₂
E-05-9b-20	0.294	0.073	20	-	18.51	4.53	31.09	5.71	4.53	4.53	31.09
E-05-9b-20	0.294	0.073	20	-	23.46	3.71	30.13	5.16	3.71	3.71	30.13
E-05-9b-20	0.294	0.073	20	-	30.35	4.27	25.46	5.93	4.27	4.27	25.46
E-05-9b-20	0.294	0.073	20	16	17.31	6.52	26.96	9.21	6.52	6.52	26.96
E-05-9b-20	0.294	0.073	20	16	19.57	5.81	27.14	8.71	5.81	5.81	27.14
E-05-9b-20	0.294	0.073	20	16	17.88	5.49	28.96	7.72	5.49	5.49	28.96
E-05-9b-90	0.294	0.073	90	-	9.19	4.60	35.20	6.62	4.60	4.60	35.20
E-05-9b-90	0.294	0.073	90	-	10.01	5.01	33.84	7.29	5.01	5.01	33.84
E-05-9b-90	0.294	0.073	90	-	8.51	4.25	36.31	6.12	4.25	4.25	36.31
E-05-9c-20	0.331	0.074	20	-	8.56	4.28	35.72	7.17	4.28	4.28	35.72
E-05-9c-20	0.331	0.074	20	-	9.76	4.88	34.80	6.00	4.88	4.88	34.80
E-05-9c-20	0.331	0.074	20	-	8.56	4.07	35.73	7.76	4.07	4.07	35.73
E-05-9c-20	0.331	0.074	20	16	13.13	5.81	29.70	10.06	5.81	5.81	29.70
E-05-9c-20	0.331	0.074	20	16	16.47	6.67	27.04	9.45	6.67	6.67	27.04
E-05-9c-20	0.331	0.074	20	16	12.43	5.47	30.97	9.21	5.47	5.47	30.97
E-05-9c-90	0.331	0.074	90	-	8.93	4.47	35.40	6.86	4.47	4.47	35.40
E-05-9c-90	0.331	0.074	90	-	8.85	4.42	35.50	6.88	4.42	4.42	35.50
E-05-9c-90	0.331	0.074	90	-	10.22	5.11	33.92	6.62	5.11	5.11	33.92
E-05-9d-20	0.389	0.074	20	-	7.00	3.50	37.84	6.82	3.50	3.50	37.84
E-05-9d-20	0.389	0.074	20	-	9.58	3.86	35.84	7.16	3.86	3.86	35.84
E-05-9d-20	0.389	0.074	20	-	21.10	3.49	30.63	7.16	3.49	3.49	30.63
E-05-9d-20	0.389	0.074	20	16	18.81	4.76	28.60	9.72	4.76	4.76	28.60
E-05-9d-20	0.389	0.074	20	16	19.11	4.75	28.39	9.86	4.75	4.75	28.39
E-05-9d-20	0.389	0.074	20	16	18.27	4.97	29.14	8.54	4.97	4.97	29.14
E-05-9d-90	0.389	0.074	90	-	11.64	5.17	31.15	10.55	5.17	5.17	31.15
E-05-9d-90	0.389	0.074	90	-	12.50	6.25	30.53	7.70	6.25	6.25	30.53
E-05-9d-90	0.389	0.074	90	-	13.13	5.15	31.30	8.81	5.15	5.15	31.30
E-05-9e-20	0.429	0.074	20	-	18.93	2.91	32.74	6.88	2.91	2.91	32.74
E-05-9e-20	0.429	0.074	20	-	12.33	3.14	35.42	7.43	3.14	3.14	35.42
E-05-9e-20	0.429	0.074	20	-	14.71	3.35	33.97	7.31	3.35	3.35	33.97
E-05-9c-20	0.429	0.074	20	16	15.75	4.55	30.28	10.04	4.55	4.55	30.28
E-05-9e-20	0.429	0.074	20	16	19.09	4.55	28.38	10.48	4.55	4.55	28.38
E-05-9e-20	0.429	0.074	20	16	17 55	5.04	28.76	9.81	5.04	5.04	28.76
E-05-9e-90	0.429	0.074	90	-	10.54	5.02	32.06	10.28	5.02	5.02	32.06
E-05-9e-90	0.429	0.074	90	-	10.31	5.15	32.48	9.28	5.15	5.15	32.48
E-05-9e-90	0.429	0.074	90	-	10.92	5.01	31.65	10.75	5.01	5.01	31.65
E-05-9f-20	0.486	0.075	20	-	7.08	3.54	36.66	8.98	3.54	3.54	36.66
E-05-9f-20	0.486	0.075	20	-	6.41	3.20	37.68	8.63	3.20	3.20	37.68
E-05-9f-20	0.486	0.075	20	-	6.50	3.25	37.60	8.54	3.25	3.25	37.60
E-05-9f-20	0.486	0.075	20	16	9.02	4.51	32.51	12.44	4.51	4.51	32.51
E-05-9f-20	0.486	0.075	20	16	10.65	5.02	31.88	10.54	5.02	5.02	31.88
E-05-9f-20	0.486	0.075	20	16	8.76	4.38	33.73	10.64	4.38	4.38	33.73
E-05-9f-90	0.486	0.075	90	-	13.93	5.15	29.02	12.56	5.15	5.15	29.02
E-05-9f-90	0.486	0.075	90	-	9.75	4.88	30.94	13.74	4.88	4.88	30.94
E-05-9f-90	0.486	0.075	90	-	8.99	4.50	32.72	12.07	4.50	4.50	32.72

Table C.3 C 1s Component Peak Areas as Percentages of Total Area (Fig. 4.6)

Membrane ID	W_{POEM}	ϕ_b	$\overline{M}_w^{comb}$ (g/mol)	Casting Temp. (°C)	HC	$\underline{C}$-COO	CH_2 (PVDF)	C-O	COO-$\underline{C}$	COO	CF_2
E-05-9g-90	0.384	0.074	6 100	90	8.40	3.50	36.81	7.49	3.50	3.50	36.81
E-05-9g-90	0.384	0.074	6 100	90	11.65	4.11	34.43	7.16	4.11	4.11	34.43
E-05-9h-90	0.402	0.074	10 800	90	10.19	4.19	33.90	9.43	4.19	4.19	33.90
E-05-9h-90	0.402	0.074	10 800	90	10.02	4.53	33.63	9.11	4.53	4.53	33.63
E-05-9d-90	0.389	0.074	15 200	90	11.64	5.17	31.15	10.55	5.17	5.17	31.15
E-05-9d-90	0.389	0.074	15 200	90	12.50	6.25	30.53	7.70	6.25	6.25	30.53
E-05-9d-90	0.389	0.074	15 200	90	13.13	5.15	31.30	8.81	5.15	5.15	31.30
E-05-9i-90	0.389	0.074	67 700	90	19.95	5.33	26.53	11.01	5.33	5.33	26.53
E-05-9i-90	0.389	0.074	67 700	90	14.89	5.31	28.93	11.32	5.31	5.31	28.93
E-05-9j-90	0.363	0.074	515 800	90	18.22	6.24	25.51	12.04	6.24	6.24	25.51
E-05-9j-90	0.363	0.074	515 800	90	18.26	5.71	26.46	11.70	5.71	5.71	26.46

Table C.4 C 1s Component Peak Areas as Percentages of Total Area (Figs. 4.7, 4.8)

Membrane ID	History	HC	$\underline{C}$-COO	CH_2 (PVDF)	C-O	COO-$\underline{C}$	COO	CF_2
F-10-9i-90	as cast	10.54	5.27	31.34	10.96	5.27	5.27	31.34
F-10-9i-90	UF of dW for 24 h at 40 psig	16.01	6.14	26.41	12.75	6.14	6.14	26.41
E-10-9a-20	as cast	9.45	3.94	33.65	11.42	3.94	3.94	33.65
E-10-9a-20	stored in dW for 32 months	12.06	4.82	29.75	13.98	4.82	4.82	29.75

Table C.5 C 1s Component Peak Areas as Percentages of Total Area (Fig. 4.14)

Membrane ID	Coag. Bath Additive	wt % Additive in Bath	HC	$\underline{C}$-COO	CH_2 (PVDF)	C-O	COO-$\underline{C}$	COO	CF_2
F-10-9k1-90	none	-	10.87	5.43	28.40	16.03	5.43	5.43	28.40
F-10-9k1-90	none	-	10.33	5.16	29.39	15.39	5.16	5.16	29.39
F-10-9k1-90	DMAc	10	12.63	5.90	26.04	17.59	5.90	5.90	26.04
F-10-9k1-90	DMAc	10	12.18	6.09	25.70	18.15	6.09	6.09	25.70
F-10-9k1-90	DMAc	15	11.06	5.53	27.96	16.44	5.53	5.53	27.96
F-10-9k1-90	DMAc	15	9.52	4.76	30.95	14.29	4.76	4.76	30.95
F-10-9k1-90	DMAc	20	6.70	3.35	36.55	10.14	3.35	3.35	36.55
F-10-9k1-90	DMAc	20	8.67	4.33	32.70	12.92	4.33	4.33	32.70
F-10-9k1-90	DMAc	30	8.47	4.24	33.04	12.73	4.24	4.24	33.04
F-10-9k1-90	DMAc	30	9.16	4.04	33.27	12.19	4.04	4.04	33.27
F-10-9k1-90	DMAc	40	5.75	2.87	38.53	8.57	2.87	2.87	38.53
F-10-9k1-90	DMAc	40	5.89	2.95	37.81	9.65	2.95	2.95	37.81
F-10-9k1-90	$CaCl_2$	10	10.02	5.01	30.02	14.93	5.01	5.01	30.02
F-10-9k1-90	$CaCl_2$	10	14.14	5.86	25.34	17.60	5.86	5.86	25.34
F-10-9k1-90	$CaCl_2$	15	29.36	4.60	21.04	14.77	4.60	4.60	21.04
F-10-9k1-90	$CaCl_2$	15	27.18	4.76	20.75	17.06	4.76	4.76	20.75
F-10-9k1-90	$CaCl_2$	20	24.48	4.63	23.47	14.72	4.63	4.63	23.47
F-10-9k1-90	$CaCl_2$	20	15.61	4.98	24.30	20.84	4.98	4.98	24.30

Table C.6 C 1s Component Peak Areas as Percentages of Total Area (Table 5.1)

Membrane ID	Bulk Composition	HC	$\underline{C}$-COO	CH_2 (PVDF)	C-O	COO-$\underline{C}$	COO	CF_2
F-10-5-90	10 wt % P(MMA-r-POEM$_5$)	13.63	6.81	24.85	16.23	6.81	6.81	24.85
F-10-9k2-90	10 wt % P(MMA-r-POEM$_9$)^k	16.48	6.56	22.14	19.56	6.56	6.56	22.14
F-10-45-90	10 wt % P(MMA-r-POEM$_{45}$)	12.15	6.07	26.80	16.04	6.07	6.07	26.80

Table C.7 C 1s Component Peak Areas as Percentages of Total Area (Fig. 5.8)

Membrane ID	$\phi_{w,b}$	ϕ_b	History	HC	$\underline{C}$-COO	CH_2 (PVDF)	C-O	COO	CF_2
E-02-9a-20	100.0	100.0	as cast	31.20	11.32	-	46.17	11.32	-
E-02-9a-20	100.0	100.0	30 min in acid	59.50	7.71	-	25.08	7.71	-
E-02-9a-20	0.05	0.075	as cast	12.92	5.06	29.84	17.28	5.06	29.84
E-02-9a-20	0.05	0.075	30 min in acid	5.49	5.32	37.22	9.43	5.32	37.22
E-05-9a-20	0.05	0.075	30 min in acid + 12h anneal	9.76	5.95	29.88	18.58	5.95	29.88

Table C.8 C 1s Component Peak Areas as % of Total Area (Fig. 5.12, Table 5.5)

Sample	$\phi_{w,b}^{POEM}$	HC	$\underline{C}$-COO	CH_2 (PVDF)	C-O	COO	CF_2	$\phi_{w,s}^{POEM}$
Pure PVDF-g-POEM^b film	0.67	13.68	3.06	12.45	55.29	3.06	12.45	0.65
Pure PVDF-g-POEM^b film	0.67	11.48	3.30	11.19	59.54	3.30	11.19	0.69
Membrane F-10-AT1-90	0.044	5.52	1.57	31.52	28.29	1.57	31.52	0.27
Membrane F-05-AT2-90	0.034	7.42	2.26	23.60	40.86	2.26	23.60	0.42
Membrane F-10-AT2-90	0.067	8.64	3.23	13.31	58.27	3.23	13.31	0.64

Table C.9 C 1s Component Peak Areas as % of Total Area (Fig. 5.15, Table 5.5)

Sample	$\phi_{w,b}^{PMAA}$	HC	$\underline{C}$-COOH	CH_2 (PVDF)	CHF	COOH	CF_2	$\phi_{w,s}^{PMAA}$
Pure PVDF-g-PMAA film	0.49	19.17	5.07	35.35	-	5.07	35.35	0.16
Pure PVDF-g-PMAA film	0.49	21.83	5.41	33.68	-	5.41	33.68	0.18
Membrane F-10-PE-90, as cast	0.049	28.74	9.19	26.44	-	9.19	26.44	0.32
Membr. F-10-PE-90, autoclaved 1h	0.049	43.06	6.51	21.96	5.08	6.51	16.88	0.29
F-10-PE-90, autocl. 1h, "back side"	0.049	41.71	9.52	19.62	4.89	9.52	14.74	0.39

Table C.10 C 1s Peak Areas as % of Total Area [P(MA-*r*-POEM₉-*r*-HPOEM₁₀)]

Membrane ID	Bulk Composition	HC	$\underline{C}$-COO⁻	CH₂ (PVDF)	C-O	COO-$\underline{C}$	COO	CF₂	ϕ_s
F-10-MA-90	10 wt % P(MA-*r*-POEM₉-*r*-HPOEM₁₀)	9.32	4.66	30.81	15.07	4.66	4.66	30.81	0.32

Appendix D. Near-Surface Composition Profile

D.1 Sampling Depth of XPS

For a particular core level photoelectron, i, the angle-dependent XPS signal $S_i(\theta)$ is given by,[223,224,289,290]

$$S_i(\theta) = K_i(\theta) \int_0^\infty n_i(z) w_i(z,\theta) dz \qquad \text{(D.1)}$$

where $K_i(\theta)$ is a constant dependent on the take-off angle (θ) relative to the plane of the sample surface, the photoelectron sensitivity factor, and the work function of the spectrometer, and $n_i(z)$ is the atomic composition as a function of the depth z. The function $w_i(z,\theta)$ is an exponential weighting function to account for the fact that photoelectron contributions to the XPS signal decrease exponentially with depth:

$$w_i(z,\theta) = \exp\left(-\frac{z}{\lambda_i \sin\theta} \right) \qquad \text{(D.2)}$$

where λ_i is the photoelectron mean free path.

A large collection of theoretical and experimental work has shown that photoelectron mean free paths are only subtly dependent on the material, but strongly dependent on the KE of the photoelectron given by Equation 3.14.[291] XPS studies of PMMA films of known thickness on silicon substrates have indicated a mean free path of $\lambda_{C1s} = 29 \pm 4$ Å for C 1s electrons excited by Al Kα radiation.[224,292] Approximately 95% of the photoelectrons contributing to the XPS signal originate from a sampling depth given by,[221,224,293]

$$d = 3\lambda \sin\theta$$ (D.3)

or ~60 Å for a polymer sample observed under the conditions used in this thesis (*i.e.*, at a 45° takeoff angle using Al Kα x-rays). The integrated near-surface atomic composition n_s measured by XPS is a weighted average of contributions from photoelectrons originating from depths $z \leq \sim d$,[294]

$$n_s = \frac{\int_0^\infty n_i(z) w_i(z,\theta) dz}{\int_0^\infty w_i(z,\theta) dz}$$ (D.4)

D.2 A Model Composition Profile Consistent with the XPS Data

Data presented in Section 4.2.1 suggest the hypothesis that, for the XPS experimental conditions used, an integrated near-surface composition of $\phi_s = \sim60$ vol % ($n_s = \sim28$ mol %) corresponds to nearly complete surface coverage of P(MMA-*r*-POEM). To evaluate the plausibility of this hypothesis, we model the near-surface composition profile using a hyperbolic tangent function,

$$\phi(z) = \phi_0 - (\phi_0 - \phi_b)\tanh\left(\frac{2z}{a_D}\right)$$ (D.5)

where ϕ_0 and ϕ_b are the volume fractions of the comb in the surface monolayer and the bulk, respectively, and a_D is the thickness of the near-surface comb depletion layer. Neutron reflectivity studies of multilayer polymer systems have commonly shown that the interlayer composition profiles are well-represented by hyperbolic tangent functions.[294,295] Irvine, *et al.*[186,280] performed SCF calculations of the equilibrium, near-

surface concentration profiles of comb copolymers in miscible blends with linear polymer matrices. In these calculations, the comb side chains were enthalpically attracted to the surface, while comb backbone and matrix units were repelled from the surface. The predicted concentration profiles $\phi(z)$ exhibited up to ~100% comb in the surface monolayer, with a rapid decay of the comb concentration to its bulk value over a depth of ~50 Å. This strongly surface-localized enrichment of the comb component is consistent with a *quasi-2-dimensional* conformation of comb molecules near the surface. That is, comb molecules nearest the surface are arranged in a "pancake"-like fashion for maximal exposure of the surface-active side chains. The high efficiency of side chain expression which would result from quasi-2D confinement of comb polymers near surfaces of blends with linear matrices has been confirmed by fluorescence labeling experiments.[186,280]

Figure D.1 shows a model near-surface composition profile for a P(MMA-*r*-POEM9) comb containing 50 wt % POEM in PVDF. This composition profile corresponds to complete surface coverage of the comb ($\phi_0 = 1$), with a depletion of the comb concentration to its bulk value ($\phi_b = 0.15$, or 10 wt % comb) over a depth of $a_D = 50$ Å. A weighting function $w(z)$, computed using a photoelectron mean free path of $\lambda_{C1s} = 29$ Å and a take-off angle of $\theta = 45°$, is shown in Figure D.1 as a dotted line. Based on these two functions, Equation D.5 was integrated numerically over the range $z = 0$ to $z = 10d$ using the trapezoidal rule,[296] with increments Δz of 0.001 Å and with conversion of volume fractions $\phi(z)$ to mole fractions $n(z)$ accomplished using molar volumes V_o^{PVDF} and V_o^{comb} calculated as described in Section 4.2.1. The XPS integrated

near-surface composition so calculated is $\phi_s = 0.66$, reasonably consistent with the largest

experimental ϕ_s values reported in Section 4.2.1 (see Fig. 4.3). Thus, it is not implausible

that the integrated near-surface membrane compositions of $\phi_s = \sim 0.60$ measured by XPS

in this thesis correspond to nearly 100% surface monolayer coverage of the comb

additive.
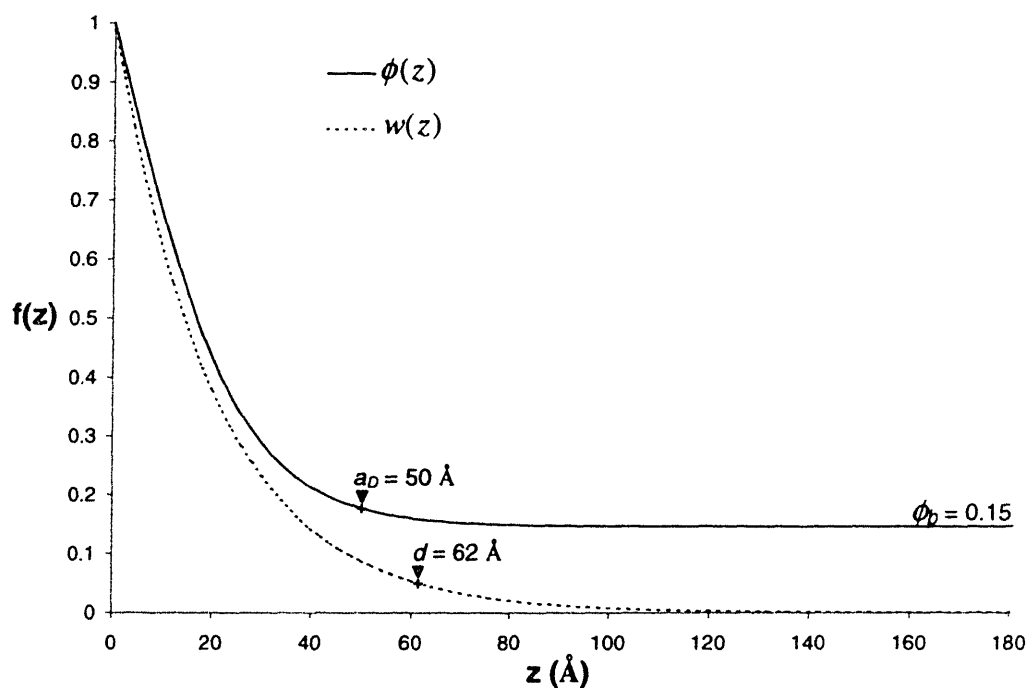
Figure D.1 Model near-surface composition profile
The composition profile $\phi(z)$ is given by Equation D.5, with $\phi_0 = 1.0$, $\phi_b = 0.15$, and $a_D = 50$ Å. The exponential weighting function (Equation D.2), with $\lambda = 29$ Å and $\theta = 45°$, is shown as a dotted line.

Appendix E. Machine Drawings

E.1 Membrane Casting Bar

| 6/9/98 | MEMBRANE CASTING BAR | JON HESTER |

ALUMINUM BAR STOCK 1"×1" CUT TO A LENGTH OF 4." TURN ON AXIS ON LATHE TO PRODUCE A CYLINDRICAL SECTION 3" LONG × 0.850" DIAMETER BETWEEN SQUARE ENDS.

$\delta_o = 0.075"$

RADIUS = 0.0425"

END VIEW

$\delta_B = 0.008"$ (SEE BELOW)

$\delta_o = 0.075"$

δ_o

δ_o

½"

3"

½"

AXIS

F

F

$\delta_B = 0.008"$

$\delta_A = 0.067"$

δ_B

δ_A

$\delta_c = \frac{1}{8}"$

SIDE VIEW

δ_c

MACHINE SQUARE ENDS AS SHOWN TO FORM STEP 0.067" DEEP BY ⅛" WIDE. GAP BETWEEN FACE F AND CYLINDRICAL BAR SHOULD BE 0.008" (CRITICAL).

Figure E.1 Machine drawing of membrane casting bar with 8 mil gate size

E.2 Membrane Cutting Die

6/9/98	MEMBRANE "COOKIE CUTTER"	JON HESTER

STEEL PIPE STOCK, APPROX. 30mm O.D. (NOT CRITICAL). CUT APPROX. 4cm LENGTH (NOT CRITICAL).

AXIS

O.D. 30mm

HALF SECTION

~4cm

~5mm

I.D. = 25mm

BORE TO 25mm I.D. (CRITICAL). SHARPEN ONE END TO A CUTTING POINT AS SHOWN.
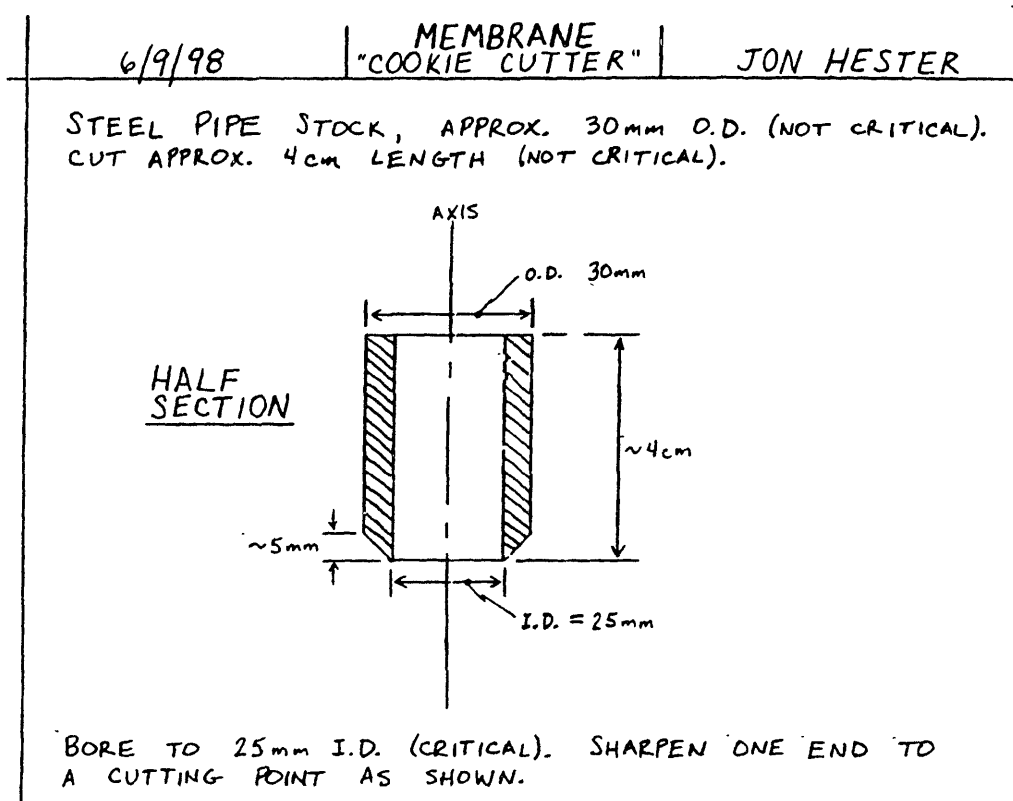
Figure E.2 Machine drawing of 25 mm diameter membrane cutting die

Appendix F. XPS Fitting Source Code

This appendix contains the source code and required peripheral file formats for the computer program used to fit all XPS data presented in this thesis. The xps program has the following useful features, which are not simultaneously available using many commercial peak deconvolution packages:

1) It allows peak positions BE_o to be set relative to a reference peak position, such that all or a subset of the peaks in a model spectrum may be shifted up or down the BE scale together while maintaining their relative positions.

2) It allows constraint of peak area ratios to any value, including non-integer values.

3) It allows numerical specification of the peak position BE_o for an internal calibrant peak, adjusting the absolute BE scale accordingly.

The FORTRAN source code for program xps (Section F.1.2) was compiled on a Sun SPARCstation 10/30 running SunOS 4.1.3 using Gnu F77 version 0.5.5.

F.1 Source Code

F.1.1 Unix Script "fit"

Following is the source code for the Unix script fit, which runs the executable FORTRAN program xps.exe. Fitting an XPS data set requires the presence of the following files in the current directory:

1) xps.exe, obtained by compiling the xps source code (Section F.1.2),
2) fit (below),
3) *.dat and *.par where "*" represents a consistent filename prefix.

The program is then run by typing at the Unix prompt,

```
fit *
```

Besides providing the filename prefix to the xps program, the fit script also makes copies of the *.log and *.par files so that they may be recovered if the current fitting attempt should lead to an undesirable result. Note that, while a file named *.par must be present to run the program, a copy of that file (named *.par.old) is actually the input for xps.exe. After the fit has terminated, xps.exe outputs an updated *.par file.

fit:

```
cp $1.log $1.log.old
cp $1.par $1.par.old

xps.exe << -+-
$1
-+-
```

F.1.2 Program xps FORTRAN Source Code

```fortran
ccccccccccccccccccccccccccccccccccccccccccccccccccccccccccccccccccccc
c
c Program Name:  XPS
c
c Author:    Jonathan Hester
c            December, 1999
c
c Description:  Fits x-ray photoelectron spectroscopy (XPS) data
c               with Gaussian-Lorentzian peaks.
c
c Required Files:
c   *.par.old - fitting parameter file (INPUT)
c   *.dat     - experimental XPS spectrum (INPUT)
c
c Output Files:
c   *.log -  fitting activity log file
c   *.bkg -  linear baseline
c   *.sub -  background-subtracted experimental spectrum
c   *.fit -  fitted model spectrum
c   *.pks -  individual model peaks
c   *.tix -  coordinates of peak center tic marks for use by CPLOT
c   *.sum -  summary report of fitted peak parameters
c   *.par -  new, updated fitting parameter file
c   _fit.scr -  CPLOT do file for screen plotting of fit
c   _bkg.scr -  CPLOT do file for screen plotting of background
c   _fit.prn -  CPLOT do file for writing a postscript file (*.ps)
c               of fit plot
c   _bkg.prn -  CPLOT do file for writing a postscript file (*.ps)
c               of backgound plot
c
c In all of the above, '*' represents the base file name, which is
c user-defined by the consistent naming of the *.par and *.dat files.
c
c References:  The loop used to adjust the parameters for minimization
c              of SSE (directly beneath the comment line 'vary fitting
c              parameters to minimize SSE') was inspired by the
c              neutron reflectivity fitting code of David Walton:
c              D. G. Walton, CREATING STABLE HYDROPHILIC SURFACES WITH
c              BLENDS OF BRANCHED AND LINEAR POLYMERS, Ph.D. Thesis,
c              Massachusetts Institute of Technology, 1997, pp. 211-
c              229.
c
ccccccccccccccccccccccccccccccccccccccccccccccccccccccccccccccccccccc
      program XPS
      implicit none
c Constant Declarations
      integer k_pmax
      parameter (k_pmax = 400)     ! Maximum number of fitting parameters
      integer k_dmax
      parameter (k_dmax = 10000)   ! Maximum number of data points
      integer k_emax
      parameter (k_emax = 100000)  ! Maximum # of points in peak envelope
      integer k_head
      parameter (k_head = 4)       ! Number of header lines in data file

c Local Declarations

      real*8  be(k_dmax)         ! Experimental binding energy
      real*8  ec(k_dmax)         ! Experimental electron counts
      real*8  bkg(k_dmax)        ! Calculated linear background
      real*8  be_sub(k_dmax)     ! Background-subtracted binding energy
      real*8  ec_sub(k_dmax)     ! Background-subtracted electron counts
      real*8  be_env(k_emax)     ! Peak envelope, binding energy
      real*8  ec_env(k_emax)     ! Peak envelope, electron counts
      real*8  ec_calc(k_dmax)    ! Calculated electron counts
      integer n_data             ! Number of experimental data points
      integer n_sub              ! Number of background-subtracted data points
      real*8  be_min             ! Minimum binding energy
      real*8  be_max             ! Maximum binding energy
      real*8  ec_max             ! Maximum electron counts in spectrum

      real*8  a(k_pmax)          ! Fitting parameters
      integer fit_a(k_pmax)      ! Fit this parameter?
                                 !   0 = no
                                 !   1 = yes
                                 !  n>1 = set value equal to m*(parameter #n)
                                 !  n<0 = set value equal to A+(parameter #(-
                                 ! n))

      real*8  a_mult(k_pmax)     ! m
      real*8  a_add(k_pmax)      ! A
      real*8  a_min(k_pmax)      ! Parameter minimum value
      real*8  a_max(k_pmax)      ! Parameter maximum value
      real*8  a_step(k_pmax)     ! Parameter step value
      real*8  a_new              ! Temporary parameter value
      real*8  a_up               ! Parameter value + step value
      real*8  a_down             ! Parameter value - step value
      integer a_fit(k_pmax)      ! List of parameters to fit
      integer n_fit              ! Number of parameters to fit
      integer n_slave            ! Number of slave parameters
      integer n_peaks            ! Number of peaks
      integer n_bkg              ! Number of points on either end of data
                                 ! to average to make linear baseline
      logical modified           ! Did we modify this parameter?
      logical minimized          ! Did we reach a minimum SSE?

      real*8  x1,y1              ! First point of linear background
      real*8  x2,y2              ! Second point of linear background
      real*8  m                  ! Slope of linear background

      real*8  ec_ave             ! Average y-value of fitted experimental data
      real*8  SSM                ! Sum of Squares about Mean
      integer DOF                ! Degree of Freedom
      real*8  rsq                ! r^2 value (Coefficient of Determination)
      real*8  rsq_DOF            ! DOF Adjusted r^2

      real*8  SSE                ! Sum of Squares due to Error
      real*8  old_SSE            ! Saved SSE value
      real*8  ref_be             ! Binding energy (eV) of reference peak
      real*8  shift              ! Difference between ref_be and HC peak pos.
      integer max_iter           ! Maximum number of iterations
      integer iter               ! Current iteration number
      integer sh_peak            ! Peak number referenced to 285eV
                                 !   (0 if no reference)
      integer i,j,k              ! Counter variables
      real*8  temp               ! Temporary storage variable
      character*30 basename      ! Base file name
      character*40 filename      ! File name
      character*70 head(k_head)  ! Data file header

c Main Program
```

```
c
c  Get base file name from user and convert to expected file names
c
      write (*,*)
      write (*,*) 'Enter filename base:'
      write (*,*) '  ( OR, enter \'?\' for help'
      write (*,*) '  OR, enter \'#\' to generate a parameter ',
     &  'file template )'
      read (*,'(a30)') basename
      write (*,*)

      if ((basename.EQ.'?').OR.(basename.EQ.'help')) then
          call Help
          goto 350
      else if (basename.EQ.'#') then
          call Template
          goto 350
      endif

      filename = basename(:index(basename,' ') - 1) // '.par.old'
      open (unit=1, file=filename, status='old', err=10)

      filename = basename(:index(basename,' ') - 1) // '.dat'
      open (unit=2, file=filename, status='old', err=10)

      filename = basename(:index(basename,' ') - 1) // '.bkg'
      open (unit=3, file=filename, status='unknown', err=10)

      filename = basename(:index(basename,' ') - 1) // '.sub'
      open (unit=4, file=filename, status='unknown', err=10)

      filename = basename(:index(basename,' ') - 1) // '.log'
      open (unit=7, file=filename, status='unknown', err=10)

      filename = basename(:index(basename,' ') - 1) // '.fit'
      open (unit=8, file=filename, status='unknown', err=10)

      filename = basename(:index(basename,' ') - 1) // '.pku'
      open (unit=9, file=filename, status='unknown', err=10)

      filename = basename(:index(basename,' ') - 1) //
     &  '_fit.scr'
      open (unit=10, file=filename, status='unknown', err=10)

      filename = basename(:index(basename,' ') - 1) //
     &  '_fit.prn'
      open (unit=11, file=filename, status='unknown', err=10)

      filename = basename(:index(basename,' ') - 1) //
     &  '_bkg.scr'
      open (unit=12, file=filename, status='unknown', err=10)

      filename = basename(:index(basename,' ') - 1) //
     &  '_bkg.prn'
      open (unit=13, file=filename, status='unknown', err=10)

      filename = basename(:index(basename,' ') - 1) // '.sum'
      open (unit=14, file=filename, status='unknown', err=10)

      filename = basename(:index(basename,' ') - 1) // '.tix'
      open (unit=15, file=filename, status='unknown', err=10)

      filename = basename(:index(basename,' ') - 1) // '.par'
      open (unit=16, file=filename, status='unknown', err=10)

      goto 20

10    write (*,*) 'ERROR: Error opening file ' // filename
      write (*,*)
      goto 350
20    continue

c
c  Read model parameters from 'filename_base.par' file
c
      read (1,*,end=30,err=30) be_min, be_max, max_iter
      read (1,*,end=30,err=30) n_peaks, n_bkg, sh_peak, ref_be

c
c  For each peak to fit, data file must include the following fitting
c  parameters, in this order:
c  1)  Peak Area (val, fit?, min, max, step)
c  2)  Peak Center, in eV (val, fit?, min, max, step)
c  3)  Full-width at half-maximum (FWHM) (val, fit?, min, max, step)
c  4)  Shape (>=0, <=1); 0 = pure Lorentzian, 1 = pure Gaussian
c  The fitting parameters for each peak are separated from the rest of
c  the 'filename_base.par' file by a single blank line.
c
      do i=1,n_peaks
          read (1,*)
          do j=3,0,-1
              k = 4*i-j
              read (1,*,end=30,err=30) a(k), fit_a(k), a_mult(k),
     &           a_add(k), a_min(k), a_max(k), a_step(k)
          enddo
      enddo
      goto 40

30    filename = basename(:index(basename,' ') - 1) // '.par'
      write (*,*) 'ERROR: Error reading file ',filename
      write (*,*)
      goto 350
40    continue

c
c  Read experimental data from 'filename_base.dat' data file.
c
      do i=1,k_head
          read (2,'(a70)') head(i)
      enddo
      i = 1
100   read (2,*,end=110,err=110) be(i), ec(i)
      i = i + 1
      goto 100
110   n_data = i - 1

c
c  Construct a linear baseline and subtract the background.
c  The two points which determine the baseline are computed as
c  averages of a number of data points (specified by the user and
c  stored in variable n_bkg) at the beginning and end of the
c  experimental data array
c
      write (*,*) 'Constructing linear baseline and subtracting ',
     &  'background'
      x1 = 0.0
```

```
      y1 = 0.0
      x2 = 0.0
      y2 = 0.0
      do i=1,n_bkg
        x1 = x1 + be(i)
        y1 = y1 + ec(i)
      enddo
      x1 = x1 / float(n_bkg)
      y1 = y1 / float(n_bkg)
      do i=(n_data-n_bkg+1),n_data
        x2 = x2 + be(i)
        y2 = y2 + ec(i)
      enddo
      x2 = x2 / float(n_bkg)
      y2 = y2 / float(n_bkg)
      m = (y2 - y1) / (x2 - x1)
      j = 1
      ec_ave = 0.0
      do i=1,n_data
        bkg(i) = m*(be(i) - x1) + y1
        if ((be(i).GE.be_min).AND.(be(i).LE.be_max)) then
          be_sub(j) = be(i)
          ec_sub(j) = ec(i) - bkg(i)
          if (ec_sub(j).LT.0.0) ec_sub(j) = 0.0
          ec_ave = ec_ave + ec_sub(j)
          j = j + 1
        endif
      enddo
      n_sub = j - 1
      ec_ave = ec_ave / float(n_sub)

      write (*,*) 'Done.'
      write (*,*)
      write (*,*) 'Number of data points read   = ',n_data
      write (*,*) 'Number of data points to fit = ',n_sub
      write (*,*) 'Number of peaks in model     = ',n_peaks

c   Prepare parameters for fitting:
c   Make a list of fitting parameters (in array a_fit)
c   Count the number of slave parameters
c   Make slave parameters equal to their masters

      n_fit = 0
      n_slave = 0
      do i=1,(n_peaks*4)
        if (fit_a(i).EQ.1) then
          n_fit = n_fit + 1
          a_fit(n_fit) = i
        else if (fit_a(i).GT.1) then
          n_slave = n_slave + 1
          a(i) = a_mult(i) * a(fit_a(i))
        else if (fit_a(i).LT.0) then
          n_slave = n_slave + 1
          a(i) = a_add(i) + a(-1*(fit_a(i)))
        endif
      enddo

      write (*,*) 'Number of parameters to fit = ',n_fit
      write (*,*) 'Number of slave parameters  = ',n_slave
      write (*,*)

c

c   Compute the initial theoretical spectrum based on the initial
c   values of the fitting parameters

      call Model(be_sub,ec_sub,ec_calc,n_sub,a,n_peaks,old_SSE)
      SSE = old_SSE
      write (*,*) 'Initial Results:'
      call PrintVals(a,fit_a,0,n_peaks)
      write (7,*) 'Initial SSE = ',old_SSE
      write (*,*) 'Initial SSE = ',old_SSE
      write (7,*)

c   Vary fitting parameters to minimize SSE

      minimized = .FALSE.
      if (n_fit.EQ.0) got. 300
      do iter1,max_iter
      modified = .FALSE.
      do j=1,n_fit
        i = a_fit(j)
        a_new = a(i)
        a_up = a(i) + a_step(i)
        a_down = a(i) - a_step(i)

c   Try up a little bit
        if (a_up.LE.a_max(i)) then
          a(i) = a_up

c   Make slaves equal to their masters
          do k=1,(n_peaks*4)
            if (fit_a(k).GT.1) then
              a(k) = a_mult(k) * a(fit_a(k))
            else if (fit_a(k).LT.0) then
              a(k) = a_add(k) + a(-1*(fit_a(k)))
            endif
          enddo

c   Compute theoretical spectrum and compare SSE to old SSE
          call Model(be_sub,ec_sub,ec_calc,n_sub,a,n_peaks,SSE)
          if (SSE.LT.old_SSE) then
            modified = .TRUE.
            old_SSE = SSE
            a_new = a_up
          endif
        endif

c   Try down a little bit
        if (a_down.GE.a_min(i)) then
          a(i) = a_down

c   Make slaves equal to their masters
          do k=1,(n_peaks*4)
            if (fit_a(k).GT.1) then
              a(k) = a_mult(k) * a(fit_a(k))
            else if (fit_a(k).LT.0) then
              a(k) = a_add(k) + a(-1*(fit_a(k)))
            endif
          enddo

c   Compute theoretical spectrum and compare SSE to old SSE
          call Model(be_sub,ec_sub,ec_calc,n_sub,a,n_peaks,SSE)
          if (SSE.LT.old_SSE) then
            modified = .TRUE.
            old_SSE = SSE
            a_new = a_down
          endif
        endif

c   Set new parameter value
        a(i) = a_new
```

```fortran
c     Make slaves equal to their masters
      do k=1,(n_peaks*4)
        if (fit_a(k).GT.1) then
          a(k) = a_mult(k) * a(fit_a(k))
        else if (fit_a(k).LT.0) then
          a(k) = a_add(k) + a(-1*(fit_a(k)))
        endif
      enddo
c
c     Save intermediate results to 'filename_base.log' file
      write (7,*) 'Iteration #',iter
      call PrintVals(a,fit_a,0,n_peaks)
      write (7,*) 'Iteration #',iter,'    SSE = ',old_SSE
      write (7,*) '    SSE = ',old_SSE
      write (7,*)
      if (.NOT.modified) then
        minimized = .TRUE.
        goto 300
      endif
      enddo
300   continue
c
c     Compute statistics of merit for the fit
      SSM = 0.0
      do i=1,n_sub
        SSM = SSM + (ec_sub(i) - ec_ave)**2.0
      enddo
      rsq = 1.0 - (old_SSE/SSM)
      DOF = n_sub - n_fit
      rsq_DOF = 1.0 - (old_SSE*float(n_sub-1))/(SSM*float(DOF-1))
c
c     Calculate and store coordinates for all the component peak
c     outlines
      call CalcEnv(a,be,be_env,ec_env,n_peaks,n_data)
c
c     Shift all data sets along x-axis such that reference peak is
c     positioned at reference binding energy of internal calibrant
      if (sh_peak.GT.0) then
        shift = ref_be - a(sh_peak*4-2)
        do i=1,n_peaks
          a(i*4-2) = a(i*4-2) + shift
          a_min(i*4-2) = a_min(i*4-2) + shift
          a_max(i*4-2) = a_max(i*4-2) + shift
        enddo
      else
        shift = 0.0
      endif
c
c     Write shifted raw data to file 'filename_base.dat'
      rewind(2)
      do i=1,k_head
        write (2,'(a70)') head(i)
      enddo
      do i=1,n_data
        write (2,*) be(i)+shift, ec(i)
      enddo
c
c     Write shifted linear baseline and the background subtracted data
c     to files 'filename_base.bkg' and 'filename_base.sub',
c     respectively
      do i=1,n_data
        write (3,*) be(i)+shift, bkg(i)
      enddo
      do i=1,n_data
        temp = ec(i) - bkg(i)
        if (temp.LT.0.0) temp = 0.0
        write (4,*) be(i)+shift, temp
      enddo
c
c     Write final theoretical spectrum to 'filename_base.fit' file
      do i=1,n_sub
        write (8,*) be_sub(i)+shift, ec_calc(i)
      enddo
c
c     Write fitted component peaks to 'filename_base.pks' file
      do i=1,n_data*n_peaks
        write (9,*) be_env(i)+shift, ec_env(i)
      enddo
c
c     Write peak center tic marks to 'filename_base.tix' file
      ec_max = 0.0
      do i=1,n_data
        temp = ec(i) - bkg(i)
        if (temp.LT.0.0) temp = 0.0
        if (temp.GT.ec_max) ec_max = temp
      enddo
      do i=1,n_sub
        if (ec_calc(i).GT.ec_max) ec_max = ec_calc(i)
      enddo
      do i=1,n_peaks
        write (15,*) a(i*4-2), ec_max*100
      enddo
c
c     Write summary of fitted peak parameters to 'filename_base_sum' file
c     Write do files for printing data and peaks using CPLOT utility
      call Summary(a,n_peaks,old_SSE,rsq,rsq_DOF,minimized,basename)
      call DoFiles(basename)
c
c     Write new version of parameter file to 'filename_base.par' file
      write (16,302) be_min+shift, be_max+shift, max_iter
302   format (f6.2,4x,f6.2,4x,i8)
      write (16,304) n_peaks, n_bkg, sh_peak, ref_be
304   format (i3,7x,i3.8x,i3.7x,f6.2)
      do i=1,n_peaks
        write (16,*)
        do j=1,3,-1
```

```
         k=4*i-3
         write (16,306) a(k), fit_a(k), a_mult(k), a_add(k),
     &      a_min(k), a_max(k), a_step(k)
306      format (f7.2,1x,i1,1x,f6 3,1x,f5.2,1x,f6 2,2x,f9.2,4x,f7 2)
         enddo
      enddo

c
c     Write final results to 'filename_base log' file
c
      write (7,*) 'Final Results:'
      write (7,*)
      call PrintVals(a,fit_a,1,n_peaks)
      write (7,*) 'Final SSE        = ',old_SSE
      write (7,*) 'r^2              = ',rsq
      write (7,*) 'DOF Adjusted r^2 = ',rsq_DOF
      write (7,*) 'Number of iterations = ',iter-1

c
c     Clean up and exit
c
      close (unit= 1, status='keep')
      close (unit= 2, status='keep')
      close (unit= 3, status='keep')
      close (unit= 4, status='keep')
      close (unit= 7, status='keep')
      close (unit= 8, status='keep')
      close (unit= 9, status='keep')
      close (unit=10, status='keep')
      close (unit=11, status='keep')
      close (unit=12, status='keep')
      close (unit=13, status='keep')
      close (unit=14, status='keep')
      close (unit=15, status='keep')
      close (unit=16, status='keep')
      write (*,*)

350   end

ccccccccccccccccccccccccccccccccccccccccccccccccccccccccccccccccccccc
c
c     Subroutine Name  Model
c
c     Description:  Computes model peak envelope based on current fitting
c                   parameter values.  Returns the sum of the squared
c                   errors (SSE) between model and experimental data
c                   points.
c
c     Parameters:   be       -> Experimental binding energy
c                   ec       -> Experimental electron counts
c                   ec_calc  <- Calculated electron counts (model)
c                   n_data   -> Number of experimental data points
c                   a        -> Fitting parameters
c                   n_peaks  -> Number of peaks in model
c                   SSE      <- Sum of the squared errors
c
ccccccccccccccccccccccccccccccccccccccccccccccccccccccccccccccccccccc
      subroutine Model(be,ec,ec_calc,n_data,a,n_peaks,SSE)
      implicit none

      integer k_pmax
      parameter (k_pmax = 400)   ' Maximum number of fitting parameters
      integer k_pkmax            ' Maximum number of peaks
      parameter (k_pkmax = 100)  ! Maximum number of data points
      integer k_dmax
      parameter (k_dmax = 10000)

      real*8  be(k_dmax)         ! Experimental binding energy
      real*8  ec(k_dmax)         ! Experimental electron counts
      real*8  ec_calc(k_dmax)    ! Calculated electron counts (model)
      integer n_data             ! Number of experimental data points
      real*8  a(k_pmax)          ! Fitting parameters
      integer n_peaks            ! Number of peaks in model
      real*8  SSE                ! Sum of squared errors
      real*8  b(k_pkmax,4)       ! Table of fitting parameters (4 per peak)
      integer i,j,k              ! Counter variables

      real*8  PeakVal            ! Function to compute y-values of model
                                 ! spectrum

      k = 1
      do j=1,n_peaks
         do i=1,4
            b(j,i) = a(k)
            k = k + 1
         enddo
      enddo

      do i=1,n_data
         ec_calc(i) = 0.0
         do j=1,n_peaks
            ec_calc(i) = ec_calc(i) + PeakVal(b,j,be(i))
         enddo
      enddo

      SSE = 0.0
      do i=1,n_data
         SSE = SSE + (ec_calc(i) - ec(i))**2.0
      enddo

      return
      end

ccccccccccccccccccccccccccccccccccccccccccccccccccccccccccccccccccccc
c
c     Function Name.  PeakVal
c
c     Description.  Function returns the y-value (electron counts, F(BE))
c                   of a component peak of the model spectrum, given the
c                   x-value (binding energy, BE).  F(BE) is given by the
c                   Gaussian-Lorentzian sum function,
c
```

$$F(BE) = 2A\left[\frac{m(\ln 2)^{1/2}}{W(\pi)^{1/2}}\exp\left[-4\ln 2\left(\frac{BE-BEo}{W}\right)^2\right] + \frac{1-m}{(pi)W\left[1+4\left(\frac{BE-BEo}{W}\right)^2\right]}\right]$$

```
c     where F(BE) is the intensity in electron counts at
c                   binding energy BE.  BEo is the peak center, W is the
```

```fortran
C     full-width at half-maximum, and m is the Gaussian-         C
C     Lorentzian mixing ratio (1 = pure Gaussian, 0 = pure       C
C     Lorentzian)                                                C
C                                                                C
C  Parameters   b       -> Table of fitting parameters (4 per peak) C
C               j       -> Peak index                            C
C               x       -> x-value of model spectrum (binding energy) C
C               PeakVal <- y-value of model spectrum (election counts)C
CCCCCCCCCCCCCCCCCCCCCCCCCCCCCCCCCCCCCCCCCCCCCCCCCCCCCCCCCCCCCCC
      real*8 function PeakVal(b,j,x)
      implicit none

      integer k_pkmax                        ! Maximum number of peaks
      parameter (k_pkmax = 100)
      real*8 k_pi                            ! pi
      parameter (k_pi = 3.14159265358585)

      real*8 b(k_pkmax,4)   ! Table of fitting parameters (4 per peak)
      integer j             ! Peak index
      real*8 x              ! x-value of model spectrum (binding energy, eV)
      real*8 temp1,temp2,temp3,temp4   ! Temporary storage variables

      temp1 = ((x - b(j,2)) / b(j,3))**2.0
      temp2 = (1.0 - b(j,4)) / (k_pi*b(j,3))*(1.0 + 4 0*temp1))
      temp3 = exp(-4.0*(log(2.0))*temp1)
      temp4 = (b(j,4)*temp3*sqrt(log(2 0)) / (b(j,3)*sqrt(k_pi))
      PeakVal = 2.0 * b(j,1) * (temp4 + temp2)

      return
      end

CCCCCCCCCCCCCCCCCCCCCCCCCCCCCCCCCCCCCCCCCCCCCCCCCCCCCCCCCCCC
C                                                              C
C  Subroutine Name:  CalcEnv                                   C
C                                                              C
C  Description.  Given the current fitting parameter values, returns C
C               the x (binding energy) and y (electron counts) values C
C               describing a single component peak of the model C
C               spectrum.                                      C
C                                                              C
C  Parameters.     a       -> List of fitting parameters       C
C                  be      -> Experimental binding energy      C
C                  be_env  <- Theoretical peak envelope, binding energy C
C                  ec_env  <- Theoretical peak envelope, electron counts C
C                  n_peaks -> Number of peaks in model         C
C                  n_data  -> Number of experimental data points C
CCCCCCCCCCCCCCCCCCCCCCCCCCCCCCCCCCCCCCCCCCCCCCCCCCCCCCCCCCCC
      subroutine CalcEnv(a,be,be_env,ec_env,n_peaks,n_data)
      implicit none

      integer k_pmax           ! Maximum number of fitting parameters
      parameter (k_pmax = 400)
      integer k_pkmax          ! Maximum number of peaks in model
      parameter (k_pkmax = 100)
      integer k_dmax           ! Maximum number of data points
      parameter (k_dmax = 10000)
      integer k_emax           ! Maximum # of points in peak envelope
      parameter (k_emax = 100000)

      real*8 a(k_pmax)         ! Fitting parameters
      real*8 b(k_pkmax,4)      ! Table of fitting parameters (4 per peak)
```

```fortran
      real*8 be(k_dmax)           ! Experimental binding energy
      real*8 be_env(k_emax)       ! Peak envelope, binding energy
      real*8 ec_env(k_emax)       ! Peak envelope, electron counts
      integer n_peaks             ! Number of peaks
      integer n_data              ! Number of experimental data points
      integer i,j,k               ! Counter variables

      real*8 PeakVal              ! Function PeakVal

      k = 1
      do j=1,n_peaks
        do i=1,4
          b(j,i) = a(k)
          k = k + 1
        enddo
      enddo

      k = 1
      do j=1,n_peaks
        do i=1,n_data
          be_env(k) = be(i)
          ec_env(k) = PeakVal(b,j,be(i))
          k = k + 1
        enddo
      enddo

      return
      end

CCCCCCCCCCCCCCCCCCCCCCCCCCCCCCCCCCCCCCCCCCCCCCCCCCCCCCCCCCCCCC
C                                                              C
C  Subroutine Name.  PrintVals                                 C
C                                                              C
C  Description.  Writes to the  log file the parameter values at the C
C               end of the current iteration.                  C
C                                                              C
C  Parameters.     a       -> List of fitting parameters       C
C                  fit_a   -> Fit this parameter?              C
C                  all     -> Print all values? (0=no, 1=yes)  C
C                  n_peaks -> Number of peaks in model spectrum C
CCCCCCCCCCCCCCCCCCCCCCCCCCCCCCCCCCCCCCCCCCCCCCCCCCCCCCCCCCCCCC
      subroutine PrintVals(a,fit_a,all,n_peaks)

      integer k_pmax          ! Maximum number of fitting parameters
      parameter (k_pmax = 400)

      real*8 a(k_pmax)        ! Fitting parameters
      integer fit_a(k_pmax)   ! Fit this parameter?
      integer all             ! Print all values?
                              ! 0 = no, just fitted parameters
                              ! 1 = yes  print all parameters
      integer n_peaks         ! Number of peaks
      integer i,j,k           ! Counter variables
      character*32 desc(k_pmax)   ! Description of parameter
      character*32 temp           ! Temporary storage variable

      do i=1,n_peaks
        temp = 'Area    - Peak #'
        desc(4*i-3) = temp( index(temp,'#'))//char(48+i)
        temp = 'Center  -
        desc(4*i-2) = temp( index(temp,'#'))// char(48+i)
        temp = FWHM    -
```

```fortran
      desc(4*i-1) = temp(:index(temp,'0'))//char(48+i)
      temp = 'Shape    0'
      desc(4*i) = temp(:index(temp,'0'))//char(48+i)
      enddo

      if (all.EQ.1) then
      do i=1,n_peaks
      do j=3,0,-1
      k = 4*i-j

c
c  If parameter was adjusted, write a '*' after its value
c  If parameter was a slave, write the number of its master after
c  its value.
c
      if (fit_a(k).EQ.1) then
      write (7,*) desc(k),' = ',a(k),' (*)'
      else if (fit_a(k).GT.1) then
      write (7,*) desc(k),' = ',a(k),' (',fit_a(k),')'
      else
      write (7,*) desc(k),' = ',a(k)
      endif
      enddo
      write (7,*)
      enddo
      else
      do i=1,n_peaks
      do j=3,0,-1
      k = 4*i-j
      if (fit_a(k).EQ.1) then
      write (7,*) desc(k),' = ',a(k)
      endif
      enddo
      enddo
      endif

      return
      end

ccccccccccccccccccccccccccccccccccccccccccccccccccccccccc
c
c  Subroutine Name:  Help
c
c  Description:  Prints out some help for the user, including a list
c                of the required and generated files.
c
ccccccccccccccccccccccccccccccccccccccccccccccccccccccccc
      subroutine Help

      write (*,*) 'Help....'
      write (*,*)
      write (*,*) 'This program fits theoretical peaks to XPS spectra '
      write (*,*) 'The peaks used are Gaussian-Lorentzian sums '
      write (*,*)
      write (*,*) 'Expected file names are '
      write (*,*) '  filename_base.par old - fit parameters (INPUT)'
      write (*,*) '  filename_base.dat     - experimental spectrum ',
     &  '(INPUT)'
      write (*,*) '  filename_base.log     - fit log'
      write (*,*) '  filename_base.bkg     - linear baseline'
      write (*,*) '  filename_base.sub     - background-subtracted ',
     &  'spectrum'
      write (*,*) '  filename_base.fit     - fitted spectrum'
      write (*,*) '  filename_base.pks     - fitted peaks'
      write (*,*) '  filename_base.tix     - peak center tic marks'
      write (*,*) '  filename_base.sum     - summary of fitted peak ',
     &  'parameters'
      write (*,*) '  filename_base.par     - updated fitting parameter',
     &  ' file'
      write (*,*) '  filename_base.fit.scr - CPLOT do file for screen ',
     &  'plotting of fit'
      write (*,*) '  filename_base.fit.prn - CPLOT do file for hard ',
     &  'copy of fit'
      write (*,*) '  filename_base.bkg.scr - CPLOT do file for screen ',
     &  'plotting of background'
      write (*,*) '  filename_base.bkg.prn - CPLOT do file for hard ',
     &  'copy of background'
      write (*,*)

      return
      end

ccccccccccccccccccccccccccccccccccccccccccccccccccccccccc
c
c  Subroutine Name:  Template
c
c  Description:  Generates a template parameter file and writes it to
c                file *.par, where '*' is chosen by the user.  The
c                number of peaks in the model spectrum is also user-
c                defined.
c
ccccccccccccccccccccccccccccccccccccccccccccccccccccccccc
      subroutine Template
      implicit none

      integer      n     ! Number of peaks in the model spectrum
      integer      i     ! Counter variable
      character*30 base  ! Base file name for template .par file
      character*40 file  ! Full file name of template file

      write (*,*) 'Enter a file name base for the .par file:'
      read (*,'(a30)') base
      write (*,*) 'How many peaks are in the model spectrum?'
      read (*,*) n

      file = base(:index(base,' ') - 1) // '.par'
      open (unit=17, file=file, status='unknown')

      write (17,400) 272.0, 292.0, 10000
400   format (f6.2,4x,f6.2,4x,i8)
      write (17,405) n, 10, 0
405   format (i3,7x,i3,8x,i3)
      do i=1,n
      write (17,*)
      write (17,410) 100.0, 0, 1.0, 0, 0.0, 100000.0, 10.0
      write (17,410) 0.0, 0, 1.0, 0, 0.0, 272.0, 292.0, 0.01
      write (17,410) 1.2, 0, 1.0, 0, 0.0, 1.0, 1.6, 0.01
      write (17,410) 0.8, 0, 1.0, 0, 0.0, 0.7, 1.0, 0.01
410   format (f7.2,1x,i3,1x,f6.3,1x,f5.2,3x,f6.2,2x,f9.2,4x,f7.2)
      enddo

      write (*,*)
      write (*,*) 'Template written to file ',file
      write (*,*)

      close (unit=17, status='keep')
```

```
      endif
      write (14,*) ' minimum SSE was reached.'

      return
      end

cccccccccccccccccccccccccccccccccccccccccccccccccccccccccccccccccc
c                                                                c
c  Subroutine Name:  DoFiles                                     c
c                                                                c
c  Description:  Writes do-files for use with the external CPLOT c
c                utility.  When CPLOT is run using the command,  c
c                'cplot dofilename,' a plot of the fit to the data (or c
c                the linear background) is generated.  This subroutine c
c                generates 4 do-files: (1) screen plot of fit to data, c
c                (2) postscript file of fit to data, (3) screen plot of c
c                background, and (4) postscript plot of background.  c
c                                                                c
c  Parameters:  basename  -> Base file name                      c
c                                                                c
cccccccccccccccccccccccccccccccccccccccccccccccccccccccccccccccccc
      subroutine DoFiles(basename)
      implicit none

      character*30  basename    ! Base file name
      character*40  filename    ! Full file name (with extension)

      write (10,*) '# do file for plotting fitted peaks using CPLOT'
      write (11,*) '# do file for printing fitted peaks using CPLOT'
      write (10,*) 'rq'
      write (11,*) 'rq'
      write (10,*) 'x11'
      filename = basename(:index(basename,' ')-1) // '.ps'
      write (11,*) 'psfilter ',filename
      write (10,*) 'zw'
      write (11,*) 'zw'
      write (10,*) 'tx t Fitted XPS Peaks for Sample ',basename
      write (11,*) 'tx t Fitted XPS Peaks for Sample ',basename
      filename = basename(:index(basename,' ')-1) // '.sub'
      write (10,*) 'gd 2 ',filename
      write (11,*) 'gd 2 ',filename
      write (10,*) 'tt 2'
      write (11,*) 'tt 2'
      write (10,*) 'tx x Binding Energy (eV)'
      write (11,*) 'tx x Binding Energy (eV)'
      write (10,*) 'tx y Electron Counts'
      write (11,*) 'tx y Electron Counts'
      write (10,*) 'sy 0'
      write (11,*) 'sy 0'
      write (10,*) 'z'
      write (11,*) 'z'
      write (10,*) 'sy 9'
      write (11,*) 'sy 9'
      write (10,*) 'zp'
      write (11,*) 'zp'
      filename = basename(:index(basename,' ')-1) // '.pks'
      write (10,*) 'gd 2 ',filename
      write (11,*) 'gd 2 ',filename
      write (10,*) 'sy L'
      write (11,*) 'sy L'
      write (10,*) 'zp'
      write (11,*) 'zp'
```

```
      return
      end

cccccccccccccccccccccccccccccccccccccccccccccccccccccccccccccccccc
c                                                                c
c  Subroutine Name:  Summary                                     c
c                                                                c
c  Description:  Writes to a file (.sum) a summary of the values of all c
c                of the parameters when fitting has terminated due to c
c                either the minimization of SSE or the expiration of c
c                the iteration limit                             c
c                                                                c
c  Parameters:  a         -> List of fitting parameters          c
c               n_peaks   -> Number of peaks in model spectrum   c
c               SSE       -> Sum of Squares due to Error          c
c               rsq       -> r^2 value (Coefficient of Determination) c
c               rsq_DOF   -> DOF Adjusted r^2                     c
c               minimized -> Did we reach a minimum SSE?          c
c               basename  -> Base file name                      c
c                                                                c
cccccccccccccccccccccccccccccccccccccccccccccccccccccccccccccccccc
      subroutine Summary(a,n_peaks,SSE,rsq,rsq_DOF,minimized,basename)
      implicit none

      integer      k_pmax     ! Maximum number of fitting parameters
      parameter (k_pmax = 400)

      real*8       a(k_pmax)   ! Fitting parameters
      integer      n_peaks     ! Number of peaks
      real*8       SSE         ! Sum of Squares due to Error
      real*8       rsq         ! r^2 value
      real*8       rsq_DOF     ! Degree-of-Freedom Adjusted r^2
      logical      minimized   ! Did we reach a minimum SSE?
      character*30 basename     ! Base file name
      character*35 temp         ! Temporary storage variable
      real*8       perc         ! Percentage of Lorentzian character
      integer      i            ! Counter variable

      temp = basename(:index(basename,' ')) // '......'
      write (14,*) '**** RESULTS SUMMARY FOR SAMPLE ',temp
      write (14,*)
      write (14,600)
600   format (1x,'PEAK NO ',8x,'AREA',4x,'POSITION (eV)',4x,
     &   'FWHM (eV)',4x,'SHAPE')
      write (14,605)
605   format (1x,8(:-'),8x,4(:-'),4x,13(:-'),4x,9(:-'),4x,5(:-'))
      do i=1,n_peaks
         perc = (1.0 - a(i*4)) * 100.0
         write (14,610) i, a(i*4-3), a(i*4-2), a(i*4-1), perc
610      format (3x,i3,4x,f11.2,7x,f9.2,7x,f5.2,5x,f5.1,
     &   ' Lorentzian')
      enddo
      write (14,*)
      write (14,*) 'Statistics of merit for this fit'
      write (14,*) '   SSE        = ',SSE
      write (14,*) '   r^2        = ',rsq
      write (14,*) '   DOF Adjusted r^2 = ',rsq_DOF
      write (14,*)
      if (minimized) then
         write (14,*) 'This fit was a minimum'
      else
         write (14,*) 'Iteration limit expired before'
```

```fortran
      filename = basename(:index(basename,' ') - 1) // '.fit'
      write (10,') 'gd 2 ',filename
      write (11,') 'gd 2 ',filename
      write (10,') 'zp'
      write (11,') 'zp'
      filename = basename(:index(basename,' ') - 1) // '.tix'
      write (10,') 'gd 2 ',filename
      write (11,') 'gd 2 ',filename
      write (10,') 'sy 7'
      write (11,') 'sy 7'
      write (10,') 'zp'
      write (11,') 'zp'
      write (10,') 'zx'
      write (11,') 'zx'

      write (12,') ' # do file for plotting background using CPLOT'
      write (13,') ' # do file for printing background using CPLOT'
      write (12,') 'zq'
      write (13,') 'zq'
      write (12,') 'xll'.
      filename = basename(:index(basename,' ') -1) // '.ps'
      write (13,') 'psfilter ',filename
      write (12,') 'zw'
      write (13,') 'zw'
      write (12,') 'tx t Fitted Background for Sample ',basename
      write (13,') 'tx t Fitted Background for Sample ',basename
      filename = basename(:index(basename,' ') - 1) // '.dat'
      write (12,') 'gd 2 ',filename
      write (13,') 'gd 2 ',filename
      write (12,') 'ft 2'
      write (13,') 'ft 2'
      write (12,') 'tx x Binding Energy (eV)'
      write (13,') 'tx x Binding Energy (eV)'
      write (12,') 'tx y Electron Counts'
      write (13,') 'tx y Electron Counts'
      write (12,') 'sy 9'
      write (13,') 'sy 9'
      write (12,') 'z'
      write (13,') 'z'
      filename = basename(:index(basename,' ') - 1) // '.bkg'
      write (12,') 'gd 2 ',filename
      write (13,') 'gd 2 ',filename
      write (12,') 'sy L'
      write (13,') 'sy L'
      write (12,') 'zp'
      write (13,') 'zp'
      filename = basename(:index(basename,' ') - 1) // '.sub'
      write (12,') 'gd 2 ',filename
      write (13,') 'gd 2 ',filename
      write (12,') 'zp'
      write (13,') 'zp'
      write (12,') 'zx'
      write (11,') 'zx'

      return
      end
```

F.2 Help Text

Following is the text printed on the screen by the xps program when the user types "?" at the prompt immediately after running the program. This text provides brief descriptions of the files input to and output by the xps.exe program.

```
Enter filename base:
  ( OR, enter '?' for help
    OR, enter '#' to generate a parameter file template )

Help...

This program fits theoretical peaks to XPS spectra.
The peaks used are Gaussian-Lorentzian sums.

Expected file names are:
  filename_base.par.old - fit parameters (INPUT)
  filename_base.dat     - experimental spectrum (INPUT)
  filename_base.log     - fit log
  filename_base.bkg     - linear baseline
  filename_base.sub     - background-subtracted spectrum
  filename_base.fit     - fitted spectrum
  filename_base.pks     - fitted peaks
  filename_base.tix     - peak center tic marks
  filename_base.sum     - summary of fitted peak parameters
  filename_base.par     - updated fitting parameter file
  filename_base_fit.scr - CPLOT do file for screen plotting of fit
  filename_base_fit.prn - CPLOT do file for hard copy of fit
  filename_base_bkg.scr - CPLOT do file for screen plotting of background
  filename_base_bkg.prn - CPLOT do file for hard copy of background
```

F.3 Examples of Required File Formats

Two files are necessary to fit an XPS data set using the xps program. Examples of these files are presented here to illustrate the required file formats.

F.3.1 Example Data File

The following is an example data (.dat) file. It contains four header lines, followed by data in a two-column format, with binding energies in column 1 in increasing order and photoelectron intensities in column 2.

```
Raw File:     example.mrs
Description:  Membrane 5-25-C4, Front Side. As cast at 90C

Binding Energy (eV)      Electron Counts
         272.00                 88.00
         272.20                 82.00
         272.40                 71.00
         272.60                 87.00
         272.80                 79.00
         273.00                103.00
         273.20                 76.00
         273.40                 79.00
         273.60                 80.00
         273.80                100.00
         274.00                 90.00
         274.20                 71.00
         274.40                 80.00
         274.60                 79.00
         274.80                 76.00
         275.00                 72.00
         275.20                 92.00
         275.40                100.00
         275.60                 87.00
         275.80                 74.00
         276.00                 82.00
         276.20                 73.00
         276.40                 77.00
         276.60                 74.00
         276.80                 81.00
         277.00                 80.00
         277.20                102.00
         277.40                 92.00
         277.60                 97.00
         277.80                 92.00
         278.00                 97.00
         278.20                107.00
         278.40                137.00
```
(and so on...)

F.3.2 Example Parameter File

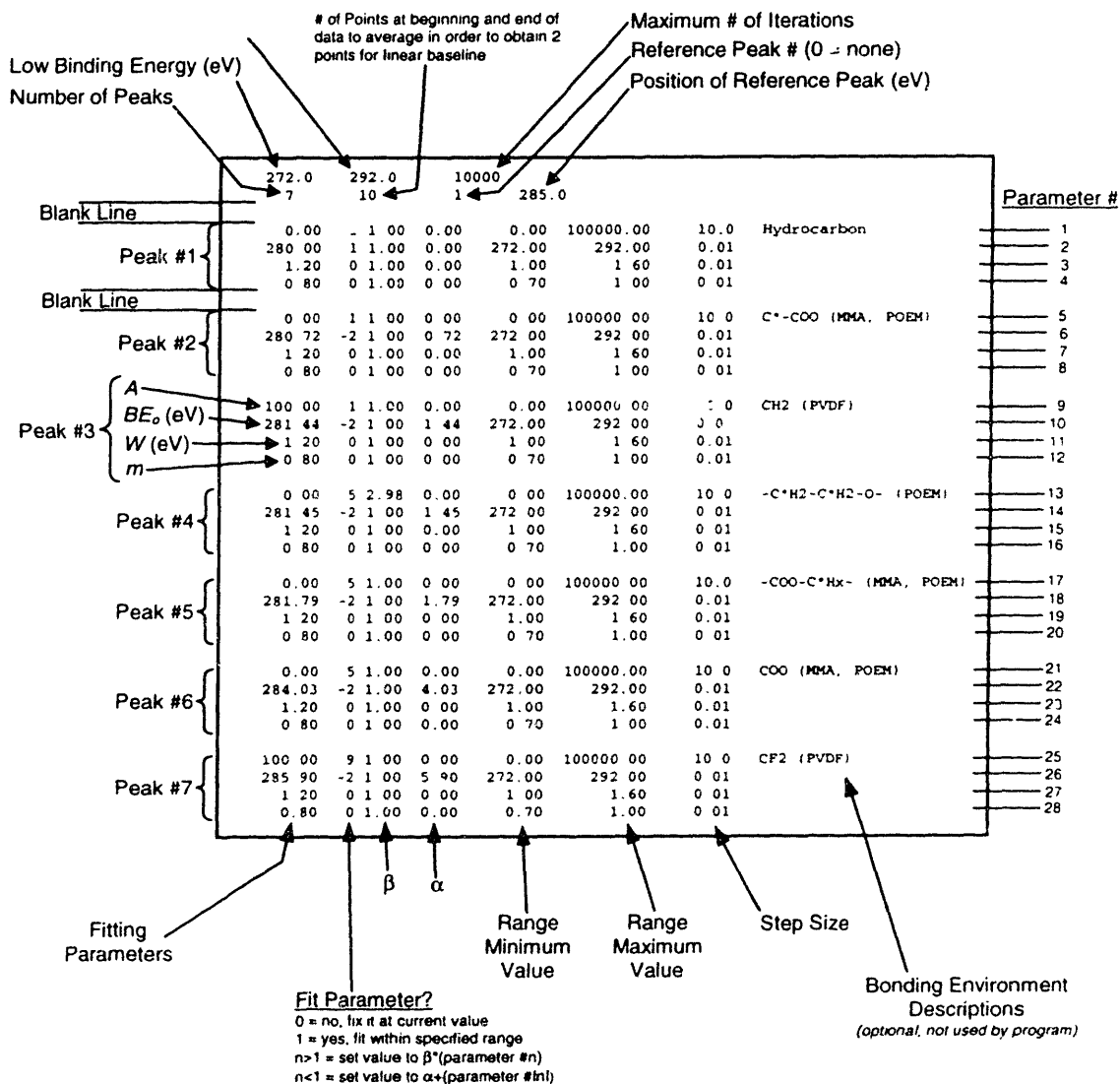Following is an example parameter (.par) file, which defines the theoretical model used to fit the experimental data.

```
                                    # of Points at beginning and end of        Maximum # of Iterations
                                    data to average in order to obtain 2        Reference Peak # (0 = none)
       Low Binding Energy (eV)      points for linear baseline                  Position of Reference Peak (eV)
       Number of Peaks

                              272.0      292.0       10000                                        Parameter #
                                7          10            1      285.0
Blank Line
              0.00    _ 1 00   0.00     0.00   100000.00    10.0   Hydrocarbon                      1
   Peak #1   280 00    1 1.00  0.00   272.00     292.00      0.01                                   2
              1.20     0 1.00  0.00     1.00        1 60      0.01                                   3
              0 80     0 1.00  0 00     0 70        1 00      0 01                                   4
Blank Line
              0 00     1 1 00  0 00     0 00   100000 00     10 0   C*-COO (MMA, POEM)              5
   Peak #2   280 72   -2 1 00  0 72   272 00     292 00      0.01                                   6
              1 20     0 1.00  0.00     1.00        1 60      0.01                                   7
              0 80     0 1 00  0 00     0 70        1 00      0 01                                   8
         A
         BE_o (eV)   100 00    1 1.00  0.00     0.00   100000 00     : 0   CH2 (PVDF)               9
Peak #3  BE_o (eV)   281 44   -2 1 00  1 44   272.00     292 00     J 0                            10
         W (eV)        1 20    0 1 00  0 00     1 00        1 60      0.01                          11
         m             0 80    0 1 00  0 00     0 70        1 00      0.01                          12

              0 00     5 2.98  0.00     0 00   100000.00    10 0   -C*H2-C*H2-O-  (POEM)           13
   Peak #4   281 45   -2 1 00  1 45   272 00     292 00      0 01                                  14
              1 20     0 1 00  0.00     1 00        1 60      0 01                                  15
              0 80     0 1 00  0 00     0 70        1.00      0 01                                  16

              0.00     5 1.00  0 00     0 00   100000 00     10.0   -COO-C*Hx-  (MMA, POEM)        17
   Peak #5   281.79   -2 1 00  1.79   272.00     292 00      0.01                                  18
              1 20     0 1 00  0 00     1.00        1 60      0.01                                  19
              0 80     0 1.00  0 00     0 70        1.00      0 01                                  20

              0.00     5 1.00  0.00     0.00   100000.00    10 0   COO (MMA, POEM)                 21
   Peak #6   284.03   -2 1.00  4.03   272.00     292.00      0.01                                  22
              1.20     0 1.00  0 00     1.00        1.60      0.01                                  23
              0 80     0 1 00  0.00     0 70        1 00      0.01                                  24

             100 00    9 1 00  0 00     0.00   100000 00     10 0   CF2 (PVDF)                     25
   Peak #7   285 90   -2 1 00  5 90   272.00     292 00      0 01                                  26
              1 20     0 1 00  0 00     1 00        1.60      0 01                                  27
             0.80     0 1.00  0.00     0.70        1.00      0 01                                  28
```

Fitting Parameters

β   α

Range Minimum Value   Range Maximum Value   Step Size

Bonding Environment Descriptions (optional, not used by program)

Fit Parameter?
0 = no, fix it at current value
1 = yes, fit within specified range
n>1 = set value to β*(parameter #n)
n<1 = set value to α+(parameter #inl)

Figure F.1 Example parameter (.par) file

The above parameter file is an example of one used to fit the C 1s data for a blend of PVDF and P(MMA-r-POEM₉). It has seven component peaks, each defined by four parameters: A, BE_o, W, and m. In this example, the positions BE_o of peaks 2-7 are constrained relative to the position of peak 1, which is started at an initial guess of 280.00 eV and allowed to vary between 272 and 292 eV. The areas A of peaks 1-3 will be fit. The areas of peaks 5 and 6 are constrained to be equal to that of peak 2, and the area of peak 4 is constrained to be 2.98 times that of peak 2. The area of peak 7 is

288

constrained to be equal to that of peak 3. Once the fit has terminated, the *BE* scale will be adjusted such that peak 1 is at a position of 285.00 eV. This adjustment will result in the rewriting of both the parameter (.par) and raw data (.dat) files.

Biographical Note

Jon Hester was born on July 28, 1971 on the Fort Bliss Army Base in El Paso, Texas, where his father, Forrest "Woody" Hester, III, was serving as a Captain in the US Army, having completed an overseas assignment in Vietnam. During Jon's brief stay in the base hospital with his mother, Louise, a tag attached to his bed read, in military style, "One Each: bed, baby; blanket." Jon resided in El Paso for only five days, after which he traveled with his parents to Good Hope, Illinois. There, his father began finishing his B.S. Degree in Pharmacy while working evenings to support the family and begin saving money for Jon's college education. (Nearly thirty years later, this thesis represents the final return on that investment.) Jon spent most of his childhood in Springfield, Illinois with his two brothers, Jason and Joshua, and his sister, Jessica (who, symmetrically, has just begun her university studies at the time of this writing).

Jon attended Purdue University, graduating in 1993 with a B.S. in Materials Science and Engineering. There, he conducted research under Prof. Eric Kvam on the epitaxial growth of single-crystal cobalt disilicide films on silicon for microelectronics applications. During the summers of 1990 and 1991, he interned at Hanson Engineers, Inc. (Springfield, IL), where he developed a computer model to conduct cost-benefit analyses of various insulation systems in residential buildings. Jon served as president of the Purdue chapter of Theta Tau Engineering Fraternity, treasurer of the Purdue chapter of Alpha Sigma Mu, and representative on the Purdue Engineering Student Council.

From 1993 to 1995, Jon served as a Peace Corps Volunteer, teaching secondary-level science and mathematics at Sandema Secondary-Technical School, a rural school in Sandema, Ghana, West Africa. Besides teaching, Jon served as a Trainer at the In-Service Training for new Peace Corps Volunteer Educators in Ghana in 1995. He also coached Sandema Sec.-Tech.'s *first* girls' soccer team. While in Ghana, Jon met his future wife, Amy, a Peace Corps physics teacher from California who was working in the not-so-nearby village of Sampa. They were married in October, 1998 in South Hadley, Massachusetts, near the University of Massachusetts - Amherst, where Amy had just completed a Masters Degree in Industrial Engineering.

Jon entered the MIT Department of Materials Science and Engineering in the fall of 1995. At MIT, he worked for a semester as a Teaching Assistant for the Undergraduate Materials Structure Laboratory (3.081) under Prof. Anne Mayes. He also had the opportunity to work as a Research Assistant under Prof. Ioannis Yannas, characterizing the surface chemistry of collagen-glycosaminoglycan scaffolds used as artificial skin implants for burn patients. The bulk of his work, including that presented in this thesis, was conducted under the direction of Prof. Anne Mayes. In 1999, Jon was awarded the Materials Research Society Graduate Student Gold Award "in recognition of outstanding performance in the conduct of research" for his work on self-organizing polymer membranes. He was a MIT Martin Graduate Fellow in Environmental Sustainability from Fall, 1999 to Spring, 2000.

Curriculum Vitae
Jonathan F. Hester
Department of Materials Science and Engineering
Polymer Science Specialization
Massachusetts Institute of Technology

EDUCATION
Massachusetts Institute of Technology, Cambridge, MA (Sept., 1995 – Sept., 2000)
Dept. of Materials Science and Engineering Doctoral Program   **GPA: 4.8/5.0**
- Specialization in Polymer Science
- Advisor: Prof. Anne M. Mayes
- Thesis Research:
  Surface segregation phenomena in water filtration membranes prepared from compatible polymer blends containing amphiphilic comb polymers as the minor component. Application of the standard immersion precipitation membrane fabrication process to drive surface localization of the comb component, providing surface modification with no additional processing steps. This strategy is used to fabricate wettable membranes from predominantly hydrophobic materials and to create membranes with regenerative, foul-resistant surface layers or with *in situ* tunable pore sizes.
- Minor: "Environmental Issues and Policy"

Purdue University, West Lafayette, IN (Aug., 1989 – May, 1993)
B.S. Materials Science and Engineering, May, 1993   **GPA: 5.83/6.0**

RESEARCH EXPERIENCE
GRADUATE RESEARCH ASSISTANT, MIT, Cambridge, MA (1996-Present)
Advisor: Prof. Anne M. Mayes, Department of Materials Science and Engineering
- ◆ Design of compatible polymer blend systems containing inexpensive, amphiphilic comb polymers as the minor component. Development of processing routes leading to surface segregation of the comb additive as an economical means to modify the surfaces of commercial polymeric articles. These include water filtration membranes with improved wettability, fouling resistance, and selectivity, as well as PVC-based medical devices having enhanced protein adsorption resistance.

Responsibilities Include:
- Design and synthesis of economical, amphiphilic comb polymers
- Fabrication of devices, including the casting of polymer membranes by immersion precipitation
- Study of the influence of comb polymer attributes (molecular weight, composition, side chain length, etc.) on surface segregation
- Study of the influence of processing parameters on surface segregation
- Development of a theoretical framework to describe the observed surface segregation phenomena
- Quantification of the benefits of surface modification (protein adsorption resistance, etc.)

Skills Include:
- Polymer Synthesis (Free-Radical, Anionic, Atom Transfer Radical Techniques)

- Immersion Precipitation (or "Phase Inversion") Casting
- Polymer Thin Film Processing
- Ultrafiltration Experimentation
- X-ray Photoelectron Spectroscopy (XPS) [wrote custom software for fitting XPS data]
- Nuclear Magnetic Resonance Spectroscopy (NMR)
- Electron Microscopy: SEM, TEM (including sample preparation)
- Immunochemical Labeling Techniques for Microscopy
- Ellipsometry
- Contact Angle Measurement
- Neutron Reflectivity
- Thermal Analysis: DSC, DTA, TGA
- Spectroscopy Techniques: FTIR, UV-Vis, EDX
- Computer Programming
- Technical and Academic Writing

GRADUATE RESEARCH ASSISTANT, MIT, Cambridge, MA (1996)
Advisor: Prof. Ioannis V. Yannas, Department of Mechanical Engineering

♦ Characterized the surface chemistry of collagen-glycosaminoglycan scaffolds used as artificial skin implants, employing electron microscopy with immunochemical labeling techniques.

RESEARCH INTERN, Purdue University, West Lafayette, IN (Summer, 1992)
Advisor: Prof. Eric P. Kvam, Department of Materials Science and Engineering

♦ Developed a process for epitaxial growth of single-crystal cobalt disilicide films on (100) silicon, using ion beam sputtering techniques.

INTERN, Hanson Engineers, Inc., Springfield, IL (Summers, 1990, 1991)
Supervisor: Walter E. Hanson

♦ Conducted cost-benefit analyses of various insulation systems in residential buildings. Developed a computer model for simulating the annual space conditioning performances of various insulation systems and components.

Publications:
- "Amphiphilic Graft Copolymers Based on Commercial Halogenated Polymers," J. F. Hester, P. Banerjee, A. Akthakul, R. A. Mickiewicz and A. M. Mayes, *In Preparation.*
- "Preparation of pH-Responsive Polymer Membranes by Self-Organization," J. F. Hester, S. Olugebefola and A. M. Mayes, *In Preparation.*
- "Optimization and Performance of Foul-Resistant Poly(vinylidene fluoride) Membranes Prepared in a Single Step by Self-Organization," J. F. Hester and A. M. Mayes, *In Preparation.*
- "Tailoring Membrane Surface Properties Economically Through Self-Organization," J. F. Hester and A. M. Mayes, *The 1999 Membrane Technology/Separations Planning Conference proceedings: as presented at the Seventeenth Annual Membrane Technology/Separations Planning Conference, Dec. 6 and 7, 1999, Newton. Massachusetts,* Business Communications Co., Inc.: Norwalk, CT, 2000.
- "Preparation of Protein-Resistant Surfaces on Poly(vinylidene fluoride) Membranes via Surface Segregation," J. F. Hester, P. Banerjee and A. M. Mayes, *Macromolecules* 1999, *32,* 1643-1650.

Patents:

- "Polymer Articles, Including Membranes, Having Hydrophilic Surfaces and Method for their Preparation," A. M. Mayes, **J. F. Hester** and D. G. Walton, International Application No. PCT/US97/16488.
- "Graft Copolymers, Methods for Grafting Vinyl Species, Including Hydrophilic Species, onto Halogenated Polymers, and Articles Thereof," P. Banerjee, **J. F. Hester**, A. Akthakul and A. M. Mayes, *US Application.*

Selected Presentations:

- *Incredible, Wettable, Uncloggable, and pH-Adjustable Self-Organizing Polymer Membranes for Water Filtration,* BP Amoco / MIT Program in Polymer Science and Technology Poster Competition, April, 2000, Cambridge, MA **(Prize Winner)**
- *Tailoring Polymer Membrane Surfaces Through Surface Segregation,* The 1999 Membrane Technology/Separations Planning Conference, Dec., 1999, Newton, MA **(Invited Talk)**
- *Self-Organizing Polymer Membranes for Water Filtration,* Materials Research Society Conference, Nov., 1999, Boston, MA **(Invited Talk)**
- *Regenerative Surfaces on Polymer Membranes via Surface Segregation,* American Physical Society Conference, March, 1999, Atlanta, GA (Contributed Talk)
- *Preparation of Protein-Resistant Surfaces on Poly(vinylidene fluoride) Membranes via Surface Segregation,* MIT Materials Processing Center Research Review Poster Session, Oct., 1998, Cambridge, MA (Poster)
- *Preparation of Hydrophilic Surfaces on Polymer Membranes via Surface Segregation,* American Chemical Society Conference, August, 1998, Boston, MA (Contributed Talk)
- *Preparation of Hydrophilic Surfaces on Polymer Membranes via Surface Segregation,* American Physical Society Conference, March, 1998, Los Angeles, CA (Contributed Talk)
- *Surface Modification of Polymer Membranes via Surface Segregation,* Annual Presentation to the MIT Center for Environmental Health Sciences, Dec., 1997, Cambridge, MA
- *Hydrophilic Surface Preparation on Fluoropolymers via Entropically-Driven Surface Segregation,* American Physical Society Conference, March, 1997, Kansas City, MO (Poster)
- *Teaching Students in the Laboratory,* Presented as part of the "Better Teaching @ MIT" program, Jan., 1996, Cambridge, MA

TEACHING EXPERIENCE

TEACHING ASSISTANT, MIT, Cambridge, MA (1995-96)

Undergraduate Materials Structure Laboratory (3.081), Fall Term, 1995, Under Prof. A.M. Mayes

- ◆ The Undergraduate Materials Structure Laboratory is designed to introduce students to the theory, experimental methods, and instruments used to characterize materials at scales ranging from the microscopic to the atomic. I led groups of 4-5 students in the hands-on performance of a series of experiments related to structure-property relationships at materials surfaces and interfaces. My responsibilities included the design and administration of the experiments, as well as the design of weekly lectures. Teaching emphasized the rational design of experiments, the physical principles behind the instrumentation, and technical reporting skills. The techniques used included XPS, AES, FTIR, TGA, profilometry, and cell counting.

VOLUNTEER, UNITED STATES PEACE CORPS - GHANA, Sandema, Ghana (1993-95)
Secondary-Level General Science and Mathematics

♦ After an intensive, 9-week training course including teaching methodology, language, and cross-cultural adaptation, I was sent to a rural secondary school in Sandema, Ghana, West Africa. At this school with a population of roughly 500 students, I was the only science teacher. I taught general science to all 500 students in grade levels equivalent to U.S. grades 10-12. I also taught mathematics to students in a grade level equivalent to U.S. grade 10.

Responsibilities:
* Development of all daily lesson plans
* Design, administration, and grading of all daily assignments and exams
* Maintenance of classroom discipline
* Design and administration of weekly lab experiments with students, often improvising with locally-available materials
* Improvement, management, and maintenance of the school's science lab and its inventory
* Development of innovative teaching materials for nationwide use by Peace Corps Volunteer Educators in Ghana

Additional Activities:
* Taught weekly night classes to aid students in preparing for the West African Exams Council external exams
* Served as faculty advisor to the school's science club
* Coached the school's *first* girls' soccer team

AWARDS
Massachusetts Institute of Technology
* Materials Research Society Graduate Student Gold Award (1999)
* Martin Fellowship (1999-2000)
* Hugh Hampton Young Fellowship (1998-1999)
* 3M Fellowship (1998-1999)

Purdue University
* Graduated With Distinction, Ranked #2 in Dept. of Materials Science and Engineering
* Induction, Alpha Lambda Delta (1992)
* Induction, Phi Eta Sigma (1992)
* Induction, Tau Beta Pi (1991)
* Purdue President's Honor Scholarship Award (1989)
* McCourtney Foundation Scholarship Award (1989)
* Robert C. Byrd Scholarship Award (1989)
* Daughters of the American Revolution Scholarship Award (1989)

POSITIONS OF LEADERSHIP
* MIT Martin Graduate Fellow in Environmental Sustainability (1999-2000)
* Trainer, In-Service Training for new Peace Corps Volunteer Educators in Ghana (1995)
* Treasurer, Purdue Chapter of Alpha Sigma Mu (1993)
* President, Purdue Chapter of Theta Tau Engineering Fraternity (1992)
* Representative, Interfraternity Presidents' Council (1992)
* Representative, Purdue Engineering Student Council (1990-1993)

THESIS PROCESSING SLIP

FIXED FIELD: ill._____ name _____

index_____ biblio _____

► **COPIES:** (Archives)   Aero   Dewey   Barker   Hum

Lindgren   Music   Rotch   (Science)   Sche-Plough

TITLE VARIES: ► ☐ _____

_____

_____

NAME VARIES: ► ☐ Forrest _____

_____

IMPRINT: (COPYRIGHT)_____

_____

► **COLLATION:** _____

_____

► **ADD: DEGREE:** _____ ► **DEPT.:** _____

► **ADD: DEGREE:** _____ ► **DEPT.:** _____

SUPERVISORS: _____

_____

NOTES:

                      cat'r: date:

                                    page:

► **DEPT:** _Nabang_ ▶ _____

► **YEAR:** _2001_ ► **DEGREE:** _Ph.D._

► **NAME:** _HESTER, _____